Huntingtin and mitosis

Maria Molina-Calavita

UNIVERSITÉ PARIS-SUD 11

ÉCOLE DOCTORALE :

INNOVATION THÉRAPEUTIQUE : DU FONDAMENTAL À L'APPLIQUÉ

PÔLE : PHYSIOPATHOLOGIE MOLECULAIRE ET CELLULAIRE

DISCIPLINE : Biologie cellulaire et moléculaire

ANNÉE 2011-2012 SÉRIE DOCTORAT N°1199

THÈSE DE DOCTORAT

soutenue le 22/10/2012

par

Maria MOLINA-CALAVITA

Huntingtine et mitose

Directeur de thèse :	Sandrine HUMBERT	DR2 INSERM (Institut Curie)
Composition du jury :		
Rapporteurs :	Arnaud ECHARD	DR2 CNRS (Institut Pasteur)
	Sonia GAREL	DR2 INSERM (IBENS)
Examinateurs :	Annie ANDRIEUX	DR1 CEA (CEA)
	Renata BASTO	DR2 CNRS (Institut Curie)
	Anselme PERRIER	CR1 INSERM (I-STEM)
	Frédéric SAUDOU	DR1 INSERM (Institut Curie)

Alla nonna

Acknowledgements

J'aimerais remercier tout d'abord les membres de mon jury de thèse - Arnaud Echard, Sonia Garel, Annie Andrieux, Anselme Perrier, Renata Basto - d'avoir accepté de lire et juger mon travail et de m'accompagner dans la dernière étape de ma thèse.

Merci à l'Institut Curie pour avoir financé ma thèse.

J'aimerais remercier chaleureusement Sandrine Humbert, ma directrice de thèse. Merci pour m'avoir accueillie dans son laboratoire. Tout au long de ces années, elle a su orienter mes recherches. J'ai particulièrement apprécié la grande liberté de fonctionnement au cours de ma thèse qui m'a permis de choisir les projets qui me tenaient à cœur et m'a donné la capacité de m'exprimer de façon personnelle dans mon travail. Merci encore pour le soutien et les conseils !

Je suis très redevable envers Frédéric Saudou, avec qui j'ai travaillé au début de ma thèse. J'ai beaucoup apprécié sa créativité scientifique. Son grand enthousiasme pour mes résultats m'a toujours motivée à continuer.

Je voudrais aussi remercier tous les membres du labo, présents ou passés. Grand merci pour votre gentillesse, vos conseils, les bonnes soirées, les discussions tant scientifiques qu'amicales et la bonne humeur ! Merci pour cette atmosphère unique au labo, pour cet esprit de groupe et pour cette bonne ambiance quotidienne. C'était vraiment sympa de travailler avec vous ! ☺ Sans les oublier, mention spéciale aux membres de l'unité 1005.

Je tiens sincèrement à remercier à ma famille, qui a toujours soutenu toutes mes décisions, cette thèse n'aura pas été possible sans vous. Vi ringrazio di cuore per essermi sempre stati vicini, anche se siamo separati da un oceano intero vi porto sempre con me. Grazie ! Y a vos David, por haberme soportado y apoyado siempre en los mejores y peores momentos de esta etapa.

Merci à tous !

Abbreviations

µm	Micrometer
µM	Micromolar
+TIP	Microtubule plus-end tracking proteins
ADP	Adenosin diphosphate
APC	Adenomatosis polyposis coli
aPKC	Atypical protein kinase C
Arp 2/3	Actin related protein 2/3
ATP	Adenosin triphosphate
bHLH	Basic helix loop helix
BDNF	Brain derived neurotrophic factor
BSA	Bovine serum albumin
CAP-Gly	Cytoskeleton-associated protein glycine-rich
Cdc42	Cell division cycle 42
Cdk	Cyclin dependent kinase
Cnn	Centrosomin
CLIP170	Cytoplasmic linker protein of 170 kDa
DIC	Dynein intermediate chain
DNA	Deoxyribonucleic acid
EB3	End-binding protein 3
ECM	Extra cellular matrix
FAT	Fast axonal transport
GFP	Green fluorescent protein
GTP	Guanosine triphosphate
HAP1	Huntingtin associated protein 1

HEAT	Huntingtin, Elongation factor 3, protein phosphatase 2A , and the yeast kinase TOR1
HIP1	Huntingtin interacting protein 1
HD	Huntington's disease
HeLa	Human adenocarcinoma epithelial cell line
HTT	Huntingtin
HTT	Human and primates HTT gene symbol
Htt	Mouse and rat HTT gene symbol
htt	Fly HTT gene symbol
IGF-1	Insulin growth factor 1
IT15	Interesting transcript 15
JNK	c-Jun N-terminal kinase
LGN	Leucine-Glycine-Asparagine enriched protein
LIMK1	LIM-kinase 1
Min	Minute
MT	Microtubule
myo	Myosin
NB	Neuroblast
nm	Nanometer
NES	Nuclear export signal
NESC	Neural epithelial stem cell
NLS	Nuclear localisation signal
NuMA	Nucleus and Mitotic Apparatus protein
PAR	Partitioning defective

PAR3	Partitioning defective 3
PCM1	Peri-centriolar molecule-1
Pins	Partner of inscuteable
pH	Power of hydrogen
PLL-PEG	PLL(20)-g[3.5]-PEG(2): poly-L-lysine (20kDa)-grafted with-poly(ethyleneglycol)(2kDa)
PtdIns(3,4,5)P3	Phosphatidylinositol-3,4,5-triphosphate
PI3K	Phosphoinositide 3-kinase
Rho	Ras homologue
RhoA	Ras homologue A
RGPC	Radial glial progenitor cell
RNA	Ribonucleic acid
s	Second
siRNA	Small interfering RNA
TBP	TATA binding protein
UV	Ultraviolet

INTRODUCTION

1 Huntington's disease

1.1 Overview and introduction to the disease

Huntington's disease (HD) is a neurodegenerative disorder first characterized as a hereditary, late-onset form of chorea by George Huntington in 1872 (Huntington, 2003). In his work (Figure 1), the description of the clinical aspects of HD is remarkably complete. The adult onsets, relentless progression, fatal outcome, mental involvement alongside the movement disorder are all recognized.

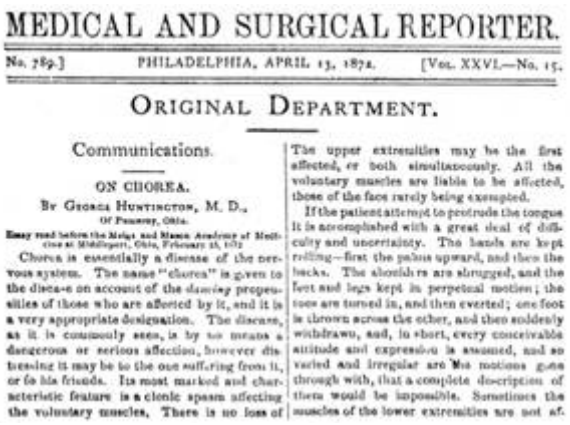

MEDICAL AND SURGICAL REPORTER.

No. 789.] PHILADELPHIA, APRIL 13, 1872. [VOL. XXVI.—No. 15.

ORIGINAL DEPARTMENT.

Communications.

ON CHOREA.

By GEORGE HUNTINGTON, M. D.,

Of Pomeroy, Ohio.

Essay read before the Meigs and Mason Academy of Medicine at Middleport, Ohio, February 28, 1872

Chorea is essentially a disease of the nervous system. The name "chorea" is given to the disease on account of the dancing propensities of those who are affected by it, and it is a very appropriate designation. The disease, as it is commonly seen, is by no means a dangerous or serious affection, however distressing it may be to the one suffering from it, or to his friends. Its most marked and characteristic feature is a clonic spasm affecting the voluntary muscles. There is no loss of

The upper extremities may be the first affected, or both simultaneously. All the voluntary muscles are liable to be affected, those of the face rarely being exempted.

If the patient attempt to protrude the tongue it is accomplished with a great deal of difficulty and uncertainty. The hands are kept rolling—first the palms upward, and then the backs. The shoulders are shrugged, and the feet and legs kept in perpetual motion; the toes are turned in, and then everted; one foot is thrown across the other, and then suddenly withdrawn, and, in short, every conceivable attitude and expression is assumed, and so varied and irregular are the motions gone through with, that a complete description of them would be impossible. Sometimes the muscles of the lower extremities are not af-

Figure 1. The title page of George Huntington's original paper "On Chorea". (1872).

In 1968, Milton Wexler started the Hereditary Disease Foundation (HDF) when his wife was diagnosed with HD. The HDF enrolled a number of scientists to work in the disease. The discovery of the gene responsible for HD was achieved by Nancy S Wexler, Milton Wexler's daughter. In 1976 the team conducted a twenty yearlong study in a Venezuelan town near Lake Maracaibo in which they collected blood samples and documented different individuals to work out a common pedigree. This work led to the development of a chromosomal test to identify potential sufferers. The HDF recruited and supported a large group composed for more than 100 scientists from all over the word named the Huntington Disease Collaborative Research Group (HDCRG). In 1993 the group reported the discovery of the gene responsible for HD and of its associated mutation (The Huntington's Disease Collaborative Research Group, 1993).

1.2 Neuropathology

The histopathology in HD is characterized by the atrophy of the caudate and putamen in the basal ganglia, as well as the cerebral cortex, reducing brain weight by up to 25-30% (Aylward, 2007; Rosas et al., 2002; Vonsattel & DiFiglia, 1998)(Figure 2).

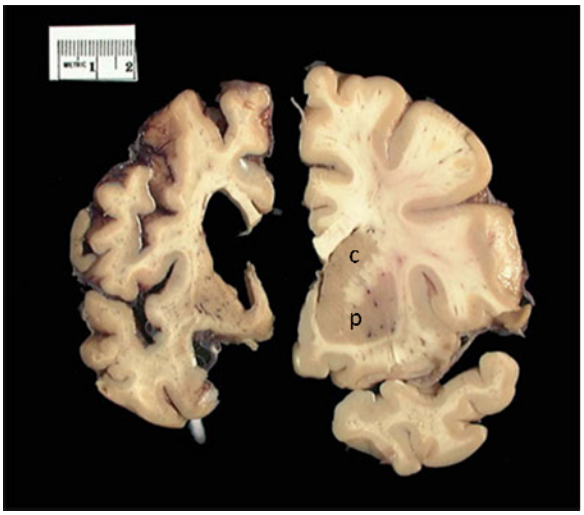

Figure 2. Atrophy of the striatum and cortex in HD brain. *Post mortem* brains from a HD patient (left) and healthy individual (right). Particularly evident is the loss of cells in the caudate (c) and putamen (p), resulting in enlarged lateral ventricles in HD brain.

The most affected neurons are GABAergic type II medium spiny projection neurons, which constitute about 80% of striatal neurons, and large neurons in layers III, IV, and V of the cortex (Hedreen et al., 1991). Interestingly, striatal interneurons are not affected (Zucker et al., 2005). Medium spiny neurons receive glutamatergic signals from the cerebral cortex, thus defects in the basal ganglia-thalamocortical pathways involved in motor control may contribute to the choreiform disorders seen in HD (Albin et al., 1990). Globus pallidus, thalamus, subthalamic nucleus, substantia nigra, white matter, and the cerebellum can be markedly affected (Vonsattel & DiFiglia, 1998). Recent work has also indicated that the hypothalamus can be significantly atrophied in HD patients (Kassubek et al., 2004; Politis et al., 2008).

The most commonly used grading system to assess the severity of HD degeneration is based on macroscopic and microscopic criteria. The pattern of striatal degeneration in *post mortem* tissues classifies HD cases into five different severity grades going from 0, as a non discernible neuropathology, to 4, with 95% of neuronal loss in caudate nuclei (Vonsattel et al., 1985).

Most clinical features of HD can be attributed to central nervous system (CNS) degeneration, but some aspects of the disease could be linked to defects outside the CNS (Figure 3). Indeed, weight loss, skeletal-muscle atrophy, cardiac failure, osteoporosis, testicular atrophy and dysfunction of blood-derived cells are observed in patients (Van Der Burg, 2009). These features of the disease are clinically important as they reduce quality of life and, in some cases, correlate with disease progression and contribute to early death.

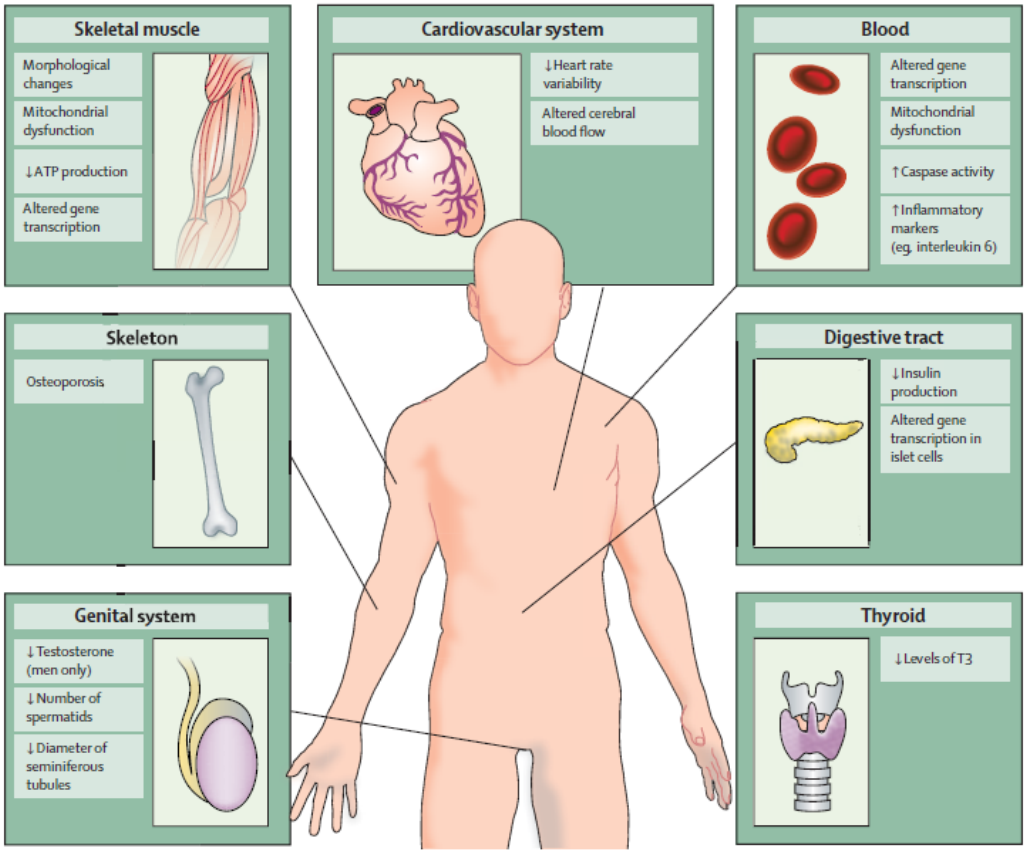

Figure 3. Peripheral pathology in patients with Huntington's disease. (Adapted from Van Der Burg et al., 2009).

1.3 Symptoms

HD symptoms comprise adult-onset personality changes, generalized motor dysfunctions, and cognitive decline. The peak age of adult-onset HD is between 35 and 50 years. A small percentage of patients (10%) develop symptoms before age 20. This corresponds to the juvenile variant of the disease usually resulting from paternal transmission. Early onset is associated with increased severity as well as with a more rapid disease progression (Beighton & Hayden, 1981).

In the early stages, HD is associated with progressive emotional, psychiatric, and cognitive disturbances such as anxiety, irritability and depression. Choreiform movements and loss of motor coordination are observed. Commonly reported symptoms in HD include progressive weight loss, alterations in sexual behaviour, and disturbances in the wake-sleep cycle that occur very early in the course of the disease and may partly be explained by hypothalamic dysfunction (Politis et al., 2008). With the progression of the disease patients show motor speech disorder (dysarthria) and difficulty in swallowing (dysphagia). Decreased movement referred as hypokinesia are also present. In the later stages, HD is characterized by progressive dementia, or gradual impairment of the mental processes involved in comprehension, reasoning, judgment, and memory (Rosenblatt, 2007). Motor problems worsen reaching a final phase of inability to initiate movements (akinesia).

Patients with advanced HD become unable to care for themselves. Life-threatening complications may result from injuries related to serious falls, poor nutrition, infection, choking, and inflammation. Death occurs 15-20 years after onset of the first symptoms. At present, there is no cure. The majority of therapeutic strategies currently used in HD are designed to ameliorate the primary symptoms of HD condition (see Annexe IV). Treatments or drugs have limited benefits, and do not delay or halt disease progression.

A top priority in the HD field is the identification of biological markers, or biomarkers. Several candidate HD biomarkers have emerged during the last years (see Annexe IV). A combination of clinical, neuroimaging, and biochemical biomarkers will be necessary to enhance the accuracy, specificity, and sensitivity in tracking disease onset and progression. Moreover, biomarkers will be important to assess the efficiency of future HD treatments.

1.4 The *HTT* gene and the mutation

In 1983, after Nancy Wexler expedition to Venezuela, the HD gene was mapped on the tip of chromosome 4 (Gusella et al., 1983). Since then, 4p16.3 was identified as the most likely position of the HD gene (Bates et al., 1991; MacDonald, Haines, et al., 1989; MacDonald, Cheng, et al., 1989; Snell et al., 1992). The HDCRG published the discovery of a new gene called IT15 (interesting transcript 15) with a polymorphic CAG (cytosine-adenine-guanine) triplet expansion in the first exon (The Huntington's Disease Collaborative Research Group, 1993). When researchers examined this region of IT15 in non-HD controls, they found that the number of CAG repeats varied from 6 to 35. Analysis of the same region in the IT15 gene in individuals with HD showed that those always had 40 or more CAG repeats. It was concluded that the trinucleotide repeat expansion was responsible for HD. The IT15 gene is now renamed the HTT gene (*HTT*) because of the name assigned to the protein. The discovery of the causal HD gene has stimulated research, and work is now focusing on molecular mechanisms of disease.

The gene encoding HTT in vertebrates is composed of 67 exons spanning over 170 kb (Figure 4). $(CAG)_n$ repeats are located in the first exon. Normal alleles are polymorphic for the CAG repeat, containing 11 to 35 CAG repeats. When the repeats reach 41 or more the disease is fully penetrant (Mcneil et al., 1997; Rubinsztein et al., 1996). Incomplete penetrance happens with 36–40 repeats I am not sure about this range, we need to check: these individuals do not develop HD but are at risk of transmitting the disease to their children, known as "genetic anticipation". This phenomenon is explained by the fact that the expanded CAG repeats are not stable and tend to expand from generation to generation specifically when the disease gene is inherited from the father (Ranen et al., 1995). Extremely large CAG repeats of 60 or greater are often associated with a disease onset during childhood or adolescence (*juvenile*).

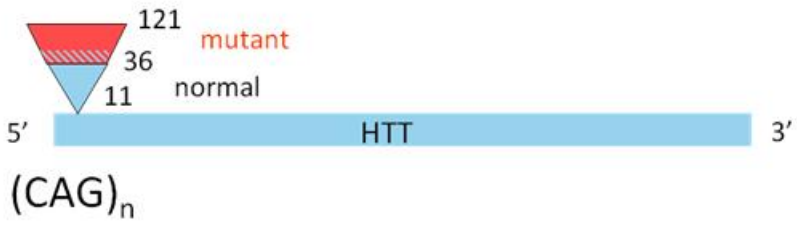

Figure 4. Human *HTT* gene. The 5' end of *HTT* has a sequence of $(CAG)_n$ repeats. 35 or less repeats are not associated with the disorder. Pathological threshold is defined by 41 or more CAG repetitions. Incomplete penetrance happens with 36 to 41 repeat. 60 or more repeats are often associated with a *juvenile* onset (before 20 years old). HTT is located on the short (p) arm of chromosome 4 at position 16.3.

There is a strong inverse correlation between CAG repeats length and age at onset of motor symptoms (Andrew et al., 1997). A recent work shows that normal allele CAG length, interaction between expanded and normal alleles and presence of a second expanded allele do not influence age at onset of motor manifestations, indicating that the rate of HD pathogenesis leading to motor diagnosis is determined by a completely dominant action of the longest expanded allele (Lee et al., 2012). However, the number of CAG repeats accounts for about 60% of the variation in age of onset and disease manifestations. This observation suggests the existence of environmental and genetic modifiers. Several studies revealed that a large set of genes distinct from the HD locus itself could contribute to modify disease onset and progression (Chattopadhyay et al., 2003; Jian-liang Li et al., 2003; Wexler, 2004). All of these modifiers relate to various mechanisms implicated in HD pathology as excitotoxicity, dopamine toxicity, metabolic impairment, transcriptional deregulation, protein misfolding, and oxidative.

Most of the patients are heterozygous for the mutant allele. Homozygous cases of the disorder show the same age of onset of the disease that heterozygous HD cases, but the rate of progression can be enhanced (Squitieri et al., 2003).

Of note, other neurodegenerative diseases are also caused by an abnormal CAG expansion in a single causative gene. This results in protein aggregation, late-onset neurodegeneration, and selective vulnerability of a subset of neurons. This includes nine other diseases with expansions in polyQ tracts: spinal and bulbar muscular atrophy (SBMA), dentatorubral and pallidoluysian atrophy (DRPLA), and spinocerebellar ataxias (SCA) 1,2,3,6,7,12,17.

1.5 Normal HTT

1.5.1 Overview

HTT gene encodes huntingtin protein (HTT), a large soluble protein with a molecular weight of 350kD (Figure 5). $(CAG)_n$ are translated in a glutamine tract. HTT has little homology to other proteins but is well conserved from *D. melanogaster* to mammals, suggesting a central role in cell homeostasis. Three putative domains of HTT have been identified in multialignment

corresponding to human HTT amino acids 1–386 (HTT1), 683–1,586 (HTT2), and 2,437–3,078 (HTT3). In particular, comparison of more divergent orthologs and quantification of evolutionary pressure on the three blocks revealed that the NH_2-terminal fragment (HTT1) is the most recently evolved part of HTT, while the COOH-terminal part represents the most conserved portion among all animals, from sea urchin to insects and mammals (Zuccato etal., 2010). HTT is a 350kDa protein. This high molecular weight hampers the production of crystals and mass spectrometry studies to elucidate its structure. Up to date, there are no clear data on the structure of the protein.

1.5.2 Expression and structure

HTT is ubiquitously expressed throughout the body; higher levels are found in brain and testis. In the brain, HTT can be found at highest levels in the cerebellar cortex, the neocortex, the striatum and hippocampus (Trottier et al., 1995). At subcellular levels, HTT has a large distribution. HTT is associated with a variety of organelles, including the nucleus, endoplasmic reticulum (ER), Golgi complex, and mitochondrion (Hilditch-Maguire et al., 2000; Hoffner et al., 2002; Kegel et al., 2002; Panov et al., 2002; Strehlow et al., 2007). HTT is also found within neurites and at synapses, where it associates with various vesicular structures such as clathrin-coated vesicles, endosomal compartments and microtubules (MT) (Difiglia et al., 1995; Hilditch-Maguire et al., 2000; Hoffner et al., 2002; Velier et al., 1998).

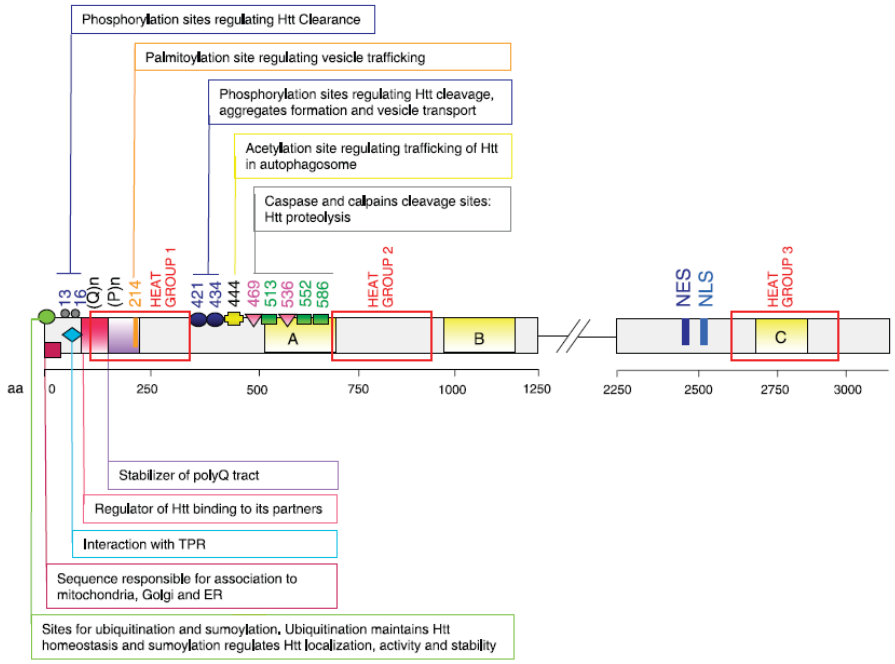

Figure 5. HTT amino acid sequence. $(Q)_n$ indicates the polyglutamine tract, which is followed by the polyproline sequence $(P)_n$; the red emptied rectangles indicate the three main groups of HEAT repeats (HEAT group 1, 2, 3). The small green rectangles indicate the caspase cleavage sites and their amino acid position (513, 552, 586), while the small pink triangles indicate the calpain cleavage sites and their amino acid positions (469, 536). Boxes in yellow: B, regions cleaved preferentially in the cerebral cortex; C, regions of the protein cleaved mainly in the striatum; A, regions cleaved in both. Posttranslational modifications: ubiquitination (UBI) and/or sumoylation (SUMO) sites (green); palmitoylation site (orange); phosphorylation at serines 13, 16, 421, and 434 (blue); acetylation at lysine 444 (yellow). The nuclear pore protein translocated promoter region (TPR, azure) is necessary for nuclear export. (Adapted from Zuccato et al., 2010)

At NH_2 terminus, glutamine stretch in human HTT begins at the 18th amino acid. A recent study suggests that the $(Q)_n$ tract may modulate a normal function of HTT (Zheng et al., 2010). *In vitro* studies on fibroblasts indicated that the $(Q)_n$ contributes in modulating longevity and energy status. Moreover, mice lacking $(Q)_n$ stretch live significantly longer than wild-type mice.

In mammals, the $(Q)_n$ region is followed by a polyproline ($(P)_n$ or polyP) stretch. It was suggested that the $(P)_n$ function may reside in the stabilization of the $(Q)_n$ tract by keeping it soluble (Steffan et al., 2004). This domain, together with Src homology 3 (SH3) region, would be implicated in protein-protein interaction.

HTT is also enriched in consensus sequences called **h**untingtin, **e**longation factor 3, protein phosphatase 2**A**, and **T**OR 1 (HEAT) repeats that are organized into protein domains important for protein-protein interactions. The repeats are well conserved in HTT through evolution. A recent study of HEAT repeats number and distribution revealed a total of 16 HEAT repeats in HTT, which are organized into 4 clusters (Tartari et al., 2008). Recombinant full-length HTT purified from insect cells has high helical content, is an elongated molecule, and remains intact despite extensive proteolytic nicking (Li et al., 2006). This preliminary characterization of HTT is consistent with a structure composed entirely of HEAT repeats, folded via a continuous hydrophobic core into a single superhelical solenoid.

A functionally active COOH-terminal nuclear export signal (NES) sequence and a less active nuclear localization signal (NLS) are present in HTT, which might indicate that the protein (or a portion of it) is involved in transporting molecules from the nucleus to the cytoplasm (Xia et al.,2003). In concordance with this, it has been show that the nuclear pore protein TPR has a role in the nuclear export of N-terminal HTT (Cornett et al., 2005). PolyQ expansion reduces this nuclear export to cause the nuclear accumulation of HTT.

HTT is subjected to several post-translational modifications that regulate its wild-type functions but also participate to HD pathology. This will be discussed in chapter 1.8 of this manuscript.

1.6 Functions of wild-type HTT

HTT ubiquitary expression and widespread subcellular localization does not facilitate the determination of its functions. However, identification of HTT interactors (see Annexe III) and development of different animal models (see Annexe I and II) put on evidence the following proposed roles for normal HTT.

1.6.1 Embryonic development

HTT is required for normal embryogenesis, as knock-out (KO) mice for HTT (*Hdh -/-*) die at an early developmental stage, E7.5. The basis of this effect appears to be increased apoptosis in the embryonic ectoderm shortly after the onset of gastrulation (Duyao et al., 1995; Nasir et al., 1995; Zeitlin et al., 1995). The inactivation of HTT gene (*htt*) does not reveal a phenotype in *D. melanogaster* embryos; *htt* is dispensable for *D. melanogaster* development but is crucial for aged adults (Zhang et al., 2009). This discrepancy might be due to intrinsic differences between mouse and fly embryogenesis as early lethality in mouse is likely to result from the absence of HTT in extraembryonic tissues (Dragatsis et al., 1998). In agreement with this hypothesis is the observation that mice deleted for *Htt* in adult stages show neurodegeneration (Dragatsis et al., 2000) and, HTT-ko adult flies show a compromised mobility and reduced viability (Zhang et al., 2009).

Conditional inactivation of the *Htt* gene in the midbrain and hindbrain in Wnt1 cell lineage results in congenital hydrocephalus (Dietrich et al., 2009). These results implicate HTT also in the regulation of cerebral spinal fluid (CSF) homeostasis.

To bypass the early lethality induced by the absence of HTT and analyze the role of the latter after gastrulation, mice expressing less than 50% of the normal of the protein were generated. These mice present defects in the formation of the precursor of the epiblast, as well as malformations of the cortex and striatum, and die shortly after birth (White et al., 1997). Analyses of chimeras created by blastocyst injection of *Htt* -/- ES cells suggest that HTT plays a specific role in neuronal survival, neuroblasts need to synthesize HTT if they are to progress in development and differentiation (Reiner et al., 2001; Reiner et al., 2003).

Finally, studies using developing zebrafish showed that a reduction in Htt levels affects the formation of most of the anterior regions of the neural plate (Henshall et al., 2009).

These data indicate that HTT is required at different steps of embryonic development and that its total absence or 50% reduced presence generates a very early phenotype in mice.

1.6.2 Antiapoptotic

Overexpression studies have demonstrated that HTT has a role in maintaining cell viability in response to acute toxic stimuli and excitotoxicity. Wild-type HTT can suppress apoptosis *in vitro* in response to exogenous toxic stimuli such as 3-nitropropionic acid, which selectively damages the striatum, presumably by preventing activation of proaspase-9 (Rigamonti et al., 2000, 2001). Similarly, HTT can protect against excitotoxicity after quinolic acid injection *in vitro* and *in vivo*, by mediating apoptosome complex activity and inhibiting caspase activation downstream of cytochrome-c release (Rigamonti et al., 2000; Leavitt et al., 2006). Cells depleted of wild-type HTT

are more sensitive to apoptotic cell death and show increased level of caspase-3 activity, with respect to control cells (Zhang et al., 2006). HTT is also implicated in anti-apoptotic pathways due to its interaction with HIP1, which reduces HIP1 and Hippi's ability to mediate procaspase-8 cleavage and apoptosis (Gervais et al., 2002).

More recently, the anti-apoptotic role of HTT has been highlighted also in non mammalian models. In fact, apoptotic cell death is observed in zebrafish embryos in which Htt is knocked-down by morpholino technology (Diekmann et al., 2009). Htt morpholino-injected zebrafish show a massively increased cell death as indicated by caspase-3 activity especially in the midbrain/hindbrain region of the developing zebrafish embryo. This increased apoptosis is accompanied by a severe underdevelopment of the CNS.

1.6.3 Pro-survival factor

Several studies have shown that HTT regulates the cellular levels of brain-derived neurotrophic factor (BDNF) (Gauthier et al., 2004; Zuccato et al., 2001). BDNF is a neurotrophin that is particularly important for the survival of striatal neurons and for the activity of the cortico-striatal synapses. However, striatal neurons depend on the supply of BDNF from the cortical afferents (Baquet et al., 2004) . Indeed, BDNF is produced by cortical neurons and transported to striatal neurons. Wild-type HTT regulates both BDNF transcription and intracellular dynamics. HTT was found to bind a BDNF transcription repressor element, REST/NRSF, and retain it in the cytoplasm permitting transcription of BDNF (Zuccato et al., 2001, 2003). HTT has also been shown to regulate BDNF delivery from the cortex to the striatum by promoting its transport through its interaction with HAP1 (Gauthier et al., 2004; Wu et al., 2010).

Further studies revealed that wild-type HTT is a substrate for the serine/threonine kinase Akt. Upon IGF-1 activation, Akt phosphorylates a number of substrates thus activating prosurvival pathways by stimulating the expression of prosurvival genes, whereas death genes such as BAX or Bcl-2 are repressed. In particular, Akt mediates prosurvival effect through HTT phosphorylation. Akt directly phosphorylates HTT at serine 421 (Emilie Colin et al., 2008; Zala et al., 2008). This phosphorylation stimulates BDNF anterograde transport in wild-type conditions. In HD, by rescuing the deficient BDNF transport, phosphorylation of serine 421 reduces mutant HTT-induced toxicity.

HTT has also been implicated in the stress response system because phosphorylation of HTT by CDK5 in response to DNA damage prevents HTT from inducing p53 dependent apoptosis (Anne et al., 2007). Additionally, phosphorylation of the N17 region of HTT regulates nuclear entry and association with chromatin in response to heat shock (Atwal et al., 2011).

1.6.4 Synaptic activity

Synapses are essential to neuronal function. Wild-type HTT interacts with cytoskeletal and synaptic vesicles proteins essential for exo- and endocytosis at the synaptic terminals, thus participating in the control of synaptic activity in neurons (Smith et al., 2005). HTT is localized post-synaptically with PSD-95 (post-synaptic density 95), a membrane-associated guanylate kinase (MAGUK) protein that binds the NMDA and kainate receptors at the postsynaptic density (Fan et al., 2009; Sun et al., 2001). HTT is also localized pre-synaptically through its interactions with synaptic vesicles, HIP1, and HIP14, suggesting roles in synaptic signaling and vesicle recycling (Stowers et al., 2007; Waelter et al., 2001). Furthermore, HTT can bind to PACSIN1/syndapin, syntaxin, and endophilin A, which collectively play a key role in synaptic transmission, as well as in synaptic vesicles and receptor recycling (Smith et al., 2005).

1.6.5 Transcriptional factor

$(Q)_n$ and $(P)_n$ regions have been demonstrated to form polar zipper structures and interact with DNA directly, suggesting HTT may function as a transcriptional activator (Gerber et al., 1994; Perutz et al., 1994). Several studies have shown interactions between HTT and various transcription factors such as the cAMP response-element binding protein (CBP) (Mccampbell et al., 2007; Steffan et al., 2000), p53 (Mccampbell et al., 2007; Steffan et al., 2000), Sp1, TAFII130 (Dunah et al., 2002), N-CoR, and Sin3A (Boutell et al., 1999; Luthi-Carter et al., 2000). By binding to these trancription factors, HTT was reported to act as a transcription activator or repressor.

HTT activates the transcirption of genes encompassing RE1 sequence, a conserved 21–23 base pair DNA Repressor element 1 (also known as the neuron-restrictive silencer element, NRSE). This sequence is recognized by the RE1-silencing transcription factor (REST; also known as neuronal restrictive silencing factor, NRSF) transcriptional regulator, which acts as a transcriptional silencer (Cattaneo et al., 2005). Thus wild-type HTT has a broad role in regulating neuronal gene transcription: cells and mice expressing increased wild-type levels also show higher levels of mRNAs transcribed from RE1/NRSE-containing neuronal genes (Zuccato et al., 2003). In particular, BDNF exon II promoter contains a RE1 sequence. Wild-type HTT thus promotes *Bdnf* transcription because it sequesters the available REST/NRSF in the cytoplasm, thereby preventing it from forming the nuclear co-repressor complex at the RE1/NRSE nuclear site and allowing gene transcription (Zuccato et al., 2003).

1.6.6 Axonal and vesicular transport

The function of HTT as a facilitator of long- and short-range transport along MT is documented in mammalian cells, *D. melanogaster* and mouse models. Much of the information gleaned from analysis of HTT interacting proteins suggests a role in intracellular transport (Figure 6).

Yeast two-hybrid screens have implicated HTT in binding HAP1 (X. J. Li et al., 1995), which is involved in axonal transport via its interaction with kinesin (Mcguire et al., 2006), dynein (Engelender et al., 1997; Rong et al., 2007), dynactin subunit p150^{Glued} (Li et al., 1998) and HIP1 and HIP14, which have roles in endocytosis (Kalchman et al., 1997; E E Wanker et al., 1997), suggesting a role for HTT in various aspects of MT and actin based intracellular transport. Dynactin is an essential co-factor for the transport of membranous organelles by the minus-end-directed microtubule motor cytoplasmic dynein.

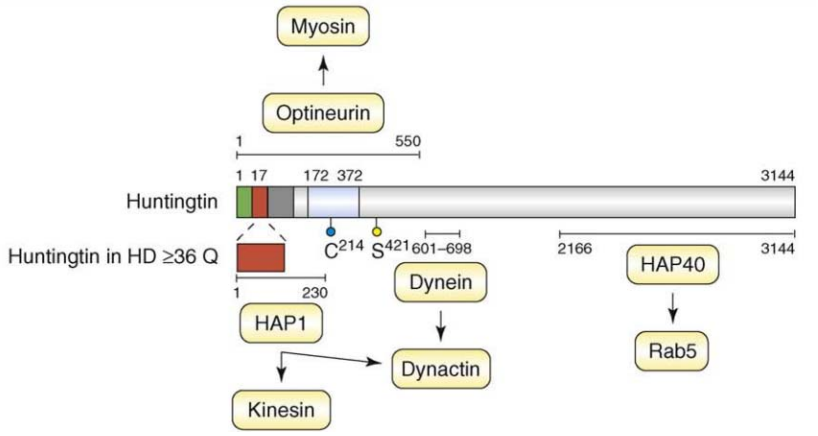

Figure 6. Schematic of HTT. The N-terminal membrane localization signal (aa1–18) is shown in green and the polyglutamine repeat region (beginning at aa17) is shown in red. The light blue region (aa172–372) has been shown to associate with acidic phospholipids at the plasma membrane. The site of palmitoylation of Cys214 by HIP14 is indicated by a blue lollipop and phosphorylation of Ser421 by Akt is indicated by a yellow lollipop. The myosin VI linker protein optineurin is known to associate with the N-terminal region of HTT. HAP1 interacts with the N-terminal region of normal HTT and the expanded polyglutamine repeat found in mutant HTT has been shown to enhance binding. HAP1 also interacts with the plus-end-directed MT motor kinesin and dynactin. The minus-end-directed MT motor dynein interacts with HTT (aa600–698) and with the dynein activator dynactin. HAP40, an effector of the small GTPase Rab5, binds to the C-terminal region of HTT (Adapted from Caviston & Holzbaur, 2009).

Additionally, we and others have shown a direct interaction between HTT and dynein. The HTT/dynein interaction was initially described by yeast two-hybrid system. This interaction was functionally validated in cell culture, by demonstrating that reduced HTT expression leads to disruption of Golgi stacks, a hallmark dynein-mediated defect (Caviston et al., 2007; Pardo et al., 2010). Mapping experiments identify a binding site for the dynein intermediate chain to residues 601–698 of HTT. Immunoprecipitation of endogenous proteins from brain extract with an anti-dynein antibody demonstrates the co-precipitation of a complex that includes cytoplasmic dynein, dynactin, HTT, kinesin and HAP1 (Caviston et al., 2007; Colin et al., 2008). In line with this, full-length versions of HTT lacking the interaction domain for dynein (Δ-DYN) and HAP1 (Δ-HAP1) fail to transport BDNF vesicles in neuronal cells (Pardo et al., 2010). These observations will be discussed in detail in the results section 5 of this thesis.

HTT has been suggested to act as a 'molecular switch' in controlling anterograde and retrograde transport of BDNF (Figure 7). Experiments in cell culture measuring transport of BDNF demonstrate that phosphorylation of serine 421 (S421) favors anterograde transport, while unphosphorylated S421 favors retrograde transport (Colin et al., 2008). A similar 'switching' mechanism has been attributed to HTT by its interaction with HAP40, a Rab5 associated protein, suggesting that HTT functions to transfer endosomes from MT to F-actin tracks (Pal et al., 2008; Peters & Ross, 2001). HTT has also been implicated in actin-based transport by its interaction with optineurin, which may physically link HTT to the actin motor myosin-VI (Sahlender et al., 2005).

Interestingly, ablation of HTT phosphorylations at S1181/S1201 leads to increased anterograde and retrograde velocities via an increased attachment of motor proteins and BDNF vesicles to MT (Ben M'Barek et al., manuscript in preparation).

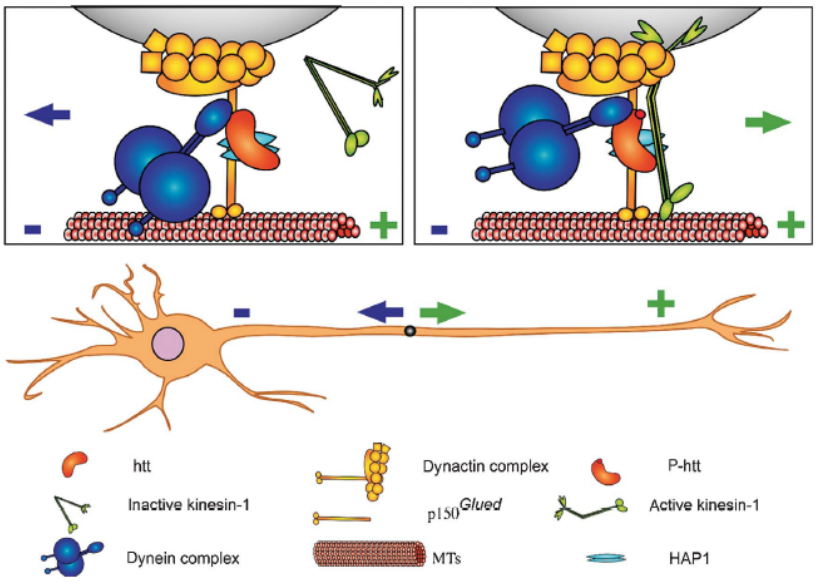

Figure 7. Proposed model of the directionality switch induced by phosphorylation of HTT. HTT binds to HAP1 and to the dynein complex. HAP1 interacts with $p150^{Glued}$ and kinesin-1. When HTT is not phosphorylated, the kinesin-1 interaction with motor complex is weak, kinesin-1 is detached from MTs and vesicles leading to retrograde transport. When HTT is phosphorylated, the kinesin-1 association with motor complex is increased and kinesin-1 is recruited to vesicles, therefore inducing a switch to anterograde transport. (Adapted from Colin et al., 2008).

A recent publication indicates that wild-type HTT is essential for protein trafficking to the centrosome and normal ciliogenesis. Ciliogenesis is regulated by an HTT-HAP1-peri-centriolar molecule-1 (PCM1) pathway. Depletion of HTT or HAP1 leads to dispersion of PCM1 from centrosomes and reduced ciliogenesis in cells (Keryer et al., 2011).

Fast axonal transport (FAT) requires consistent energy over long distances to fuel the molecular motors that transport vesicles. A recent study from our laboratory (Zala et al., manuscript in preparation) shows that FAT depends on glycolytic but not on mitochondrial ATP. Indeed, FAT

would use ATP that is directly generated on vesicles from glyceraldehyde 3-phosphate dehydrogenase (GAPDH) and phosphoglycerate kinase (PGK) activities. GAPDH is a very abundant protein present both in the cytoplasm and the nucleus and localizes on fast moving vesicles within axons. Consistent evidence show that would HTT scaffolds GAPDH on vesicles with depletion of HTT reducing GAPDH attachment to vesicles.

1.7 Mutant HTT and its down-stream effect: *HTT-mediated toxicity*

Down-stream amino acid 17, HTT has a polymorphic $(Q)_n/(P)_n$ rich domain. The abnormal expansion of $(Q)_n$ (polyQ) stretch encoded by the nucleic acids $(CAG)_n$ causes HD. HD is an autosomal dominant disorder. This suggests that the mutation leads to a toxic gain of function. Accordingly, several cellular and animals models were developed by over-expressing mutant HTT. But there is evidence that a loss of protective function of HTT could act synergistically with the gain of toxic functions (Figure 8). Mutant HTT is found in both the nucleus and the cytoplasm of HD brain (Benn et al., 2005; Gutekunst et al., 1999). Hypothesis about the nuclear effects of mutant HTT focuses mainly on transcriptional dysregulation, while toxicity of HTT in the cytoplasm involves ubiquitin/proteasome dysfunction, aberrant caspase activity and cell death, synaptic dysfunction, excitotoxicity, mitochondrial dysfunction, autophagy and impaired axonal transport.

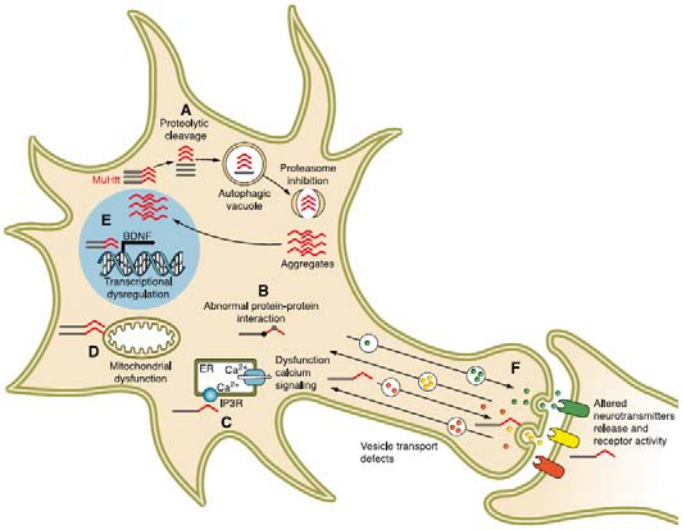

Figure 8. Key cellular pathogenic mechanisms in HD. (A): the mutation in HTT causes a conformational change of the protein that leads to partial unfolding or abnormal folding of the protein, which can be corrected by molecular chaperones. Full-length mutant HTT is cleaved by proteases in the cytoplasm. In an attempt to eliminate the toxic HTT, fragments are ubiquitinated and targeted to the proteasome for degradation. However, the proteasome becomes less efficient in HD. Induction of the proteasome activity as well as of autophagy protects against the toxic insults of mutant HTT proteins by enhancing its clearance. (B): NH2-terminal fragments containing the polyQ strech accumulate in the cell cytoplasm and interact with several proteins causing impairment of calcium signaling and homeostasis (C) and mitochondrial dysfunction (D). (E): N-terminal mutant HTT fragments translocate to the nucleus where they impair gene transcription or form intranuclear inclusions. (F): the mutation in HTT alters vesicular transport and recycling. (Adapted from Zuccato et al., 2010).

1.7.1 Cleavage by caspases and nuclear translocation

HTT is found cleaved in cellular and mouse HD models and in HD patients. The cleavage events occur both in normal and mutant huntingtin, but the latter is more susceptible to proteolysis and generates N-terminal fragments that are found in the cytoplasm and nucleus of neuronal and non neuronal cells.

HTT cleavage is a key event in the pathology. Indeed, inhibition of HTT cleavage prevents neurodegeneration and toxicity *in vivo* (Gafni et al., 2004; Graham et al., 2006). Further supporting the importance of mutant HTT cleavage, expression of different N-terminal fragments with expanded polyQ is sufficient to induce a HD-like pathology, whereas longer fragments are less toxic in cellular and animals models (de Almeida et al., 2002; Karpuj et al., 1999; Lunkes et al., 1998; Saudou et al., 1998).

Several consensus cleavage sites have been identified in HTT (Figure 5). Caspases 1,3,6,7 and 8 as well as calpain can cleave HTT *in vivo* and *in vitro* (Difiglia, 2002; Gafni et al., 2004; Gafni & Ellerby, 2002; Hermel et al., 2004; Mende-Mueller et al., 2001). In particular, studies have strengthened the evidence for a role of caspase-6-mediated cleavage in the disease process. Activation of caspase-6 may be a primary event in the proteolytic process of mutant HTT. This would then lead to the activation of additional proteolytic caspase activities (for example, to activation of caspase-2 and -3), exacerbating neurodegeneration and contributing to the appearance of the disease phenotype.

Once HTT is cleaved, N-terminal fragments are translocated to the nucleus. This nuclear translocation of mutant HTT induces neuronal apoptosis (Saudou et al., 1998) Accumulation of small N-terminal fragments could be in part a result of a diminution in the interaction of HTT with the nuclear pore protein TPR (translocated promoter region) in a mutant context (Cornett et al., 2005). The decreased mutant HTT-TPR interaction would reduce the export toward the cytoplasm of mutant fragments.

PTM are suggested as important regulators of huntingtin proteolysis (see below). In fact, HTT phosphorylation at S434 by Cdk5 prevents the cleavage of the protein, while phosphorylation at S421 reduces huntingtin cleavage by caspase-6 and the nuclear accumulation of caspase-6 fragments (Luo et al., 2005; Warby et al., 2005, 2009).

1.7.2 Aggregation and toxicity

Progressive accumulation of abnormal protein aggregates associated with neuronal loss is a common molecular event observed in al polyQ diseases, but also in other neurodegenerative diseases such as Parkinson's disease (PD), Alzheimer disease (AD) amyothrophic lateral sclerosis (ALS). HTT fragment length and amount, as well as the length of the $(Q)_n$, are critical factors in

determining the aggregation process (Chen et al., 2002; Hackam et al., 1998; Li et al., 2001; Li et al., 1998).

Two major aggregation pathways are in competition with each other and explain how the polyQ expansion can facilitate aggregation: The first pathway is mediated by aggregation of the polyQ stretch. PolyQ aggregation displays kinetics of nucleated-growth polymerization with a prolonged lag-phase required for forming an aggregation nucleus, followed by a fast extension phase during which additional polyglutamine monomers rapidly join the growing aggregate (G. Bates, 2003; Paoletti et al., 2008; Erich E Wanker, 2000). The second pathway depends on the first 17 N-terminal amino acids and involves intermediate structures. It is characterized by the formation of oligomers having the first 17 amino acids of the protein in their core and polyQ sequences exposed on the surface (Thakur et al., 2009).

Toxicity of nuclear mutant HTT aggregates is still under debate. However, the field is reaching a consensus. The absence of correlation between nuclear aggregates and cell death show that HTT inclusions are not pathogenic *per se* but rather an attempt of the cells to sequester toxic soluble fragments (Arrasate et al., 2004; Gutekunst et al., 1999; Saudou et al., 1998). In agreement, inhibition of ubiquitination increases mutant HTT toxicity while decreasing aggregates formation. However, while aggregates are not directly responsible for the induction of cell death they are physically interfering with key cellular functions such as intracellular transport and transcription thus leading to neuronal dysfunction.

Misfolded mutant HTT could impair with chaperone and proteasome systems. This would lead to the accumulation of misfolded or damaged proteins and aggregates formation, inducing a cellular stress response that leads to cell death. Indeed, earlier studies have provided evidence that misfolded toxic polyQ HTT protein induces a global impairment of the ubiquitin–proteasome system (UPS) that is pathogenic in HD (Bennett et al., 2005). However, other studies showed an accumulation of polyubiquitinated proteins in HD in the absence of a general UPS impairment (Bett et al., 2006; Bett et al., 2009; Bett et al., 2009; Maynard et al., 2009). This suggested that the UPS is generally functional in HD, but that pathogenic HTT may impair selectively the ubiquitination process of specific substrates. A recent study from our lab exposed that HTT binds to β-catenin and to the destruction complex by interacting with β-TrCP and axin. The presence of an abnormal polyQ expansion in mutant HTT leads to a decreased binding to β-catenin therefore impairing the binding of β-catenin to the destruction complex and subsequently resulting in β-catenin accumulation (Godin et al., 2010). Finally, recruitment of chaperones to polyQ aggregates would induce mutant HTT accumulation with an abnormal conformation (Hay et al., 2004).

1.7.3 Transcriptional deregulation

DNA transcription is a highly regulated cellular process that is impaired in HD, resulting in altered levels of expression for a number of genes. Both wild-type and mutant HTT have been shown to

interact with a range of transcription factors, giving rise to the hypothesis that abnormal interactions between mutant HTT and proteins involved in transcription lead to transcriptional deregulation, which is an early event in HD pathogenesis (Sugars & Rubinsztein, 2003)

Wild-type and polyQ HTT are cleaved by caspases, resulting in N-terminal fragments that enter the nucleus and alter transcription (Difiglia et al., 1995; Steffan et al., 2000). PolyQ tracts and glutamine rich regions are common in transcription factors, arguing that wild-type HTT may act in a similar manner, and the expanded polyQ could alter its endogenous interactions with transcription factors and DNA.

Wild-type HTT is known to bind the RE1-silencing transcription factor/neuron-restrictive silencer factor (REST/NRSF) complex (Figure 9). This interaction is likely mediated by HAP1, dynactin, and the REST/NRSF-interacting LIM domain protein (RILP) (Shimojo, 2008). The interaction between HTT and REST/NRSF is reduced in HD, allowing translocation of REST/NRSF into the nucleus. This reduces the transcription of BDNF, as well as of many other neuronal genes under the control of the REST complex, which is a global regulator of neuronal gene transcription (Zuccato et al., 2007, 2008; Zuccato & Cattaneo, 2007).

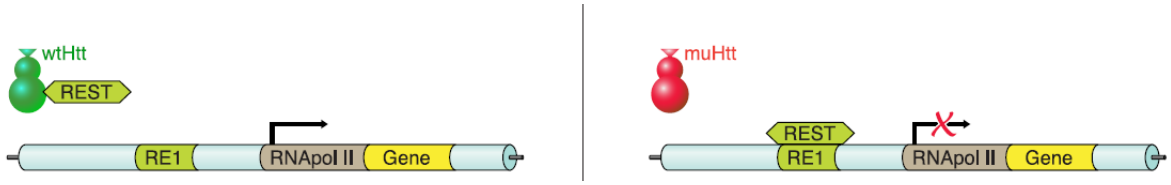

Figure 9. The transcription factor REST/NRSF binds to RE1/NRSE elements in neuronal gene promoters such as in the BDNF gene. Wild-type HTT sustains the production of BDNF by interacting with REST/NRSF in the cytoplasm, thereby reducing its availability in the nucleus to bind to RE1/NRSE sites. Under these conditions, transcription of BDNF and of other RE1/NRSE regulated neuronal genes is promoted. Mutant HTT fails to interact with REST/NRSF in the cytoplasm, which leads to increased levels of REST/NRSF in the nucleus. Under these conditions, REST/NRSF binds avidly to the RE1/NRSE sites, suppressing the transcription of BDNF and of other RE1/NRSE regulated neuronal genes. (Adapted from Zuccato et al., 2010).

TAFII-130, a cofactor for CREB dependent transcription accumulates in mutant HTT nuclear aggregates (Figure 10). PolyQ tract, impairs the soluble association of TAFII130 with Sp1, and directly interfers with the binding of Sp1 to DNA (Dunah et al., 2002; M. Shimohata et al., 2005; T. Shimohata et al., 2000). A role for Sp1 is supported by the downregulation of two relevant gene promoters in cell models: dopamine D2 receptor and nerve growth factor receptor. Sp1 disruption appears to occur early in human HD pathogenesis, being detectable even in presymptomatic grade 1 postmortem tissue (Dunah et al., 2002; M. Shimohata et al., 2005; T. Shimohata et al., 2000).

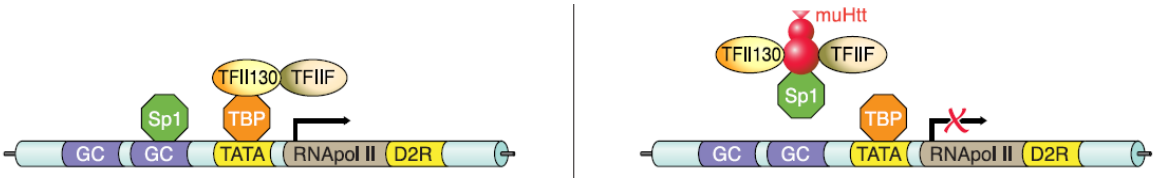

Figure 10. Mutant HTT represses transcription of Sp1-dependent promoters (i.e., dopamine receptors D1 and D2 genes) by abnormally interacting with specific transcription cofactors such as Sp1 itself, TFIIF, and TFII130. (Adapted from Zuccato et al., 2010).

Transcriptional dysregulation in HD is also linked to energy deficits (Figure 11). Particularly, mutant HTT inhibits expression of PGC-1α, a master regulator of mitochondrial biogenesis and function, by interfering with CREB/TAF4 at the PGC-1α promoter (Cui et al., 2006).

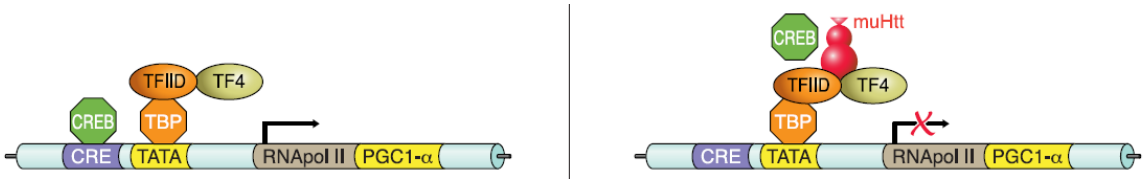

Figure 11. The transcription factor cAMP-responsive element (CRE)-binding protein (CREB) binds to DNA elements that contain a CRE sequence, as in the promoter of the PGC1-α gene, a master regulator of genes involved in mitochondrial function and energy metabolism. Mutant HTT interferes with CREB and TFIID, leading to reduced activation of PGC1-α gene, reduced PGC1-α protein levels, and consequently, downregulation of its mitochondrial target genes. (Adapted from Zuccato et al., 2010).

The transcription of genes involved in cholesterol and lipid metabolism was also reported to be affected in HD. HD cells showed reduced sterol responsive element binding protein (SREBP) nuclear translocation and reduced activity of a SRE-reporter gene in the presence of mutant HTT (Figure 12) (Valenza et al., 2005). These results imply that less SREBP reaches the transcriptionally active sites in the nucleus causing reduced expression of SRE-regulated genes involved in cholesterol and lipid metabolism.

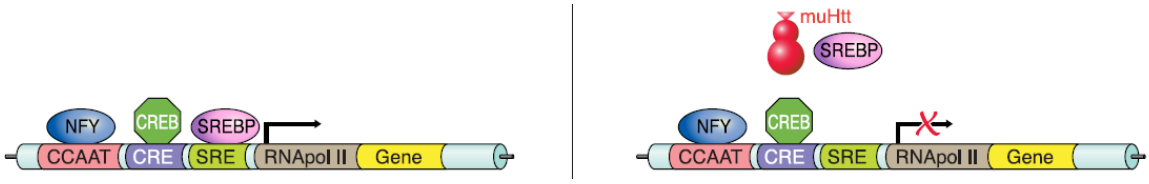

Figure 12. SREBP binds to SRE to regulate the transcription of genes involved in the cholesterol biosynthesis pathway. Under physiological conditions, SREBP is transported from the endoplasmic reticulum to the Golgi region, where it is cleaved to obtain a fragment that enters the nucleus and activates cholesterogenic genes. In the presence of mutant HTT, this mechanism is impaired, which leads to the reduced expression of SREBP-dependent genes and decreases the biological effects of cholesterol biosynthesis. (Adapted from Zuccato et al., 2010).

Mutant HTT may also cause transcriptional deregulation by inhibiting the action of histone acetylases such as CBP, p300, and P/CAF through binding of the expanded polyQ tract to acetyltransferase domains (Steffan et al., 2001) (Figure 13). Acetylation of histones through

histone acetyltransferase activity facilitates unwinding of chromatin, rendering it transcriptionally active; conversely, inhibition of histone acetylase (HAT) activity results in repression of gene transcription. In agreement, administration of histone deacetylase (HDAC) inhibitors rescues neurodegeneration in cellular, fly, and mouse models of HD (Ferrante et al., 2003; Hockly et al., 2003; Steffan et al., 2001).

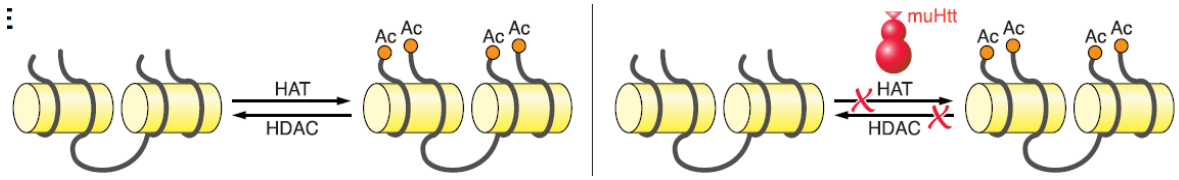

Figure 13. Levels of histone acetylation at specific lysine residues are determined by concurrent reactions of acetylation (Ac) and deacetylation, which are mediated by histone acetylases (HATs) and histone deacetylases (HDACs). Histone acetylation is vital for establishing the conformational structure of DNA-chromatin complexes suitable for transcriptional gene expression. Mutant HTT leads to disruptions in HAT and HDAC balance, leading to general transcriptional repression. (Adapted from Zuccato et al., 2010).

1.7.4 Excitotoxicity

Excitotoxicity occurs from either overactive glutamate release, reduced glutamate uptake by glial cells, or glutamate hypersensitivity of NMDA receptors (NMDAR) or downstream signaling pathways in the striatal cells. As striatal cells depend on glutamatergic activation from cortical cells, excitotoxicity is an appealing mechanism to explain mutant HTT-mediated toxicity in striatal cells. Early evidence for this came from human patient brain slices demonstrating reduced NMDAR binding specifically in the striatum (Young et al., 1988). YAC128 mouse models expressing full-length mutant HTT also display excitotoxic sensitivity in striatal cells (Benn et al., 2007).

Possible mechanisms for this effect include changes in NMDAR protein levels or post-translational modifications (Ali & Levine, 2006; Cepeda et al., 2001). Defective glutamate clearance from the synaptic cleft by glia has also been suggested as a possible cause of excitotoxicity. The transporter GLT1, a glial glutamine transporter, appears down-regulated in mouse models of HD, increasing levels of glutamine in the synaptic cleft (Estrada-Sánchez et al. , 2009). Mutant HTT induced excitotoxicity could also be the result of a decrease interaction with PSD-95. PSD-95 recruits NMDA receptors and facilitates their activation, but in a HD pathological context, PSD-95 is not properly recycled and NMDA receptors become hypersensitive (Sun et al., 2001).

In addition to glutamate, other neurotransmitter systems that control the activity of the corticostriatal synapse contribute to render striatal neurons more sensitive to excitotoxic stimuli (Bamford et al., 2004). Adenosine A2 receptors (A2AR) and cannabinoid receptors (CB1R) are particularly abundant on the corticostriatal terminals, where, when activated, they increase glutamate release. A crucial input to the striatum comes from the substantia nigra pars compacta, whose fibers represent the main striatal source of dopamine. Dopamine can directly regulate glutamate release from corticostriatal terminals by stimulating the D2 receptors (D2R) located on the cortical afferents

Impaired clearance of glutamate from the synaptic cleft may contribute to enhance excitotoxic neurodegeneration in HD (Tzingounis & Wadiche, 2007). Glial cells may play important roles through cell-cell interactions. For example, decreased glutamate uptake in glial cells by GLT-1, the Na^+dependent glial transporter of glutamate, contributes to increased neuronal vulnerability and neuronal excitotoxicity in neurons.

1.7.5 Mitochondrial-based defects, energy and trafficking

Many studies have indicated that mitochondrial dysfunction may contribute to neurodegenerative diseases, including HD. Mitochondria are the 'powerhouses' of the cell, generating adenosine-5'-triphosphate (ATP) and maintaining cellular homeostasis. Neurons have intense energy demands that are met by mitochondria: ATP is essential in neurons to fuel ionic pumps and ATP-dependent enzymes (Johri et al., 2011). Mitochondria also buffer intracellular calcium levels and sequester apoptotic factors, playing a vital role in neuronal function and survival. Dysfunction of mitochondria can lead to metabolic insufficiency, oxidative damage, excitotoxicity, and neurodegeneration (Hollenbeck & Saxton, 2005).

There is extensive evidence for bioenergetic deficits and mitochondrial dysfunction in HD: such as a pronounced weight loss despite sustained caloric intake; nuclear magnetic resonance spectroscopy showing increased lactate in the cerebral cortex and basal ganglia; decreased activities of oxidative phosphorylation (OXPHOS) complexes II and III, and reduced aconitase activity in the basal ganglia; abnormal mitochondrial membrane depolarization in patient lymphoblasts; abnormal ultrastructure of mitochondria in cortical biopsies obtained from patients with both juvenile and adult-onset HD; pathologic grade dependent reductions in numbers of mitochondria in HD postmortem brain tissue; and in striatal cells from mutant HTT knock-in mice: both mitochondrial respiration and ATP production are significantly impaired (Johri & Beal, 2012).

HD patient post mortem brain slices and mouse models demonstrate decreased levels of cAMP and ATP/ADP ratios, indicating defective mitochondrial energy metabolism (Gines et al., 2003). Positron emission tomography (PET) imaging in the striatum of patients during presymptomatic or early stages of HD revealed increased oxygen over glucose utilization, suggesting early defects in glycolysis (Powers et al., 2007). The R6/2 mouse model shows increased oxygen consumption and increased uncoupling protein-2 mRNA levels in the brown adipose tissue, which suggests inefficient coupling of the electron transport and ATP synthesis (van der Burg et al., 2008). Similarly, HD patients often demonstrate severe chorea-independent weight loss (Djoussé et al., 2002). Defects in the mitochondrial respiratory chain complex II and III have been observed specifically in the caudate and putamen, but not cerebellum or cortex of HD patients (Brennan et al., 1985; Gu et al., 1996; Tabrizi et al., 1999). Together these results point to cell specific defects associated with mitochondrial energy production in areas of the brain prone to neurodegeneration in HD. Because many of these effects are seen pre-symptomatically, defects may represent early events in pathogenesis which could provide useful targets for therapeutics.

Mitochondria must be positioned properly to serve the needs of the cell. In neurons, mitochondria are delivered to and remain in areas of the axon where metabolic demand is high, such as synapses, active growth cones and branches, nodes of Ranvier, distal initial segments, myelination boundaries and regions of demyelination or axonal protein synthesis (Hollenbeck & Saxton, 2005). Long-distance fast axonal transport of mitochondria requires MTs. Mitochondrial movement implicate motor proteins of the kinesin superfamily in anterograde organelle transport and those of the dynein family in retrograde transport (Hollenbeck, 1996). Mitochondrial transport defects have been demonstrated in several models of HD. Results suggest aggregation-independent defects owing to a role for wild- type HTT in mediating fast axonal transport of mitochondria (Li et al., 2010; Trushina et al., 2004) as well as aggregation-dependent defects resulting from large HTT aggregates blocking axonal transport in neuritic processes (Lee et al., 2004).

1.7.6 Intracellular transport alteration

Many studies have highlighted a potential role for defective axonal transport in neurodegenerative diseases. Neurons rely on fast axonal transport (FAT) to transport vesicles, organelles, nucleic acids, and signalling molecules between the cell body and the synapse via microtubule tracks (Schliwa & Woehlke, 2003). HTT is found predominantly in the cytoplasm of neurons and is enriched in compartments containing vesicle-associated proteins (Velier et al., 1998). Accumulating data on roles for HTT in endocytosis, endosomal motility and axonal transport have led to an emerging model for HTT as an integrator of transport along the cellular cytoskeleton (Caviston & Holzbaur, 2009)(see also chapter 1.6.6 of this manuscript).

Mutant HTT expression has been shown to alter axonal transport of mitochondria (Lee et al., 2004; Sinadinos et al., 2009), synaptic vesicles (Lee et al., 2004), neurotrophic factors such as BDNF (Gauthier et al., 2004), and other organelles (Chang et al., 2006).

The alteration of axonal transport observed in HD is linked, at least in part, to a defect in HTT function in transport. This was shown in particular for the vesicular transport of BDNF (Charrin et al., 2005). BDNF is an important factor in HD. It is produced in the cortex and transported to the striatum, the major site of degeneration in HD, where it supports neuronal differentiation and survival. Normal full-length HTT stimulates BDNF transport. The mutant form has lost this ability, leading to reduced BDNF support and thus to increasing susceptibility of striatal neurons to death. This phenotype is mediated by HAP1, which interacts with huntingtin and with the $p150^{Glued}$ subunit of dynactin. HTT normally interacts with $p150^{Glued}$ via HAP1 and stimulates BDNF transport. In contrast, when HTT contains an abnormal polyQ expansion, it interacts more strongly with HAP1 and $p150^{Glued}$, leading to the detachment of the molecular motors from the microtubules and thus to less efficient transport of BDNF vesicles (Charrin et al., 2005; Gauthier et al., 2004). Phosphorylating mutant HTT at S421 completely restores its ability to transport BDNF-containing vesicles. Mutant HTT phosphorylation leads to a restoration of the interaction properties between HTT and the molecular motors and a recovery of HTT and $p150^{Glued}$ capacities to interact with MTs

(Zala et al., 2008). Gene replacement experiments, leading to a complete silencing of endogenous HTT and exogenous expression of a full-length form of wild-type or mutant HTT (pARIS-HTT), were used to assess vesicular transport in cellular models (Pardo et al., 2010). In this context, mutant HTT failed to correctly reassembly the Golgi apparatus after MT depolymerisation and to stimulate the dynamic of BDNF containing vesicles. These results support the notion of HTT as a scaffold protein linking vesicles and MTs and promoting the association and regulation of components of the molecular motor machinery, including HAP1 and the motors dynein or kinesin.

N-terminal HTT fragments and their aggregates accumulate in axonal processes and terminals (Li, et al., 2000) and cause axonal transport defects (Gunawardena et al., 2003; Lee et al., 2004; Szebenyi et al., 2003; Trushina et al., 2004), which subsequently induce neuronal death. Alteration in transport could then be due to a physical blockage of vesicles but could also involve the titration by mutant huntingtin aggregates of motor proteins (particularly $p150^{Glued}$ and kinesin heavy chain) from other cargoes and pathways.

1.7.7 Synaptic dysfunction

A specialized function of neurons involves transmission and reception of signals across the synaptic cleft. Evidence of both pre- and postsynaptic dysfunction is observed in HD, and could underlie cognitive and motor symptoms of the disease.

After synaptic vesicle fusion to the plasma membrane and neurotransmitter release, endocytosis is necessary to recycle vesicle membranes and may also capture retrograde signals from the postsynaptic cell. Neurotransmitter release may be affected by abnormal associations between mutant HTT with binding partners involved in endocytosis, binding more strongly to HAP1, PACSIN1, endophilin B1b, and SH3G13, and more weakly to HIP1 and HIP14 (Smith et al., 2005). Decreased synaptic vesicle density and neurotransmitter release are seen in a transgenic HD mouse model corresponding to a diminution in the association of HAP1 with vesicles (H. Li et al., 2003). This decreased synaptic vesicle density was also reported to result from high levels of mutant HTT in presynaptic terminals (Difiglia et al., 1995).

Postsynaptic defects in HD may arise from impaired interaction between mutant HTT and the postsynaptic density protein PSD-95, a protein that plays a key role in regulation of synaptic plasticity and synaptogenesis (Che et al., 2000). Mutation of HTT decreases its interaction with PSD-95, leading to NMDA receptor oversensitivity and excitotoxic cell death (Sun et al., 2001). Other receptors are also affected by expression of mutant HTT. Metabotropic glutamate receptors or mGluR2 and 3 receptors and dopamine receptors are downregulated, and alpha-amino-3-hydroxy-5-methyl-4-proprionate (AMPA), kainate, and dopamine D1 and D2 receptors all exhibit decreased ligand binding in R6/2 mice (Cha et al., 1998). The mGLuR receptor interacts with optineurin. Mutant HTT expression leads to an increase in optineurin binding to mGLUR and increased antagonism of mGLUR signalling (Anborgh et al., 2005).

Electrophysiological evidence for synaptic pathology in HD include long-term potentiation (LTP) defects in hippocampal slices from R6/2 HD mice (Murphy et al., 2000), YAC HD mice (Hodgson et al., 1999) and knock-in mice (Usdin et al., 1999). LTD defects were also reported in R6/1 HD mice (Milnerwood et al., 2006). Finally, striatal neurons from R6/2 mice exhibit more depolarized resting potentials, which may indicate removal of the voltage-dependent magnesium block of NMDA channels and vulnerability to excitotoxic neurodegeneration (Raymond et al., 2011).

1.8 Post-translational modification

Studying the post-translational modifications (PTM) of HTT has proven to be a potent tool to analyze HTT functions in health and HD.

Phosphorylations: There are various known phosphorylation sites in HTT (Figure 5).

IkappaB kinase (IKK) complex, previously shown to directly interact with HTT, phosphorylates HTT S13 and may activate phosphorylation of S16. Phosphorylation of these residues promotes modification of the adjacent lysine residues and targets wild-type HTT clearance by proteasomal and the lysosomal pathways. The presence of a polyQ expansion reduces the efficiency of this phosphorylation and mutant HTT clearance (Thompson et al., 2009). Furthermore, stress-induced phosphorylation of residues S13 and S16 can modulate nuclear entry, subnuclear localization and toxicity (Atwal et al., 2011). Phosphorylation of S16 reduces the interaction of HTT with the nuclear pore protein TPR, thus reducing its nuclear entry (Havel et al., 2011).

HTT is phosphorylated at S421 upon IGF1/Akt pathway activation (Humbert et al., 2002). Akt is able to counteract the proapoptotic properties of mutant HTT *in vitro* and *in vivo* (Humbert et al., 2002; Pardo et al., 2006; Warby et al., 2005). S421 phosporylation plays a key role in vesicular transport: when phosphorylated at S421, mutant HTT is as efficient as wild-type HTT in vesicular transport, thus leading to increased neuronal survival (Zala et al., 2008). In addition, phosphorylation of wild-type HTT is also important in physiological conditions as it acts as a molecular switch dictating the anterograde versus retrograde directionality of vesicles (Emilie Colin et al., 2008). Further studies have shown that phosphorylation of S421 results in reduced nuclear accumulation of caspase-6 cleavage fragments by reducing the activity of caspase-6 (Havel et al., 2011; Warby et al., 2009).

HTT is phosphorylated at S434 by cyclin-dependent kinase 5 (Cdk5), which reduces mutant HTT cleavage, aggregation, and cell death (Luo et al., 2005). Moreover, increase in the activity of Cdk5 in response to DNA damage results in the phosphorylation of other HTT serines, serines 1181 and 1201. These phosphorylations are crucial to regulate neuronal cell death through the p53 pathway (Anne et al., 2007). Mice models for the absence or constitutive phosphorylation at these sites show that absence of phosphorylation of wild-type HTT at S1181/1201 reduces

anxiety/depression-like behaviors through increased hippocampal neurogenesis (Ben M'Barek et al., manuscript in preparation).

More systematically, the phosphorylation sites of full-length HTT were mapped by mass spectrometry (Schilling et al., 2006). Additional phosphorylation sites were identified at positions 533-5-6, 2076, 2653 and 2657 (Schilling et al., 2006). More work is needed to explore their regulatory effects.

SUMOylation, ubiquitination, acetylation and palmitoylation:

N-terminal HTT fragments of HTT can also be modified by small ubiquitin-like modifier (SUMO)-1 or ubiquitin at lysine residues. SUMOylation of HTT stabilizes N-terminal fragments, reduces aggregation, increases nuclear localization, and increases neurodegeneration in a *D. melanogaster* model of HD (Steffan et al., 2004). Ubiquitination of lysines K6, K9, and K15 targets HTT to the proteasome for degradation. However, misfolded forms of HTT are not effectively degraded by this pathway, leading to global defects in the ubiquitination-proteasome pathway that can result in increased levels of pro-apoptotic proteins (Jana et al., 2001).

Acetylation of mutant HTT at lysine 444 has been shown to increase its trafficking to autophagosomes, decreasing overall levels and improving cell viability (Jeong et al., 2009). HTT is also palmitoylated at cysteine-214 by its copartner, HTT- interacting protein 14 (HIP14, a palmitoyl transferase) (Yanai et al., 2006). The palmitoylation of HTT is consistent with its proposed role in regulating vesicular trafficking, since palmitoylated proteins are often involved in the dynamic assembly of the components that control vesicle trafficking and synaptic vesicle function. Expansion of the polyQ tract in HTT results in decreased palmitoylation, which contributes to the formation of inclusion bodies and enhanced neuronal toxicity.)

1.9 Mechanisms of cell death

Mutant HTT cell death was reported to be linked to two major pathways: autophagy and apoptosis (detailed below). Signs of necrosis were also observed in HD. In particular, calpain activation was reported in HD cellular and mouse models, being its activation a feature of necrosis. Moreover, calpain cleaves HTT in smaller fragments that are toxic (Gafni et al., 2004; Gafni & Ellerby, 2002).

1.9.1 Autophagy

Autophagy is a dynamic cellular pathway involved in the turnover of proteins, protein complexes, and organelles through lysosomal degradation. The integrity of postmitotic neurons is heavily dependent on high basal autophagy compared to non-neuronal cells as misfolded proteins and damaged organelles cannot be diluted through cell division. Moreover, neurons contain specialized structures for intercellular communication, such as axons, dendrites and synapses, which require the reciprocal transport of proteins, organelles and autophagosomes over significant distances from the soma. Defects in autophagy affect the intercellular communication and subsequently, contribute to neurodegeneration (Son et al., 2012).

Accumulation of mutant HTT activates the endosomal-lysosomal system and contributes to an autophagic process of cell death (Kegel et al., 2000). Mammalian target of rapamycin (mTOR) sequestration in mutant HTT aggregates has been observed in cell and mice models, as well as in human HD brains (Ravikumar et al., 2004). The sequestration of mTOR impairs its kinase activity and induces autophagy. This autophagy protects against polyglutamine toxicity, as rapamycin attenuates HTT accumulation and cell death in cell models of HD and inhibition of autophagy has the opposite effects. Using cellular and mouse models of HD and cells from HD patients, a primary defect in the ability of autophagic vacuoles to recognize cytosolic cargo, was identified in HD cells (Martinez-Vicente et al., 2010). Autophagic vacuoles form at normal rates and are adequately eliminated by lysosomes, however, they failed to efficiently trap cytosolic cargo in their lumen.

Another mechanism underlying the intracellular accumulation of mutant HTT involves beclin 1: an essential protein for the formation of autophagosomes and cytosol- to-vacuole vesicles. Mutant HTT recruits beclin 1 and impairs the beclin 1-mediated long lived protein turnover (Shibata et al., 2006). Thus, the sequestration of beclin 1 in the neuronal population expressing mutant HTT might further reduce beclin 1 function and autophagic degradation of mutant HTT. Wild-type HTT protein has been proposed to act as an endoplasmic reticulum (ER) sentinel, regulating autophagy in response to ER stress. As a result, cells expressing mutant HTT may have perturbed ER function and have increased autophagic vesicles (Atwal & Truant, 2008).

The initial increase in autophagic vacuoles and autophagy observed in HD models may represent an attempt to remove mutant HTT protein and over time the autophagy machinery becomes dysfunctional, leading to neurodegeneration. Thus, therapeutic induction and recovery of autophagy may enhance the clearance of mutant HTT protein and reduce its toxic effect in HD neurons (Son et al., 2012).

1.9.2 Apoptosis

Mutant HTT also leads to cell death/degeneration through activation of caspases, which initiate and execute the apopototic program of cell death. Signs of cell death, such as DNA fragmentation, have been observed in HD brain (Dragunow et al., 1995; Portera-Cailliau et al., 1995; Thomas et al., 1995), with the degree of fragmentation positively correlated with polyQ expansion length (Butterworth et al., 1998). Activation of caspases is observed in HD striatum (Ona et al., 1999; Sanchez et al., 1999) and in mutant HTT expressing lymphoblasts (Maglione et al., 2006). An increase in caspase-1 activity is also observed in presymptomatic and early symptomatic transgenic HD mice, while inhibition of caspase-1 activity slows disease pathology (Ona et al., 1999). This indicates that caspase-mediated cell death may play a key role in initiation and progression of HD pathogenesis.

Normal and mutant HTT are both cleaved into N-terminal fragments by caspase-1 and caspase-3 (Goldberg et al., 1996; Wellington et al., 2002; Wellington et al., 2000). In a positive feedback loop, increased nuclear entry of N-terminal mutant fragments then upregulates caspase-1 expression, leading to more HTT cleavage. Caspase-1 may then activate caspase-3, which can execute the apoptotic program (S-H Li et al., 2000). Additionally, the initiator caspases-8 and -10 are auto-activated through sequestration into mutant HTT aggregates (Sanchez et al., 1999; U et al., 2001), while cytochrome c release from dysfunctional mitochondria found in HD activates caspase-9, also triggering cascades leading to apoptosis (Kiechle et al., 2002).

Proteolysis of HTT at the caspase-6 cleavage site is a crucial and rate-limiting step in the pathogenesis of HD. Activated caspase-6 is present in the brains of pre-symptomatic and early-grade human HD patients, as well as murine HD models. Intriguingly, activated caspase-6 levels correlate with CAG size in human HD brains and inversely correlate with age of disease onset (Graham et al., 2010). There is growing evidence in favor of the cleavage at the 586 amino acid caspase-6 site in mutant HTT being involved in an amplification loop for caspase-6 activation in HD (Graham et al., 2011). Caspase-6 clives and activates caspase-3, and down-stream activation of caspase-3 results in cell death (Graham et al., 2010; Hermel et al., 2004).

Other mechanisms are involved. For example, overexpression of mutant HTT in a rat hippocampal neuronal cell line induced c-Jun N-terminal kinases (JNK) activation and apoptotic cell death (Liu, 1998). It has also been suggested that the presence of an abnormal polyQ expansion in HTT affects its interaction with pro-apoptotic factors. For instance, mutant HTT promotes translocation of the pro-apoptotic factors Smac/Diablo and HtrA into the cytosol with subsequent reduction in levels of cytosolic Inhibitor of Apoptosis Protein-1 (IAP1) and X-linked inhibitor apoptosis (XIAP) (Goffredo et al., 2005). Levels of IAP1 and XIAP are decreased in HD brain tissues (Goffredo et al., 2005). Finally, mutant HTT binds more efficiently to p53 than wild-type HTT (Bae et al., 2005). This enhanced binding leads to the increased level of nuclear p53 thus promoting its transcriptional activity in neuronal cultures and in HD mice. Indeed, protein levels of the p53 targets, Bax and Puma, are significantly elevated by mutant huntingtin.

2 Mitosis

2.1 Overview

One key feature of living cells is their ability to proliferate. With the goal of creating two genetically identical daughter cells, cell division culminates in the equal segregation of sister chromatids. Mitosis represents the last stage in the life of an individual cell.

2.2 Cell cycle

The eucaryotic cell cycle is traditionally divided into four sequential phases: G1, S, G2, and M (Figure 14). G1, S, and G2 together are called interphase. In a typical human cell proliferating in culture, interphase might occupy 23 hours of a 24 hour cycle, with 1 hour for M phase. DNA duplication occurs during S phase (S for synthesis). After S phase, chromosome segregation and cell division occur in M phase (M for mitosis). M phase involves a series of dramatic events that begin with nuclear division. Most cells require much more time to grow and double their mass of proteins and organelles than they require to replicate their DNA and divide. To allow more time for growth, extra G (G for gap) phases are inserted in most cell cycles: a G1 phase between M phase and S phase and a G2 phase between S phase and M. The two gap phases also provide time for the cell to monitor the internal and external environment to ensure that conditions are suitable and preparations are complete before the cell commits itself to the major upheavals of S and M phases. The G1 phase is especially important in this respect. Its length can vary greatly depending on external conditions and extracellular signals from other cells. If extracellular conditions are unfavourable, for example, cells delay progress through G1 and may even enter a specialized resting state known as G0 (G zero). If extracellular conditions are favourable and signals to grow and divide are present, cells in early G1 or G0 progress through a commitment point near the end of G1 known as Start (in yeasts) or the restriction point (in mammalian cells). After passing this point, cells are committed to DNA replication, even if the extracellular signals that stimulate cell growth and division are removed (Alberts et al., 2002).

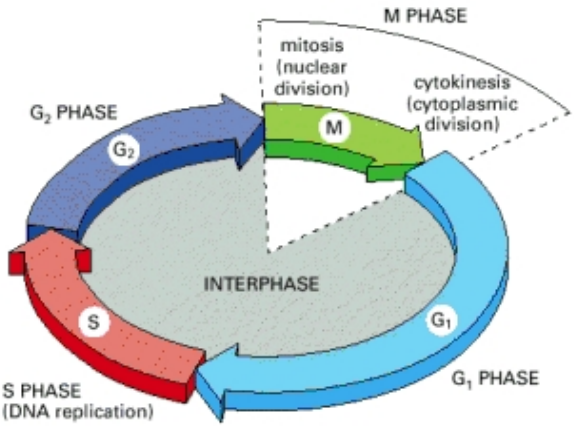

Figure 14. The cell cycle. The cell grows continuously in interphase, which consists of three phases: DNA replication is confined to S phase; G1 is the gap between M phase and S phase, while G2 is the gap between S phase and M phase. In M phase, the nucleus and then the cytoplasm divide. (Adapted from Alberts et al., 2002).

There are two classes of cell cycle regulatory molecules: cyclins and CDKs. CDKs have been proposed as cell cycle engines, driving cells through the cell cycle. Cyclins form the regulatory subunits and CDKs the catalytic subunits of an activated heterodimer. When activated by a bound cyclin, CDKs phosphorylates target proteins to orchestrate coordinated entry into the next phase of the cell cycle. Different cyclin-CDK combinations determine the downstream proteins targeted. CDKs are constitutively expressed in cells whereas cyclins are synthesised at specific stages of the cell cycle, in response to various molecular signals (Nurse, 2000).

Mitosis is divided in different phases (Figure 15). At prophase, replicated chromosomes condense and the mitotic spindle consisting of MTs assembles between the two centrosomes that have separated and move to opposite directions. After nuclear envelope breakdown (NEB) chromosomes attach to the spindle MTs via their kinetochores and undergo active movement towards an equilibrium position between the two spindle poles, thereby aligning at the equator of the spindle (prometaphase). Spindle poles are interacting with the chromosomes through spindle MTs, but also with the actin cortex of the mitotic cell through astral MTs. A complete equilibrium is reached in metaphase, with kinetochores of sister chromatids attached to MTs from opposite poles. The sister chromatids finally separate and are slowly pulled towards the poles (anaphase), where a new nuclear envelope reassembles around them during telophase. Eventually, the mother cell constricts due to increased acto-myosin contractility at the cell equator giving rise to two daughter cells.

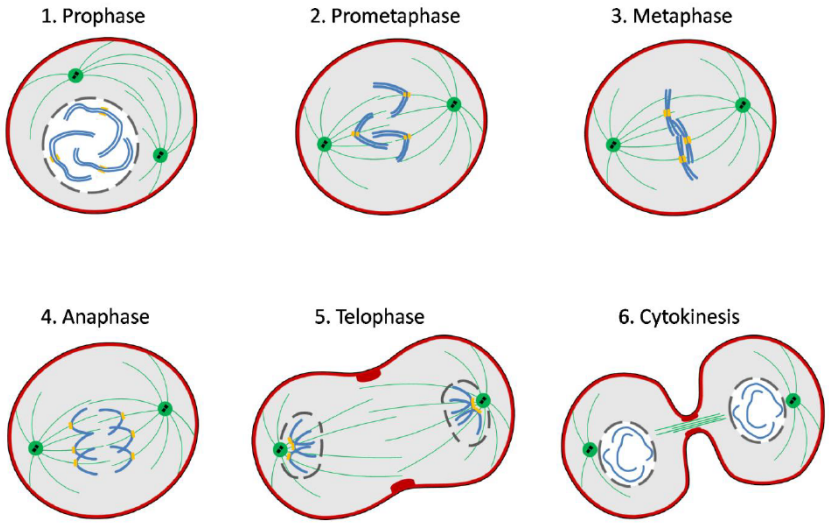

Figure 15. Mitosis and cytokinesis. 1) Prophase. Duplicated centrosomes migrate around the nucleus. 2) Prometaphase. The nuclear envelope breaks down allowing MTs to move chromosomes to the equator. C) Metaphase. Sister chromatids face opposite poles at the equator. 4) Anaphase. Chromatids are moved to opposite poles. Pole-pole spacing increases. 5) Telophase. Nuclear envelopes reassemble around decondensing segregated sisters. 6) Cytokinesis. A barrier between the daughter cells develops and constricts the spindle mid-zone into a structure called midbody. The two daughter cells are separated. (Adapted from Alberts et al., 2002).

2.3 The mitotic spindle

During mitosis, the mitotic spindle ensures the separation of the genetic material and positions the cytokinesis furrow, therefore coordinating karyokinesis and cytokinesis. The mitotic spindle is an elongated dynamic structure consisting of three classes of MTs (Figure 16) nucleated from spindle poles: kinetochore-fibers (K-fibers) attach to the chromosomes to separate sister chromatides at anaphase; interpolar MTs form an antiparallel array between the spindle poles and are implicated in positioning the furrow at cytokinesis; and astral MTs dynamically anchor the mitotic spindle to the cortex and also participate in furrow positioning.

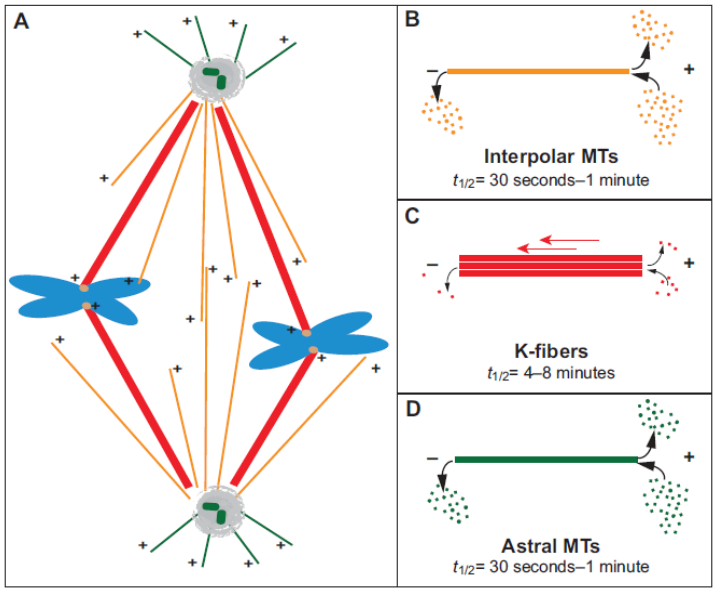

Figure 16. The three subclasses of spindle MTs. (A) Schematic metaphase spindle, showing its three different MT subclasses: interpolar MTs (orange), K-fibers (red) and astral MTs (green). The '+' indicates the plus-ends of the MTs. (B–D) Representation of the three kinds of spindle MTs and their dynamic properties. Astral MTs have dynamic properties that are similar to those of the interpolar MTs. K-fibers are less dynamic and undergo a constant polewards tubulin flux (arrows). $T_{1/2}$ is average half-life. (Adapted from Meunier & Vernos, 2012).

Spindle MTs dynamically grow and shrink through the addition and removal of tubulin dimers, a property referred to as 'dynamic instability'. MT dynamic instability allows probing for microtubule anchor sites, and can be coupled to spindle positioning force generation. Spindle positioning typically involves pulling-forces exerted on astral microtubules, which can be generated by plus-end depolymerization of astral MTs that remain attached to the cell cortex, cortically-attached MT minus-end directed motor activity or translocation of MT plus-ends by attachment to actin-based motors. Regulation of MT dynamic instability is critical for correct spindle positioning (Siller & Doe, 2009).

2.4 Positioning of the mitotic spindle

2.4.1 Spindle orientation in development and tissue organization

Cell division orientation during animal development serves to correctly organize shape tissues and create cellular diversity. The underlying cellular mechanism is oriented cell division (OCD). OCD serves two purposes: first, to elongate cell sheets and shape tissues and, second, to generate cellular diversity. In order to achieve these two mutually non-exclusive functions, the orientation of the mitotic spindle has to be controlled. Depending on the developmental context, extrinsic signals or intrinsic cues control the correct orientation of the mitotic spindle. Cell geometry is another determinant of spindle orientation (Gillies & Cabernard, 2011).

Organ shape depends on the coordination between cell proliferation and the spatial arrangement of cells during development. At the same time, cell division is coordinated with cell growth to determine the number of cells and the size of multicellular organisms (Goranov & Amon, 2010). The processes by which the cells are systematically distributed can be accomplished either by random division of cells that later migrate locally to new positions (cell allocation) or through polarized cell division (Baena-López et al., 2005).

Most divisions in an organism are symmetric, and many have a stereotypical orientation. Cell division orientation is the main 'driving force' for tissue elongation. OCD may contribute to tissue elongation by two distinct mechanisms: (1) cell growth is isotropic and tissue elongation occurs by positioning daughter cells along the axis of elongation; (2) and cell growth can be anisotropic either due to an increase of cortical tension perpendicular to the tissue elongation axis or to a global anisotropic constraint along the tissue elongation axis. The two models are not mutually exclusive: OCD itself might generate a local elongation of neighboring cells, and this elongation might in return trigger an anisotropic cell growth (Morin & Bellaïche, 2011).

Cell division orientation can be switched during development to contribute to tissue morphogenesis. The switch from symmetric, proliferative divisions towards asymmetric, diversifying divisions occurs in several different cell types. A clear example is mammalian skin epidermis (Figure 17). In mice, it has been shown that the stratification of the epidermis consists of two phases: a proliferative, amplification phase in which symmetric divisions increase the surface area of the epithelium, followed by an asymmetric division phase generating distinct molecular identities (Lechler & Fuchs, 2005; Williams et al., 2011). Thus, stratification occurs through a change in the division axis of dividing cells. Further studies revealed that epidermal cells are not committed to one type of division but can change between symmetric and asymmetric divisions (Poulson & Lechler, 2010).

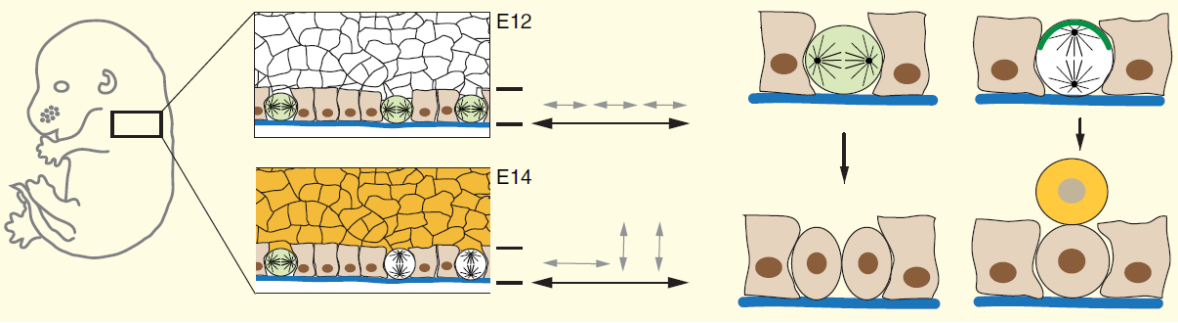

Figure 17. Switching the division axis to generate cellular diversity. Mouse epidermis. At embryonic day 12, basal cells divide preferentially within the plane of the epithelium (grey arrows). From embryonic day 15.5 onwards, perpendicular asymmetric cell divisions occur, producing differentiating siblings (yellow). Intrinsic cues (green) are diffusely localized (light green throughout the cell) in symmetrically dividing basal cells but becomes asymmetrically localized (green crescent) from embryonic day 15.5 onwards, inducing asymmetric cell division. (Adapted from Gillies & Cabernard, 2011).

OCD axis is strongly associated with tissue elongation, but, other mechanisms like anisotropic cell growth, cell-cell rearrangements and apoptosis have been demonstrated to shape tissues as well

(Rauzi et al., 2008; Su & O'Farrell, 1998; Toyama et al., 2008). Future studies will clarify the specific contribution of each mechanism in different tissues and organisms.

2.4.2 Spindle orientation in cell fate specification

The ability of dividing cells to produce daughter cells with different fates is an important developmental mechanism conserved from bacteria to fungi, plants and metazoan animals. Spindle orientation can influence the generation of symmetric or asymmetric cell fates depending on cell-intrinsic polarity cues and cell-extrinsic cues.

Two mechanisms are possible for asymmetric outcomes of the daughter cells: asymmetric distribution of intrinsic fate determinants during mitosis (asymmetric cell division or ACD) or placement of equal daughter cells (symmetric cell division or SCD) into different microenvironments providing extrinsic differentiation signals. Those extrinsic signals can be as simple as changes in substrate stiffness (Engler et al., 2006).

ACD is often proposed to be composed of three steps: (1) a cell polarity axis is specified; (2) cell polarization is translated into the asymmetric localization of cell fate determinants; and (3) the mitotic spindle aligns with the cell polarity axis, thereby leading to the segregation of fate determinants in only one daughter cell.

ACD has mostly been studied in invertebrate systems such as *D. melanogaster* neuroblasts (NBs) (Figure 18) and *C. elegans* zygote (Figure 19). *D. melanogaster* NB model exemplify how intrinsic polarity cues can align the mitotic spindle, whereas *C. elegans* zygote illustrates the down-stream effects of an extrinsic signal (fertilization) in asymmetric localization of determinants.

D. melanogaster NBs are cells that delaminate from the ventral neuroectoderm during embryogenesis. In embryos, NBs undergo up to 20 rounds of asymmetric cell division to generate the neurons of the larval nervous system, and they become quiescent at the end of embryogenesis. During the larval stages of development, NBs re-enter the cell cycle and continue to divide asymmetrically to generate the neurons of the adult fly brain (Ito & Hotta, 1992). Type I NBs divide into a large cell that remains a NB and a smaller ganglion mother cell (GMC); the GMC subsequently divides into two terminally differentiated neurons (Figure 18a). During mitosis, NBs orientate their mitotic spindle along the apical-basal axis, defined by polarity complexes asymmetrically distributed along the cell (Figure 18b). Apical cortical complex is formed from late interphase/early prophase onward, and basal determinants are localized slightly after. These complexes provide astral MT anchoring activity and mitotic spindle pulling forces that will orientate the mitotic spindle. As a consequence, daughter cells inherit different fate determinants to self-renew or differentiate (Knoblich, 2010; Morin & Bellaïche, 2011)

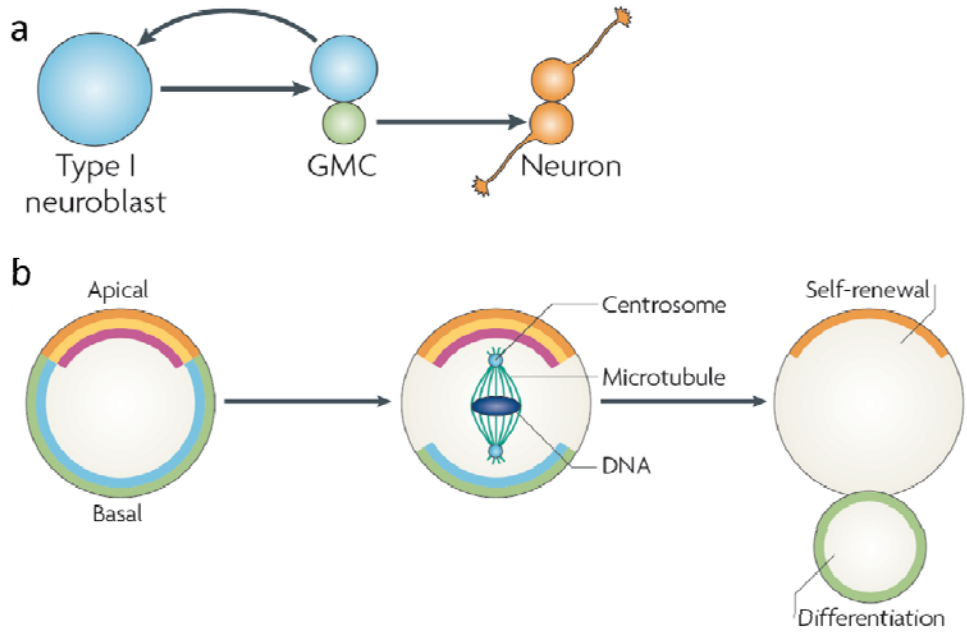

Figure 18. ACS in *D. melanogaster* NBs. a) Type I NBs divide asymmetrically, resulting in an apical self-renewed NB and a basal GMC. The GMC divides terminally into two neurons. b) Schematic NB showing the apical (orange, yellow, pink) and basal (light blue, green) polarity complexes. Mitotic spindle orients along the apical-basal axis. Cell fate determinants are asymmetrically inherited by daughter cells. (Adapted from Knoblich, 2010).

The fertilized *C. elegans* one-cell embryo is elongated along the anterior-posterior axis (Figure 19). Upon fertilization, the movement initiated by the sperm centrosome starts when the entire cortical actin cytoskeleton moves towards the anterior pole. Sperm centrosome and cortex interaction allow cortical cues accumulation at the posterior cortex, while proteins that are initially uniformly distributed, concentrate at the anterior side after fertilization. These cortical cues are translated in mechanical forces pulling on astral MTs. The two pro-nuclei and their associated centrosomes form the nucleus centrosome complex in the posterior half of the zygote. The centrosomes align perpendicular to the anterior-posterior axis. Before the first mitosis, the nucleus centrosome complex moves to the cell centre in a posterior to anterior direction and rotates 90˚ to align the centrosome pair along the anterior-posterior axis (Siller & Doe, 2009). The first cell division generates a large anterior blastomere (AB) and a smaller posterior one (P1) which are both endowed with distinct cell fate determinants (Knoblich, 2010; Morin & Bellaïche, 2011).

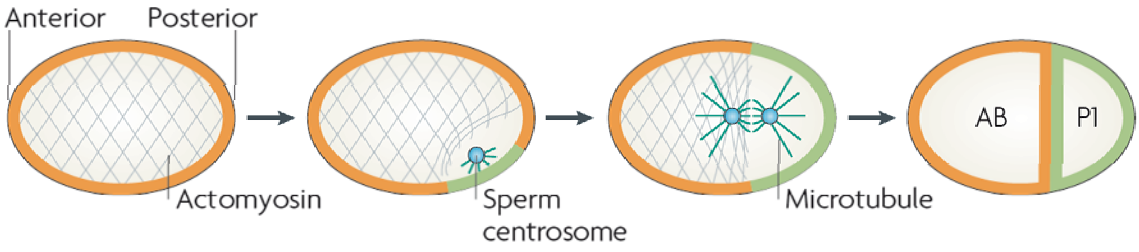

Figure 19. Spindle orientation and positioning in the *C. elegans* zygote. Polarization starts after fertilization. Sperm centrosome creates movements of actomyosin and anterior-posterior asymmetric localisation of cortical cues. Mitotic spindle aligns along the anterior-posterior axis. The first cell division generates an anterior AB cell and a posterior P1 cell. (Adapted from Knoblich, 2010).

2.5 Key players in mitotic spindle orientation

2.5.1 Cell shape

120 years ago, applying mechanical forces on sea urchin embryos, which trigger a cell shape deformation, revealed that cells tend to divide along their long axis: the so-called '*Hertwig rule*' (Hertwig, 1893). This pushed forward the notion that mitotic spindle orientation originates from a mechanical regulation, whereby the cells are able to sense their shape or the applied stress (Figure 20). The divisions of, for example, the yeast *S. pombe*, mouse oocytes and of mammalian cells cultured *in vitro* seems to follow this rule (Moseley & Nurse, 2010; Piel & Tran, 2009; Théry & Bornens, 2006). Many animal cells, especially cultured mammalian cells, drastically change geometry during mitosis and round up, whereas others, such as blastomeres of early developing animals, maintain their stereotypical shape throughout interphase and mitosis (Minc & Piel, 2012).

However several exceptions to the Hertwig rule have been found for cells in tissues, where the polarized cell cortex overrides the influence of the cell shape: In dorsal tissue elongation during zebrafish gastrulation cell division axis is dominated by planar cell polarity (PCP) signalling and does not follow the Hertwig rule (Gong et al., 2004). In the mouse epidermis mitotic spindles align either along the cell's longest axis or perpendicular to it, both under the control of cell–cell junctions (Lechler & Fuchs, 2005).

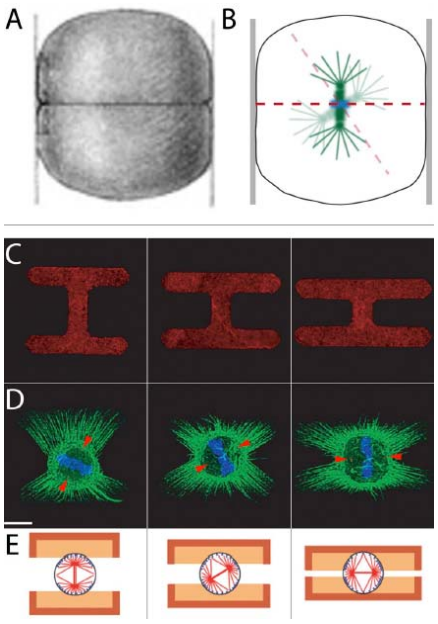

Figure 20. Cell shape controls mitotic orientation. (A) Drawing by O. Hertwig of the confined frog embryo after its first division illustrating Hertwig's rule (Hertwig, 1893). (B) Without apparent interactions with the cell boundary, we might expect the small mitotic spindle in a large cell to position randomly, but it orients according to Hertwig's rule. (C) Fibronectin micropatterns in various geometries results in well-defined mitotic spindle orientations (D) determined by actin-rich retraction fibers (green). DNA (blue), positions of spindle poles (red arrowheads). (E) Computational modeling predicts the expected orientation based on adhesion pattern shape (Théry et al., 2007). (Adapted from Shah, 2010).

2.5.2 Cell-cell junctions (cadherins) and focal adhesions (integrins)

Cadherins: In multicellular organisms, cell–cell contacts that are mediated by classic cadherins are essential in many fundamental processes, including morphogenesis, maintenance of tissue integrity, wound healing and cell polarity (Kobielak & Fuchs, 2004). These cadherins (for example E-cadherin) possess an extracellular segment that consists of five distinct Ca^{2+} binding domains, a transmembrane domain and a conserved cytoplasmic domain, which binds β-catenin. The extracellular part interacts with cadherins on the surface of neigbouring cells to form adherens junctions (Figure 21). The cytoplasmic tail binds indirectly to the actin cytoskeleton. Thus classic cadherins are good candidates to transmit extracellular information to the cytoskeleton inside the cell. In addition to their function as connectors, adherence junctions actively regulate and organize the actin cytoarchitecture (Kobielak & Fuchs, 2004).

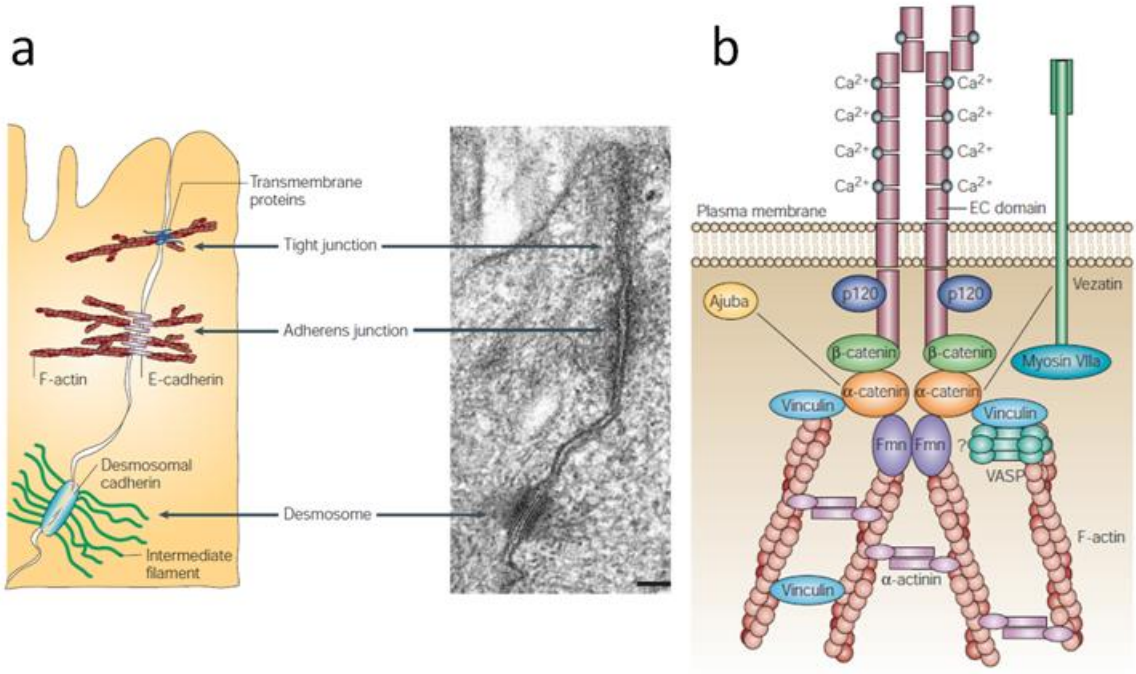

Figure 21. Localization and molecular structure of adherence junctions. a) Electron micrograph and corresponding schematic depict the main types of intercellular junction in epithelial cells: tight junctions, adherens junctions and desmosomes. b) Molecular structure of an adherens junction. (Adapted from Kobielak and Fuchs 2004).

In some model systems such as *D. melanogaster* germline stem cells (GSCs), mitotic spindles are oriented toward the adherens junction formed between stem cells and the niche component (Inaba et al., 2010; Yamashita, et al., 2003). This has led to speculation that the adherens junction might provide a polarity cue for spindle orientation. Such orientation leads to asymmetric stem cell division, with one daughter of the stem cell division staying within the niche and the other being displaced away from the niche. In non-stem cell systems, abundant evidence shows that adherens junction components, including E-cadherin and β-catenin, are responsible for spindle orientation. For example, in epithelial cells of *D. melanogaster* embryos, spindle poles are closely

associated with the adherens junctions present between neighboring cells, leading to orientation of spindles parallel to the epithelial surface and ensuring symmetric cell division (Lu et al., 2001). In *D. melanogaster* NBs, spindle orientation correlates with contact with epithelial cells, implying that the adherens junction is involved in spindle orientation. In addition, E-cadherin is concentrated at the interface between the NB and GMCs (Siegrist & Doe, 2006). More recently, the E-cadherin/adherens junction was shown to be sufficient to polarize mammalian cells in culture (Desai et al., 2009; Dupin et al., 2009), though centrosomes were oriented away from the adherens junctions in these cases.

Integrins: Focal adhesions are large, dynamic protein complexes through which the actin cytoskeleton of a cell connects to the extracellular matrix (ECM) (Figure 22) (Petit & Thiery, 2000). A complex interplay between the actin cytoskeleton and cell adhesion sites (Figure 23) leads to the generation of membrane protrusions and traction forces. External stimuli that control cell migration are transduced into intracellular biochemical signals through the interactions of transmembrane integrins that bind to ECM proteins, growth factors that bind to their related cell-surface receptors, or mechanical stimuli (such as shear stress that promote deformation of the actin cytoskeleton) (Mitra et al., 2005).

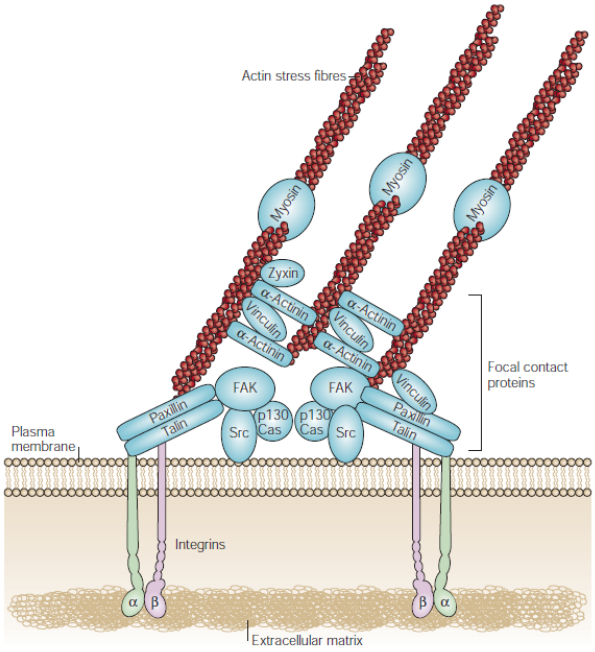

Figure 22. Molecular architecture of focal contacts. The extracellular matrix, integrins (α- and β-transmembrane heterodimeric proteins) and the cell cytoskeleton interact at sites called focal contacts. The composition of a focal contact is constantly varying depending on external cues and cellular responses. (Adapted from Mitra et al. 2005).

The connection to ECM is mediated by heterodimeric α–β integrins that possess a binding domain for ECM proteins (e.g. fibronectin, laminin, collagens, vitronectin), a transmembrane domain and a binding domain for the focal adhesion protein talin (Figure 22). Integrin activity is conformationally regulated by proteins that bind to its β-tail (Geiger et al., 2009; Mitra et al., 2005).

Focal adhesions contain over 100 different proteins, which suggests a considerable functional diversity (Geiger et al., 2009). Indeed focal adhesion signalling (Figure 23) plays essential roles in important biological processes including cell migration, cell proliferation and survival, cell differentiation and gene expression (Geiger et al., 2009; Mitra et al., 2005; Petit & Thiery, 2000).

The importance of integrin/focal adhesion signaling in oriented cell division has been demonstrated *in vivo* in *D. melanogaster* and mouse models: In *D. melanogaster* ovarian follicular epithelium, spindle alignment parallel to the basement membrane is required to keep the integrity of the monolayer. This symmetric division depends on integrins and ensures that both daughter cells remain adhered to the basement membrane to prevent inappropriate stratification (Fernandez-Miñan et al., 2007). Accumulating evidence suggests that adhesion molecules participate in spindle orientation in some stem cell models, including mammalian neuronal stem cells and skin stem cells (Lechler & Fuchs, 2005; Loulier et al., 2009; Marthiens et al., 2010; Taddei et al., 2008), both of which require integrins for correct spindle orientation. Integrin signaling is also essential for spindle orientation in cultured cells: In HeLa cells spindles orient parallel to the fibronectin substrate (Mitsushima et al., 2009; Toyoshima & Nishida, 2007a, 2007b). This orientation is perturbed if cells grow on poly-lysine substrates (onto which integrins cannot bind) or if β1 integrin functioning is inhibited by siRNA or function-blocking antibodies.

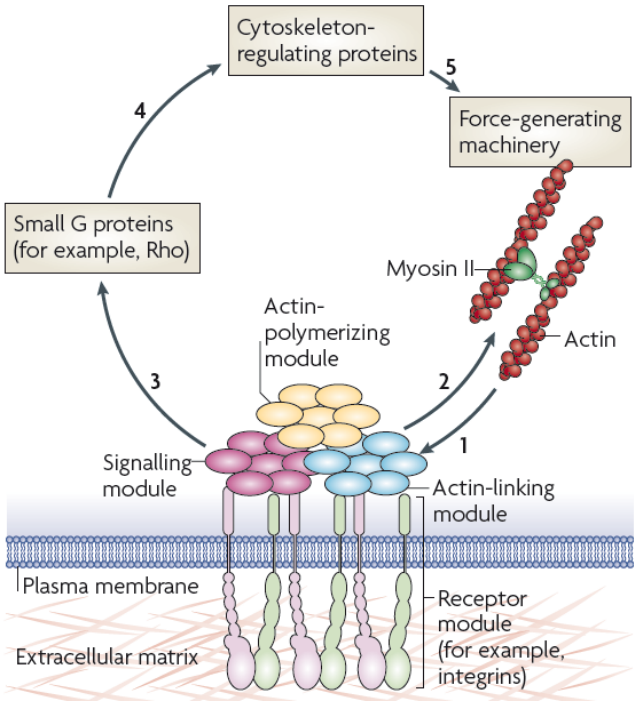

Figure 23. Actin cytoskeleton-focal adhesion interplay. Feedback loops that interconnect the actin machinery and integrin-mediated adhesions. Step 1: forces generated by actin polymerization affect the mechanoresponsive network (actin-linking module, the receptor module, the associated actin-polymerizing module and the signalling module). Step 2: integrated response of the entire system affect actin cytoskeleton. Step 3: Stimulation of the signalling module activates small G proteins. Step 4: activated G proteins affect actin polymerization and actomyosin contractility through cytoskeleton-regulating proteins. Step 5: as a result, the force-generating machinery is modulated. (Adapted from Geiger et al., 2009).

2.5.3 Microtubules: overview

MTs are involved in a large number of processes, such as protein and organelle transport, cell polarity, cell shape, cell motility and cell division. They are assemblies of α- and β- tubulin heterodimers (Figure 24). The orientation of the α- and β-tubulin heterodimers within the MT confers an intrinsic polarity that is defined by a minus-end (where α-tubulin is exposed) and a plus-end (where β-tubulin is exposed). Interestingly, each end has distinct dynamic properties and the plus-end is the dominant site for the addition of tubulin subunits and MT elongation. MTs are dynamic filaments that undergo successive cycles of growth and shrinkage, called dynamic instability. A large number of factors are involved in mechanisms that favour MT stabilization or destabilization. Dynamic instability allows the cell to regulate the parameters of MT dynamics and to reorganize its MT network. This occurs, for example, during cell division, when MTs form the mitotic spindle. As the cell commits to divide, MTs nucleated by the centrosomes become shorter and more dynamic; this leads to the disassembly of the interphase MT network. In addition, after nuclear envelope breakdown, the chromosomes direct *de novo* MT assembly and a separate mechanism drives MT amplification. The local stabilization and organization of these centrosomal and non- centrosomal MTs lead to the assembly of a bipolar spindle that aligns the chromosomes on the metaphase plate and segregates them into the two daughter cells (Gatlin & Bloom, 2010; Tanenbaum & Medema, 2010; Walczak et al., 2010; Walczak & Heald, 2008).

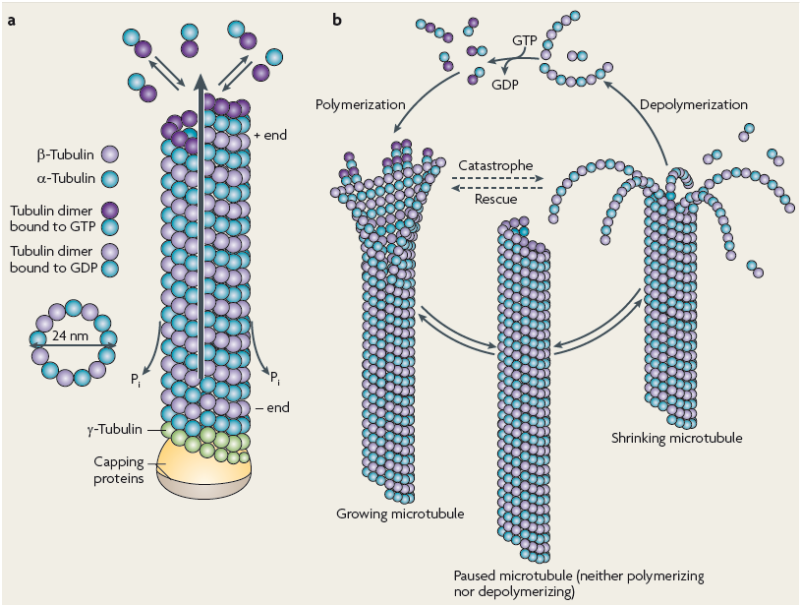

Figure 24. MT dynamics. a) MTs are polarized structures composed of α- and β-tubulin heterodimer subunits assembled into linear protofilaments. A single MT is comprised of 10–15 protofilaments that associate to form a 24 nm wide hollow cylinder. A third tubulin isoform, γ-tubulin, functions as a template for the correct assembly of MTs. Polymerization of GTP bound αβ-tubulin dimers attach preferentially to the fast growing plus end. Once incorporated into the microtubular structure the GTP hydrolyses creating a protecting GTP cap at the plus end. Loss of the GTP cap promotes microtubule depolymerisation. b) MTs undergo periods of polymerization and depolymerization and interconvert randomly between these states. Conversion from growth to shrinkage is termed 'catastrophe', whereas the switch from shrinkage to growth is called 'rescue'. (Adapted from Conde & Cáceres, 2009).

MT dynamics and function are modulated by interactions with other proteins, microtubule motor proteins and non-motor microtubule-associated proteins (MAPs). The two major families of microtubule motors are the kinesins and dyneins. The heterogeneous group of non-motor MAPs comprises proteins that stabilize MTs (for example, the neuronal proteins tau, MAP1 and MAP2) but also severing proteins, such as spastin and katanin, which destabilize the microtubule lattice (Janke & Bulinski, 2011). Another group of intensively studied MAPs is that of the MT plus end-tracking proteins (+TIPs): MT growth and catastrophe are regulated by proteins that specifically attach to the plus- or minus-ends of MT. Plus-end proteins (e.g. EB1) accumulate around the MT plus tip, thereby forming a cap structure that favours filament growth, reduces catastrophe frequencies and recruits further proteins (Akhmanova & Steinmetz, 2010; Steinmetz & Akhmanova, 2008). Plus-end proteins are also required to connect proteins present in the actin cytoskeleton or at the plasma membrane to transduce polarization cues from the actin to the microtubules network (Akhmanova & Hoogenraad, 2005; discussed in chapter 2.5.5).

In animal cells, MTs are primarily emanating from the centrosome which organizes most of the MTs in interphase. Centrosome consists of a pair of centrioles linked together through their proximal regions by a matrix consisting in part of large coiled-coil proteins of the pericentrin family, which anchor other matrix components. The centrioles contain cylindrical arrays of triplet MTs organized with nine-fold radial symmetry and the proximal region is structurally similar to the basal bodies of cilia and flagella (Azimzadeh & Bornens, 2007). MTs are nucleated in the matrix associated with both mother and daughter centrioles, but only the mother centriole is able to anchor them (Piel et al., 2000). MTs are nucleated by the γ-tubulin ring complex (γ-TuRC). γ-tubulin is present throughout the cell cycle in the matrix, close to the proximal walls of centrioles. Its levels increase dramatically prior to mitosis, concomitantly with the recruitment of MT-associated proteins required for mitotic spindle formation. Following their nucleation by the γ-TuRC, MTs are either released into the cytoplasm or recaptured and anchored at the centrosome. The subdistal appendages of the mother centriole are thought to be a major site for MT anchoring, and this activity requires ninein. PCM1 and p150^{Glued} subunit of the dynactin complex also seem to play an important role in collaboration with the MT-associated protein EB1 to anchor MT at the centrosome (Azimzadeh & Bornens, 2007).

2.5.4 Microtubule post-translational modifications

Cells generate distinct MT subtypes through expression of different tubulin isotypes and through PTM, such as detyrosination and further cleavage to Δ2-tubulin, acetylation, polyglutamylation and polyglycylation (Figure 25). Recent advances draw a clearer picture of the importance of tubulin PTMs in diverse MT functions.

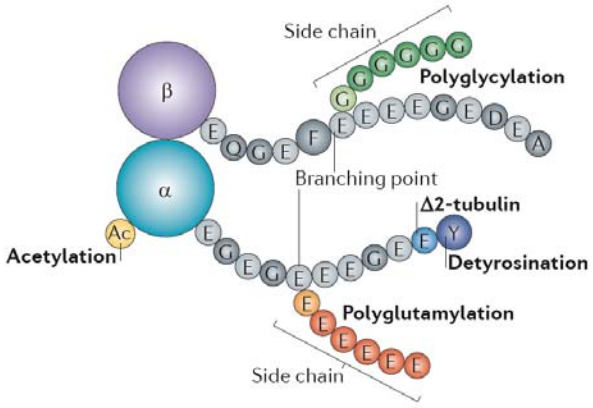

Figure 25. Tubulin PTMs. Schematic representation of the α-tubulin–β-tubulin dimer and its associated modifications. The C-terminal tails of both tubulins are represented as amino acid sequences. Both α-tubulin and β-tubulin can be modified by polyglutamylation and polyglycylation on different E (glutamic acid) residues within those tails. Together with detyrosination at the C-terminus and the follow-up removal of the penultimate E residue (which generates Δ2-tubulin), these modifications are specific to the C-terminal tails of tubulin. Acetylation (Ac) of Lys40 is localized at the amino-terminal domain of α-tubulin. (Adapted from Janke & Bulinski, 2011).

Studies of cultured cell lines with PTM-specific antibodies demonstrated that detyrosination, acetylation and polyglutamylation are enriched in the mitotic spindle, but less so in astral microtubules of the spindle (Bobinnec, Khodjakov, et al., 1998; Bobinnec, Moudjou, et al., 1998; Gundersen & Bulinski, 1986; Piperno et al., 1987). During cytokinesis, the midbody also shows high levels of these PTMs. These observations indicate that specific patterns of tubulin PTMs could mediate specialized functions of MT subsets during cell division. For example, they might participate in the stabilization of k-fibres that connect the spindle poles with the chromosomes, thus explaining their less dynamic behaviour (Zhai et al., 1995). The importance of polyglutamylation in cell division is consistent with the observed increase in polyglutamylase activity at the onset of mitosis (Regnard et al., 1999).

Detyrosination and polyglutamylation may control distinct aspects of mitotic spindle or midbody functions. The tyrosination state of α-tubulin regulates the activity of the depolymerizing motor mitotic centromere- associated kinesin (MCAK), which is essential for proper chromosome segregation in anaphase (Peris et al., 2009). Thus, detyrosination could be an essential regulator of chromosome segregation. Accordingly, tubulin detyrosination regulates CAP-Gly proteins recruitment at MT plus-end. Mislocalization of these proteins correlate with defects in both spindle positioning during mitosis and cell morphology during interphase (Peris et al., 2006).

Polyglutamylation induces enzymatic microtubule severing and might therefore be critical for controlling the length of the mitotic spindle via katanin-mediated microtubule severing (Lacroix et al., 2010; Sonbuchner et al., 2010). Similarly, polyglutamylation may also ensure timely abscission during cytokinesis by controlling spastin-dependent severing (Connell et al., 2009). The emerging picture is that the temporal and spatial control of tubulin PTMs may restrict the functions of multiple MT-interacting proteins during cell division.

MTs from neurons carry elevated levels of PTMs. Biochemical and immunological analyses of tubulin in mammalian brain tissue or cultured neurons demonstrated enrichment for detyrosinated, acetylated, and polyglutamylated tubulin, as well as for Δ2-tubulin. High levels of PTMs were observed in centrioles as well as in cilia and flagella (Janke & Bulinski, 2011).

2.5.5 Microtubule plus-end tracking proteins (+TIP)

In mammalian cells, MT minus-ends are often stably anchored, whereas the plus-ends are highly dynamic and stochastically switch between phases of growth and shrinkage. Cells possess a complex protein machinery that associates with the MT plus-ends, involved in several function such as: regulation of MT dynamics, linking MT-ends to cellular structures, generation of pushing and pulling at MT-ends and recruitment of signalling factors. MT end-binding proteins can be divided into MT destabilising factors, which include Kin I kinesins and MT plus-end-tracking proteins (+TIPs) (Akhmanova & Hoogenraad, 2005).

MT plus-end tracking proteins (+TIPs) are a structurally and functionally diverse group of proteins that are distinguished by their specific accumulation at MT plus-ends. Despite this diversity, they often colocalize and share common activities, and are therefore difficult to classify according to functional aspects. However, +TIPs can be classified in different families according to their structure (Figure 26).

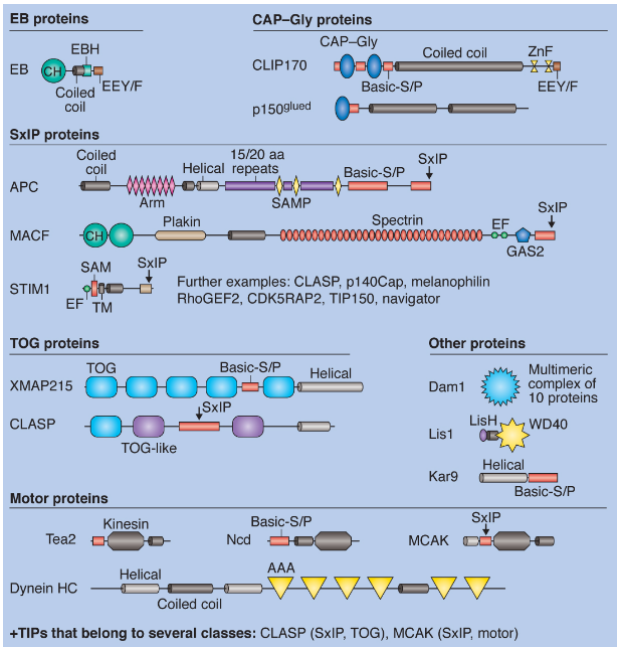

Figure 26. Structural classification of +TIPs. Ranging in size from a few hundred up to thousands of residues, +TIPs are multi-domain and/or multi-subunit proteins. +TIPs comprise combinations of a limited set of evolutionarily conserved modular binding domains, repeat sequences and linear motifs. Five families of +TIPs were identified: EB proteins, CAP-Gly proteins, SxIP proteins, TOG proteins and motor proteins. There are other +TIPs that cannot be grouped in one of the five classes (other proteins). (Adapted from Akhmanova & Steinmetz, 2010).

EB proteins: End-binding (EB) family proteins contain a highly conserved N-terminal domain that adopts a calponin homology (CH) fold that is responsible for MT binding (Hayashi & Ikura, 2003). The C-terminus of EB proteins harbours an α-helical coiled-coil domain that mediates parallel dimerization of EB monomers. It further comprises the unique EB homology (EBH) domain and an acidic tail encompassing a C-terminal EEY/F motif (Komarova et al., 2005). EB proteins are now generally accepted to represent core components of +TIP networks because they autonomously track growing MT plus ends independently of any binding partners (Akhmanova & Steinmetz, 2008; Bieling et al., 2008; Dixit et al., 2009). Moreover, EB proteins directly associate with almost all other known +TIPs and, by doing so, target them to growing MT plus-ends.

CAP-Gly proteins: The cytoskeleton-associated protein glycine-rich (CAP-Gly) domain is a small globular module that contains a unique conserved hydrophobic cavity and several characteristic glycine residues. Prominent examples are the CLIP proteins (CLIP170 and CLIP115) and the large subunit of the dynactin complex p150^{Glued} (Steinmetz & Akhmanova, 2008). CAP-Gly domains use their hydrophobic cavity to confer interactions with MT and EB proteins by specifically recognizing C-terminal EEY/F sequence motifs (Weisbrich et al., 2007). CLIPs and p150^{Glued} contain coiled-coil domains that mediate their homotypic association and result in the formation of parallel dimers. A single CAP-Gly domain of CLIP-170, together with the adjacent serine-rich region, can track growing MT ends (K. K. Gupta et al., 2009). The most evolutionarily conserved property of CAP-Gly proteins is their capacity to interact with tubulin monomers, tubulin dimers and/or MT. CLIPs stabilize MTs by preventing catastrophes or by stimulating rescues. In addition, CLIP170 participates in the plus-end recruitment dynein: CLIP170 associates with MT and EB through its CAP-Gly motifs, p150^{Glued} binds to the C-terminal of CLIP170 and is recruited to the plus ends, and dynein associates with dynactin (Coquelle et al., 2002; Galjart, 2005). Together with dynein, CLIP170 is also present at the kinetochores of mitotic cells, where it might participate in MT capture (Tanenbaum et al., 2006).

SxIP proteins: The major group of +TIPs is the group of the so-called SxLP proteins. It comprises large and complex, often multi-domain proteins containing low-complexity sequence regions that are rich in basic, serine and proline (basic-S/P) residues. They share the small four-residue motif Ser-x-Ile-Pro (SxIP, where x denotes any amino acid), which is specifically recognized by the EBH domain of EB proteins (Honnappa et al., 2009; Kumar & Wittmann, 2012). Important examples of this diverse class of +TIPs are the adenomatous polyposis coli (APC) tumour suppressor, the spectraplakin microtubule–actin crosslinking factor (MACF) and the MCAK (Akhmanova & Steinmetz, 2010). It has been proposed that the SxIP motif acts as a general microtubule tip localization signal (MtLS) (Buey et al., 2012; Honnappa et al., 2009). Detailed knowledge on MtLSs is expected to help predicting the +TIP proteome in different species and can lead to the discovery of novel +TIPs.

TOG proteins: Proteins with tumour-overexpressed gene (TOG) or TOG-like domains include members of the XMAP215/Dis1 family and CLIP-associating proteins (CLASPs). Tandemly arranged TOG domains mediate binding to tubulin and are probably responsible for MT growth-promoting activity of these proteins (Slep, 2009). Additional domains, such as SxIP motifs in CLASPs, are

required for targeting of these proteins to MT plus-ends and other subcellular sites. Moreover, CLASPs are MT-stabilizing proteins that can mediate the interaction between distal MT-ends and the cell cortex (Goodson & Folker, 2006; Lansbergen et al., 2006).

Motor proteins: Both MT plus- and minus-end directed motor proteins can track growing MT-ends. Examples are the MT-depolymerising kinesin 13 family members, such as MCAK) and cytoplasmic dynein. Sequences outside the microtubule-binding motor domains, like the SxIP motif of MCAK (Honnappa et al., 2009), might be needed for the microtubule tip-tracking behaviour of these proteins.

Other +TIPs cannot be grouped in one of the five classes above mentioned. For example the Dam1 complex is found in yeast but not in higher organisms. Other examples are the *S. cerevisiae* protein Kar9 and the highly conserved cytoplasmic dynein accessory factor lissencephaly-1 protein (Lis1) (Akhmanova & Steinmetz, 2010). LIS1 comprise an N-terminal LIS homology (LISH) domain and a C-terminal WD40 repeat-containing β-propeller domain. MT end tracking by LIS1 protein seems to require the ability of the β-propeller domain to target CLIP170, dynein and dynactin, rather than microtubules directly (Akhmanova & Steinmetz, 2008; Coquelle et al., 2002; Vallee & Tsai, 2006).

+TIPs can bind to the plus-ends of depolymerizing MTs ends or to the tips of stable MTs. However, most +TIPs decorate only growing MT plus-ends, which indicates that certain aspects of MT dynamics regulate their local accumulation (Figure 27). The likely reason for +TIP accumulation at growing MT ends is a structural difference between the end and the remainder of the tube. *In vivo*, minus-ends never grow in cells. This difference could be the presence of the GTP cap at the end of the freshly polymerized MTs or some specific protofilament arrangement (Coquelle et al., 2009). Most +TIPs exhibit a weak affinity for the MT lattice and it is possible that some of them use one-dimensional diffusion along MTs to arrive at the tips. Some +TIPs can be transported to growing tip of MTs by kinesins (Carvalho et al., 2004; Carvalho et al., 2003). +TIPs can track the ends of growing microtubules in a non-autonomous manner. For example, hitchhiking on MT bound EB proteins. Others recognize more complex binding sites that encompass domains of both EB proteins and tubulin (Akhmanova & Steinmetz, 2010; Bieling et al., 2008; K. K. Gupta et al., 2010; Honnappa et al., 2009) (Figure 27a). The idea that +TIPs can either recognize growing plus ends or co-polymerize with tubulin implies that individual +TIPs are transiently immobilized at the growing MT ends. Dissociation of +TIPs from MT ends can occur spontaneously or can be driven by structural changes in the MT lattice: a mechanism known as treadmilling (Akhmanova & Steinmetz, 2008; Carvalho et al., 2003)(Figure 27b). This mechanism has not found support in the *in vitro* reconstitution studies using EB and CLIPs but might still apply to some other proteins (Bieling et al., 2008; Dixit et al., 2009).

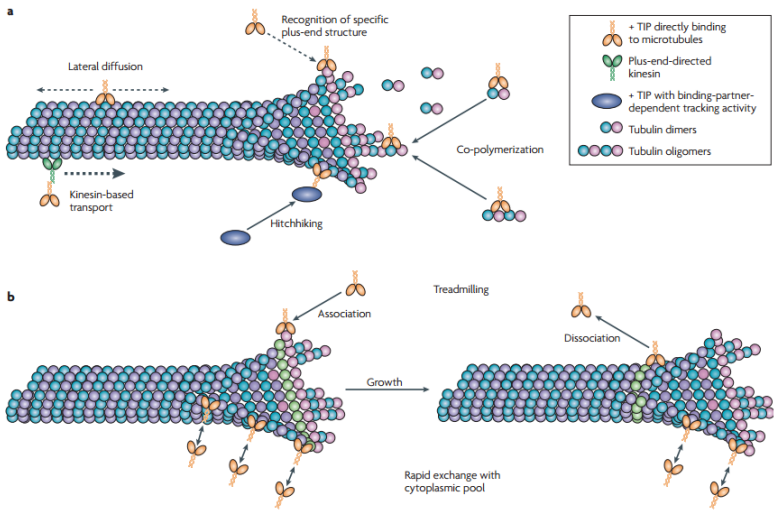

Figure 27. Mechanisms of microtubule plus-end tracking. a) +TIPs can arrive at the MT tips by diffusion in the cytoplasm or along the MT lattice. Alternatively, they can also be transported to MT plus-ends by kinesins. In all these cases, +TIP accumulation at the MT ends can be caused by their preference for a specific structural or chemical property associated with MT polymerization. The affinity of some +TIPs for the MT end may depend on their binding partners (hitchhiking). Finally, some +TIPs might co-polymerize with tubulin. b) +TIPs that recognize a specific structure at the growing MT end (or co-polymerize with tubulin) might be immobilized at the ends until this structure is converted into the regular MT lattice (treadmilling; visualized in green). Alternatively, +TIPs may exchange rapidly at their binding sites at the MT ends, while these binding sites decay over time during MT lattice maturation. (Adapted from Akhmanova & Steinmetz, 2008).

Differential regulation of +TIP association with MT ends throughout the cell can give individual MTs a specific identity, either as a result of specific motor-based loading, regional control of post-translational modifications or intramolecular interactions. Therefore, different microtubule populations that are required for particular processes, such as cell division, polarity and differentiation, can be formed (Akhmanova & Steinmetz, 2008).

2.5.6 The actin cortex

Actin is the monomeric subunit of two types of filaments in cells: microfilaments, one of the three major components of the cytoskeleton, and thin filaments, part of the contractile apparatus in muscle cells. In vertebrates, three main groups of actin isoforms, α, β, and γ have been identified. The α actins, found in muscle tissues, are a major constituent of the contractile apparatus. The β and γ actins coexist in most cell types as components of the cytoskeleton, and as mediators of internal cell motility (Doherty & McMahon, 2008). The dynamic network of polar actin filaments represents a key element of cell cytoskeleton. It is for example important for mechanical stability, cell polarization, migration and cell division.

Globular (G)-actin monomers can associate to form helical filaments called filamentous (F)-actin. F-actin is asymmetric and the two extremities retain different kinetic characteristics (Figure 28). Actin monomers assemble much more rapidly at the 'barbed-end' compared to the 'pointed-end'.

Monomeric actin binds either ATP or ADP. ATP monomers assemble at a far higher rate than ADP ones. Following assembly on a treadmilling filament, ATP is hydrolysed to ADP and this induces a change in the filament conformation, resulting in a less stable form at the pointed end, which depolymerizes. A treadmilling filament therefore contains ATP- bound subunits at the barbed end, whereas the ones at the pointed end are ADP-bound. Many proteins bind to actin and influence its dynamics or state: actin-binding proteins (ABPs). Among ABPs, some link actin filaments in a loose network (crosslinking proteins) or in a tight bundle (bundling proteins), or anchor filaments to membranes. Others bind to the barbed end of the filament and prevent further elongation (capping proteins), whereas some cause fragmentation of filaments (severing proteins) or might favour the depolymerization of pointed ends. ABPs also regulate the addition of monomers by sequestering them or favouring ADP/ATP exchange (Revenu et al., 2004).

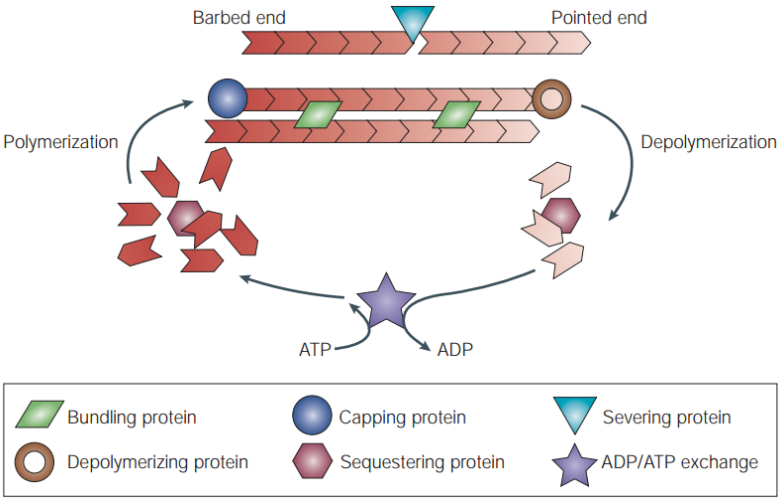

Figure 28. Structure and dynamics of actin filaments. G-actin monomers can associate to form helical filaments. These filaments (F-actin) are asymmetric and highly dynamic, continuously polymerizing and depolymerising, structures. Numerous proteins bind to actin thereby regulating its dynamics. (Adapted from Revenu et al., 2004).

Numerous proteins are known to dynamically control actin polymerization and organization: for example the Arp2/3 complex can initiate actin branching. Fascin, α-actinin and formins bundle filaments, whereas the protein fimbrin shows crosslinking activity. Reorganization of the actin structures requires furthermore the disassembly of preexisting actin filaments. This is achieved through the action of the cofilin family of proteins, which catalyse the severing of ADP-actin filaments (Chhabra & Higgs, 2007; Revenu et al., 2004).

In interphase, actin filaments assemble into different structures: they can form branched networks in membrane protrusions (lamelliopodia), align parallel to build cables (stress fibres, filopodia) and they can closely attach to the cell's membrane, being the main structural element of the cell cortex. Due to their organization and molecular composition lamellipodia are rather soft and flexible (Laurent et al., 2005). They are located at adhesive sites and arise when the growing actin

meshwork pushes the membrane forward. Stress fibres are rigid and highly contractile (Peterson et al., 2004; Rotsch & Radmacher, 2000), since myosin 2 motor proteins bridge the bundled actin filaments and move them in relation to each other. Stress fibres connect to the substrate via focal adhesions (Figure 29).

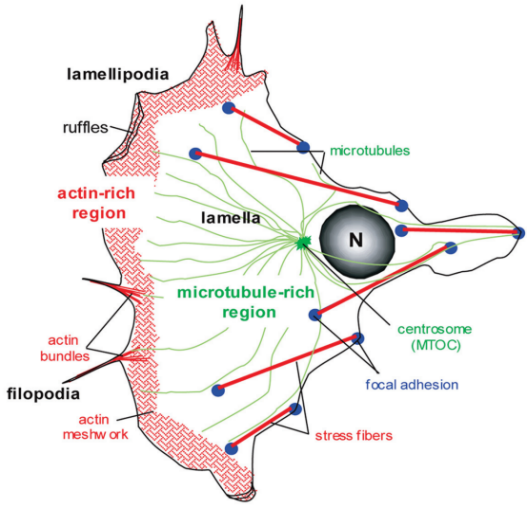

Figure 29. Actin organizes into different structures in the cell. Two regions can be distinguished in a migrating cell: an actin-rich region (red) comprising actin bundles organized into filopodia, a dense actin meshwork forming a ruffling lamellipodia; and the region where actin structures are essentially limited to stress fibers (thick red lines), anchored to the substrate via focal adhesions (blue dots). MTs are depicted in green. MTOC is microtubule-organizing center. N is the nucleus. (Adapted from Etienne-Manneville, 2004).

Local assembly and disassembly of these structures is regulated in response to a variety of intra- or extra-cellular stimuli through the Rho family of small GTPases: Rho, Rac and Cdc42. Rac controls actin polymerization and thereby lamelipodia formation, whereas Rho regulates stress fibres assembly and contractility (DeMali & Burridge, 2003; Etienne-Manneville & Hall, 2003; Ridley & Hall, 1992). Rac and Rho are thus antagonists and it has been demonstrated that Rac inhibits Rho activity to avoid locally counteracting activities (Nimnual et al., 2003). Cdc42 promotes the formation of actin-rich, finger-like membrane extensions (filopodia) and activates Rac in fibroblasts (Etienne-Manneville & Hall, 2002).

2.5.7 Spatial reorganization of the mitotic cell

In animal cells, the interphasic actin cytoskeleton undergoes dramatic changes at the onset of mitosis, since the whole structure needs to be disassembled and reformed to ensure proper cell rounding (Kunda & Baum, 2009; Théry & Bornens, 2006). The transformation of an object into a sphere can be performed either by a volume increase or an area reduction. It has been shown that during mammalian cell rounding in mitosis, the cell volume is reduced (Boucrot & Kirchhausen, 2008). This is made possible by an important cell surface reduction. A large part of the surface is endocytosed and transformed in small internal vesicles (Boucrot & Kirchhausen, 2007). Another

part of the surface is folded in many small membrane spikes, wrinkles and fibers that have been observed in electronic microscopy (Théry & Bornens, 2008).

Mitotic rounding force depends both on the actomyosin cytoskeleton and the cells' ability to regulate osmolarity. The rounding force itself is generated by an osmotic pressure. It has been shown show that in cells, osmotic pressure is balanced by inwardly directed actomyosin cortex contraction. Thus, by locally modulating actomyosin-cortex-dependent surface tension and globally regulating osmotic pressure, cells can control their volume, shape and mechanical properties (Stewart et al., 2011).

When entering mitosis, lamellipodial formation stops and the whole actin cytoskeleton gets severed by cofilin. Cofilin activity is subsequently inhibited in prometaphase through phosphorylation by LIM kinase and by interaction with AIP/WDR1 (Fujibuchi et al., 2005). This inactivation appears to be important, as continuous severing by cofillin causes the instability of the actin cortex and inhibits cell rounding (Fujibuchi et al., 2005; Kaji et al., 2008). After cofilin inactivation new filaments form, elongate and organize close to the cell surface *via* Ezrin/Radixin/Moesin (ERM) family proteins. The latter have been proposed to align actin filaments parallel to the plasma membrane due to their actin filament and transmembrane receptor binding domains, thereby driving cell rounding (Kunda & Baum, 2009; Théry & Bornens, 2008). Simultaneously to the actin reorganization the cell weakens its adhesion to the substrate (Figure 30). However, the cell does not loose completely contact with the substrate. Retraction fibres are formed during cell rounding connecting the mitotic cell body to remaining anchoring site. These fibres contain stationary parallel actin bundles pointing with their barbed ends away from the cell body. They furthermore contain Ezrin that probably crosslinks the actin bundles to the surrounding membrane (Kunda & Baum, 2009; Théry et al., 2005; Théry & Bornens, 2008).

The resulting shell of cross-linked and membrane associated actin provides the basis for proper spindle assembly and/or orientation as has been shown by numerous experiments for in *C. elegans* (Cowan & Hyman, 2007), Drosophila S2 cells (Carreno et al., 2008; Kunda et al., 2008) and mammalian cells *in vitro* (Fink et al., 2011; Théry et al., 2005; Toyoshima & Nishida, 2007b).

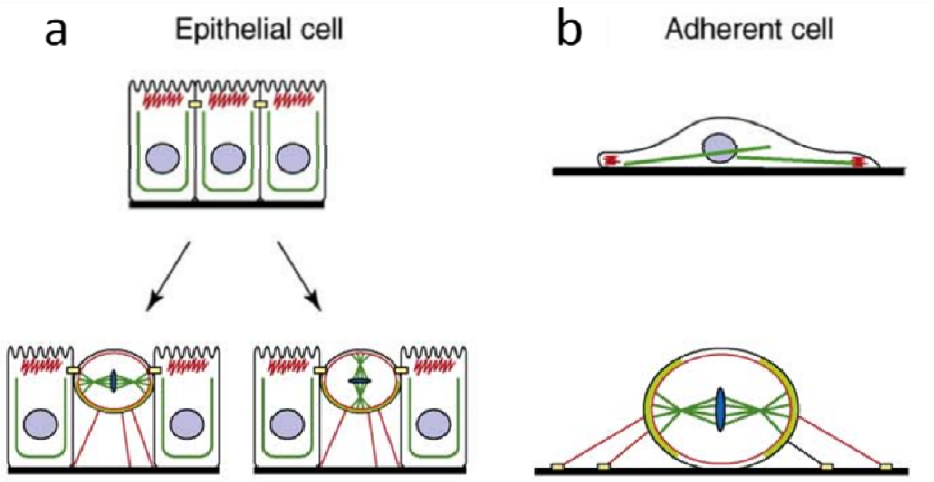

Figure 30. The cell cortex and spindle positioning. a) in epithelial cells, spindle orientation is determined by cortical cues that orientate it either parallel (symmetric) or perpendicular (asymmetric) to the plane of division, depending on genes expressed. This probably occurs by altering the way cortical cues are read by astral MTs. b) In adherent animal cells, spindles usually align parallel to the substrate. At onset of mitosis, cells retract their margins, leaving thin actin cables attached to the substrate. These cables define cortical marks within the cell cortex. Astral MTs then read these cues in the rigid, rounded mitotic cell cortex to assemble, orientate and position the mitotic spindle. Actin structures in red, MTs in dark green, DNA in blue, adhesion molecules in yellow, cortical cues in light green. (Adapted from Kunda & Baum, 2009).

2.5.8 Cortex polarization

Spindle alignment along the predetermined axis requires both astral microtubules and the actin cytoskeleton and is believed to involve dynein-dependent microtubule pulling forces functioning at the cell cortex (Laan et al., 2012).

Cdc42 is required for proper spindle positioning in polarized cells such as budding yeast and the *C. elegans* zygote, which both undergo asymmetric cell division (Gotta et al., 2001). Two new pathways for spindle orientation under the control of Cdc42 in non-polarized HeLa cells have been described: Cdc42 would regulate integrin dependent spindle positioning parallel to the substrate by controlling actin cytoskeleton organization and the cortical polarization of the lipid second messenger phosphatidylinositol (3,4,5)-trisphosphate (PtdIns(3,4,5)P3). Both pathways lead to the accumulation of the dynein/dynactin motor complex at the equatorial cortex plane in metaphase (Mitsushima et al., 2009; Toyoshima et al., 2007).

In many animal cells the Par complex is required to establish cortical polarity that directs spindle positioning. It consists of three proteins: partitioning defective 3 and 6 (Par-3 and Par-6) and the atypical protein kinase aPKC. Par-3 is required for the polarized cortical localization of Par-6 and aPKC. Par-6 regulates the kinase activity of aPKC. aPKC finally regulates cortical polarity by phosphorylating target proteins (Siller & Doe, 2009). The Par complex localizes to the anterior cortex in the *C. elegans* zygote and to the apical cortex of epithelial cells, including epidermal and neuronal progenitors in invertebrates and vertebrates.

Par-dependent spindle positioning is mediated through polarized localization of the NuMA family of proteins and the Dynein-Dynactin motor complex (Markus & Lee, 2011) (Dynein-Dynactin will be discussed in the section 2.5.9). NuMA (lin-5 in *C. elegans* and mud in *D. melanogaster*) encodes a large coiled-coil protein with multiple interaction partners, and was initially discovered and intensely studied for its role in mitotic spindle assembly in vertebrate cells in culture (Radulescu & Cleveland, 2010). The first hint at a possible role for NuMA in spindle orientation came from the discovery of its association with the vertebrate Partner of Inscuteable (Pins, also known as mPins, LGN, and GPSM2) (Du & Macara, 2004), whose homologs in *D. melanogaster* (Pins) and *C. elegans* (GPR-1 and GPR-2, thereafter referred to as GPR-1/2) are involved in ACD (Colombo et al., 2003; Gotta et al., 2003). Thus, Inscuteable (Insc) couples cortical cell polarity and spindle orientation (Figure 31).

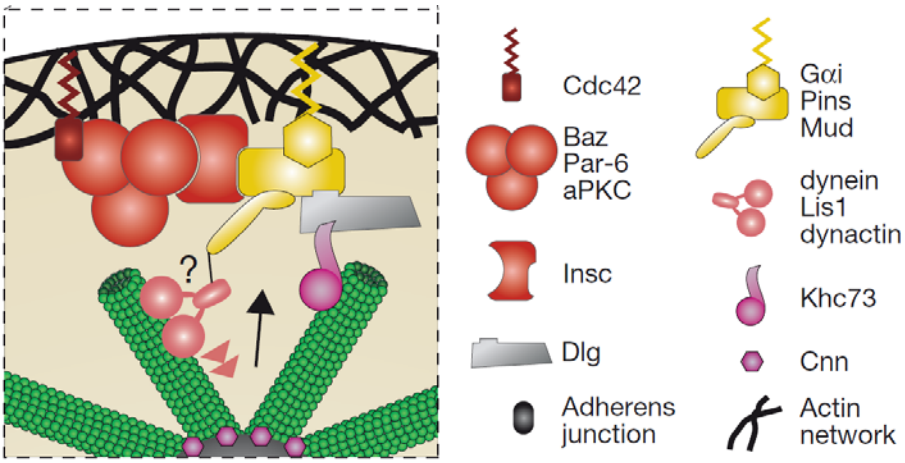

Figure 31. Linking cortical polarity and spindle orientation. Detail of the cortex of a dividing *D. melanogaster* NB. Note the presence of the evolutionary conserved Par complex (red) responsible for cortex polarization by recruiting the Gαi/Pins/Mud complex (yellow). The latter complex interacts with astral microtubules and motor proteins and can thereby transmit the cortex polarization to the mitotic spindle. (Adapted from Siller & Doe 2009).

2.5.9 Microtubule-actin interaction in mitosis

The interaction between the microtubule network, that builds up the spindle and organizes the chromosomes, and the stiff actin cortex, that gets polarized due to external cues, is achieved by several evolutionary conserved protein families. These proteins not only bind and stabilize MTs, but also exert forces on them.

The APC protein has been shown to interact with MTs directly and indirectly *via* EB1 protein, which is located at the microtubule plus-ends (Dikovskaya et al., 2001; Etienne-Manneville & Hall, 2003). APC is often recruited to the actin cortex where APC–EB1 interaction is thought to stabilize microtubules (Dikovskaya et al., 2001). The importance of APC and EB1 for spindle orientation has been demonstrated in symmetric division of the *D. melanogaster* neuroepithelium (Lu et al., 2001) and for asymmetric stem cell divisions (Quyn et al., 2010; Yamashita et al., 2003). In both cases APC polarization is achieved by its recruitment to adherens junctions and thus depends on their

distribution. Accordingly, EB1 siRNA knockdown in cultured cells resulted in the absence of astral MTs and therefore in spindle misorientation (Toyoshima & Nishida, 2007b).

Besides getting stabilized, astral MTs are often actively pulled towards the cortex by motor proteins. These pulling forces drive spindle positioning in yeast, worms, insect and mammalian cells (Knoblich, 2001; Siller & Doe, 2009). Emerging data from diverse model systems have led to the prevailing view that, during mitotic spindle positioning, polarity cues at the cell cortex leads to the recruitment of NuMA and cytoplasmic dynein. The NuMA/dynein complex is believed to connect, in turn, to the mitotic spindle *via* astral MTs, thus aligning and tethering the spindle.

Dynein is an evolutionary conserved motor protein complex that uses ATP hydrolysis to move towards MTs minus-end, thus towards the spindle poles in mitosis. Dynein associates with the multiprotein dynactin complex, through the p150^{Glued} subunit, which increases dynein processivity and tethers dynein to its cargo proteins (Schroer, 2004). p150^{Glued} uses its CAP-Gly domain to accumulate at MT plus-ends and at mitotic kinetochores, where contributes to dynein function. p150^{Glued} is also present at the centrosome where its CAP-Gly domain participates in anchoring MT minus-ends (Steinmetz & Akhmanova, 2008) (Figure 32).

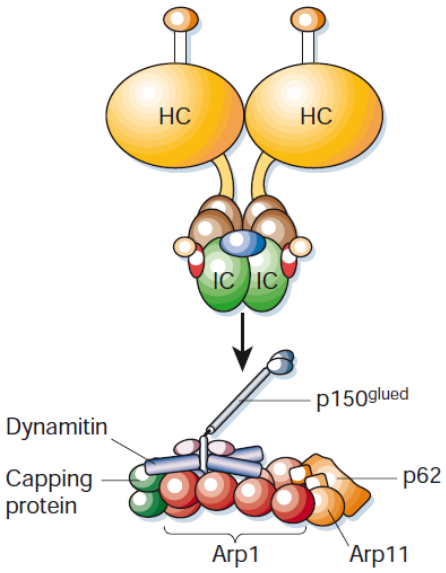

Figure 32. The dynein–dynactin complex. The dynein molecule, itself a complex of heavy (HC), intermediate (IC) and light chains, interacts with the p150^{Glued} subunit of the dynactin complex through its intermediate chains (arrow). The most prominent component of the dynactin complex is a short filament of the actin-related protein Arp1. (Adapted from Schliwa & Woehlke, 2003).

The dynein/dynactin complex and its regulators (Lis1/Nde/Ndl) have been proven essential for mitotic spindle positioning in many systems (Siller & Doe, 2008, 2009). Lis1 is required for the targeting of dynein to MT plus-ends and consequently the cell cortex. Lis1 may be important to maintain dynein at the plus-end by keeping the motor in an 'off' state, thus preventing it from

walking toward the minus-end (Markus & Lee, 2011; O'Connell & Wang, 2000). Ndl, a NudE-like protein, and Ndl are required for the normal wild-type frequency of dynein targeting to astral MT plus-ends. Ndl may stabilize or enhance the efficiency of Lis1 binding to dynein at the plus-end (Li et al., 2005).

Being fixed at the cell cortex and simultaneously moving along microtubules, dynein motor complexes effectively generate pulling forces that move MTs towards the cortex. This process is more efficient when coordinated with slow MT plus-end depolymerization to avoid counteracting forces due to microtubule pushing against the cortex (Laan et al., 2012; Moughamian & Holzbaur, 2012; Siller & Doe, 2009).

The mammalian protein NuMA links the dynein/dynactin-LIS1 complex to the cortically polarized LGN protein. NuMa couples therefore dynein motor activity to cortex polarity cues (Du & Macara, 2004; Siller & Doe, 2009).

2.6 Determination of the division plane

After separation of sister chromatids in telophase, the mother cell constricts giving rise to two daughter cells. To ensure equal partitioning of the genetic material, different mechanisms have evolved (Oliferenko et al., 2009).

In eukaryotes, mainly two mechanisms exist for determining the constriction site of the mother cell: mitotic apparatus independent positioning in yeast, and mitotic apparatus dependent positioning in animal cells.

The cleavage plane in animal cells is dictated by the position and orientation of the mitotic spindle at late anaphase (Burgess & Chang, 2005; Rappaport, 2005); although exceptions have been recently reported for NB asymmetric divisions in *D. melanogaster* (Cabernard et al., 2010) and *C. elegans* (Ou et al., 2010). Basically, astral MTs connect the centrosome to the actin cortex and the central spindle, consisting of overlapping MT bundles at the cell midzone after chromosome segregation (Oliferenko et al., 2009). It is widely accepted that these MTs control cortical contractility by maintaining active gradients of the small GTPase Rho which is crucial for cleavage furrow induction (Drechsel et al., 1996). Thereby GTP- bound, active Rho triggers F-actin assembly (Watanabe et al., 1997) and activates myosin II (Kimura et al., 1996) at the cell equator which causes cortical constriction.

Three mechanisms for cleavage plane positioning have been proposed (Figure 33):

(a) The cortex contractility at the equatorial zone is stimulated by the central spindle (central spindle stimulation). A number of proteins important for cytokinesis are known to accumulate at the central spindle during anaphase (Oliferenko et al., 2009), for example the kinesin-like protein MKLP1 that causes Rho activation.

(b) The cortex contractility is stimulated at the equatorial zone where subpopulations of stable astral MTs from the two poles converge. These MTs are thought to deliver stimulating factors (astral MTs stimulation).

(c) Astral MTs inhibit cortex contractility opposite to the spindle poles (polar relaxation). This results in the establishment of a gradient of cortical tension with the highest tension at the equator leading to its constriction (Paluch et al., 2006).

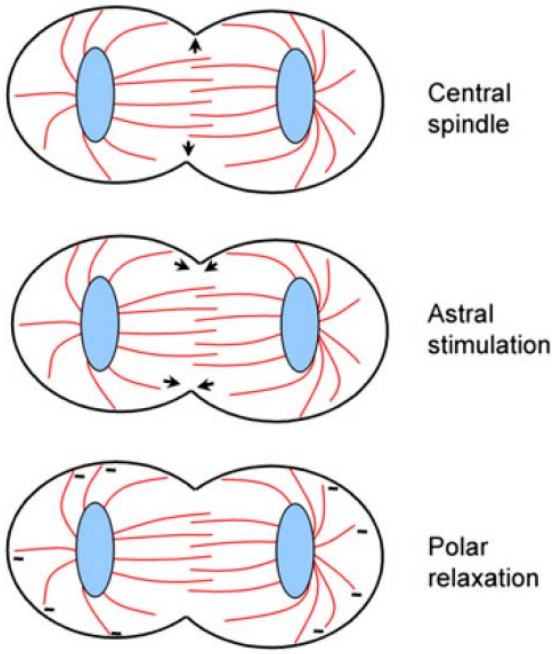

Figure 33. Models for cleavage plane positioning in animal cells. After chromosome segregation, the overlapping MT bundles at the cell midzone known as the central spindle specify the cleavage plane. In certain cell types, astral MTs stimulate cleavage furrow formation at the division site, whereas in some cases, astral MTs inhibit cortical contractility at the cell ends to promote cleavage furrow formation at the division site. (Adapted from Oliferenko et al., 2009).

Simultaneous inhibition and stimulation of cortical contractility could be achieved by different subsets of astral MTs, mainly varying in their stability (Foe & von Dassow, 2008; Murthy & Wadsworth, 2008): Stable MTs contacting the equatorial midzone could deliver Rho –activating proteins (like MKLP1) whereas astral MTs contacting the polar regions are highly dynamic and therefore too unstable to deliver the factors. Has been proposed that MTs specify the cleavage plane by directing the formation and spatial extent of a highly localized zone of RhoA activity (Bement et al., 2005).

The three proposed mechanisms are redundant and it has been shown that they work together to ensure the fidelity of the division site (Bringmann & Hyman, 2005).

3 Neural development

3.1 Overview

Neural development is the process that generates, shape, and reshapes the nervous system (NS), from the earliest stages of embryogenesis to the final years of life. The NS is an organ system that consists in two parts: the central nervous system (CNS) and the peripheral nervous system (PNS). NSs are found in most multi-cellular animals, but vary greatly in complexity. Defects in neural development can lead to cognitive, motor, and intellectual disability, as well as neurological disorders. The development of the NS proceeds in three phases: first, nerve cells are generated through cell division; then, having ceased dividing, they send out axons and dendrites to form profuse synapses with other, remote cells so that communication can begin; last, the system of synaptic connections is refined and remodelled according to the pattern of electrical activity in the neural network (reviewed in Albert et al., 2002).

During development, neural stem cells (NSCs) give rise to all the neurons of the mammalian CNS. They are also the source of the two types of macroglial cell in the CNS, astrocytes and oligodendrocytes. NSCs exist not only in the developing NS but also in the adult NS of all mammalian organisms, including humans (Gage, 2000). The adult brain show high neuroplasticity. Neurogenesis continues into adult life in restricted germinal layers. During adulthood, the two major locations of neurogenesis are the sub-ventricular zone (SVZ) adjacent to the lateral ventricules and the sub-granular zone (SGZ) in the dentate gyrus of the hippocampus.

3.2 Brain development

3.2.1 Neural tube formation

The nervous system is derived from the ectoderm, the outermost tissue layer of the embryo (reviewed in Albert et al., 2002). The mesoderm, middle layer, forms muscles and bones. The endoderm, inside layer, forms the epithelial lining of multiple systems. The neuroectoderm appears and forms the neural plate along the dorsal side of the embryo (Figure 34). This neural plate is the source of the majority of all neurons and glial cells. The neural plate wraps in on itself to make a hollow neural tube. The neural tube gives rise to both the spinal cord and the brain. Neural crest cells are also created during neurulation. Neural crest cells migrate away from the neural tube and give rise to a variety of cell types, including pigment cells and neurons. Signal proteins secreted from the ventral and dorsal sides of the neural tube act as opposing morphogens, causing neurons born at different dorsoventral levels to express different gene regulatory proteins. The notochord, a midline structure, is apparently responsible

for inducing the development of the brain and spinal cord. The notochord itself is mesodermal tissue and eventually gives rise to the vertebral column and cranium, which enclose and protect the brain and spinal cord.

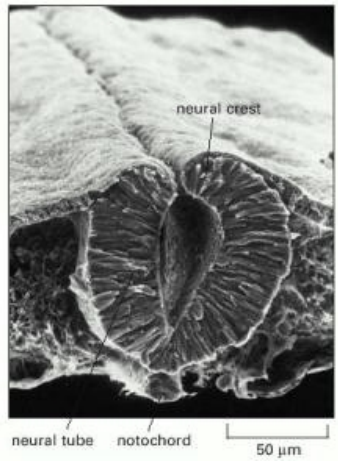

Figure 34. The neural tube. Scan electron micrograph showing a cross section through the trunk of a 2-day chick embryo. The neural tube is about to close and pinch off from the ectoderm; at this stage it consists (in the chick) of an epithelium that is only one cell thick. (Adapted from Albert et al., 2002).

3.2.2 Brain development

There are four subdivisions of the neural tube that will each eventually develop into distinct regions of the CNS by division of NSCs: The prosencephalon, the mesencephalon, the rhombencephalon and the spinal cord (Figure 35).

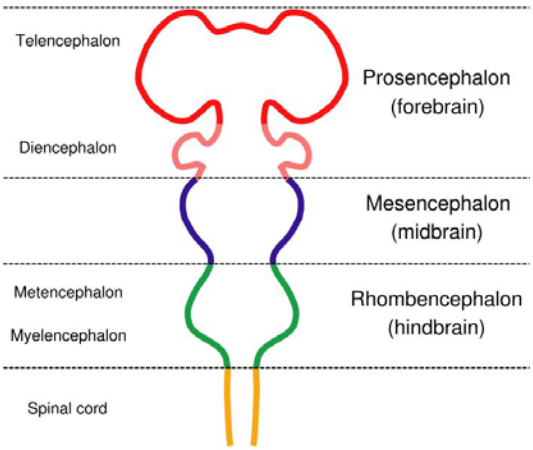

Figure 35. Diagram depicting the main subdivisions of the embryonic vertebrate brain. The encephalon begins to form when the neural tube swells and subdivides, first into the three primary vesicles (the prosencephalon, mesencephalon and rhombencephalon), and then into the five secondary vesicles (the telencephalon, diencephalon, mesencephalon, metencephalon and myelencephalon) (Extracted from File:EmbryonicBrain.svg; author Nrets,).

The telencephalon is the most rostral of the secondary vesicles. Two buds emerge from either side of its rostral portion to form the two telencephalic vesicles and will form the two cerebral hemispheres. Another pair of vesicles will become the olfactory bulbs and other structures that contribute to the sense of smell. The neurons of the telencephalon wall proliferate to form three distinct regions—the cerebral cortex, the basal telencephalon, and the olfactory bulb. The axons of these neurons will constitute the cortical white matter and corpus callosum. In the the remaining space between the telencephalon and the diencephalon on either side, the two lateral ventricles form, while the third ventricle forms in the space at the centre of the diencephalon.

The diencephalon also differentiates into distinct areas: the thalamus and the hypothalamus. On either side of the diencephalon also develop the optic vesicles. The optic vesicles lengthen and fold inward to form the optic peduncles and optic cups, which will give rise to the retinas and the optic nerves.

Compared with the prosencephalon, the mesencephalon undergoes far less transformation. The metencephalon differentiates into two major structures: the cerebellum and the pons. The myelencephalon forms the medulla oblongata. Lastly, the central canal, which persists while the medulla is forming, becomes the fourth ventricle. The entire portion of the neural tube that lies caudal to the five secondary vesicles becomes the spinal cord.

3.3 Neurogenesis

Vertebrate embryonic neurogenesis is a highly dynamic process during which a limited number of NSCs produce a highly diverse number of glial and neural cell types. NSCs are initially found as a single layer of neuroepithelial cells (NESCs) forming the neural tube. These cells first undergo a phase of massive proliferation, during which their number increases exponentially through symmetric divisions. Later on, the system switches to a neurogenic mode during which neuroepithelial progenitors start to divide in an asymmetric manner to self-renew and produce a more committed progeny (Figure 36).

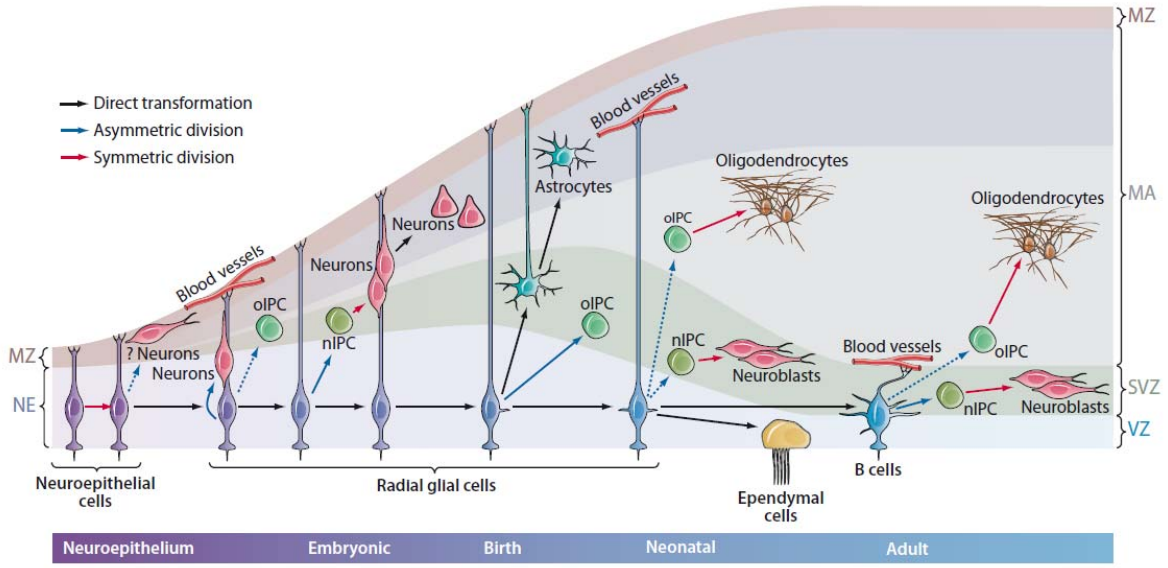

Figure 36. NSCs in developing and in the adult brain. Neuroepithelial cells in early development divide symmetrically to generate more neuroepithelial cells. As the developing brain epithelium thickens, neuroepithelial cells elongate and convert into radial glial (RG) cells. RG cells divide asymmetrically to generate neurons directly or indirectly through intermediate progenitor cells (nIPCs). RG cells have apical-basal polarity: apically, RG contact the ventricle, where they project a single primary cilium; basally, RG contact the meninges, basal lamina, and blood vessels. At the end of embryonic development, most RG begin to detach from the apical side and convert into astrocytes while oIPC production continues. A subpopulation of RG retain apical contact and continue functioning as NSCs in the neonate. Type B cells continue to function as NSCs in the adult. IPC, intermediate progenitor cell; MA, mantle; MZ, marginal zone; NE, neuroepithelium; nIPC, neurogenic progenitor cell; oIPC, oligodendrocytic progenitor cell; RG, radial glia; SVZ, subventricular zone; VZ, ventricular zone. (Adapted from Kriegstein & Alvarez-Buylla, 2009).

3.3.1 Progenitors cells

The neural plate is initially formed by a single layer of progenitor cells, theNESCs, which form the neuroepithelium (Figure 36). NESCs have epithelial characteristics and are highly polarized along their apico-basal axis with apical attachments to the ventricular surface and a basal fiber connecting the pial (basal) surface. The neuroepithelium is pseudostratified, with NESC nuclei found all along the apico-basal axis. These nuclei undergo interkinetic nuclear migration (INM), moving back and forth between the apical and basal sides of the tissue during their cell cycle, and undergoing mitosis at the ventricular surface. NESCs have a small apical domain, forming the ventricular surface and a large baso-lateral domain. These two membrane domains are separated by tight junctions preventing lateral diffusion of apical proteins. Before the onset of neurogenesis, NESCs undergo a phase of massive proliferation by symmetric division allowing the expansion of the neural progenitor cell population (Peyre & Morin, 2012). At the onset of neurogenesis, they switch to an asymmetric mode of divisions allowing self-renewal and neuron generation (Götz & Huttner, 2005).

Simultaneous with the beginning of neurogenesis, NESCss acquire characteristics associated with glial cells and are then called radial glial cells (RGCs) (Figure 36). They repress the expression of epithelial markers and start to express astroglial markers. Newly-born neurons use RG basal fibers

as a migration scaffold toward cortical layers. This results in progressive cortical thickening and basal fiber elongation. Tight junctions evolve into adherens junctions delimited by a Zona Occludens 1 (ZO-1) domain and higher amount of N-cadherin (Aaku-Saraste et al., 1996). These junctional complexes anchor the RGCs to each other and to the ventricular surface, they also allow the recruitment of cytoplasmic proteins such as Par3, aPKC, Par6 (Joberty et al., 2000), as well as, β-catenin and δ-catenin (Ho et al., 2000; Zhadanov et al., 1999). It is important to note that neural progenitor cells form a continuum from early development (NESC) through neurogenesis (RGC) and into adulthood (adult stem cells) (Merkle et al., 2004). As they maintain an apical attachment and divide apically, NES and RG cells are more generally called apical progenitors (APs).

Neurons derive from asymmetric division of RGCs either directly in a process called direct neurogenesis, or indirectly, through the production of intermediate progenitors (Figure 37). Indirect neurogenesis was first revealed in the neocortex by the identification of monopolar neural progenitor cells migrating basally in the SVZ to divide (Haubensak et al., 2004; Miyata et al., 2004; Noctor et al., 2004). These cells are called basal progenitors (BP) or intermediate progenitors (IP) (Figure 36). IP differ from RGC at the morphological and molecular levels. When produced by asymmetric division of a RGC, IP retract their apical attachment and basal extension, do not exhibit hallmarks of apico-basal polarity and migrate basally before they undergo mitosis (Attardo et al., 2008; Noctor et al., 2008). In their majority, RG-cderived IPs divide once symmetrically to give rise to two neurons (Noctor et al., 2004). This population of IP cells is a transit amplification compartment that allows indirect neurogenesis to increase the number of neurons (Lui et al., 2011).

It has been known that primates develop an additional germinal zone (outer subventricular zone or OSVZ) outside of the SVZ during brain development (Figure 37). Recently, these progenitors were identified as a new subtype of self-renewing progenitors named outer RGC (oRGCs) (Hansen et al., 2010). These cells maintain some RGC properties, such as the ability to self-renew, RG marker expression and the basal process. However, they do not possess an apical process or apico-basal polarity, nor do they undergo INM (Fietz et al., 2010; Hansen et al., 2010). Similar to RGCs, oRGCs divide asymmetrically to self-renew and produce the more committed cells (Hansen et al., 2010). oRG-like cells also exist in other species, including ferret (intermediate radial glial cells, IRGC) and mouse (outer VZ progenitor cells, oVZ cells), during the middle to late neurogenic stage (Fietz et al., 2010; Reillo et al., 2011; Shitamukai et al., 2011; Wang et al., 2011). The number of oRG cells is correlated with brain size, which is larger in animals with bigger brains (e.g., humans, monkeys, and ferrets) and smaller in the animals with smaller brains (e.g., mice and rats). Therefore, oRG cells are thought to be the key to the evolution of brain size (Lui et al., 2011; Reillo et al., 2011). However, the mechanism of their production and maintenance is largely unknown.

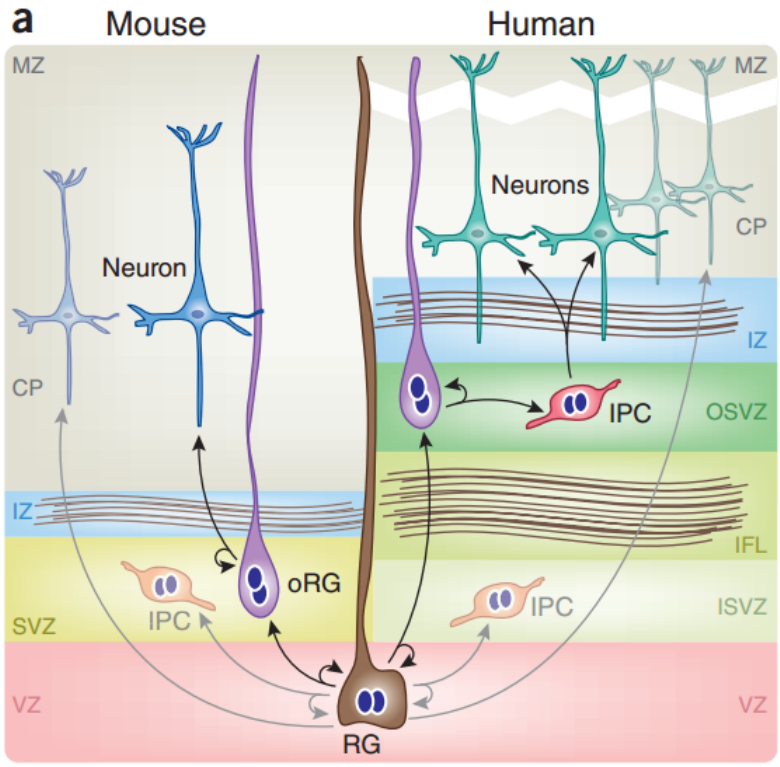

Figure 37. Comparisons of mouse and human cortical germinal zones. Similar progenitor cell types reside in the mouse (left) and human (right) developing cortex. These include the RGCs (brown), which divide at the ventricular surface to generate either an IPC (orange), an oRG progenitor cell (purple) or a neuron (blue) while also renewing themselves (circular arrows). The mouse and human OSVZ or oRG progenitor cells both lack contact with the ventricular (apical) surface but maintain their pial (basal). However, the human cortex differs from that of the mouse in two respects. First, human but not mouse has a cytoarchitectonically distinct extra germinal zone, the OSVZ (dark green), that is separated from the ISVZ by an inner fiber layer. Second, oRG cells in mouse generate neurons directly through self-renewing asymmetric division, whereas human oRG cells generate neurons through transit-amplifying cells (that is, IPCs). (Adapted from Molnár et al., 2011).

3.3.2 Molecular control of neurogenesis

Regulation pathways of the transition from one progenitor stage to the next (e.g. from NESC to RGC, or from RGC to IP) have been identified. A small number of 'proneural genes', which encode transcription factors of the basic helix-loop-helix (bHLH) class, are both necessary and sufficient, in the context of the ectoderm, to initiate the development of neuronal lineages and to promote the generation of progenitors that are committed to differentiation (Bertrand et al., 2002).

An essential role of proneural proteins is to restrict their own activity to single progenitor cells. Proneural genes inhibit their own expression in adjacent cells, thereby preventing these cells from differentiating. This is achieved through activation of the Notch signalling pathway (Bertrand et al., 2002). The Notch signalling pathway and its main effectors, the Hes proteins, have a role in keeping progenitors undifferentiated and insulating them from specification signals, so that progenitors that escape Notch inhibition at different times acquire distinct fates (Guillemot, 2005). However, Notch signalling does not appear to straightforwardly maintain all progenitor cells, since

Notch activation has been shown to promote RGC identity (Yoon & Gaiano, 2005). Notch signalling is activated by the cell-cell interaction between Notch-expressing cells and Delta-expressing cells. The Notch receptor is mainly expressed in the RGCs and is distributed along the entire cell membrane. A Notch ligand, Delta-like 1, is specifically and transiently expressed in the differentiating cells, particularly in the VZ (Yoon & Gaiano, 2005). It is most likely that Notch-Delta interaction efficiently occurs at the apical side of the VZ. IPCs and migrating neurons along the basal process of RGCs are also thought to contribute Notch-Delta interactions and maintain RG proliferation (Lui et al., 2011; Yoon et al., 2008). However, oRGCs that are located outside of the VZ require Delta from their sibling cell, which appears to interact with the sister oRG cell body (Shitamukai et al., 2011).

Numb is an intracellular inhibitor of Notch. In mice, loss of Numb leads to severe defects that differ dramatically depending on when Numb activity is eliminated in the cortex (Fishell & Kriegstein, 2005, 2003). This indicates that Numb and Numb-like have complex roles in neurogenesis that may involve interactions with additional pathways besides Notch.

Wnt signalling is also central to regulate neural stem cell activity. In the cortex, a stabilized form of β-catenin promotes either the self-renewal (Chenn & Walsh, 2002) or the neuronal differentiation of progenitors (Hirabayashi et al., 2004), depending on when it is expressed during cortical development, suggesting that a timing mechanism modifies the response of cortical progenitors to the Wnt pathway (Hirabayashi & Gotoh, 2005). The fibroblast growth factor (FGF) signalling pathway has also been shown to modify the response of cortical progenitors to β-catenin, mediating a switch from proliferation (in the presence of FGF2) to neuronal differentiation (in its absence) (Israsena et al., 2004). FGF signalling promotes self-renewal, possibly through activation of *Olig2* (Hack et al., 2004), and induces the RG phenotype, suggesting possible interactions between Notch and FGF signalling pathways in maintaining this progenitor population.

REST/NRSF, a factor known to repress neuronal genes in non-neuronal cells, turns out to be another important regulator of neuronal lineage progression (Ballas et al., 2005). The transition from pluripotent stem cells to neural stem cells and then to neurons involves a progressive reduction of REST binding to neuronal promoters. Moreover, the timing of neural gene expression may be regulated by differential affinity of REST binding sites (Ballas et al., 2005).

Once neurogenesis is achieved, gliogenesis is initiated by several developmentally regulated gliogenic signals, such as FGF2 (Figure 38). These signals activate glial differentiation and, in parallel, inhibit neurogenesis through various mechanisms: activation of proneural inhibitors, degradation of proneural protein and repression of proneural gene transcription. Notch signalling has been shown to have a gliogenic activity and is likely to act, in part, by inhibiting proneural gene activity (Bertrand et al., 2002).

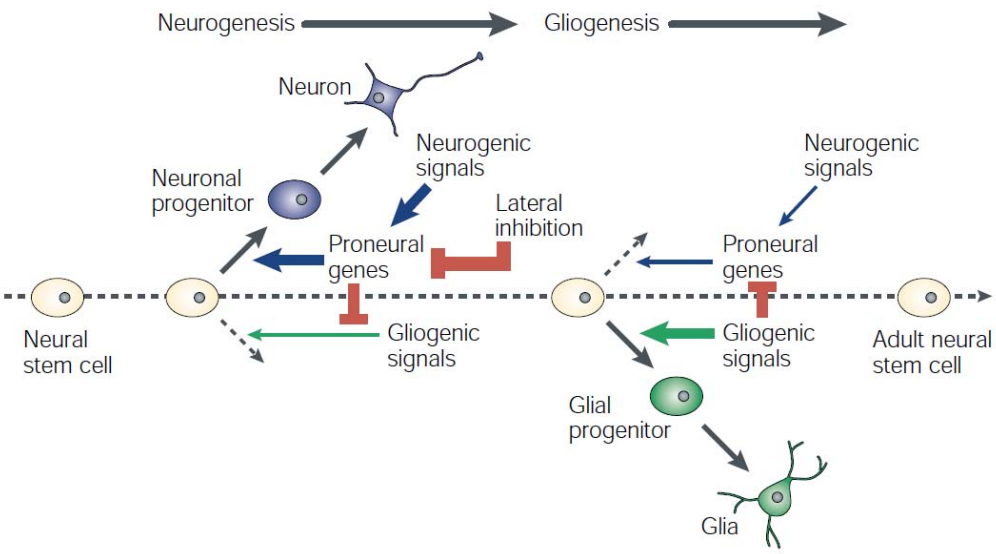

Figure 38. Role of vertebrate proneural genes during the neurogenic and gliogenic phases of neural development. Proneural proteins accumulate at high level in progenitor cells, resulting in the activation of a neuronal-differentiation pathway, the inhibition of glial differentiation, and cell-cycle arrest. Notch signalling (lateral inhibition) downregulates and/or inhibits proneural genes in other cells that are thereby prevented from entering the neuronal pathway. Gliogenesis is initiated by several developmentally regulated gliogenic signals (e.g. FGF2). These signals activate glial differentiation and inhibit neurogenesis. Stem cells persist in the adult brain. (Adapted from Bertrand et al., 2002).

3.3.3 Cell division of neural progenitors and cell fate

At the onset of neurogenesis, progenitor cells switch from symmetric to asymmetric divisions in order to produce committed neural cells. The orientation of the axis of division has been shown to be correlated with the choice between symmetric and asymmetric modes of cell division in a number of systems (Peyre & Morin, 2012).

Ventricular NE progenitors harbour a small cortical apical domain and a basal-lateral domain that includes a thin and extended basal process connected to the pial surface of the tissue (Figure 39). During an initial proliferative phase, NE progenitors amplify their pool through symmetric (proliferative) divisions. Recent studies using zebrafish provide some clues to understanding NE cell divisions during the proliferative stages (Alexandre et al., 2010). In zebrafish development both apical and basal processes are able to re-establish themselves, even after the epithelial structure is asymmetrically segregated. Re-extension of the basal process has also been observed in the early neurogenic stage in mice, whereas it is rarely observed in the middle-to-late stage (Miyata et al., 2004; Shitamukai et al., 2011). NE progenitors later switch to a neurogenic phase during which they divide asymmetrically to renew RGCs and produce a more committed daughter cell, which migrates basally.

RGCs maintain their marked apico-basal polarity and undergo asymmetric cell division to self-renew and also to produce a daughter that is either a neuron or an IPC (Figue 38). Daughter neurons often migrate along parental RG fibers and neuronal migration continues even while the

guiding RG cell is dividing (Noctor et al., 2004, 2008). IPC frequently have multipolar processes and do not appear to contact the ventricle or pial surface, but they do display a predilection to divide with a cleavage plane parallel to the ventricular surface (Haubensak et al., 2004; Noctor et al., 2004, 2008). IPCs undergo symmetrical divisions to produce two neurons or may divide symmetrically to produce two additional IPCs (Haubensak et al., 2004; Miyata et al., 2004; Noctor et al., 2004). Similar to RGCs, oRGCs divide asymmetrically to self-renew and produce the more committed cells (Hansen et al., 2010).

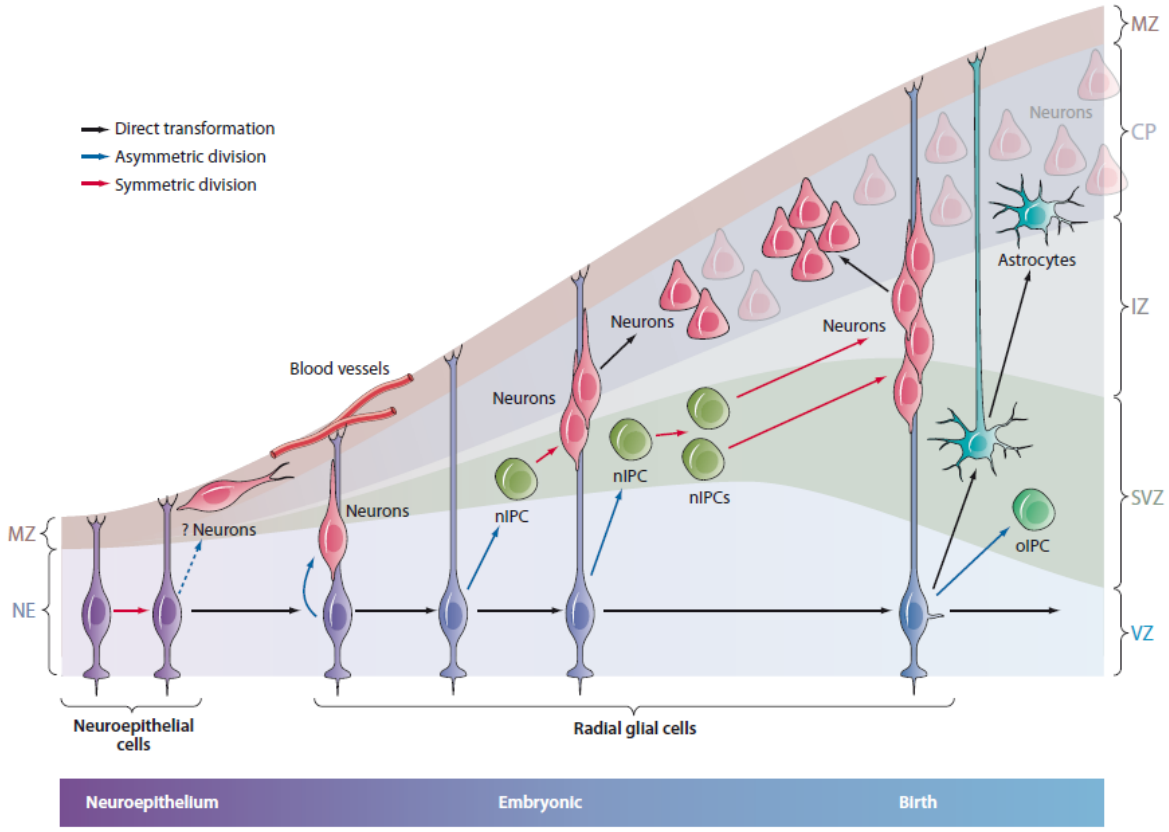

Figure 39. Division of neural progenitors. During an initial proliferative phase, NE progenitors amplify their pool through symmetric divisions. RGCs generate neurons directly through asymmetric division, indirectly by generation of nIPCs and one or two round of amplification. This additional amplification stage may be fundamental to increase cortical size during evolution. oIPCs generate oligodendrocytes. RGCs begin to detach from the apical side and convert into astrocytes. CP, cortical plate; IZ, intermediate zone; MZ, marginal zone; nIPC, neurogenic intermediate progenitor cell; RG, radial glia; SVZ, subventricular zone; VZ, ventricular zone (Adapted from Kriegstein & Alvarez-Buylla, 2009).

Initial observations in the ferret neocortex suggested that apico-basal divisions are asymmetric and neurogenic, whereas planar divisions are symmetric and proliferative. However, the vast majority of neural progenitors divide with a near planar orientation even at stages where asymmetric divisions predominate (Kosodo et al., 2004; Noctor et al., 2008). This suggested that minor shifts in spindle orientation may regulate symmetric versus asymmetric division by causing

the cleavage plane to respectively either bisect or bypass the apical domain, whose constituents could act as cell fate determinant(s) maintaining the RG fate (Kosodo et al., 2004; Marthiens & Ffrench-Constant, 2009).

Segregation of the apical membrane exclusively to one daughter cell normally occurs in no more than 10–20% of apical divisions during the neurogenic stage (Asami et al., 2011; Konno et al., 2008; Shitamukai et al., 2011). Because both daughters inherit the apical membrane during most RGC divisions, structural asymmetry could be instead generated by the asymmetric inheritance of the basal process in the majority of RGC divisions (Miyata et al., 2004; Shitamukai et al., 2011). RGC fate has also been shown to be tightly correlated with inheritance of the basal process, whereby the daughter cell that does not inherit the basal process mostly differentiates into neurons or IP cells (Shitamukai et al., 2011; Shitamukai & Matsuzaki, 2012). In the majority of RGC divisions, one daughter cell inherits the entire epithelial structure and maintains the capability to acquire RGC identity, whereas the other cell inherits only the apical epithelial domain and is thus committed to differentiate into a neuron or IPC.

A prediction of this model is that the loss of planar spindle orientation should favour asymmetric divisions and lead to accelerated neurogenesis. Indeed, studies analyzing the loss of function of a number of different genes have described a correlation between spindle orientation defects and premature neuronal differentiation at the expense of RGCs in the cortex (Feng & Walsh, 2004; Gauthier-Fisher et al., 2009; Godin, Colombo, et al., 2010; Yingling et al., 2008). However, in the mouse cortex and in the chick spinal cord, the high proportion of oblique divisions resulting from randomization of spindle orientation by Pins or NuMA loss of function did not accelerate neurogenesis but caused the scattering of progenitors in the SVZ (Konno et al., 2008; Morin et al., 2007; Peyre et al., 2011). Clonal fate analysis *in vivo* showed that these ectopic progenitors retain the molecular signature of their ventricular counterpart, indicating that they have not changed their identity (Konno et al., 2008; Morin et al., 2007; Shitamukai et al., 2011).

The “nuclear residence hypothesis” predicts that a signal influencing AP fate in an INM-dependent manner should be highly polarized along the apical-basal axis. In the developing mouse cortex, slowing-down of apical-to-basal INM by myosin II inhibition has been found to result in a cell fate change, in this particular case yielding more neurogenic IPs at the expense of proliferative APs (Schenk et al., 2009; Taverna & Huttner, 2010). Thus, INM can control the exposure of AP nuclei to proliferative versus neurogenic signals along the apical-basal axis, thereby also influencing AP fate.

3.3.4 Interkinetic nuclear migration

One aspect of NECs activity retained by RGCs is the complex mitotic behavior known as interkinetic nuclear migration (INM). The NECs exhibit two remarkable features that, intriguingly, are interrelated: pseudostratification and INM. Pseudostratification refers to the fact that although all NECs extend from the apical surface of the neuroepithelium to the basal lamina

throughout their cell cycle, their nuclei are found at various positions along this apical-basal axis resulting in a multilayer appearance (Baye & Link, 2007; Miyata, 2008). INM refers to the fact that mitosis of NECs occurs at (or very close to) the apical surface of the neuroepithelium, whereas S phase usually takes place at a more basal location, with apical-to-basal nuclear migration in G1 and basal-to-apical nuclear migration in G2 (Baye & Link, 2007; Miyata, 2008). Hence, INM is responsible for the pseudostratified appearance of the neuroepithelium. INM can be regarded as a highly specialized form of the evolutionary conserved process of nuclear migration and positioning (Taverna & Huttner, 2010).

The transformation from NE to RG cells is associated with a major change with regard to INM. Whereas in NECs INM may extend over their entire apical-basal axis, INM in RGCs does not extend into the portion of the cell that traverses the neuronal layers, but is confined to the portion of the cell residing in the VZ and, when present, the SVZ (Götz & Huttner, 2005).

A study reports evidence that inhibition of INM does not affect cell cycle progression. Specifically, upon interference with INM in the developing mouse cortex using the myosin II inhibitor blebbistatin, no difference in the length of the various cell cycle phases and in progression through mitosis of progenitors in the VZ was observed (Schenk et al., 2009). On a general note, the findings that INM is dispensable for cell cycle progression of apical progenitors (NECs and RGCs) is not surprising, given the existence of other neural progenitors that progress through the cell cycle without INM, such as IPs (Taverna & Huttner, 2010). Notably, the converse does not hold true: INM has been found to depend on cell cycle progression, as shown in several studies of developing mouse cortex. Specifically, pharmacological treatments inducing S phase or G2/M arrest resulted in concomitant inhibition of INM in the basal and apical region of the VZ, respectively (Baye & Link, 2007).

The localization of APs primary cilium and centrosomes at the apical plasma membrane, implies that the INM during G1 is directed away from the centrosome (ab-centrosomal INM), and that during G2 is directed toward the (by then duplicated) centrosomes (ad-centrosomal INM) (Figure 40). There is a lack of physical proximity between nucleus and centrosomes in APs in interphase. This distinguishes APs from their progeny: IP, OSVZ progenitors and neurons, which also show nucleokinesis but in which the centrosomes are located in the perinuclear area (Farkas & Huttner, 2008; Fietz et al., 2010; Hansen et al., 2010; Taverna & Huttner, 2010).

In basal-to-apical INM (ad-centrosomal), the AP nucleus is moved, as a cargo, along MT tracks (Figure 40). As the orientation of MT is with their minus-ends toward the centrosome, such nuclear movement would be expected to be mediated by minus-end-directed MT-based motor proteins, such as dynein (Baye & Link, 2007). Evidence that this is so has come from studies of the centrosomal proteins Cep120, TACCs, and Hook3 (Ge et al., 2010; Xie et al., 2007) and of the Lis1 protein (Gambello et al., 2003; Tsai et al., 2005). Upon reduction of Lis1 levels in the developing rodent cortex, basal-to-apical INM is inhibited, and mitoses are no longer confined to the apical surface but observed throughout the VZ. Further support for dynein motors mediating the basal-to-apical INM has come from studies of the developing zebrafish CNS (Schroer, 2004). In the

developing mouse cortex, SUN-KASH complexes mediate the coupling between the nucleus and the centrosome and provide anchors in the nuclear envelope for cytoplasmic dynein/dynactin during neuronal migration (X. Zhang et al., 2009). These studies provide compelling evidence that the MT minus-end-directed dynein motor system is involved in basal-to-apical INM and that APs possess a protein-protein interaction network that links the nucleus to microtubules via the dynein motor system. Plus end-directed MT-based motors of the kinesin type may be involved in apical-to-basal INM (ab-centrosomal). The outer nuclear envelope KASH-domain-containing protein Syne2 interacts with kinesin complexes (X. Zhang et al., 2009) and the MTs in APs are oriented parallel to the apical-basal axis, with the plus ends directed away from the centrosomes (Norden et al., 2009), thus providing a possible track to move the nucleus via a plus end-directed motor.

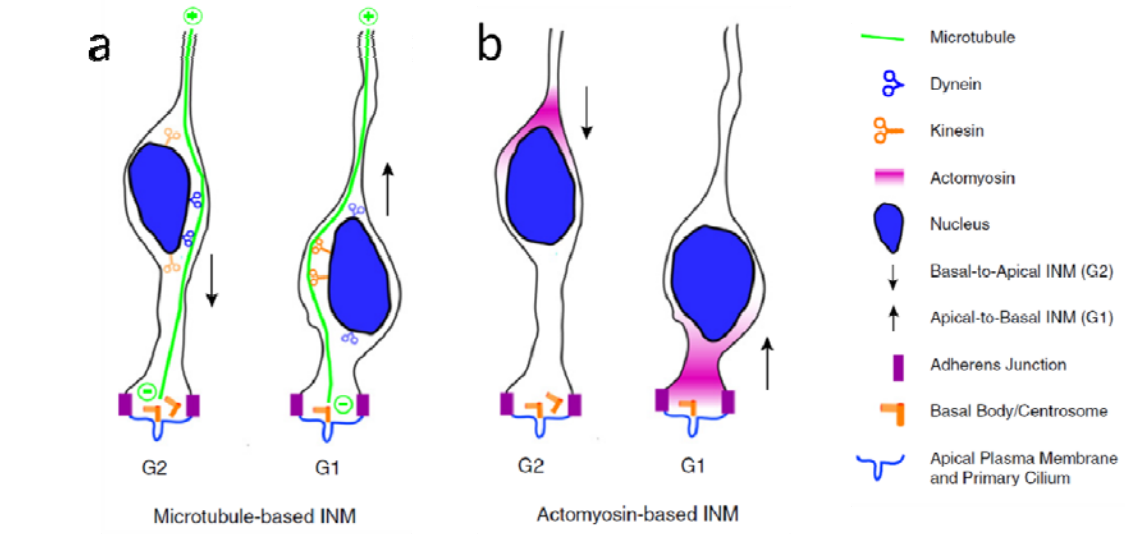

Figure 40. MT-based and Actomyosin-based INM. a) Ad-centrosomal, MT minus end-directed, dynein-based basal-to-apical INM in G2; ab-centrosomal, MT plus end-directed, kinesin-based apical-to-basal INM in G1. b) Basal-to-apical INM in G2, and apical-to-basal INM in G1, both driven by directional actomyosin constriction. (Adapted from Taverna & Huttner, 2010).

Actomysin plays also a role in basal-to-apical INM. Direct evidence comes from a study on the zebra fish retina (Norden et al., 2009). During most of the cell cycle, nuclear movement is a largely stochastic process. Persistent directed movement of the nucleus was observed only immediately before and after mitosis. Pharmacological inhibition of myosin II function prevented basal-to-apical INM but not interference with dynactin and microtubule function. This work suggests that in this system MT minus-end-directed dynein motors play only a minor role (Norden et al., 2009). It was proposed that the actomyosin-based apical- to-basal INM is mechanistically different from the MT-based basal-to-apical INM in that the nucleus is not moved as a cargo but, rather, via directional myosin-II-dependent constriction (Schenk et al., 2009).

It has been proposed that INM influences AP fate by determining the time the AP nucleus spends at any given location along the apical-basal axis during the cell cycle.

3.4 Mechanisms of mitotic spindle orientation in vertebrate neural progenitor cells

Live imaging in the chick neuroepithelium has shown that the mitotic spindle initially forms with a random orientation and that planar orientation is achieved through directed spindle rotation during early metaphase (Peyre et al., 2011; Roszko et al., 2006). LGN is enriched in the lateral membrane of both mouse and chick dividing neural progenitors (Konno et al., 2008; Peyre et al., 2011) and this lateral distribution is necessary for the rotation and for planar orientation of the spindle (Konno et al., 2008; Morin et al., 2007; Peyre et al., 2011) (Figure 41). LGN is recruited to the cell cortex by GDP-bound Gαi subunits and recruits NuMA to the lateral cortex. Removing LGN, NuMA, or Gαi, as well as interfering with the LGN/Gαi interaction, suppress spindle rotation during metaphase and result in defects in final spindle orientation at anaphase. Conversely, homogenization of the complex at the cell cortex by overexpression of Gαi subunits results in erratic spindle movements and random orientation. It is postulated that the restricted localization of the LGN complex concentrates pulling forces at the lateral cortex to dictate the plane of cell division. Interestingly, Lis1 has been reported to be involved in planar spindle orientation (Gauthier-Fisher et al., 2009; Yingling et al., 2008). Remarkably, both loss of LGN and of Lis1 result in almost complete spindle randomization in apical progenitors (Konno et al., 2008; Morin et al., 2007; Peyre et al., 2011; Yingling et al., 2008), suggesting that the cortically anchored LGN complex, together with the dynein/dynactin complex, is the key player in the transmission of forces from the cell cortex to astral MTs and the spindle.

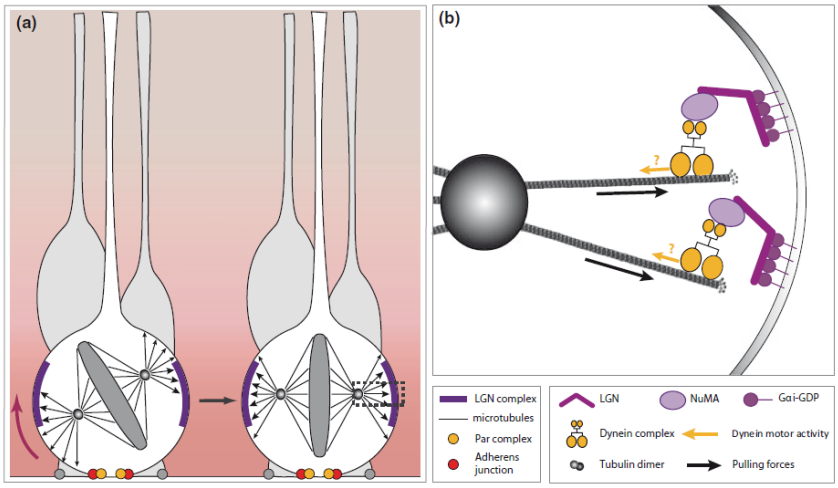

Figure 41. Mechanisms of mitotic spindle orientation in vertebrate neural progenitor cells. a) At the onset of mitosis the mitotic spindle is formed with a random orientation relative to the cell's apico-basal polarity (left). The spindle then undergoes a rapid movement of rotation and aligns with the apical surface. This planar orientation is maintained until anaphase. The LGN complex (purple) is enriched in a ring located at the lateral cell cortex where it concentrates pulling forces on astral microtubules (large arrowheads). Outside of the ring, pulling forces are weaker or absent (small arrowheads), and this results in a force imbalance and rotation of the spindle until it reaches a planar orientation. b) The LGN complex: Cortically anchored Gαi-GDP subunits interact with LGN and allow the recruitment of NuMA to the cell cortex. Together orient and maintain the mitotic spindle in a planar position. The complex could interact with the Dyein/Dynactin complex via NuMA to generate pulling forces on the MTs (Adapted from Peyre & Morin, 2012).

In the mouse developing neocortex, where low levels of Insc are expressed, apico-basal and oblique divisions are rare, and most cells divide in a planar fashion. Remarkably, in these cells, loss of Insc function increases the number of planar divisions, while its overexpression favors oblique and apico-basal divisions (Konno et al., 2008; Postiglione et al., 2011). Basal levels of Insc may induce a background level of imprecision that could control the balance between divisions in which the cleavage plane bisects or bypasses the apical domain in a stochastic manner (Postiglione et al., 2011). Insc is enriched apically in dividing cells (Konno et al., 2008; Postiglione et al., 2011), possibly in a Par3 dependent manner (Izaki et al., 2006). Insc may actively orient the spindle by recruiting the LGN complex apically through the conserved Insc/LGN interaction (Izaki et al., 2006). Specific defects in spindle orientation have not been reported in NE or RG cells lacking Par complex members, although gain and loss of function of Par3 and Par6 affect the mode of division (proliferative versus neurogenic) of mouse cortical progenitors (Costa et al. 2008; Bultje et al. 2009).

Adhesion complexes, such as adherens junctions, may help position LGN and NuMA. In mouse RGCs, inhibition of β1-integrin at the apical cell surface as well as knockout of α2-laminin, resulted in slightly more planar divisions than in the control situation (Loulier et al., 2009).

Any major defect in spindle assembly, such as the formation of mono or multipolar spindles is likely to affect spindle orientation. Subtle defects in the molecular composition of spindle poles and in the production of astral microtubules may have more relevant effects. For example, loss of Lis1 (Yingling et al., 2008), Nde1 (Yuanyi Feng & Walsh, 2004), HTT (Godin, Colombo, et al., 2010) from spindle poles and Lfc and Tctex from spindle MTs (Gauthier-Fisher et al., 2009) results in significant defects in spindle orientation and neurogenesis.

4 Context of the project

HTT is a large and ubiquitously expressed protein. Addressing its normal function is a priority in order to understand the pathology, HD. In this context, my PhD project was devoted to the functional validation of a novel tool, pARIS-htt, and the description of HTT role during mitosis.

Generate and validate a HTT synthetic gene to study its normal functions in a full-length context

HTT large size has hampered studies using the full-length protein. Up to date, most of the models for HD, including cell lines, flies, worms, zebrafishes, mice and rats, were generated using only the Exon 1 of HTT. Taking into account that Exon 1 represents only 3% of the full-length HTT, the development of a new tool that would permit the expression of the full-length protein and the study of the function of wild-type HTT was crucial.

We designed a construction called pARIS-htt encoding the full-length protein with a wild-type (23Q) or pathologic (100Q) expansion. We validated pARIS-htt using a Golgi reassembly assay. We used HeLa cells stably expressing GFP-mannosidase II that permitted us to monitor the dissambly/reassembly of Golgi particles after MT depolymerisation. Furthermore, we analyzed the dynamics of BDNF-eGFP-containing vesicles in mouse neuronal cells using fast 3D videomicroscopy. The requirements for HTT in the organisation and maintenance of the Golgi as well as in vesicular dynamics are linked to the interaction between HTT and components of the dynein/dynactin complex (Caviston et al., 2007; Colin et al., 2008; Gauthier et al., 2004; Zala et al., 2008). For that reason, we also generated mutant versions of pARIS-htt unable to interact with protein partners such as dynein and HAP1.

Investigate the role of wild-type and mutant HTT during mitosis

Given the predominant neurological signs and striking neuronal death in HD, most studies on HTT function have focused on postmitotic neurons and have revealed major roles for HTT in transcription, apoptosis protection and axonal transport. Nevertheless HTT is a scaffold protein and has many interactors. Within the cell, HTT is found in the nucleus and in the cytoplasm, in neurites and at synapses and it associates with various organelles and structures. In addition, molecular motors implicated in vesicular transport and with which HTT interacts, are important for correct spindle positioning during cell division.

As a first approach, we investigated the loss of function of wild-type HTT in dividing cells. We depleted endogenous HTT from cells in culture using siRNAs. We measured the spindle angle and the localization of important proteins involved in cell division: NuMa, dynein, $p150^{Glued}$. *In vivo* we inactivated *Htt* gene, by *in utero* electroporation and genetic ablation, and measure the cleavage plane of apical progenitors and their cell fate during corticogenesis. As a model of asymmetric cell division, we used NBs from transgenic *D. melanogaster*.

It has been reported that HTT polyQ mutation leads to disorganization of the centrosome and a subsequent disruption of the cell cycle leading to aneuploidy, micronuclei and dysmorphic cells (Sathasivam et al., 2001). Impaired adult neurogenesis was revealed in the DG of HD mouse models (Phillips et al., 2005; Simpson et al., 2010). In contrast, embryonic neurogenesis in HD condition has been poorly addressed. However, premanifest HD mutation carriers have smaller intracranial adult brain volume compared with controls that could result from an abnormal development (Nopoulos et al., 2010). Thus, it was a prioritary question for us to address the effect of the polyQ expansion in HTT during cell division and embryonic neurogenesis.

First observations were done regarding MT dynamics in wild-type and polyQ conditions and measuring the spindle angle. We used HeLa cells transfected with wild-type and mutant HTT constructs, neuronal cells lines derived from knock-in mice and mouse embryonic fibroblasts (MEFs). Analysis of the localization and interaction of +TIP, such as EB3, $p150^{Glued}$, CLIP-170, and dynein was also performed. We explored the role of HTT phosphorylation at S421 by Akt using phospho-HTT specific antibodies and HTT point-mutants. Concerning embryonic neurogenesis, we used HD mouse models to measure the cleavage plane of neural progenitors at different stages. The cell fate of the newly generated cells was also studied. To conclude, we utilized *D. melanogaster* models of HD and analysed NBs division.

RESULTS AND DISCUSSION

5 pARIS-htt: a new tool to study huntingtin functions

5.1 Study presentation

HTT is a multi-domain protein whose function is yet to be fully understood. This absence of information is due in part to the difficulty of manipulating large DNA fragments by using conventional molecular cloning techniques. Consequently, few studies have addressed the cellular function(s) of full-length HTT and its dysfunction(s) associated with the disease.

We describe a flexible synthetic vector encoding full-length HTT called pARIS-htt (**A**daptable, **R**NAi **I**nsensitive & **S**ynthetic). pARIS-htt was designed with the aim to facilitate mutagenesis, tagging and cloning into diverse expression plasmids. To achieve that, the cDNA coding for full-length human HTT was modified. As a result, pARIS-htt is insensitive to four different siRNAs allowing gene replacement studies, contains unique restriction sites (URSs) dispersed throughout the entire sequence and multiple cloning sites (MCS) at the N and C-terminal ends and finally, is Gateway compatible.

HTT regulates dynein/dynactin-dependent trafficking of vesicles, such as BDNF-containing vesicles, and of organelles, including reforming and maintenance of the Golgi (Caviston et al., 2007; Gauthier et al., 2004). Based on this, we used different cellular assays to validate pARIS-htt constructs. We demonstrated that wild-type pARIS-htt compensates for the defect induced by silencing endogenous HTT in Golgi apparatus reformation following reversible MT disturbance. Similarly, it rescues the defective BDNF transport in absence of endogenous HTT. A mutant form of pARIS-htt that contains a 100Q expansion as well as HTT devoid of either HAP1 or dynein interaction domains are unable to rescue loss of endogenous HTT.

5.2 Article I

Raúl Pardo*, **Maria Molina-Calavita***, Ghislaine Poizat, Guy Keryer, Sandrine Humbert and Frédéric Saudou. **pARIS-htt: an optimised expression platform to study huntingtin reveals functional domains required for vesicular trafficking.** Mol. Brain. 2010

*equal first authors

Molecular Brain

RESEARCH Open Access

pARIS-htt: an optimised expression platform to study huntingtin reveals functional domains required for vesicular trafficking

Raúl Pardo[†1,2,3], Maria Molina-Calavita[†1,2,3], Ghislaine Poizat[1,2,3], Guy Keryer[1,2,3], Sandrine Humbert[1,2,3] and Frédéric Saudou[*1,2,3]

Abstract

Background: Huntingtin (htt) is a multi-domain protein of 350 kDa that is mutated in Huntington's disease (HD) but whose function is yet to be fully understood. This absence of information is due in part to the difficulty of manipulating large DNA fragments by using conventional molecular cloning techniques. Consequently, few studies have addressed the cellular function(s) of full-length htt and its dysfunction(s) associated with the disease.

Results: We describe a flexible synthetic vector encoding full-length htt called pARIS-htt (**A**daptable, **R**NAi **I**nsensitive &**S**ynthetic). It includes synthetic cDNA coding for full-length human htt modified so that: 1) it is improved for codon usage, 2) it is insensitive to four different siRNAs allowing gene replacement studies, 3) it contains unique restriction sites (URSs) dispersed throughout the entire sequence without modifying the translated amino acid sequence, 4) it contains multiple cloning sites at the N and C-ter ends and 5) it is Gateway compatible. These modifications facilitate mutagenesis, tagging and cloning into diverse expression plasmids. Htt regulates dynein/dynactin-dependent trafficking of vesicles, such as brain-derived neurotrophic factor (BDNF)-containing vesicles, and of organelles, including reforming and maintenance of the Golgi near the cell centre. We used tests of these trafficking functions to validate various pARIS-htt constructs. We demonstrated, after silencing of endogenous htt, that full-length htt expressed from pARIS-htt rescues Golgi apparatus reformation following reversible microtubule disruption. A mutant form of htt that contains a 100Q expansion and a htt form devoid of either HAP1 or dynein interaction domains are both unable to rescue loss of endogenous htt. These mutants have also an impaired capacity to promote BDNF vesicular trafficking in neuronal cells.

Conclusion: We report the validation of a synthetic gene encoding full-length htt protein that will facilitate analyses of its structure/function. This may help provide relevant information about the cellular dysfunctions operating during the disease. As proof of principle, we show that either polyQ expansion or deletion of key interacting domains within full-length htt protein impairs its function in transport indicating that HD mutation induces defects on intrinsic properties of the protein and further demonstrating the importance of studying htt in its full-length context.

Background

Huntingtin (htt) is a protein of 350 kDa that when mutated causes Huntington's disease (HD). HD is a devastating inherited neurodegenerative disorder characterized by the selective dysfunction and death of particular neurons in the brain [1,2]. The causative mutation is an abnormally expanded CAG tract in the 5'coding region of the htt gene that is translated into a long polyglutamine (polyQ) stretch in the N-terminal part of the protein. HD occurs when there are more than the threshold of 36 glutamines. The mechanisms leading to disease are not fully understood but involve both the gain of new toxic functions and the loss of normal htt function(s) [1-3]. For example, loss of htt function in the transcription of brain-derived neurotrophic factor (BDNF) and in its microtubule (MT)-dependent transport participates in HD pathogenesis [4,5]. We and others have contributed to the

* Correspondence: Frederic.Saudou@curie.fr
[1] Institut Curie, F-91405 Orsay, France
[†] Contributed equally
Full list of author information is available at the end of the article

identification and characterization of postranslational modifications within htt that regulate the function(s) of both the wild-type protein and the toxicity induced by the mutant version. These findings demonstrate the importance of the protein context. The first identified modification of htt was its phosphorylation at serine 421 (S421). Htt S421 is phosphorylated by Akt and the *Serum and Glucocorticoid-induced kinase* (SGK) and is dephosphorylated by calcineurin [6-9]. Phosphorylation at S421 is abnormally low in disease [9-11]. Dephosphorylation of S421 is associated with reduced htt function in the MT-dependent transport of BDNF in neurons and may contribute to the selective neurodegeneration in cases of HD [12,13]. Htt is cleaved by several proteases, including caspase 6 which may play a crucial role and modify disease progression [14]. PolyQ-htt susceptibility to cleavage is regulated by phosphorylation of serine 434 by Cdk5 [15] and of serine 536 by an unidentified kinase [16]. Also, the specific acetylation of mutant htt at lysine 444 leads to its selective degradation by autophagy, thereby reducing toxicity [17]. Subcellular trafficking of htt and its association with lipid membranes can be modified by palmitoylation of cysteine 214 [18]. Palmitoylation-resistant mutants accelerate formation of inclusions and neuronal toxicity. Mass spectrometry experiments have identified additional phosphorylation sites in the central and carboxy-terminal parts of the protein [16] which may be involved in additional mechanisms regulating its cellular functions. Sequence analysis revealed at least 36 HEAT (**h**untingtin, **e**longation factor 3, PR65/A subunit of protein phosphatase 2**A** and m**T**or) repeats dispersed throughout the protein [19,20]. The presence of these domains and the predicted structure of htt are consistent with a cellular role as a scaffold protein [21,22]. In agreement, more than one hundred interactors have been reported in yeast-two-hybrid screens using various htt fragments as baits [23,24]. The protein sequence, including the central and carboxy-terminal part of the protein, has been very highly conserved throughout evolution. These various observations all indicate the importance of the full-length protein context when addressing htt functional studies. They have also led to the emerging notion that understanding normal htt function is essential if we are going to understand the pathogenic and regulatory events that occur during disease progression in HD patients.

Various cellular and molecular biology techniques can be used to study the function(s) of a particular protein and its dysfunction(s) when mutated. Many of these techniques require cloning the gene of interest into appropriate vector(s) for subsequent characterization. This step can be extremely laborious and time consuming especially when dealing with large proteins, like htt, and may constitute a difficult technical obstacle for extensive functional and genetic analyses. Because of this problem, and despite the very large number of publications concerning HD since the cloning of the htt gene in 1993, most studies have used only short N-terminal fragments of the htt protein and focused on the gain of toxic function elicited by the polyQ stretch. Indeed, expression of short N-terminal fragments (containing the pathogenic expansion), for example the 89 amino acid fragment corresponding to the exon 1, are sufficient to generate a neurological phenotype in mice and to induce the death of various cell types [25]. Although these models reproduce some pathological features observed in HD patients, exon 1 encodes less than 3% of the full-length htt protein; consequently, such studies do not necessarily provide a complete image of the function(s) of the protein and the dysfunction(s) operating during HD. In particular, the translational product of exon 1 does not contain important sites of post-translational modifications, notably S421, L444 and C214, that critically regulate mutant htt toxicity. In addition, events such as caspase 6 proteolysis of the full-length protein are bypassed in such models. Also, functional studies on the role of htt in MT-dependent transport have shown that wild-type full-length htt, but not short amino-terminal fragments such as that encoded by exon 1, stimulates the transport of BDNF-containing vesicles [5]. These observations make clear the need for appropriate tools to study wild-type and pathogenic htt in its full-length protein context.

We report the construction and validation of a complete synthetic htt gene with wild-type and mutant versions. We demonstrate that the wild-type htt encoded by this gene has a positive effect in regulating the trafficking of vesicles and organelles; the pathogenic mutant htt does not. We exploited the versatility of this synthetic htt gene to generate internal deletions and demonstrate that the regions interacting with HAP1 and dynein are required to mediate htt function in cellular trafficking. Thus, this fully synthetic construct will be useful for investigations of htt function and the pathogenic mechanisms underlying HD.

Results

pARIS-htt, a synthetic cDNA encoding a tagged full-length version of human huntingtin

We designed a synthetic cDNA covering the entire sequence of human htt as part of a modular and versatile plasmid expression platform to study the function(s) of the protein. This system includes all the benefits of the Gateway system from Invitrogen. We named this platform pARIS-htt (**A**daptable, **R**NAi **I**nsensitive &**S**ynthetic). The sequence of human htt (GenBank access NM_002111) was optimized for eukaryotic codon usage. We also exploited the degenerate nature of the genetic code to eliminate various restriction sites from the sequence and introduce others, resulting in a synthetic

DNA sequence with unique restriction sites every 1-1.5 kbp on average without modifying the amino acid sequence encoded (GenBank access NP_002102)(Figure 1A). The overall construction strategy required first the synthesis and cloning of eight fragments separately in the vector pUC19. The full-length version of the htt gene was then generated by assembling the eight fragments (Figure 1A). In the resulting construct, the entire sequence can be divided into eight different fragments, each single fragment being flanked by unique restriction sites.

The multi-cassette nature of pARIS-htt is advantageous. Any desired mutation of the full-length context can be generated in two steps. The first step is the introduction of the desired mutation into the corresponding 1 to 1.5 kbp fragment in pUC19. The second step is to reintroduce the mutated fragment into the full-length htt cDNA by conventional restriction enzyme digestion and ligation. PolyQ expansion in the htt protein causes HD, so we produced pARIS-htt versions with and without a sequence encoding an abnormal polyQ stretch. We generated a pARIS-htt version encoding a pathogenic polyQ expansion of 100Q by introducing alternate CAG-CAA repeats, because the alternating codons are genetically more stable [26]. The NotI site upstream from the sequence encoding the first N-ter 17 amino acids and the SacI site downstream from that encoding the poly-proline stretch (amino acid position 92) allow the introduction of a sequence encoding a synthetic N-terminal fragment with CAG repeats of any desired size by simple digestion with NotI/SacI followed by insertion of a compatible cassette coding for the polyQ sequence of desired length. We generated two different cassettes coding for 23 and 100Q.

To facilitate functional studies, the pARIS-htt constructs were designed to allow production of various fusion proteins: tagging of the amino terminus of the encoded protein with a 6× histidine-tag to allow protein purification on Ni^{2+} columns, and fusion to the mCherry protein; the C-terminus was tagged with haemaglutinin (HA) that can be used for immunoprecipitation or immunohistochemistry, and a tetracysteine tag (TC-Tag) that allows the fusion protein to be specifically recognized in living cells by biarsenic labelling reagents such as FlAsH-EDT_2 and ReAsH-EDT_2 [27,28]. The sequences encoding the tags can be easily removed by using the unique NotI and EcoRI restriction sites and multicloning sites (MCS) at the two extremities (Figure 1A; sequences and vector maps are provided in additional files 1 and 2). Another important feature of pARIS-htt is its full compatibility with the Gateway technology, which allows recombination-based cloning and all its benefits in terms of time and simplicity. This property is provided by the inclusion of the specific recombination sites attB1 and attB2 flanking the htt coding sequence. First, the htt coding wild-type and mutant sequences were transferred to a general donor plasmid (pDONR201, Invitrogen) to generate Entry vectors in which pARIS-htt is flanked by attL sequences (BP clonase reaction). These Entry vectors are referred as follows: pARIS-htt-N[His-mCherry]Q23-C[HA-TC] and pARIS-htt-N[His-mCherry]Q100-C[HA-TC]. pARIS-htt sequences can then be transferred to the desired destination vector though a second recombination (LR clonase reaction) to generate an expression clone. Numerous commercially available destination vectors can be used for straightforward expression of synthetic human htt protein in diverse biological systems (transient expression in mammalian cells, baculovirus-mediated infection of insect cells, lentiviral-mediated delivery to neural cells or expression in *Drosophila melanogaster*).

pARIS-htt drives expression of full-length huntingtin and is insensitive to siRNAs targeting the endogenous protein

To validate pARIS-htt constructs, we first generated a pcDNA-based (pcDNA3.2-DEST, Invitrogen) expression vector to drive pARIS-htt expression in mammalian cells. The constructs pARIS-$htt^{pcDNA3.2}$-N[His-mCherry]Q23-C[HA-TC] (pARIS-mCherry-httQ23) and pARIS-$htt^{pcDNA3.2}$-N[His-mCherry]Q100-C[HA-TC] (pARIS-mCherry-httQ100) were used to transfect HEK cells and protein expression was analyzed by immunoblotting with various htt-specific antibodies recognizing different epitopes within the protein, including htt-4C8 whose epitope maps to positions 443-457 of the amino acid sequence and the htt-2C1 antibody raised against the carboxy-terminal region (2788-2990) [29,30] (Figure 1A). These two antibodies gave strong signals for the synthetic htt constructs with migration shifts due to the presence of the tags for pARIS-mCherry-httQ23 and that of the expanded polyQ stretch for pARIS-mCherry-httQ100 (Figure 1B). pARIS-mCherry-httQ100 but not Q23 was selectively recognized by antibody 1C2 that binds specifically to pathogenic polyQ expansions [31]. The synthetic constructs containing a C-terminal HA tag were also efficiently recognized by anti-HA antibodies. We next investigated whether expression of pARIS-htt in transfected Cos7 cells could be detected by direct immunofluorescence due to its N-terminal mCherry fluorescent tag. The fluorescent signals corresponding to pARIS-mCherry-httQ23 and pARIS-mCherry-httQ100 were mainly cytosolic and colocalized with htt-4C8 staining (Figure 1C). This localization is in agreement with previous studies [29].

The pARIS constructs are suitable for use in gene replacement strategies. Indeed, the sequence was modified to make it insensitive to various siRNAs that efficiently silence human, rat or mouse htt (see Methods section for the list of siRNAs that can be used and addi-

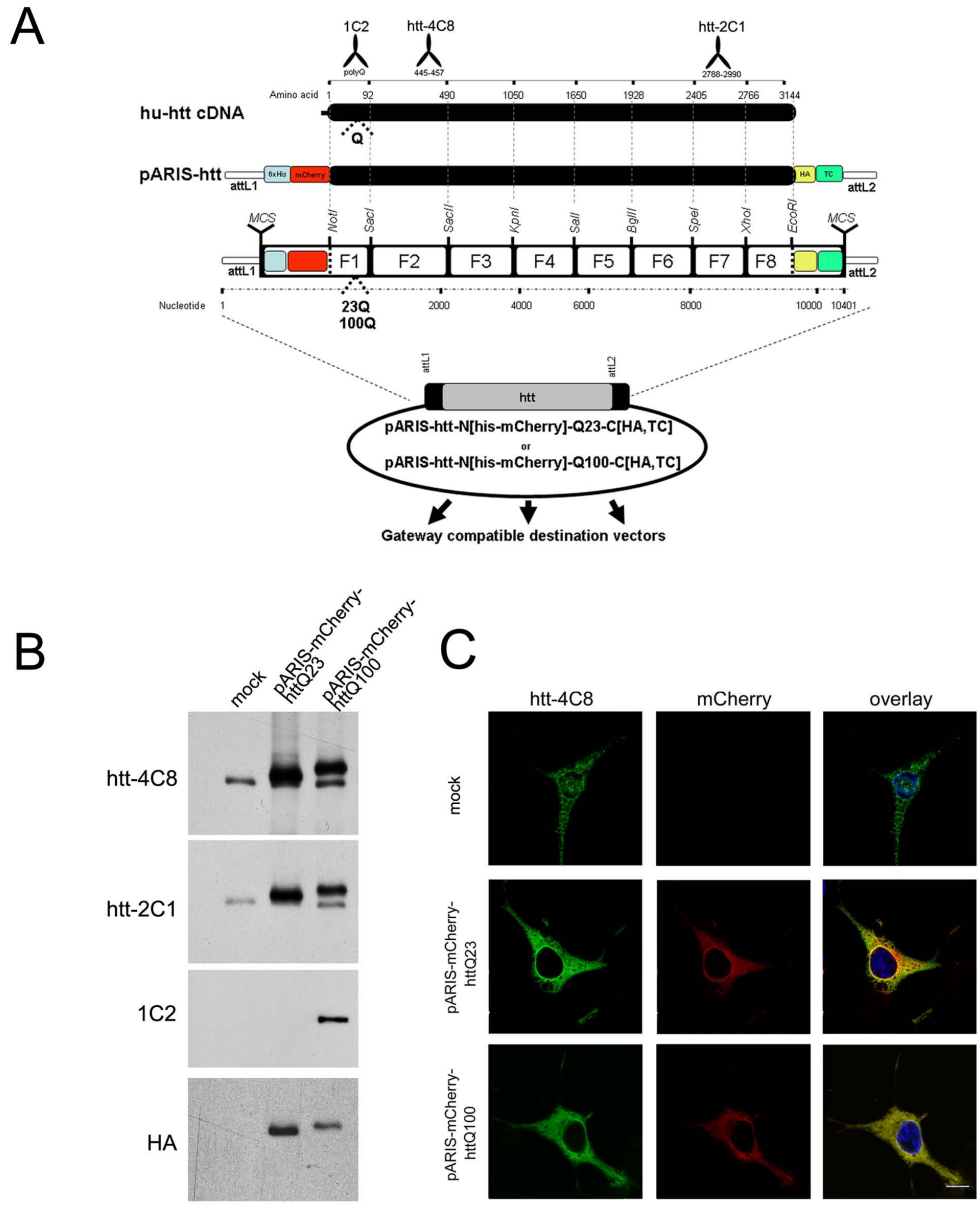

Figure 1 pARIS-htt an Adaptable, RNAi Insensitive & Synthetic construct encoding human huntingtin. A) Schematic representation of pARIS-htt. The entire coding sequence is divided into 8 different fragments, each fragment being flanked by unique restriction sites every 1-1.5 kbp and cloned independently into a modified pUC19 backbone. A multi-cassette full-length htt plasmid (pARIS-htt) was generated by assembly of these 8 individual fragments. pARIS-htt construct was tagged with 6×His followed by a mCherry on the amino terminus. The carboxy-terminal part contains HA and tetracysteine (TC) tags. The synthetic construct is fully compatible with the Gateway technology thanks to the introduction of flanking attL sites. (B) pARIS-htt triggers the expression of full-length htt in HEK cells. Cells mock transfected and transfected with pARIS-mCherry-httQ23 or pARIS-mCherry-httQ100 were analyzed by western blot using antibodies raised against different regions of htt: the amino-terminal part (htt-4C8), the carboxy-terminal part (htt-2C1) or the pathogenic polyQ stretch (1C2). The exact epitopes for these antibodies are illustrated in (A). Expression of the different constructs was detected using a high affinity anti-HA antibody. (C) Confocal images of Cos7 mock transfected cells and cells transiently transfected with pARIS-mCherry-httQ23 or pARIS-mCherry-httQ100 constructs. Expression of pARIS-htt is detected as a cytosolic mCherry fluorescent signal which codistributes with htt-4C8 antibody staining. Scale bar 10 μm.

tional file 1 for their positions within htt sequence). We previously reported a similar strategy for replacing endogenous htt with exogenous N-ter amino acid fragments of htt [9,13]. Here, we significantly improved the pertinence of this approach, because pARIS-htt allows the re-expression of full-length htt versions in various cellular contexts (human, mouse or rat cells) in which the endogenous htt is silenced. As a proof of principle, we specifically silenced endogenous htt in HeLa cells using a human specific siRNA, siRNA-hu-htt-585, which is particularly effective for knocking-down htt expression in cells of human origin (data not shown). HeLa cells were transfected with control RNA (scRNA) or siRNA-hu-htt-585 using lipofectamine, transfected 24 h later with pARIS-htt constructs, and then incubated for an additional 24 h. Expression of both endogenous and exogenous htt was analyzed by Western blotting (Figure 2A). Production of endogenous htt was completely abolished by the siRNA without affecting pARIS-mCherry-httQ23/Q100, whose expression was detected using an anti-HA antibody. Thus, pARIS-htt is fully insensitive to siRNAs targeting htt and therefore can be used for replacement strategy experiments in cells.

pARIS-htt can substitute endogenous huntingtin in a Golgi reassembly assay

We exploited this RNAi insensitivity to develop a cellular test and to validate pARIS-htt as a functional htt protein. Htt is found in the Golgi apparatus (GA) [32-34]. In our hands, a significant fraction of pARIS-mCherry-httQ23 was similarly localized in discrete sites in the GA (data not shown). Knock-down of htt in cells results in the disruption of GA structure, leading to the suggestion that htt plays an active role in the maintenance of the GA structure near the cell centre [34]. Studies in which microtubules (MTs) were depolymerized or molecular motors were inactivated indicate that MTs and minus end-directed motors are also required to ensure the structural integrity and the perinuclear localization of the GA [35-40]. The requirement for htt in the organisation and maintenance of the Golgi is linked to the interaction between htt and components of the dynein/dynactin complex [34]. We therefore set up a cellular test to assess htt function in the transport of Golgi-derived vesicles. We used HeLa cells stably expressing GFP-mannosidase II, a key enzyme of N-linked glycan processing often used as a medial Golgi marker [41]. As expected, silencing of htt was associated with the disruption of the GA structure as shown by the dispersion of Ctr433, a marker of the cis/median Golgi [42](Figure 2B). Most cells depleted of endogenous htt displayed spread GA, which was in many cases fully vesicular instead of being organized into compact perinuclear stacks as observed in most control (scRNA-treated) cells (Figure 2B). We next investigated the role of htt in MT-dependent assembly of the GA (Figure 2C-2E). To do so, we treated the cells with nocodazole (NZ, 4 μM, 120 min) to allow complete depolymerization of the MT network (Figure 2C, upper panel) and dispersion of the GA into numerous ministacks (Figure 2E, upper row) that localize at the exit sites of the endoplasmic reticulum [43]. GA integrity was then analyzed 120 min after NZ washout (Figure 2E, lower row). In scRNA-treated cells the Golgi structure became centrally reorganized again, after NZ washout, concomitant with the reformation of the MT network (Figure 2C, lower panel). In most if not all htt-silenced cells, the Golgi remained dispersed 120 min after NZ washout (Figure 2E, lower row) despite the MT network being completely reconstituted (not shown).

We next tested whether exogenous expression of pARIS-htt could complement the loss of endogenous htt for MT-dependent assembly of the GA. Expression of endogenous htt was knocked-down by treatment with siRNA-htt. Then, pARIS-mCherry-httQ23, insensitive to the siRNA-htt used, was expressed and cells were treated with NZ for 120 min (Figure 3A). We assessed the reassembly of the GA 120 min after NZ washout. A significant fraction of siRNA-htt-treated cells expressing pARIS-mCherry-httQ23 could efficiently reorganize the GA into stacks in the perinuclear region (Figure 3B). Thus, pARIS-mCherry-httQ23 can substitute for endogenous htt to reassemble the GA into tight stacks.

The role of wild-type htt in GA maintenance has been previously studied [34]. However, it is not known whether pathogenic htt has altered functions in the reassembly of Golgi-derived membranes. We therefore used the same approach but with expression of pARIS-mCherry-httQ100 in cells depleted of endogenous htt. After NZ washout, the highly dispersed GA was unable to reassociate completely into a well-defined perinuclear structure (Figure 3B). Next we developed a system to quantify GA reassembly in this experimental model. We determined the mean volume of Golgi particles before (t = 0) and 120 min after NZ washout (t = 120, figure 3C). NZ treatment induced the complete disintegration of the GA into numerous ministacks with a mean volume of 0.28 ± 0.04 μm^3. In control cells (scRNA), 120 min after NZ washout, the mean volume per particle increased approximately 15 fold (4.13 ± 0.77 μm^3, $p < 0.0001$). In cells depleted of endogenous htt, Golgi-derived vesicles completely failed to cluster and fuse (siRNA-htt, t = 0 vs t = 120; p = 0.634, NS). Expression of pARIS-mCherry-httQ23 in htt-depleted cells completely restored the assembly of Golgi ministacks (3.763 ± 0.71 μm^3, t = 0 vs t = 120, $p < 0.0001$) and their transport to perinuclear regions. By contrast, pARIS-mCherry-httQ100 was unable to promote reassembly of the GA (p = 0.432, NS). This experiment indicates that synthetic-Q23 htt restores MT-dependent

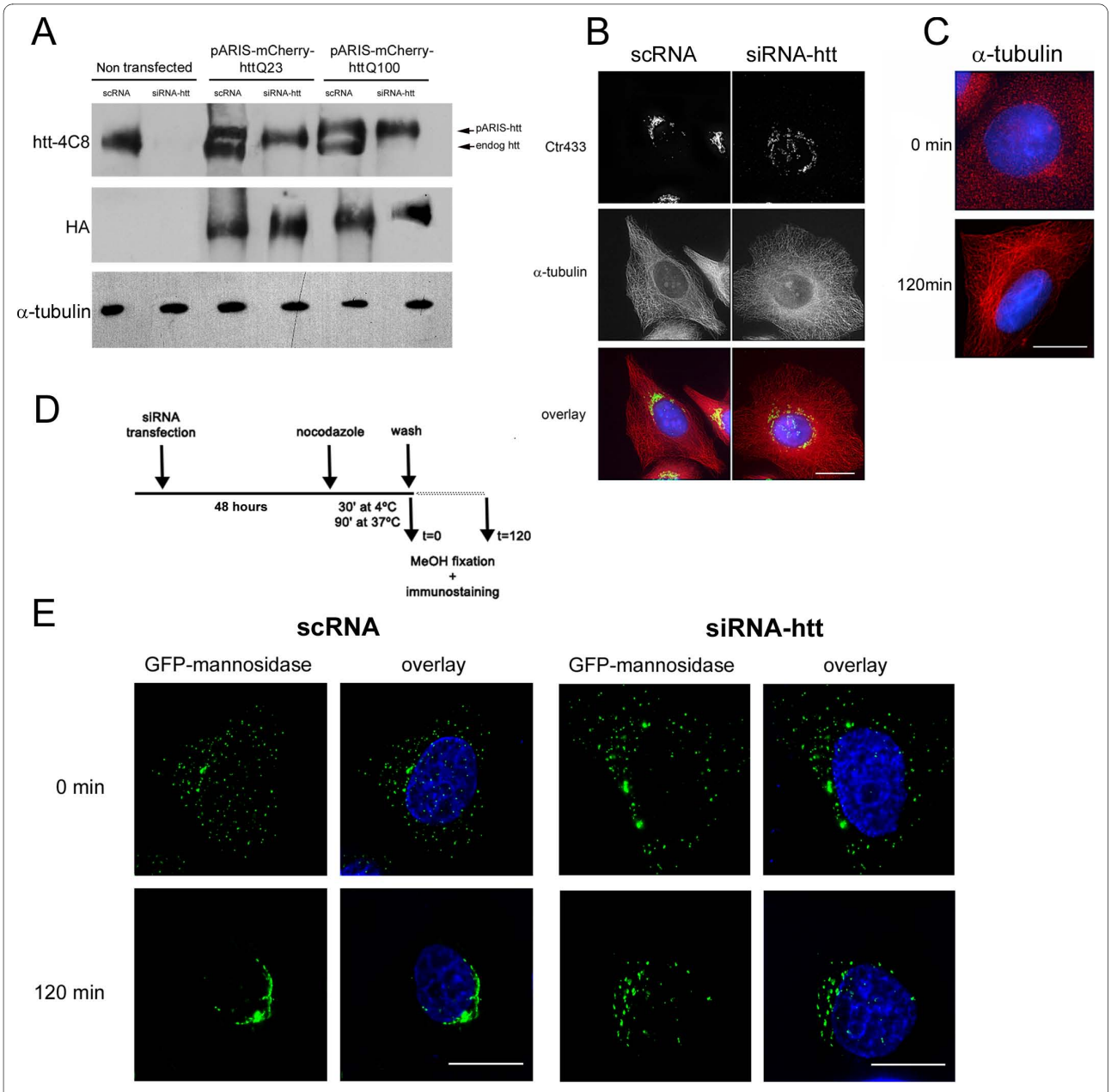

Figure 2 Huntingtin depletion impairs Golgi reformation after microtubule disruption. A) HeLa cells were sequentially transfected with scRNA or siRNA-htt and pARIS-mCherry-httQ23/Q100 and finally analyzed by western blot using antibodies that recognize either endogenous and exogenous htt (htt-4C8) or only exogenous htt (HA). Treatment with siRNA-htt (second lane) results in the complete silencing of endogenous htt. Compared to endogenous htt, pARIS-htt displays lower mobility due to fusion with tags. Note that expression levels of pARIS-mCherry-httQ23/Q100 are not modified by siRNA-htt treatment (lanes 4 and 6). α-tubulin is used as a protein loading control. (B) HeLa cells were transfected with scRNA or siRNA-htt, fixed and processed for staining of a Golgi marker (Ctr 433) and α-tubulin. Unlike scRNA-treated cells, cells silenced for endogenous htt display a dispersed Golgi phenotype but an intact MT network. (C) α-tubulin staining before and after nocodazole (NZ) treatment reveals that MT network is entirely reformed 120 min after NZ removal in HeLa cells. (D) A schematic description of the transfection protocol is summarized. (E) HeLa cells stably expressing GFP-mannosidase II were transfected with scRNA or siRNA-htt and treated with NZ for 120 min to allow a complete MT depolymerization. Golgi reformation was monitored 120 min after NZ washout. In scRNA-treated cells the GA becomes again centrally organized. However, cells depleted from endogenous htt still present a dispersed GA at the same time point. Scale bars 10 μm.

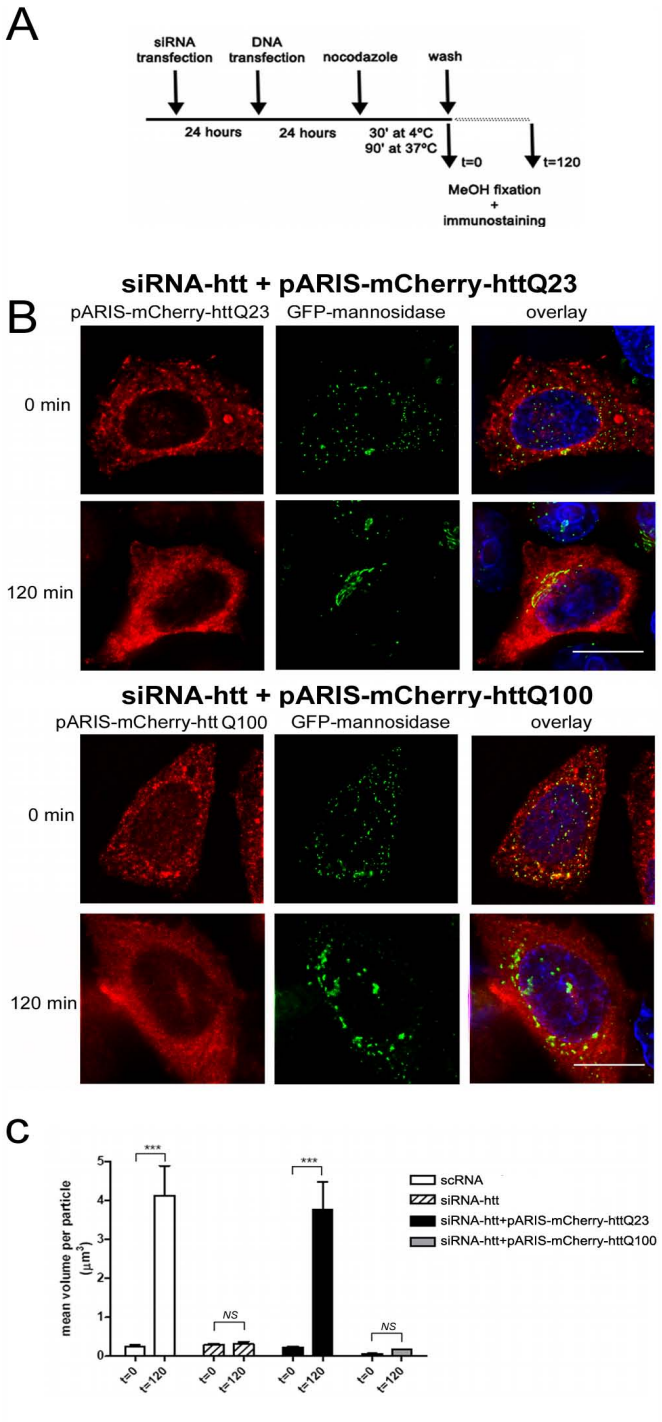

Figure 3 pARIS-mCherry-httQ23 but not pARIS-mCherry-httQ100 restores Golgi reassembly after endogenous huntingtin depletion. A) Gene replacement experiments and Golgi reformation assays were performed adding back pARIS-mCherry-httQ23/Q100 in cells depleted from endogenous htt following the protocol indicated in the scheme. (B) Representative images of cells expressing pARIS-mCherry-httQ23 (upper pannel) or pARIS-mCherry-httQ100 (lower panel) at t = 0 and t = 120 after NZ washout. While cells expressing pARIS-mCherry-httQ23 completely reassemble the GA into tight stacks, cells expressing pARIS-mCherry-httQ100 display scattered Golgi fragments that are unable to reassemble in the perinuclear region. (C) Quantification of the GA reassembly is presented as an analysis of mean Golgi particle volume (μm^3) before and after NZ washout for different treatments. Results were obtained from 3 independent experiments in which 280 cells were analyzed. One way ANOVA followed by Fisher's *Post-hoc* test: ***$p < 0.0001$; NS non significant. All comparisons are t = 0 vs t = 120; scRNA: 0.283 ± 0.044 vs 4.126 ± 0.771; siRNA-htt 0.073 ± 0.008 vs 0.158 ± 0.06; siRNA-htt + pARIS-mCherry-httQ23: 0.222 ± 0.035 vs 3.763 ± 0.712; siRNA-htt + pARIS-mCherry-httQ100: 0.062 ± 0.006 vs 0.171 ± 0.013.

assembly of the GA in cells with no endogenous htt. More importantly, it shows that the pathogenic polyQ expansion impairs the htt function allowing Golgi reassembly.

The dynein/dynactin-interacting domains of huntingtin are required for Golgi apparatus reassembly

Our findings indicate that physiological organization of the GA requires wild-type htt and that this function of htt is impaired by polyQ expansion. This is in agreement with previous studies linking htt function to the dynein/dynactin-dependent transport of organelles along MTs [5,12,13,34]. Htt interacts with the dynein intermediate chain (DIC) via a minimal interaction region mapping to amino acid positions 536-698 of htt [34] and with dynactin via HAP1 [44-46] with a minimal interacting region corresponding to amino acids 171-230 of htt [47]. We have previously shown that the htt/HAP1 complex is necessary for vesicle transport along MTs. Depletion of HAP1 through siRNA treatment impairs BDNF transport along MTs in neuronal cells [5]. We have also shown that expression of wild-type exon 1 of htt that lacks the HAP1 binding region, does not stimulate BDNF transport in neuronal cells; by contrast, a 480 amino acid N-ter fragment can stimulate such transport. Although informative, these experiments have limited relevance because, due to the difficulty of manipulating full-length htt, they are based on the expression of truncated forms with most of the protein being deleted. Therefore, it is unknown whether these domains are required within a full-length htt context as mediators of htt regulatory function in the dynein/dynactin complex.

To investigate the htt-dynein interaction, we generated a version of pARIS-htt from which part of the dynein-interacting region was deleted (pARIS-mCherry-httQ23-Δdyn). We used immunoprecipitation experiments to test the ability of this deletion mutant to bind dynein. We used an antibody raised against htt (htt-4C8) to pull-down both endogenous and synthetic htt from non transfected cells and from cells expressing pARIS-mCherry-httQ23 (Figure 4A, upper panel). Under these conditions, dynein co-immunoprecipitated with htt provided the cells express either endogenous htt or pARIS-mCherry-httQ23. Similarly, both endogenous and exogenous htt were co-immunoprecipitated with dynein as shown by the presence of a doublet band (Figure 4A, lower panel). This doublet band was observed in cells transfected with pARIS-mCherry-httQ23 but was absent from non transfected cells and from cells expressing pARIS-mCherry-httQ23 but silenced for endogenous htt. Silencing experiments and re-expression of htt siRNA-insensitive constructs were then used to assess the interaction between dynein and the various exogenous htt constructs. In particular, we tested the interaction between dynein and full-length htt lacking the internal dynein-binding domain. Anti-htt antibodies could not immunoprecipitate dynein from pARIS-mCherry-httQ23-Δdyn expressing cells silenced for endogenous htt (Figure 4B, upper panel). Conversely, although endogenous htt was efficiently immunoprecipitated by an anti-dynein antibody, pARIS-mCherry-httQ23-Δdyn was not (Figure 4B, lower panel). This strongly indicates that pARIS-mCherry-httQ23-Δdyn lacking the dynein-interaction domain does not bind dynein.

Next we studied the effect of the expression of pARIS-mCherry-httQ23-Δdyn on GA reassembly. Unlike in cells expressing pARIS-mCherry-httQ23 (Figure 3B, upper panel), GA stacks remained dispersed in cells expressing pARIS-mCherry-httQ23-Δdyn (Figure 4C). We then quantified GA reassembly (as in Figure 3C) and found that the GA clearly failed to reassemble following NZ washout (Figure 4D). This demonstrates a strong defect in the fusion of Golgi-derived mini-stacks in the presence of pARIS-mCherry-httQ23-Δdyn (siRNA-htt + pARIS-mCherry-httQ23-Δdyn, t = 0 vs t = 120; p = 0.4883, NS). In summary, we show that the htt-dynein interaction is required for the positive effect of htt on GA fusion and transport.

Another mechanism by which htt may regulate the dynein-dynactin complex involves the interaction between htt and huntingtin-associated protein 1 (HAP1), the first htt-interacting protein described. The association between these two proteins is enhanced when htt contains a pathogenic polyQ stretch [44]. HAP1 interacts with dynactin [45,46] and plays a key role in MT-dependent transport of organelles in concert with htt [5,12,48]. Since the minimal interacting region of htt for HAP1 has been mapped to amino acid positions 171-230 of htt [47], we generated a version of pARIS-httQ23 deleted for this domain referred to hereafter as pARIS-mCherry-httQ23-ΔHAP1.

We analyzed whether the pARIS-mCherry-httQ23-ΔHAP1 mutant could bind to HAP1. We co-transfected HEK cells with GFP-tagged HAP1 and either pARIS-mCherry-httQ23 or pARIS-mCherry-httQ23-ΔHAP1. Co-immunoprecipitation experiments demonstrated that the htt construct not containing the 170-268 amino acid region did not bind to HAP1 (Figure 5A) and therefore that this region is necessary for interaction between full-length htt and HAP1. We next tested the effect of this deletion on Golgi reassembly. Unlike cells expressing pARIS-mCherry-httQ23, cells expressing pARIS-mCherry-httQ23-ΔHAP1 could not reorganize the GA even 120 min after NZ washout (Figure 5B), despite complete reorganization of the MT network (not shown). Quantification of the mean volume of Golgi-derived particles (Figure 5C) confirmed the substantial defect in the fusion of GA ministacks in cells expressing pARIS-mCherry-httQ23-ΔHAP1 (t = 0 vs t = 120, p = 0.63, NS).

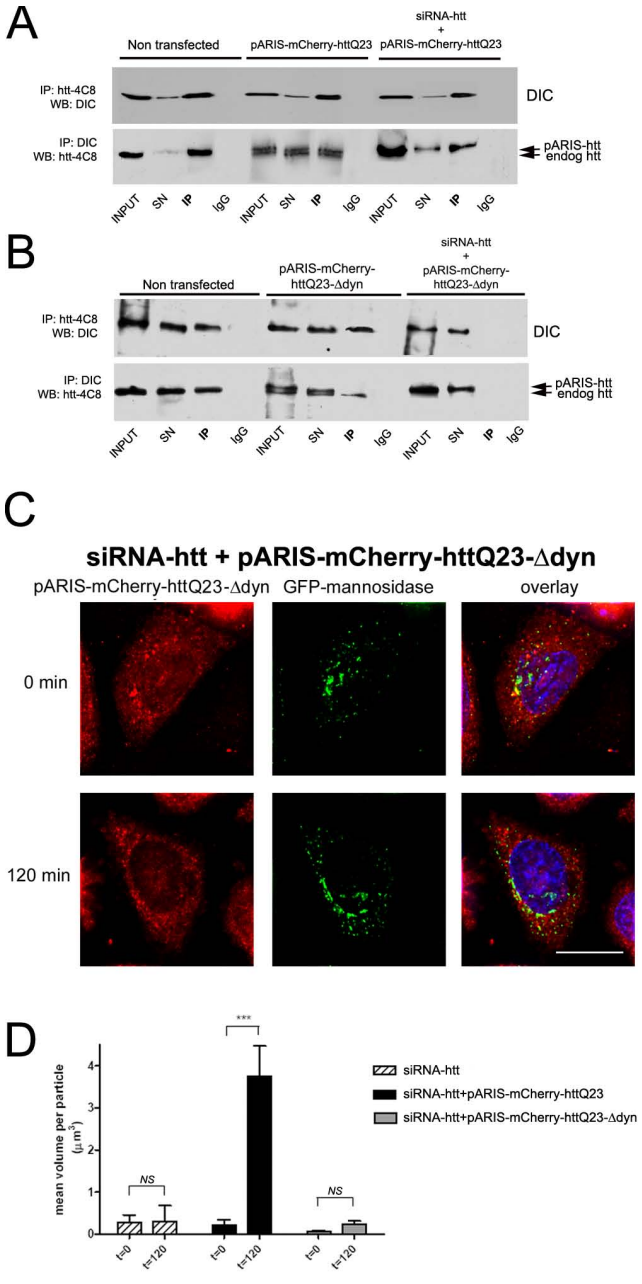

Figure 4 Htt requires dynein interacting domain to facilitate the transport of Golgi-derived vesicles. A) HEK cells were treated with scRNA or siRNA-htt prior transfection with pARIS-mCherry-httQ23. Cellular lysates were immunoprecipitated using htt-4C8 or anti-dynein (DIC) antibodies and immunocomplexes were subjected to SDS-PAGE to detect either htt or dynein. Dynein co-precipitates with htt when htt-4C8 antibody is used to pull-down endogenous and exogenous htt (Upper panel). Conversely, immunoprecipitation of dynein (lower panel) pulls down both endogenous and exogenous htt (indicated by arrows, lower mobility band corresponding to pARIS-mCherry-httQ23). The same amount of mouse or rabbit IgG's were used as internal immunoprecipitation controls. SN stands for supernatant; IP denotes immunoprecipitation. B) A deletion mutant lacking the minimal dynein interaction domain, denoted as pARIS-mCherry-httQ23-Δdyn, is unable to bind to endogenous dynein (lane 11). (C) Golgi reassembly was monitored in HeLa cells stably expressing GFP-mannosidase II, silenced for endogenous htt and expressing pARIS-mCherry-httQ23-Δdyn as the only cellular source of htt. Most of the cells expressing pARIS-mCherry-httQ23-Δdyn failed to reassemble the GA after NZ washout, suggesting that htt-dynein interaction is required to transport retrogradely Golgi-derived vesicles. Scale bar 10 μm. (D) Quantification of the Golgi dispersion as the mean volume per Golgi particle (μm^3) before and after after NZ washout for the different treatments. Results were obtained from 3 independent experiments in which 192 cells were scored. One way ANOVA followed by Fisher's *Post-hoc* test: ***$p < 0.0001$; NS non significant. All comparisons t = 0 vs t = 120; siRNA-htt 0.073 ± 0.008 vs 0.158 ± 0.06; siRNA-htt + pARIS-mCherry-httQ23: 0.222 ± 0.035 vs 3.763 ± 0.712; siRNA-htt + pARIS-mCherry-httQ23-Δdyn: 0.073 ± 0.010 vs 0.244 ± 0.072.

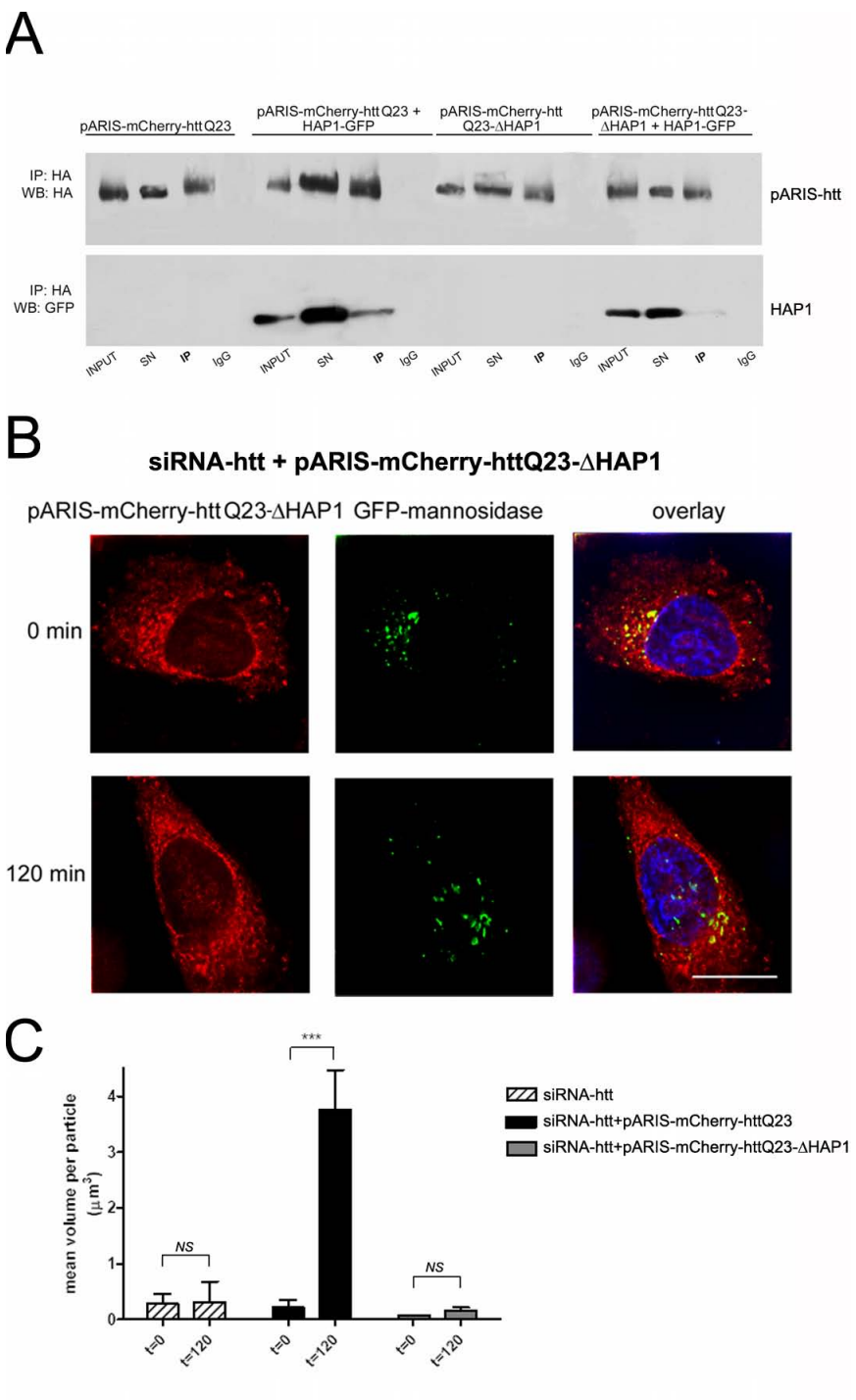

Figure 5 Htt requires HAP1 interacting domain to facilitate the transport of Golgi-derived vesicles. A) HEK cells were transfected with pARIS-mCherry-httQ23 or a deletion mutant for the minimal HAP1 interaction domain (denoted as pARIS-mCherry-httQ23-ΔHAP1) in the absence or presence of HAP1-GFP. Exogenous htt was immunoprecipitated (IP) from cell lysates using a HA antibody and immunocomplexes were analyzed for the presence of HAP1-GFP. Immunoprecipitations with mouse IgGs were used as a specificity control. (B) Golgi reformation assays were done in HeLa cells stably expressing GFP-mannosidase II as described previously. Representative image of a pARIS-mCherry-httQ23-ΔHAP1 expressing cell failing to reconstitute the GA after NZ washout. Scale bar 10 μm. (C) Quantification of the Golgi dispersion as the mean volume per Golgi particle (μm³) before and after NZ washout for the different treatments. Results were obtained from 3 independent experiments in which 190 cells were scored. One way ANOVA followed by Fisher's *Post Hoc* test: ***p < 0.0001. NS, non significant. All comparisons t = 0 vs t = 120; siRNA-htt 0.073 ± 0.008 vs 0.158 ± 0.06; siRNA-htt + pARIS-mCherry-httQ23: 0.222 ± 0.035 vs 3.763 ± 0.712; siRNA-htt + pARIS-mCherry-httQ23-ΔHAP1: 0.073 ± 0.080 vs 0.159 ± 0.060.

Our results show the importance of HAP1 in the MT-dependent transport of GA-derived vesicles.

Together, our results further extend the role of htt in the maintenance of GA. Indeed, we demonstrate that the capacity of htt to regulate the retrograde transport of dispersed Golgi vesicles to form highly organized stacks around the perinuclear region requires a functional interaction between htt and both dynein and HAP1.

pARIS-httQ23 but not pARIS-httQ100, pARIS-httQ23-Δdyn nor pARIS-httQ23-ΔHAP1 promotes BDNF transport in neuronal cells

MT-dependent transport of vesicles, such as BDNF, is regulated by the association between htt and the dynein/dynactin complex [5,12,13,34]. Wild-type htt has a positive effect on vesicular dynamics whereas this function is lost in HD [5,12,13,34]. Therefore, the regulatory functions of htt in vesicular trafficking can be evaluated by comparing neurons that express wild-type htt or mutant htt. We previously described the effect of wild-type and pathogenic versions of htt on the dynamics of vesicles that contain eGFP or mCherry-tagged BDNF [5,12,13]. These approaches are sensitive enough to be used to evaluate drugs that restore MT-dependent transport that is altered during HD [5,9,12,13,49].

We analyzed the dynamics of BDNF-eGFP-containing vesicles in mouse neuronal cells using fast 3D videomicroscopy followed by deconvolution. Videomicroscopy was performed one day after electroporation of cells with BDNF-eGFP alone or BDNF-eGFP with pARIS-mCherry-httQ23 and pARIS-mCherry-httQ100, in conditions in which no apparent toxicity was observed. The combination of mCherry-htt and BDNF-eGFP facilitated identification of cells to be recorded during videoexperiments. pARIS-mCherry-httQ23 showed a similar transport function as wild-type htt, significantly increasing the mean velocity of BDNF vesicles (1.132 ± 0.030 μm/s compared to the control value: 0.733 ± 0.044 μm/s; ***p < 0.0001, figure 6A). The presence of pARIS-mCherry-httQ100 did not stimulate BDNF transport (0.810 ± 0.056 μm/s). In cells expressing pARIS-mCherry-httQ100, the pausing time, corresponding to the percentage of time the vesicles spent without moving, was significantly longer than in controls (from 3.09 ± 0.49% in control cells to 5.83 ± 1.03%, figure 6B). The pausing time in cells expressing pARIS-httQ23 was not significantly different from control values (3.00 ± 0.38%).

Htt function in MT-dependent transport of BDNF also involves dynein/dynactin and HAP1. We therefore investigated BDNF dynamics in neuronal cells expressing pARIS-mCherry-httQ23-Δdyn or pARIS-mCherry-httQ23-ΔHAP1. Relative to control values, pARIS-mCherry-httQ23 increased BDNF trafficking in cells, whereas each pARIS-mCherry-httQ23-Δdyn and pARIS-mCherry-httQ23-ΔHAP1 mutants reduced the mean velocity (Figure 6A). Similarly, we also observed a significantly longer pausing time of BDNF-containing vesicles in cells expressing pARIS-mCherry-httQ23-Δdyn or -ΔHAP1 mutants than in cells expressing pARIS-mCherry-httQ23 (Figure 6B). These findings further extend the functional role of full-length htt as a key regulator of MT-dependent transport of organelles in cells. Furthermore, we clearly show that in mammalian neuronal cells, in a physiological full-length protein context, this positive function is mediated by two independent domains of htt protein: the HAP1- and dynein-interacting regions.

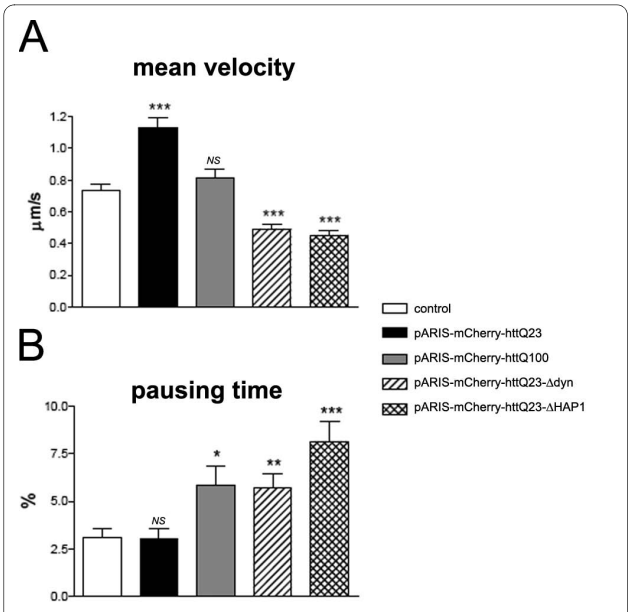

Figure 6 pARIS-mCherry-httQ23 facilitates BDNF transport through interaction with dynein and HAP1. A) Fast 3D videomicroscopy was performed to analyze the dynamics of BDNF-eGFP-containing vesicles in mouse neuronal cells expressing BDNF-eGFP alone or cotransfected with pARIS-mCherry-httQ23/Q100 or dynein/HAP1 deletion mutants. Overexpression of pARIS-mCherry-httQ23 recapitulates the transport function of wild-type htt and significantly increases the mean velocity of BDNF-containing vesicles compared to controls values (BDNF transfection alone). Nor the polyQ version neither pARIS-htt deletion mutants are able to stimulate the transport of BDNF containing vesicles. The pausing time of moving vesicles is quantified in (B). Mean overall velocity is indicated as μm/sec. Data were obtained from three independent experiments (control: 4805 tracks from 39 cells; pARIS-mCherry-httQ23: 1970 tracks from 20 cells; pARIS-mCherry-httQ100: 1670 tracks from 18 cells; pARIS-mCherry-httQ23-Δdyn: 4603 tracks from 25 cells; pARIS-mCherry-httQ23-ΔHAP1: 4029 tracks from 20 cells). Fisher's analysis: *P < 0.05; **P < 0.01, NS, non significant.

Discussion

There is currently substantial evidence consistent with htt being a scaffold protein required for diverse cellular functions, including various intracellular trafficking pro-

cesses. Unravelling htt functions in different tissues and how these functions are spatially and temporally tuned to the needs of the cell (via a plethora of post-translational modifications) is extremely complex. In particular, it requires working in the context of the full-length protein. Due in part to htt being a very large protein, this approach has been technically difficult and most experiments addressing htt function, toxicity or post-translational modifications have used short N-terminal fragments of htt; many studies have been based on exon-1 that corresponds to less than 3% of the protein. Here we present a flexible platform to render working with the full-length protein much more straightforward. Our pARIS-htt platform can be used for the construction of tagged and mutant versions of htt in a full-length context. We successfully produced tagged versions of wild-type and mutant htt in various cell lines and generated mutants unable to interact with known protein partners: dynein and HAP1 (pARIS-mCherry-httQ23-Δdyn and pARIS-mCherry-httQ23-ΔHAP1). In the absence of htt, the GA is disrupted, indicating that htt is required to maintain GA organization around the centrosome [33,50]. Indeed, a fraction of htt localizes to the GA and may serve to regulate the post-Golgi trafficking of proteins [32]. We used this property to establish reconstitution experiments to validate our pARIS-htt constructs. Our experimental model is based on the complete silencing of endogenous htt and the expression of various synthetic htt constructs in HeLa cells stably expressing a fluorescent GA-resident protein (GFP-mannosidase II). We used NZ treatment and monitored subsequent reassembly of the GA. In cells expressing pARIS-mCherry-httQ23, the GA was completely reassembled 120 min after NZ washout. By contrast, cells expressing any of the three mutant pARIS-htt constructs (pARIS-mCherry-httQ100, pARIS-mCherry-httQ23-Δdyn or pARIS-mCherry-httQ23-ΔHAP1) failed to reassemble their GA: dispersed ministacks were observed, instead of tightly organized GA around the cell centre, suggesting a defect in the retrograde transport of Golgi-derived vesicles. Quantification of the mean volume of Golgi-derived particles revealed a profound defect in the fusion events in cells expressing any of the mutants, a defect which was not observed in cells expressing pARIS-mCherry-httQ23. These data are in agreement with previous results linking htt function to the maintenance of the GA via dynein [50]. We also validated pARIS-htt constructs for their function in the MT-dependent transport of BDNF-containing vesicles: pARIS-mCherry-httQ23 made a positive contribution to transport whereas this function was lost in neuronal cells expressing pARIS-mCherry-httQ100. Interestingly, BDNF transport, as assessed by measuring BDNF vesicle velocities, was disrupted more strongly by pARIS-mCherry-httQ23-Δdyn and pARIS-mCherry-httQ23-ΔHAP1 than by pARIS-mCherry-httQ100. These experiments demonstrate the requirement of the dynein (633-672) and HAP1 (168-270) interacting regions for htt function in the context of the full-length protein. Furthermore, they suggest that htt regulates vesicular trafficking via distinct but functionally important domains. These results support the notion of htt as a scaffold protein linking vesicles and MTs and promoting the association and regulation of components of the molecular motor machinery, including HAP1 and the motors dynein or kinesin. In agreement with this view, phosphorylation of htt at S421 regulates the recruitment of kinesin-1 to the motor complexes thereby coordinating the directionality of vesicular transport in cells [12]. Moreover, our results strongly suggest that pathogenic polyQ expansions may influence the protein's conformation and its association with motor complexes.

The study of htt function(s) in health and disease is complex, because the protein is widely distributed, but the pathological mutant disables only a small subset of neurons and does so only after many years. Numerous questions concerning the cellular functions of wild-type htt remain unanswered. The role of htt in the regulation of vesicular trafficking is one of its best-described functions [5,12,13,34] and is certainly not limited to its association with dynein or HAP1. Indeed, the contribution of htt to different membrane trafficking events involves other protein partners, such as HIP-1 [51], HAP40 [52], Rab8/optineurin [32,53] or Rab11 [54]. Determination of the true contribution of the reported vesicular trafficking defects to the pathology of HD will certainly require more comprehensive studies. Any such studies would be strengthened by working with the full-length protein, so pARIS-htt constitutes a valuable expression platform for future investigations.

Finally, the combination of yeast-two-hybrid techniques with biochemical approaches led to the identification of more than 100 non redundant htt-interactors. These factors can be classified into different functional groups, including proteins involved in cytoskeletal organization, signal transduction, synaptic transmission, proteolysis and regulation of transcription or translation [23,24,55]. It is important to validate these interacting proteins as *bona fide* genetic modifiers, so that they can then be used to provide insight into the normal function of htt in neuronal and non-neuronal cells, and into the molecular pathogenesis of HD. Here again, pARIS-htt may be a valuable tool for use with other biological approaches for exploring these issues.

Conclusions

We present a comprehensive set of vectors designed for mutation/tagging and expression of full-length huntingtin. We hope this vector platform will be of value to the

scientific community and facilitate functional and genetic studies of htt in the near future.

Methods

Statistical analyses

InfoStat software version 2009 (InfoStat Group, FCA, Cordoba National University, Argentina) was used for the analysis of variance and followed by a *post hoc* LSD Fisher's test. Data are expressed as mean +/- S.E.M. *P < 0.05;**P < 0.01;***P < 0.001.

Constructs and siRNA

The plasmid encoding BDNF-eGFP was previously described [5,56]. BDNF-eGFP shows cellular localization, processing, and secretion properties indistinguishable from those of endogenous BDNF. The plasmid encoding for the huntingtin-associated protein 1 (HAP1) tagged with GFP was a gift of XJ Li (Emory University, Atlanta, USA). The siRNA targeting human huntingtin (siHtt-hu585, Eurogentec, Seraing, Belgium) corresponds to the coding region 279-298 of human htt mRNA (NCBI ref. seq. NM_002111). The control RNA (scRNA, ATCGAGCTACCACGAACGCTT, Eurogentec) has a unique sequence which does not match to any sequence in the genome of interest.

Construction of pARIS-htt

pARIS-htt was engineered based on the cDNA of full-lengh human htt using OptGene (Ocimum Biosolutions, Hyderabad, India) gene optimizing tool. Gene synthesis was performed by assembly of oligonucleotides using proprietary in-house protocols of BaseClear BV (Leiden, Netherlands). The original sequence was designed with a polyglutamine stretch of 23 glutamines. Glutamine repeats were encoded by alternate CAG/CAA codons to provide more genetic stability. The first base on the start translation codon is considered position number 1.

The pARIS-htt sequence has been rendered insensitive to different siRNAs commonly used in our laboratory: siHtt-1.1 AAGAACTTTCAGCTACCAA (human specific, position 275-293); siHtt-hu585 AACTTTCAGCTACCAAGAAAG (human specific, position 279-298); siHtt-6: AAGCTTTGATGGATTCTAA (human specific, position 474-492); siHtt-13: GCAGCTTGTCCAGGTTTAT (human, rat and mouse specific, position 1062-1080). siHtt-hu585 was used in this study because it is particularly effective to knock-down endogenous htt expression in cells of human origin (referred as siRNA-htt throughout the text).

The full-length engineered pARIS-htt construct was entirely sequenced and inserted into HindIII/BamHI sites of a pUC19 variant (Baseclear BV) for amplification. The pARIS-htt sequence contains flanking attL1 and attL2 sites to allow recombination into pDON201 donor vector (BP clonase reaction, Invitrogen, Carlsbad, USA). A second recombination with pcDNA3.2-DEST (Invitrogen) using LR clonase was necessary to generate a pcDNA3-based destination vector. Recombinations were done in a 10 μl final volume following instructions provided by the manufacturer. Amplification of the constructs was done in TOP10 or DH5α E. coli strains (Invitrogen). A DNA fragment of htt containing a polyQ stretch of 100 glutamines was synthesized using alternative protocols by Geneart AG (Regensburg, Germany) and inserted into NotI/SacI sites of pARIS-htt to replace the 23Q stretch. Vector maps are available in additional file 1.

We use the following nomenclature to describe the first step constructs in the Entry vector: pARIS-htt-N[His-mCherry]Q23-C[HA-TC] and pARIS-htt-N[His-mCherry]Q100-C[HA-TC]. These constructs were transposed to pcDNA3.2 to generate pARIS-htt$^{pcDNA3.2}$-N[His-mCherry]Q23-C[HA-TC] (pARIS-mCherry-httQ23) and pARIS-htt$^{pcDNA3.2}$-N[His-mCherry]Q100-C[HA-TC] (pARIS-mCherry-httQ100).

To generate the htt construct deleted for the dynein-interacting domain, the deletion was first generated within the F3 fragment (pUC19-F3Δ633-672), transposed to Entry-based pARIS-htt by insertion of SacII/KpnI (fragment 3) generating pARIS-htt-N[His-mCherry]Q23-Δ633-672-C[HA-TC] and next transposed to pcDNA3.2 to generate pARIS-htt$^{pcDNA3.2}$-N[His-mCherry]Q23-Δ633-672-C[HA-TC] hereafter denoted pARIS-mCherry-httQ23-Δdyn. To generate the htt construct deleted for the HAP1 binding domain, the deletion was first generated within the F2 fragment (pUC19-F2Δ170-268), transposed to Entry-based pARIS-htt by insertion of SacI/SacII (fragment 2) generating pARIS-htt-N[His-mCherry]Q23-Δ170-268-C[HA-TC] and next transposed to pcDNA3.2 to generate pARIS-htt$^{pcDNA3.2}$-N[His-mCherry]Q23-Δ170-268-C[HA-TC] hereafter denoted pARIS-mCherry-httQ23-ΔHAP1. Requests for constructs may be sent to the following e-mail address: paris-htt.constructs@curie.fr.

Cell Culture

HEK and Cos7 cells were grown at 37°C in 5% CO2 in Dulbeco's modified Eagle's medium (DMEM) supplemented with 10% bovine calf serum, 1% L-glutamine and antibiotics (50 units/ml penicillin and 50 μg/ml streptomycin). HeLa cells stably expressing GFP-mannosidase II (gift of F. Perez, Institut Curie, Paris, France), were grown at 37°C in 5% CO_2 and cultured in DMEM supplemented with 10% bovine calf serum, 1% L-glutamine and 400 μg/ml geneticin (Gibco, Carlsbad, USA). Mouse neuronal cells, ST*Hdh*$^{+/+}$ cells derived from immortalized striatal progenitor cells were grown as previously described [57].

Cell Transfection

For pARIS-htt expression analysis, HEK cells were transfected with pARIS-mCherry-httQ23, pARIS-mCherry-httQ100 or equivalent amount of empty vector, using the calcium phosphate method [58]. Western blot analysis was performed after 24-48 h.

For immunofluorescence experiments, Cos7 cells seeded in 12-well plates with 18 mm coverslips were transfected with pARIS-mCherry-httQ23, pARIS-mCherry-httQ100 or equivalent amount of empty vector using FuGENE reagent (Roche, Mannheim, Germany) according to the manufacturer's instructions. Immunostaining was done after 48 h.

For gene replacement experiments, HeLa cells stably expressing GFP-mannosidase II were seeded in 12-well plates with 18 mm coverslips. Sequential transfection was performed as following: attached cells were first transfected using Lipofectamine 2000 (Invitrogen) with siRNA-htt or scRNA. After 24 h, cells were transfected again with pARIS-mCherry-httQ23, pARIS-mCherry-httQ100, pARIS-mCherry-httQ23-Δdyn or pARIS-mCherry-httQ23-ΔHAP1. Cells were processed for western blotting or immunostaining 24 h after. DNA, siRNA and Lipofectamine 2000 quantities were used according to the manufacturer's instructions.

To perform co-immunoprecipitation experiments, HEK cells were transfected using Lipofectamine 2000 with siRNA-htt as described above. After 24 h the cells were transfected with pARIS-mCherry-Htt constructs and/or HAP1-GFP using the calcium phosphate method. Immunoprecipitation assays were performed after 24 h.

For videomicroscopy experiments mouse neuronal cells were electroporated with Kit L Nucleofector according to the supplier's manual (Amaxa, Köln, Germany). BDNF-eGFP and pARIS-htt DNA or equivalent amount of empty vector were added to the electroporation mix. After electroporation, cells were seeded in 12 well plates with 18 mm coverslips.

Nocodazole treatment

Transfected HeLa GFP-mannosidase II cells were treated with 4 μM nocodazole for 30 min at 4°C and 90 min at 37°C to allow a complete depolymerization of microtubules. Cells were washed twice with DMEM prior to methanol fixation (2 min at -20°C).

Antibodies

Anti-huntingtin antibodies used in this study htt-4C8, htt-2C1 and 1C2 were previously described [29,31], α-tubulin was from Sigma (St Louis, USA), high affinity anti-HA and anti-GFP were from Roche, anti-dynein intermediate chain (DIC) was from Chemicon (Billerica, USA), secondary IgG-HRP antibodies were from Jackson ImmunoResearch (WestGrove, USA), the mouse monoclonal antibody against the cis/medial Golgi marker CTR433 was previously described [42]. Alexa Fluor secondary antibodies used in immunofluorescence experiments were from Invitrogen.

Western Blot

Transfected cells were harvested and lyzed in 50 mM Tris-HCl, pH 7.5, containing 0.1% Triton X-100, 2 mM EDTA, 2 mM EGTA, 50 mM NaF, 10 mM β-glycerophosphate, 5 mM sodium pyrophosphate, 1 mM sodium orthovanadate, 0.1% (v/v) β-mercaptoethanol, 250 μM PMSF, 10 mg/ml aprotinin and leupeptin. Cell lysates were centrifuged at 20,000 g for 10 min at 4°C. Equal amounts of protein were subjected to SDS-PAGE on 6% polyacrylamide gels and transferred to nitrocellulose membranes (Whatman, Dassel, Germany). Blocked membranes (5% milk in TBS-0.1% Tween-20) were incubated with mouse anti-huntingtin antibodies (htt-4C8, htt-2C1), mouse anti-polyQ expansion (1C2), rat anti-HA, mouse anti-GFP, mouse anti-DIC or mouse anti-α-tubulin antibodies and washed three times with TBS-0.1% Tween-20 for 10 min. Membranes were then labelled with secondary IgG-HRP antibodies raised against each corresponding primary antibody. After three washes, the membranes were incubated with SuperSignal West Pico Chemiluminescent Substrate (Pierce, Erembodegem, Belgium) according to the instructions of the supplier. Membranes were exposed to Amersham Hyperfilm™ MP (GE Healthcare, Buckinghamshire, UK) films and developed.

Immunoprecipitation

Immunoprecipitations were performed as described [59] with minor modifications. Cell lysis and wash of the immunocomplexes were done in 50 mM of Tris 1 M (pH 8), 150 mM NaCl and 1% of NP40 containing protease and phosphatase inhibitors. Briefly, transfected cells were harvested and lyzed on ice. Lysates were centrifuged at 16,000 g (15 min at 4°C) and precleared (30 min at 4°C) using protein A-Sepharose beads (Sigma). Cleared lysates were incubated for 2-3 h at 4°C with protein A-Sepharose beads conjugated to mouse htt-4C8, mouse DIC or rat HA antibodies. Immunoprecipitates were washed three times and analyzed by Western blot as described.

Immunofluorescence

After methanol fixation cells were blocked for 1 h at RT with PBS-BSA 3% and incubated with primary antibodies for 1 h prior staining with Alexa Fluor secondary antibodies. Nuclei were stained with DAPI (Roche). The mounting medium was 0.1 g/ml Mowiol 4-88 (Calbiochem, Darmstadt, Germany) in 20% glycerol.

Image acquisition

Images on fixed samples were acquired at RT with a Leica SP5 laser scanning confocal microscope equipped with a 63 × oil-immersion objective or with a Leica DM RXA microscope with a PL APO oil 63 × NA of 1.4 objective coupled to a piezzo and a Micromax RTE/CCD-1300-Y/HS camera controlled by Metamorph software (Molecular Devices, Sunnyvale, CA). Z-stack step was of 0.2 μm. All stacks were treated by automatic batch deconvolution using the PSF of the optical system, Meinel algorithm with parameters set at 7 iterations, 0.7 sigma and 4 frequencies.

Computer morphometric analysis of the Golgi apparatus

Images of fixed cells were acquired as described (see above, image aquisition). Only HeLa cells stably expressing GFP-mannosidase II and transfected with our pARIS-htt constructs were analyzed. Once deconvolved, images were analyzed with ImageJ software using 3D object counter plugin ([60]; available at http://imagej-docu.tudor.lu/doku.php?id=plugin:analysis:3d_object_counter:start). The quantification was achieved tagging each identified object within the z-stacks (around 30 z-stacks per image), treating each Golgi particle as an individual object. Statistics about each object were calculated, volume as: number of voxels of the object × x calibration × y calibration × z calibration. The overall measurements were obtained from 3 independent experiments and analyzed to determine the mean volume per particle for each condition.

Videomicroscopy

Mouse neuronal transfected cells were grown on glass coverslips and mounted in a Ludin's chamber. The microscope and the chamber were kept at 33°C. Live videomicroscopy was carried out using a Leica DM IRBE microscope and a PL APO oil 100 × objective with a numerical aperture of 1.40-0.70, coupled to a piezo device (PI) and recorded with Photometrics CoolSNAP HQ2 camera (Roper Scientific, Trenton, NJ) controlled by Metamorph software. Images were collected in stream set at 2 × 2 binning with an exposure time of 50-150 ms (frequency of 2 s) with a Z-step of 0.3 μm. Deconvolution was performed as described for fixed samples. All dynamic parameters of intracellular transport were obtained from three independent experiments with a total of about 1500-5000 measures from 18-39 independent cells. Dynamics were characterized by tracking positions of eGFP vesicles as a function of time with an especially developed plugin (available at http://rsb.info.nih.gov/ij/plugins/track/track.html) for Image J.

Additional material

Additional file 1 Sequences and maps of pARIS-htt constructs used in the study. The file includes vector maps, DNA sequences, protein translation and additional information for pARIS-mCherry-httQ23/Q100 plasmids in Entry vector. They were generated using Gene Construction Kit (Textco BioSoftware, West Lebanon, USA) and Serial Cloner 2.0 (available at http://serialbasics.free.fr/Serial_Cloner.html.) software.

Additional file 2 Sequence text files of pARIS-htt constructs used in the study. It includes sequences of pARIS-mCherry-httQ23/Q100 plasmids in Entry and pcDNA vectors.

Abbreviations

The abbreviations used are BDNF: brain-derived neurotrophic factor; GA: Golgi apparatus; HD: Huntington's disease; htt: huntingtin; IP: immunoprecipitation; MT: microtubule; NZ: nocodazole; polyQ: polyglutamine; RT: room temperature; WB: western blot.

Competing interests

The authors declare that they have no competing interests.

Authors' contributions

RP, MMC, GK, SH and FS designed the experiments. RP, MMC and GP performed the experiments. RP, MMC, SH and FS analyzed the data. RP, MMC, SH and FS wrote the paper. All authors read and approved the final manuscript.

Acknowledgements

We thank E van Rijn and BaseClear BV (Leiden, Netherlands) for discussions, help in the design and completion of the synthetic gene project. We acknowledge K Colombo, JR Pineda and D Zala for help in data analysis and all the members of the Saudou and Humbert's laboratories for helpful comments; FP Cordelières and the Institut Curie Imaging Facility for image acquisition and treatment; M Bornens, XJ Li and F Perez for providing materials and reagents. This work was supported by grants from Agence Nationale pour la Recherche (ANR-MRAR-018-01 and ANR-08-MNP-039 to FS), Fondation pour la Recherche Médicale (FRM) and Fondation BNP Paribas (FS). RP was supported by a Beatriu de Pinós fellowship from Generalitat de Catalunya (Spain) and MMC by Institut Curie Ph.D. fellowship. FS and SH are investigators from Institut National de la Santé et de la Recherche Médicale. SH is co-investigator at Assistance Publique-Hôpitaux de Paris.

Author Details

[1]Institut Curie, F-91405 Orsay, France, [2]Centre National de la Recherche Scientifique, Unité Mixte de Recherche 3306, F-91405 Orsay, France and [3]Institut National de la Santé et de la Recherche Médicale, Unité U1005, F-91405 Orsay, France

Received: 27 April 2010 Accepted: 1 June 2010
Published: 1 June 2010

References

1. Borrell-Pages M, Zala D, Humbert S, Saudou F: **Huntington's disease: from huntingtin function and dysfunction to therapeutic strategies.** *Cell Mol Life Sci* 2006, **63(22):**2642-2660.
2. Li S, Li XJ: **Multiple pathways contribute to the pathogenesis of Huntington disease.** *Mol Neurodegener* 2006, **1(1):**19.
3. Cattaneo E, Zuccato C, Tartari M: **Normal huntingtin function: an alternative approach to Huntington's disease.** *Nat Rev Neurosci* 2005, **6(12):**919-930.
4. Zuccato C, Ciammola A, Rigamonti D, Leavitt BR, Goffredo D, Conti L, MacDonald ME, Friedlander RM, Silani V, Hayden MR, Timmusk T, Sipione S, Cattaneo E: **Loss of huntingtin-mediated BDNF gene transcription in Huntington's disease.** *Science* 2001, **293(5529):**493-498.
5. Gauthier LR, Charrin BC, Borrell-Pages M, Dompierre JP, Rangone H, Cordelieres FP, De Mey J, MacDonald ME, Lessmann V, Humbert S, Saudou F: **Huntingtin controls neurotrophic support and survival of neurons by enhancing BDNF vesicular transport along microtubules.** *Cell* 2004, **118(1):**127-138.

6. Humbert S, Bryson EA, Cordelieres FP, Connors NC, Datta SR, Finkbeiner S, Greenberg ME, Saudou F: **The IGF-1/Akt pathway is neuroprotective in Huntington's disease and involves Huntingtin phosphorylation by Akt.** *Dev Cell* 2002, **2(6):**831-837.
7. Rangone H, Poizat G, Troncoso J, Ross CA, MacDonald ME, Saudou F, Humbert S: **The serum- and glucocorticoid-induced kinase SGK inhibits mutant huntingtin-induced toxicity by phosphorylating serine 421 of huntingtin.** *Eur J Neurosci* 2004, **19(2):**273-279.
8. Pardo R, Colin E, Regulier E, Aebischer P, Deglon N, Humbert S, Saudou F: **Inhibition of calcineurin by FK506 protects against polyglutamine-huntingtin toxicity through an increase of huntingtin phosphorylation at S421.** *J Neurosci* 2006, **26(5):**1635-1645.
9. Pineda JR, Pardo R, Zala D, Yu H, Humbert S, Saudou F: **Genetic and pharmacological inhibition of calcineurin corrects the BDNF transport defect in Huntington's disease.** *Mol Brain* 2009, **2(1):**33.
10. Colin E, Regulier E, Perrin V, Durr A, Brice A, Aebischer P, Deglon N, Humbert S, Saudou F: **Akt is altered in an animal model of Huntington's disease and in patients.** *Eur J Neurosci* 2005, **21(6):**1478-1488.
11. Warby SC, Chan EY, Metzler M, Gan L, Singaraja RR, Crocker SF, Robertson HA, Hayden MR: **Huntingtin phosphorylation on serine 421 is significantly reduced in the striatum and by polyglutamine expansion in vivo.** *Hum Mol Genet* 2005, **14(11):**1569-1577.
12. Colin E, Zala D, Liot G, Rangone H, Borrell-Pages M, Li XJ, Saudou F, Humbert S: **Huntingtin phosphorylation acts as a molecular switch for anterograde/retrograde transport in neurons.** *Embo J* 2008, **27(15):**2124-2134.
13. Zala D, Colin E, Rangone H, Liot G, Humbert S, Saudou F: **Phosphorylation of mutant huntingtin at S421 restores anterograde and retrograde transport in neurons.** *Hum Mol Genet* 2008, **15; 17(24):**3837-46.
14. Graham RK, Deng Y, Slow EJ, Haigh B, Bissada N, Lu G, Pearson J, Shehadeh J, Bertram L, Murphy Z, Warby SC, Doty CN, Roy S, Wellington CL, Leavitt BR, Raymond LA, Nicholson DW, Hayden MR: **Cleavage at the caspase-6 site is required for neuronal dysfunction and degeneration due to mutant huntingtin.** *Cell* 2006, **125(6):**1179-1191.
15. Luo S, Vacher C, Davies JE, Rubinsztein DC: **Cdk5 phosphorylation of huntingtin reduces its cleavage by caspases: implications for mutant huntingtin toxicity.** *J Cell Biol* 2005, **169(4):**647-656.
16. Schilling B, Gafni J, Torcassi C, Cong X, Row RH, Lafevre-Bernt MA, Cusack MP, Ratovitski T, Hirschhorn R, Ross CA, Gibson BW, Ellerby LM: **Huntingtin phosphorylation sites mapped by mass spectrometry: Modulation of cleavage and toxicity.** *J Biol Chem* 2006, **281:**23686-23697.
17. Jeong H, Then F, Melia TJ Jr, Mazzulli JR, Cui L, Savas JN, Voisine C, Paganetti P, Tanese N, Hart AC, Yamamoto A, Krainc D: **Acetylation targets mutant huntingtin to autophagosomes for degradation.** *Cell* 2009, **137(1):**60-72.
18. Yanai A, Huang K, Kang R, Singaraja RR, Arstikaitis P, Gan L, Orban PC, Mullard A, Cowan CM, Raymond LA, Drisdel RC, Green WN, Ravikumar B, Rubinsztein DC, El-Husseini A, Hayden MR: **Palmitoylation of huntingtin by HIP14 is essential for its trafficking and function.** *Nat Neurosci* 2006, **9(6):**824-831.
19. Andrade MA, Bork P: **HEAT repeats in the Huntington's disease protein.** *Nat Genet* 1995, **11(2):**115-116.
20. Takano H, Gusella JF: **The predominantly HEAT-like motif structure of huntingtin and its association and coincident nuclear entry with dorsal, an NF-kB/Rel/dorsal family transcription factor.** *BMC Neurosci* 2002, **3(1):**15.
21. Palidwor GA, Shcherbinin S, Huska MR, Rasko T, Stelzl U, Arumughan A, Foulle R, Porras P, Sanchez-Pulido L, Wanker EE, Andrade-Navarro MA: **Detection of alpha-rod protein repeats using a neural network and application to huntingtin.** *PLoS Comput Biol* 2009, **5(3):**e1000304.
22. Grinthal A, Adamovic I, Weiner B, Karplus M, Kleckner N: **PR65, the HEAT-repeat scaffold of phosphatase PP2A, is an elastic connector that links force and catalysis.** *Proc Natl Acad Sci USA* 2010, **107(6):**2467-2472.
23. Goehler H, Lalowski M, Stelzl U, Waelter S, Stroedicke M, Worm U, Droege A, Lindenberg KS, Knoblich M, Haenig C, Herbst M, Suopanki J, Scherzinger E, Abraham C, Bauer B, Hasenbank R, Fritzsche A, Ludewig AH, Bussow K, Coleman SH, Gutekunst CA, Landwehrmeyer BG, Lehrach H, Wanker EE: **A protein interaction network links GIT1, an enhancer of huntingtin aggregation, to Huntington's disease.** *Mol Cell* 2004, **15(6):**853-865.
24. Kaltenbach LS, Romero E, Becklin RR, Chettier R, Bell R, Phansalkar A, Strand A, Torcassi C, Savage J, Hurlburt A, Cha GH, Ukani L, Chepanoske CL, Zhen Y, Sahasrabudhe S, Olson J, Kurschner C, Ellerby LM, Peltier JM, Botas J, Hughes RE: **Huntingtin interacting proteins are genetic modifiers of neurodegeneration.** *PLoS Genet* 2007, **3(5):**e82.
25. Mangiarini L, Sathasivam K, Seller M, Cozens B, Harper A, Hetherington C, Lawton M, Trottier Y, Lehrach H, Davies SW, Bates GP: **Exon 1 of the HD gene with an expanded CAG repeat is sufficient to cause a progressive neurological phenotype in transgenic mice.** *Cell* 1996, **87(3):**493-506.
26. Peters MF, Ross CA: **Preparation of human cDNas encoding expanded polyglutamine repeats.** *Neurosci Lett* 1999, **275(2):**129-132.
27. Gaietta G, Deerinck TJ, Adams SR, Bouwer J, Tour O, Laird DW, Sosinsky GE, Tsien RY, Ellisman MH: **Multicolor and electron microscopic imaging of connexin trafficking.** *Science* 2002, **296(5567):**503-507.
28. Ju W, Morishita W, Tsui J, Gaietta G, Deerinck TJ, Adams SR, Garner CC, Tsien RY, Ellisman MH, Malenka RC: **Activity-dependent regulation of dendritic synthesis and trafficking of AMPA receptors.** *Nat Neurosci* 2004, **7(3):**244-253.
29. Trottier Y, Devys D, Imbert G, Saudou F, An I, Lutz Y, Weber C, Agid Y, Hirsch EC, Mandel JL: **Cellular localization of the Huntington's disease protein and discrimination of the normal and mutated form.** *Nat Genet* 1995, **10(1):**104-110.
30. Cong SY, Pepers BA, Roos RA, Van Ommen GJ, Dorsman JC: **Epitope mapping of monoclonal antibody 4C8 recognizing the protein huntingtin.** *Hybridoma (Larchmt)* 2005, **24(5):**231-235.
31. Trottier Y, Lutz Y, Stevanin G, Imbert G, Devys D, Cancel G, Saudou F, Weber C, David G, Tora L, *et al.*: **Polyglutamine expansion as a pathological epitope in Huntington's disease and four dominant cerebellar ataxias.** *Nature* 1995, **378(6555):**403-406.
32. del Toro D, Canals JM, Gines S, Kojima M, Egea G, Alberch J: **Mutant huntingtin impairs the post-Golgi trafficking of brain-derived neurotrophic factor but not its Val66Met polymorphism.** *J Neurosci* 2006, **26(49):**12748-12757.
33. Strehlow AN, Li JZ, Myers RM: **Wild-type huntingtin participates in protein trafficking between the Golgi and the extracellular space.** *Hum Mol Genet* 2007, **16(4):**391-409.
34. Caviston JP, Ross JL, Antony SM, Tokito M, Holzbaur EL: **Huntingtin facilitates dynein/dynactin-mediated vesicle transport.** *Proc Natl Acad Sci USA* 2007, **104(24):**10045-10050.
35. Corthesy-Theulaz I, Pauloin A, Pfeffer SR: **Cytoplasmic dynein participates in the centrosomal localization of the Golgi complex.** *J Cell Biol* 1992, **118(6):**1333-1345.
36. Echeverri CJ, Paschal BM, Vaughan KT, Vallee RB: **Molecular characterization of the 50-kD subunit of dynactin reveals function for the complex in chromosome alignment and spindle organization during mitosis.** *J Cell Biol* 1996, **132(4):**617-633.
37. Thyberg J, Moskalewski S: **Role of microtubules in the organization of the Golgi complex.** *Exp Cell Res* 1999, **246(2):**263-279.
38. Burkhardt JK, Echeverri CJ, Nilsson T, Vallee RB: **Overexpression of the dynamitin (p50) subunit of the dynactin complex disrupts dynein-dependent maintenance of membrane organelle distribution.** *J Cell Biol* 1997, **139(2):**469-484.
39. He Y, Francis F, Myers KA, Yu W, Black MM, Baas PW: **Role of cytoplasmic dynein in the axonal transport of microtubules and neurofilaments.** *J Cell Biol* 2005, **168(5):**697-703.
40. Levy JR, Sumner CJ, Caviston JP, Tokito MK, Ranganathan S, Ligon LA, Wallace KE, LaMonte BH, Harmison GG, Puls I, Fischbeck KH, Holzbaur EL: **A motor neuron disease-associated mutation in p150Glued perturbs dynactin function and induces protein aggregation.** *J Cell Biol* 2006, **172(5):**733-745.
41. Gomez M, Scales SJ, Kreis TE, Perez F: **Membrane recruitment of coatomer and binding to dilysine signals are separate events.** *J Biol Chem* 2000, **275(37):**29162-29169.
42. Jasmin BJ, Cartaud J, Bornens M, Changeux JP: **Golgi apparatus in chick skeletal muscle: changes in its distribution during end plate development and after denervation.** *Proc Natl Acad Sci USA* 1989, **86(18):**7218-7222.
43. Cole NB, Sciaky N, Marotta A, Song J, Lippincott-Schwartz J: **Golgi dispersal during microtubule disruption: regeneration of Golgi stacks at peripheral endoplasmic reticulum exit sites.** *Mol Biol Cell* 1996, **7(4):**631-650.

44. Li XJ, Li SH, Sharp AH, Nucifora FC Jr, Schilling G, Lanahan A, Worley P, Snyder SH, Ross CA: **A huntingtin-associated protein enriched in brain with implications for pathology.** *Nature* 1995, **378(6555):**398-402.
45. Engelender S, Sharp AH, Colomer V, Tokito MK, Lanahan A, Worley P, Holzbaur EL, Ross CA: **Huntingtin-associated protein 1 (HAP1) interacts with the p150Glued subunit of dynactin.** *Hum Mol Genet* 1997, **6(13):**2205-2212.
46. Li SH, Gutekunst CA, Hersch SM, Li XJ: **Interaction of huntingtin-associated protein with dynactin P150Glued.** *J Neurosci* 1998, **18(4):**1261-1269.
47. Bertaux F, Sharp AH, Ross CA, Lehrach H, Bates GP, Wanker E: **HAP1-huntingtin interactions do not contribute to the molecular pathology in Huntington's disease transgenic mice.** *FEBS Lett* 1998, **426(2):**229-232.
48. McGuire JR, Rong J, Li SH, Li XJ: **Interaction of Huntingtin-associated protein-1 with kinesin light chain: implications in intracellular trafficking in neurons.** *J Biol Chem* 2006, **281(6):**3552-3559.
49. Dompierre JP, Godin JD, Charrin BC, Cordelieres FP, King SJ, Humbert S, Saudou F: **Histone deacetylase 6 inhibition compensates for the transport deficit in Huntington's disease by increasing tubulin acetylation.** *J Neurosci* 2007, **27(13):**3571-3583.
50. Caviston JP, Holzbaur EL: **Huntingtin as an essential integrator of intracellular vesicular trafficking.** *Trends Cell Biol* 2009, **19(4):**147-155.
51. Wanker EE, Rovira C, Scherzinger E, Hasenbank R, Walter S, Tait D, Colicelli J, Lehrach H: **HIP-I: a huntingtin interacting protein isolated by the yeast two-hybrid system.** *Hum Mol Genet* 1997, **6(3):**487-495.
52. Pal A, Severin F, Lommer B, Shevchenko A, Zerial M: **Huntingtin-HAP40 complex is a novel Rab5 effector that regulates early endosome motility and is up-regulated in Huntington's disease.** *J Cell Biol* 2006, **172(4):**605-618.
53. Hattula K, Peranen J: **FIP-2, a coiled-coil protein, links huntingtin to Rab8 and modulates cellular morphogenesis.** *Curr Biol* 2000, **24:**1603-1606.
54. Li X, Standley C, Sapp E, Valencia A, Qin ZH, Kegel KB, Yoder J, Comer-Tierney LA, Esteves M, Chase K, Alexander J, Masso N, Sobin L, Bellve K, Tuft R, Lifshitz L, Fogarty K, Aronin N, DiFiglia M: **Mutant huntingtin impairs vesicle formation from recycling endosomes by interfering with Rab11 activity.** *Mol Cell Biol* 2009, **29(22):**6106-6116.
55. Faber PW, Barnes GT, Srinidhi J, Chen J, Gusella JF, MacDonald ME: **Huntingtin interacts with a family of WW domain proteins.** *Hum Mol Genet* 1998, **7(9):**1463-1474.
56. Haubensak W, Narz F, Heumann R, Lessmann V: **BDNF-GFP containing secretory granules are localized in the vicinity of synaptic junctions of cultured cortical neurons.** *J Cell Sci* 1998, **111:**1483-1493.
57. Trettel F, Rigamonti D, Hilditch-Maguire P, Wheeler VC, Sharp AH, Persichetti F, Cattaneo E, MacDonald ME: **Dominant phenotypes produced by the HD mutation in STHdh(Q111) striatal cells.** *Hum Mol Genet* 2000, **9(19):**2799-2809.
58. Saudou F, Finkbeiner S, Devys D, Greenberg ME: **Huntingtin acts in the nucleus to induce apoptosis but death does not correlate with the formation of intranuclear inclusions.** *Cell* 1998, **95:**55-66.
59. Crespo PM, Silvestre DC, Gil GA, Maccioni HJ, Daniotti JL, Caputto BL: **c-Fos activates glucosylceramide synthase and glycolipid synthesis in PC12 cells.** *J Biol Chem* 2008, **283(45):**31163-31171.
60. Bolte S, Cordelieres FP: **A guided tour into subcellular colocalization analysis in light microscopy.** *J Microsc* 2006, **224(Pt 3):**213-232.

doi: 10.1186/1756-6606-3-17
Cite this article as: Pardo *et al.*, pARIS-htt: an optimised expression platform to study huntingtin reveals functional domains required for vesicular trafficking *Molecular Brain* 2010, **3**:17

5.3 Discussion

In the presented article **"pARIS-htt: an optimised expression platform to study huntingtin reveals functional domains required for vesicular trafficking"** we report the validation of a synthetic gene encoding full-length HTT protein that will facilitate analyses of its structure and function.

There is currently substantial evidence consistent with HTT being a scaffold protein required for diverse cellular functions, including intracellular trafficking processes. Unravelling HTT functions in different tissues and how these functions are spatially and temporally tuned to the needs of the cell (via a plethora of post-translational modifications) is extremely complex. In addition, HTT is widely distributed. Working in a HTT full-length context is crucial, however due in part to HTT being a very large protein, this approach has been technically difficult. Most experiments addressing HTT function, toxicity or PTM have used short N-terminal fragments of HTT. Many studies have been based on exon-1 that corresponds to less than 3% of the protein. Working with truncated forms of HTT leads to a restricted view of the function(s) of HTT as phosphorylations, clivages and others PTM take place on the entire HTT sequence. Furthermore, these modifications can occur at the same time to tightly regulate temporally and locally different cellular functions. For example, phosphorylation by Akt at S421 has been show to modulate vesicular transport directionality (Colin et al., 2008; Pineda et al., 2009) and Cdk5 phosphorylations at S1181/1201 to regulate vesicles velocity (Ben M'Barek at al., in preparation). We can imagine these two phosphorylations taking place simultaneously to satisfy specific cellular requirements. Modelling the combinations of absence/constitutive phosphorylations at these sites has to be done on full-length HTT with an easy to manipulate tool.

We generated pARIS-htt deletion mutants for the interaction domain of HTT with HAP1 and dynein, two important HTT interactors in vesicular transport. As for the HD mutant condition, these constructs induced reduced vesicular mean velocity and increased pausing time. Interestingly, this was more accentuated in Δdynein and ΔHAP1 than in the HD mutant condition. These results demonstrate the requirement of the dynein and HAP1 interacting regions for HTT function in a full-length context. We suggest that HTT regulates vesicular trafficking via distinct but functionally important domains. Furthermore, HTT solely interaction with dynein or HAP1 was not sufficient to rescue the lost of interaction with the other partner protein. This observation reinforces the hypothesis of HTT being a central scaffold element in vesicular transport.

Here we present a flexible platform to work with the full-length protein much more straightforward. Our pARIS-htt platform can be used for the construction of tagged and mutant versions of HTT in a full-length context. We hope this vector platform will be of value to the HD community and facilitate functional and genetic studies of HTT in the near future.

6 Role of HTT during mitosis

6.1 Study presentation

Knock-out of HTT in mouse results in embryonic lethality at E7.5, demonstrating its indispensible role during mammalian development.

In this study, we identified a previously undescribed role for HTT in mitosis. We found that HTT localizes to the spindle pole where it participates to the recruitment of several key mitotic players to the spindle apparatus. More interestingly, HTT is specifically required for modulating the orientation of the mitotic spindle without changing other parameters of the cell cycle. Knocking-down HTT by siRNA resulted in the mislocalization of dynein/dynactin complex and NuMA from the spindle pole.

HTT is critically required by neural progenitors of the developing cerebral cortex. Depletion of HTT by either siRNA interference or conditional knockout leads to significantly increased spindle misorientation that is in favor of apical-basal cleavages. Such alteration of mitotic cleavage orientation is correlated with the depletion of the progenitor pool and the increased production of postmitotic cortical neurons. Interestingly, HTT function is conserved in *D. melanogaster* as depletion of *htt* results in altered mitotic spindle orientation in embryonic NBs.

6.2 Article II

Juliette D. Godin*, Kelly Colombo*, **Maria Molina-Calavita**, Guy Keryer, Diana Zala, Bénédicte C. Charrin, Paula Dietrich, Marie-Laure Volvert, François Guillemot, Ioannis Dragatsis, Yohanns Bellaiche, Frédéric Saudou, Laurent Nguyen, and Sandrine Humbert. **Huntingtin is required for mitotic spindle orientation and mammalian neurogenesis.** Neuron. 2010.

*equal first authors

Neuron
Article

Huntingtin Is Required for Mitotic Spindle Orientation and Mammalian Neurogenesis

Juliette D. Godin,[1,2,3,8] Kelly Colombo,[1,2,3,8] Maria Molina-Calavita,[1,2,3] Guy Keryer,[1,2,3] Diana Zala,[1,2,3] Bénédicte C. Charrin,[1,2,3] Paula Dietrich,[4] Marie-Laure Volvert,[5] François Guillemot,[6] Ioannis Dragatsis,[4] Yohanns Bellaiche,[1,7] Frédéric Saudou,[1,2,3] Laurent Nguyen,[5] and Sandrine Humbert[1,2,3,*]
[1]Institut Curie
[2]CNRS UMR 3306
[3]INSERM U1005
Orsay F-91405, France
[4]Department of Physiology, University of Tennessee Health Science Center, Memphis, TN 38163, USA
[5]Developmental Neurobiology Unit, GIGA-Neurosciences, University of Liège, Liège, B-4000, Belgium
[6]Division of Molecular Neurobiology, National Institute for Medical Research, The Ridgeway, Mill Hill, NW71AA London, UK
[7]CNRS UMR 3215, INSERM U934, Paris 6 University, Paris F-75248, France
[8]These authors contributed equally to this work.
*Correspondence: sandrine.humbert@curie.fr
DOI 10.1016/j.neuron.2010.06.027

SUMMARY

Huntingtin is the protein mutated in Huntington's disease, a devastating neurodegenerative disorder. We demonstrate here that huntingtin is essential to control mitosis. Huntingtin is localized at spindle poles during mitosis. RNAi-mediated silencing of huntingtin in cells disrupts spindle orientation by mislocalizing the p150^{Glued} subunit of dynactin, dynein, and the large nuclear mitotic apparatus NuMA protein. This leads to increased apoptosis following mitosis of adherent cells in vitro. In vivo inactivation of huntingtin by RNAi or by ablation of the *Hdh* gene affects spindle orientation and cell fate of cortical progenitors of the ventricular zone in mouse embryos. This function is conserved in *Drosophila*, the specific disruption of *Drosophila* huntingtin in neuroblast precursors leading to spindle misorientation. Moreover, *Drosophila* huntingtin restores spindle misorientation in mammalian cells. These findings reveal an unexpected role for huntingtin in dividing cells, with potential important implications in health and disease.

INTRODUCTION

Mutation of huntingtin (htt) causes Huntington's disease (HD), a neurodegenerative disorder characterized by severe psychiatric, cognitive, and motor deficits and selective neuronal death in the brain. The mechanisms leading to disease are not fully understood, but increasing evidence suggest that in addition to the gain of new toxic properties, loss of wild-type htt function also contributes to pathogenesis (Borrell-Pages et al., 2006; Cattaneo et al., 2005). Given the predominant neurological signs and striking neuronal death in HD, most studies on htt function have focused on postmitotic neurons and have revealed major roles for htt in transcription and axonal transport (Caviston et al., 2007; Gauthier et al., 2004; Zuccato et al., 2001). Wild-type htt interacts with microtubules, the dynein/dynactin complex and kinesin to regulate the microtubule-dependent transport of organelles in neurons (Caviston et al., 2007; Colin et al., 2008; Gauthier et al., 2004; McGuire et al., 2006). However, no studies have investigated the possible role of htt during division. Indeed, htt is not restricted to differentiated neurons but is found at high levels in dividing cells where it associates to the centrosomal region and microtubules (Gauthier et al., 2004; Gutekunst et al., 1995; Hoffner et al., 2002; Sathasivam et al., 2001).

Spindle regulation is crucial to ensure the proper segregation not only of chromosomes, but also of cell fate determinant factors. The orientation of the mitotic spindle involves several steps, including the proper assembly and positioning of the spindle. These two steps are controlled by various molecular components. Among them, the dynein/dynactin complex ensures the correct spindle formation and, when anchored at the cell cortex, also generates pulling forces that are essential for proper cell division (Busson et al., 1998; Carminati and Stearns, 1997; Farkasovsky and Kuntzel, 2001; Nguyen-Ngoc et al., 2007; O'Connell and Wang, 2000; Skop and White, 1998). During mitosis, dynein and dynactin localize along spindle microtubules with an enrichment at spindle poles (Fant et al., 2004). This location at the spindle pole is linked to the dynein's ability to move toward the minus ends of microtubules. The dynein/dynactin complex is thought to focus microtubule minus ends at the spindle poles. In agreement with this idea, disrupting the dynein/dynactin complex by the use of specific antibodies alters spindle assembly (Merdes et al., 2000). Similarly, expressing the p50/dynamitin subunit of dynactin prevents the formation of a functional dynactin complex and subsequently impairs mitotic spindle morphology (Echeverri et al., 1996; Merdes et al., 2000). Finally, dynactin is required for spindle assembly in *Drosophila* neuroblasts (Siller et al., 2005). These data implicate dynein/dynactin as a central player in spindle pole organization.

Htt facilitates the dynein/dynactin-mediated transport of organelles along microtubules in neuronal cells. We thus investigated whether htt could also function during mitosis. We found that htt localized to the spindle poles during mitosis, from prophase to anaphase. The downregulation of htt led to a defect in spindle orientation reminiscent of the phenotype obtained from the silencing of $p150^{Glued}$ subunit of dynactin. We showed that siRNA targeting htt mislocalized $p150^{Glued}$, dynein, and the large nuclear mitotic apparatus (NuMA) protein, an essential player in mitotic assembly and maintenance (Radulescu and Cleveland, 2010). Furthermore, htt was required for proper spindle orientation and for cell fate determination of murine neuronal progenitors in vivo. Finally, this role of htt was conserved in *Drosophila*. Our study now establishes a link between htt, proper spindle orientation, and neurogenesis in mammals.

RESULTS

Huntingtin Localizes to Spindle Poles during Mitosis

We analyzed the subcellular localization of htt in mouse neuronal cells using various antibodies (Trettel et al., 2000) (Figure 1A). We first used a polyclonal antibody, pAb SE3619. During interphase, htt showed a punctuated distribution in the nucleus, reminiscent of stainings previously described using other anti-htt antibodies (Anne et al., 2007; Kegel et al., 2002) (Figure 1B). During mitosis, htt was specifically located at the spindle poles, between prophase to late anaphase. Htt staining was also observed at the spindle midzone during anaphase (Figure 1B).

We then checked the specificity of the htt antibody by transfecting cells with small interfering RNAs (siRNA) directed against htt (si-htt1). This treatment led to a selective, and statistically significant, reduction of signal intensity at the spindle pole (Figures 1B–1D). We further confirmed the subcellular localization of htt using several other anti-htt antibodies directed against various epitopes of the htt protein (Lunkes et al., 2002) (Figures 1A, 1E, and S1). These antibodies showed htt to be concentrated at the spindle poles particularly during metaphase, consistent with our observations using the pAb SE3619 (Figures 1E and S1).

Huntingtin Modulates Mitotic Spindle Orientation

We next investigated the putative function of htt at spindle poles. We transfected neuronal cells with scramble siRNA or si-htt1 targeting the mouse htt sequence. We immunostained cells with an antibody against γ-tubulin to analyze in Z-series stacks the position of the spindle poles with respect to the substratum plane (Figures 2A and 2C). In control cells, the majority of the spindles were properly oriented parallel to the substratum plane ($\sim$75%, n = 66) (Figure S2A). In contrast, in 53% of htt depleted cells (n = 89) the spindle was not correctly aligned (more than nine stacks of 0.2 μm between the two poles, $\Delta Z > 1.8$ μm). Spindle misorientation was then measured during metaphase by determining the angle between the pole-pole axis (axis of the metaphase spindle) and the substratum plane (Figure 2D). Whereas control cells show an angle mostly smaller than 10° (7.9° ± 1.3, n = 42), the average angle in si-htt1-transfected cells was significantly higher (20.4° ± 3.8, n = 48), indicating aberrant spindle orientation relative to the substratum (Figure 2E, right graph). Spindle misorientation was also supported by the fact that the proportion of cells showing a relative distribution of spindle angles under 10° was markedly lower among si-htt1-transfected cells (30%) than among control cells (70%). A significant proportion (48%) of htt-depleted cells had spindle angles greater than 20° (Figure 2E). No correlation between spindle angles and cell area in metaphase was observed (Figure S2B), indicating that the changes in the spindle angle do not result from changes in cell dimensions. To confirm these results, we reduced htt levels using si-htt2 whose target sequence is located in the C terminus (Figures 1A, 2B, and 2C). Similar results showing a misoriented spindle when downregulating htt were obtained (Figure 2F). Next we introduced an N-terminal 1301 amino acid fragment of htt (Figures 2B, 2C, and 2F) (Anne et al., 2007). The si-htt2 targeted the endogenous mouse htt and had no effect on the expression of htt-1301 fragment (Figure 2B). This N-terminal fragment restored the spindle orientation defect observed with si-htt2 to the control situation (Figures 2C and 2F). Thus loss of htt leads to spindle misorientation and the htt-1301 fragment recapitulates the function of htt during mitotic spindle orientation.

Given that htt is also expressed in nonneuronal cells (Tao and Tartakoff, 2001), we tested the possibility that the function of htt in spindle orientation extended to other cell types. We analyzed the role of htt in HeLa cells, which have been widely used to study different aspects of mitosis (Figures S2C–S2F). Htt levels were similar in HeLa and in neuronal cells (data not shown). Htt was concentrated at the spindle poles during mitosis (Figure S2C). Depletion of htt by RNA interference induced a statistically significant increased percentage of HeLa cells with misorientated spindles during mitosis (more than nine stacks of 0.2 μm between the two poles, $\Delta Z > 1.8$ μm) (Figures S2D–S2F) as in neuronal cells (Figure 2; Figure S2A). These findings suggest that htt ubiquitously regulates spindle orientation.

Huntingtin Is Required for the Recruitment of Dynein/Dynactin and NuMA to the Spindle and for Its Positioning

What are the underlying mechanisms by which htt monitors spindle orientation? We performed immunostainings for α-tubulin to analyze the morphology of mitotic spindles and astral microtubules. The general morphology of the spindle and asters emerging from the poles were comparable in htt-depleted and control mouse neuronal cells (Figure 3A). However, si-htt1-treated cells exhibited smaller spindles (Figures 3A and 3B). The smaller spindles were correlated to the smaller size of these cells (Figure 3C). As mitotic spindle and the formation of asters are dynamic microtubule-based structures, we depolymerized microtubules with nocodazole and followed microtubule regrowth after washout of the drug in si-htt1 and scramble RNA-treated neuronal cells. Microtubules regrowth was allowed for 4, 8, 12, and 18 min (t = 0 and t = 12 min are shown in Figure 3D). The nucleation at these different time points was similar in both conditions (Figure 3D and data not shown). Further, the speed of microtubule plus-end binding protein 3 fused to GFP (EB3-GFP) comets was similar in si-htt1 and scramble-treated cells (si-htt1: 0.23 ± 0.11 μm/s, n = 18; scramble: 0.24 ± 0.14 μm/s, n = 17; mean ± SEM). In conclusion, depletion of htt leads to smaller mitotic spindle without affecting microtubule nucleation and growth.

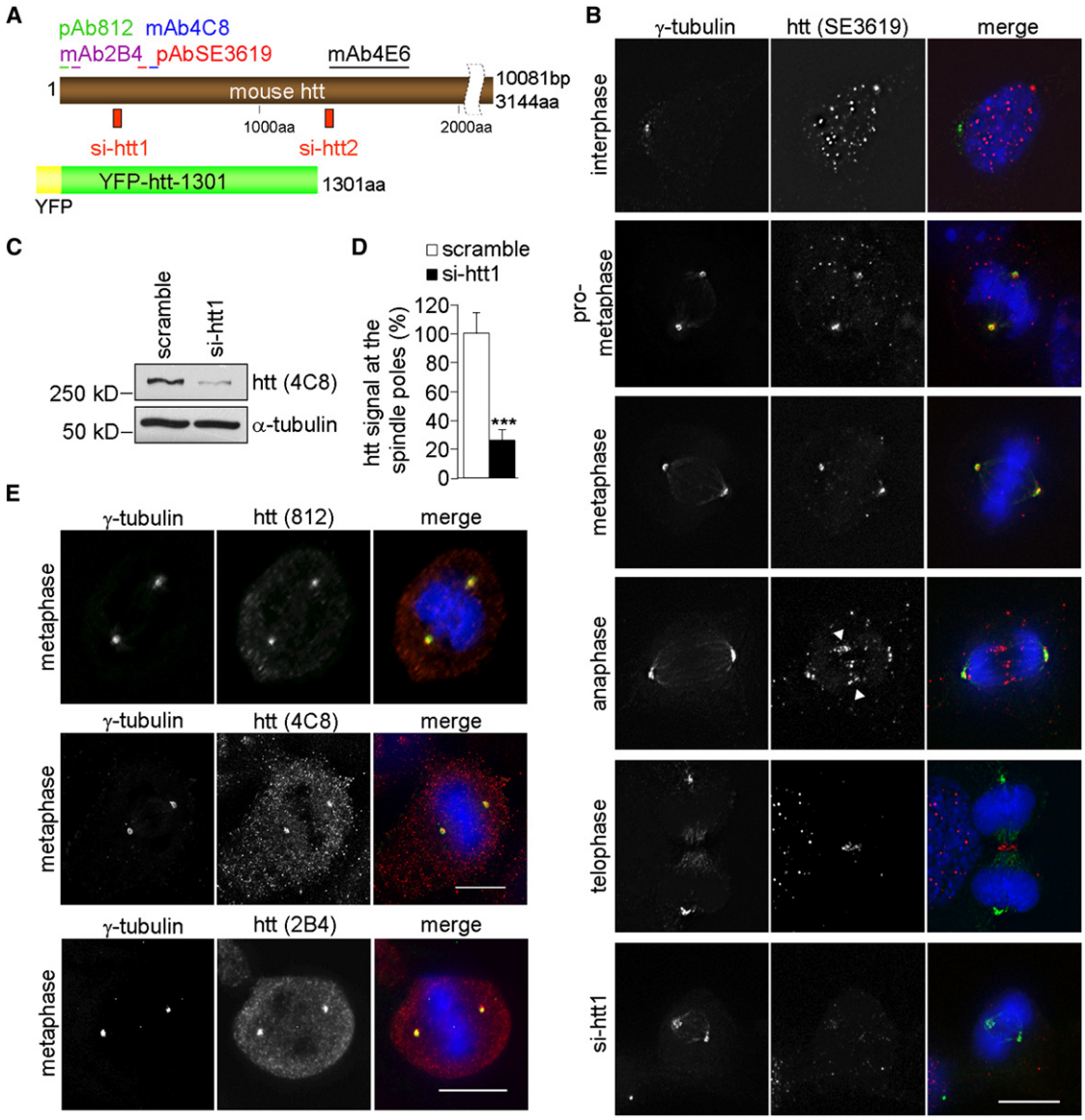

Figure 1. Huntingtin Localizes to Spindle Poles during Mitosis

(A) Schematic representation of htt.

(B) Immunostaining of mouse neuronal cells with anti-γ-tubulin and anti-htt (SE3619, red) antibodies and DAPI counterstaining.

(C) Lysates from scramble and si-htt1 RNA-treated cells are analyzed by immunoblotting using anti-htt (4C8) and anti-α-tubulin antibodies.

(D) Quantification of anti-htt (SE3619) signal at the spindle poles. ***$p < 0.001$.

(E) Immunostaining of metaphase mouse neuronal cells using 812, 4C8, and 2B4 htt antibodies.

All scale bars, 5 μm. Error bars, SEM.

The p150^{Glued} subunit of dynactin associates with cytoplasmic dynein to regulate spindle orientation (Carminati and Stearns, 1997; Moore et al., 2008; Siller et al., 2005; Skop and White, 1998). Htt forms a complex with dynein/dynactin to stimulate axonal transport in neurons (Gauthier et al., 2004). NuMA is another essential component in mitotic spindle pole formation (Merdes et al., 1996; Radulescu and Cleveland, 2010), which was reported to interact with htt by yeast two-hybrid screening (Kaltenbach et al., 2007). We first compared the phenotype observed in htt-depleted cells to that induced by the silencing of p150^{Glued} (Figure 2A). Spindle misorientation was observed to similar extends after silencing either htt or p150^{Glued} with an increase in the average spindle angle and distribution (Figures 2C–2E). As with htt depletion, in p150^{Glued}-depleted cells, no correlation between spindle angles and cell area in metaphase was observed, while the spindle length was reduced (Figures 3B, 3C, 4B, and S2B). We also investigated whether the depletion of htt affects the distribution of p150^{Glued}. Consistent with previous studies, p150^{Glued} was observed at the spindle poles and at the spindle during mitosis (Figure 4A) (Busson et al.,

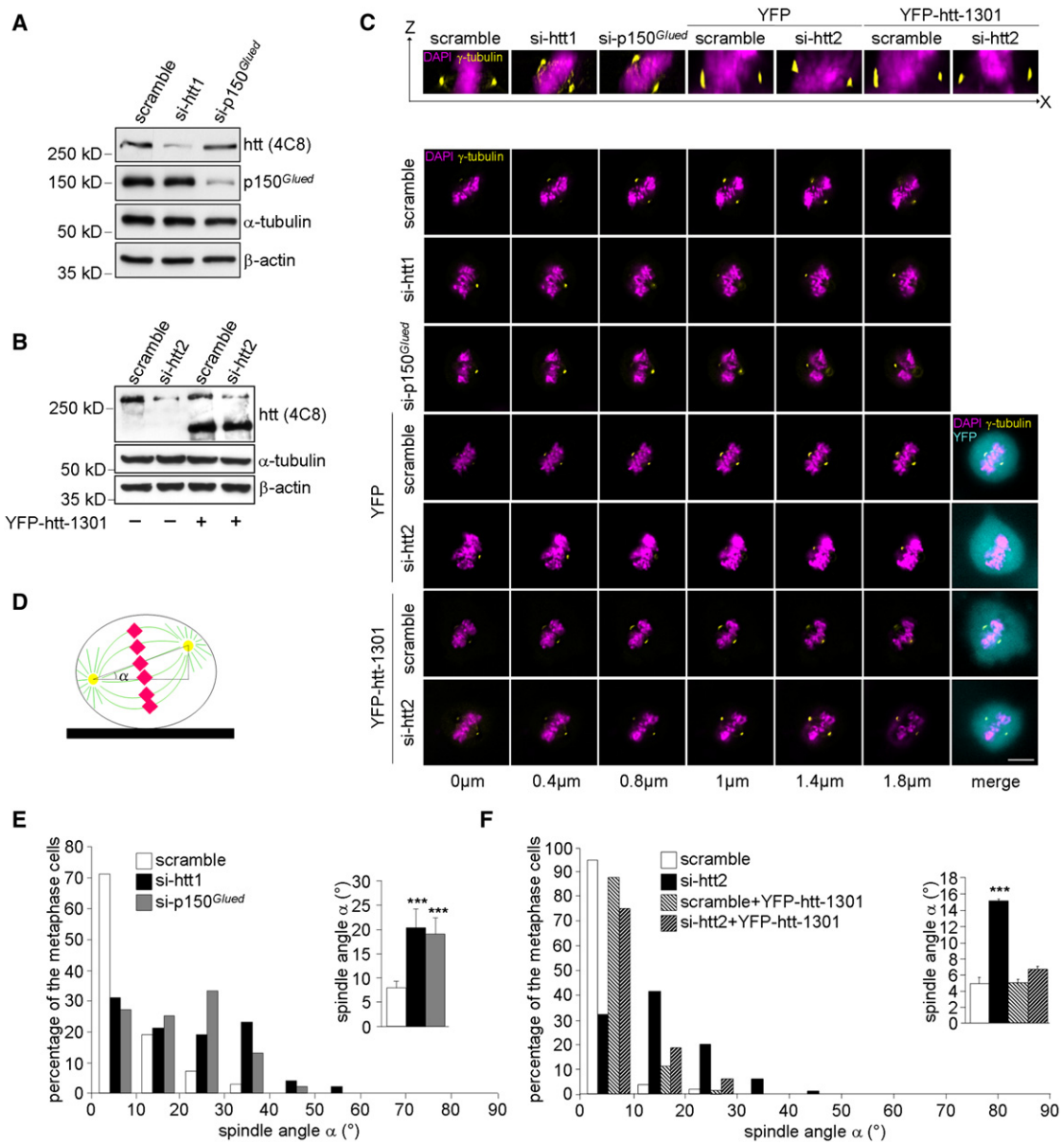

Figure 2. Loss of Huntingtin Causes Spindle Misorientation

(A) Immunoblotting of scramble, si-htt1, and si-p150^{Glued} RNA-treated mouse neuronal cell extracts using anti-htt (4C8), anti-p150^{Glued}, anti-α-tubulin, and anti-β-actin antibodies.

(B) Immunoblotting of extracts from scramble and si-htt2 RNA-treated mouse neuronal cells expressing htt 1301 N-terminal fragment (YFP-htt-1301) or empty vector (YFP) using anti-htt (4C8), anti-α-tubulin, and anti-β-actin antibodies.

(C) Immunostaining of mouse neuronal cells treated as in (A) and (B) with γ-tubulin and DAPI and Z-X projections (top) or Z-stacks (bottom). Scale bar, 10 μm.

(D) Scheme illustrating the measurement of the spindle angle α.

(E and F) Distribution and average of spindle angles of metaphase cells in mouse neuronal cells treated with scramble, si-htt1, or si- p150^{Glued} RNAs (E) and (F) with scramble, si-htt2, scramble + YFP-htt-1301, and si-htt2 + YFP-htt-1301.

All graphs ***$p < 0.001$. Error bars, SEM.

1998). The depletion of htt resulted in partial mislocalization of p150^{Glued} from the spindle poles (Figures 4A and 4E). Conversely, the silencing of p150^{Glued} induced a significant increase in the level of htt at spindle poles (Figures 4B and 4F), demonstrating interplay between these two proteins. We next evaluated the effect of depleting htt on dynein and NuMA localizations. Dynein and NuMA were enriched at the spindle poles in metaphase cells with NuMA showing a typical crescent shape pattern (Figures 4C and 4D). When htt was depleted, these proteins were dispersed around the spindles poles.

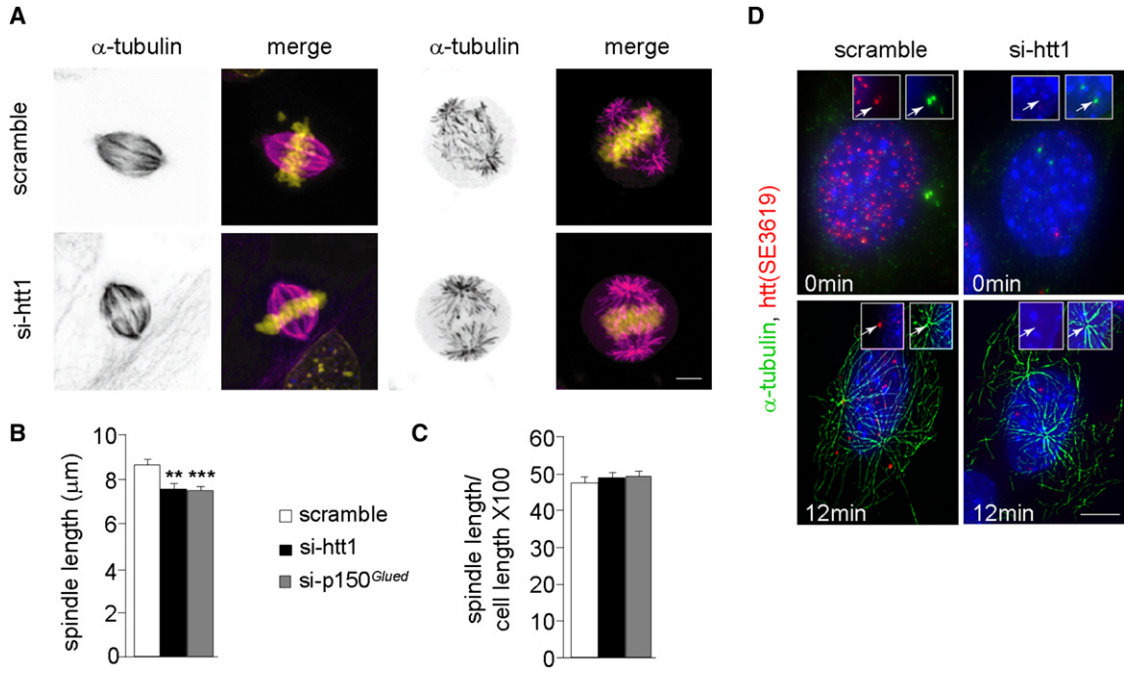

Figure 3. Loss of Huntingtin Leads to Shortened Spindles

(A) Immunostainings of scramble or si-htt1 RNA-treated mouse neuronal cells with α-tubulin and DAPI counterstaining.

(B and C) Quantification of spindle length of metaphase cells. **$p < 0.01$ and ***$p < 0.001$.

(D) Effect of htt depletion on microtubule regrowth. Mouse neuronal cells transiently transfected with scramble or si-htt1 RNAs, treated with nocodazole for 1 hr and incubated 30 min on ice are labeled using anti-α-tubulin and anti-htt (SE3619) antibodies to visualize microtubules upon regrowth. White arrow shows centrosomes and htt.

All scale bars, 5 μm. Error bars, SEM.

Finally, we investigated the dynamic positioning of the spindle by video-recording dividing HeLa cells stably expressing fluorescent core histone 2B (cherry) and α-tubulin (GFP) treated with scramble or si-Huhtt RNAs (Steigemann et al., 2009) (Figure 4I and Movie S1). The duration of mitosis was similar in HeLa cells treated with si-Huhtt or scramble RNAs (si-Huhtt: 32.44 ± 1.73 min, n = 18; scramble: 33.17 ± 2.33 min, n = 8; mean ± SEM). Once reaching anaphase, the angles between the pole-pole axis and the substratum plane were retrospectively calculated each minutes and represented as a function of time (Figure 4J). In HeLa cells treated with si-Huhtt, the mitotic spindle angle to the substratum plane was more variable during mitosis compared with the control. Calculation of the amplitude of spindle angle also revealed a difference between both conditions (Figure 4K) with the spindle pole showing more oscillations before finding its final position in htt-depleted cells. Taken together, these observations suggest that htt controls spindle orientation by ensuring the proper localization of several key components of the spindle and, as a consequence, the positioning of the spindle.

Huntingtin Regulates the Orientation of the Plane of Cell Division

To investigate the consequences of htt regulation of spindle orientation in cultured adherent cells, we performed time-lapse recordings of dividing mouse neuronal cells. As previously described for other cells (Toyoshima and Nishida, 2007), we observed two types of cell division: cells that divide in and cells that divide outside the plane of the substratum (Figure 5A). Forty-eight hours posttransfection, cells were video-recorded for 20 hr, and the time-lapse sequences were analyzed to determine the frequency of each type of cell division. Most of the divisions occur in the plane of the substratum (Figure 5A). However, consistent with the role of htt in the proper orientation of the spindle, we observed a higher number of cells dividing outside the substratum plane in si-htt1-transfected cells than in scramble-transfected cells (Figure 5B).

In cell culture, impairment of cell division relative to the substratum plane can promote cell death through detachment-induced apoptosis. We found an increased rate of postmitotic cell death when htt was silenced (Figure 5C). Mitotic index showed no significant difference between cells treated with si-htt1 and scramble RNAs (Figure 5D). We also analyzed the distribution of cells across mitotic phases based on chromosome configurations. As previously described, disturbing dynactin resulted in a prometaphase arrest (Figure 5E) (Echeverri et al., 1996). However, si-htt1-treated cells were distributed across all mitotic phases showing no difference with the control situation. Consistent with this, the duration of the mitosis was the same in si-htt1 and scramble conditions (Figure 4I). These data suggest that htt controls the plane of division of mitotic cells without affecting their progression through the cell cycle.

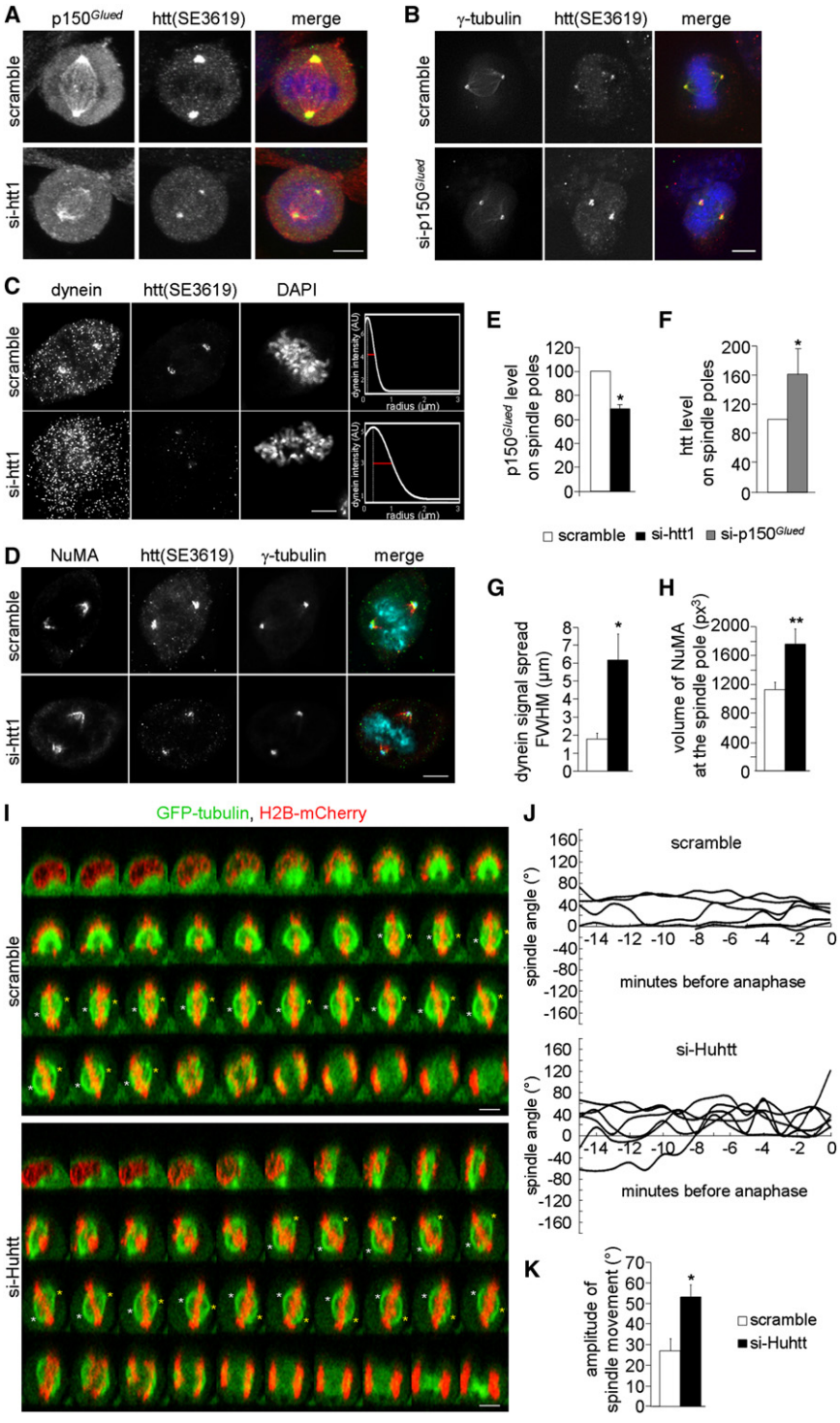

Figure 4. Loss of Huntingtin Perturbs Molecular Motor Distribution at Spindle Poles

(A and E) Immunostainings of metaphase mouse neuronal cells treated with scramble or si-htt1 RNAs with anti-htt (SE3619), anti-p150^{Glued} antibodies, and DAPI counterstaining. Quantification (E).

(B and F) Mouse neuronal cells are treated with scramble or si-p150^{Glued} RNAs and immunostained with anti-γ-tubulin and anti-htt (SE3619) antibodies and counterstained with DAPI. Quantification (F).

(C and G) Mouse neuronal cells treated as in (A) and immunostained with anti-dynein and anti-htt (SE3619) antibodies and counterstained with DAPI (C). Analyses of dynein intensities in htt-depleted cells at increasing distance from the pole (C, graph). Full-width at half maximum (G, FWHM) is used as an estimator of the dynein signal spread.

(D and H) Immunostaining of metaphase mouse neuronal cells treated as in (A) with anti-htt (SE3619), anti-NuMA, anti-γ-tubulin antibodies and DAPI counterstaining. Quantification (H).

(I–K) HeLa cells stably expressing GFP–tubulin and H2B–mCherry are transfected with scramble or si-Huhtt RNAs and video-recorded for 2 hr. (I) Z-X projection of representative example of dividing cells for both conditions (from prophase to anaphase). Images are collected every minute. Position of each spindle pole is indicated with yellow and white stars. (J) Representation of angles between the pole-pole axis and the substratum plane as a function of time. (K) Amplitude of spindle pole movement.

All graphs *$p < 0.05$, **$p < 0.01$; (A–D) Scale bars 5 μm, (I) 10 μm. Error bars, SEM.

In Vivo Silencing of Huntingtin Modifies Spindle Orientation of Mouse Cortical Progenitors and Promotes Neurogenesis in the Neocortex

During cortical development, progenitor cells located in the ventricular zone (VZ) undergo divisions to ultimately generate post-mitotic neurons that migrate radially to form successive cell layers organized in an inside-out manner (Gonczy, 2008; Knoblich, 2008; Siller and Doe, 2009). To address whether htt controls mitosis in vivo, we carried out in utero electroporation-based transfection of cortical progenitors from E14.5 mouse embryos with GFP-expressing vectors and scramble or si-htt1 RNA. Two days after electroporation, we analyzed mitotic cleavage planes in GFP-expressing cortical progenitors, by measuring the angle between a line segregating the daughter chromosomes and the surface of the VZ, also named apical surface (Figures 6A–6C). This method allows us to predict the cleavage furrow position based on chromatin staining (Konno et al., 2008). Angles of the mitotic cleavage plane were comprised between 72° and 90° in 68.8% of control GFP-labeled dividing cells. In contrast, silencing htt with si-htt1 resulted in a smaller percentage of dividing progenitors displaying mitotic angles between 72° and 90° (65%) and a greater proportion of cells

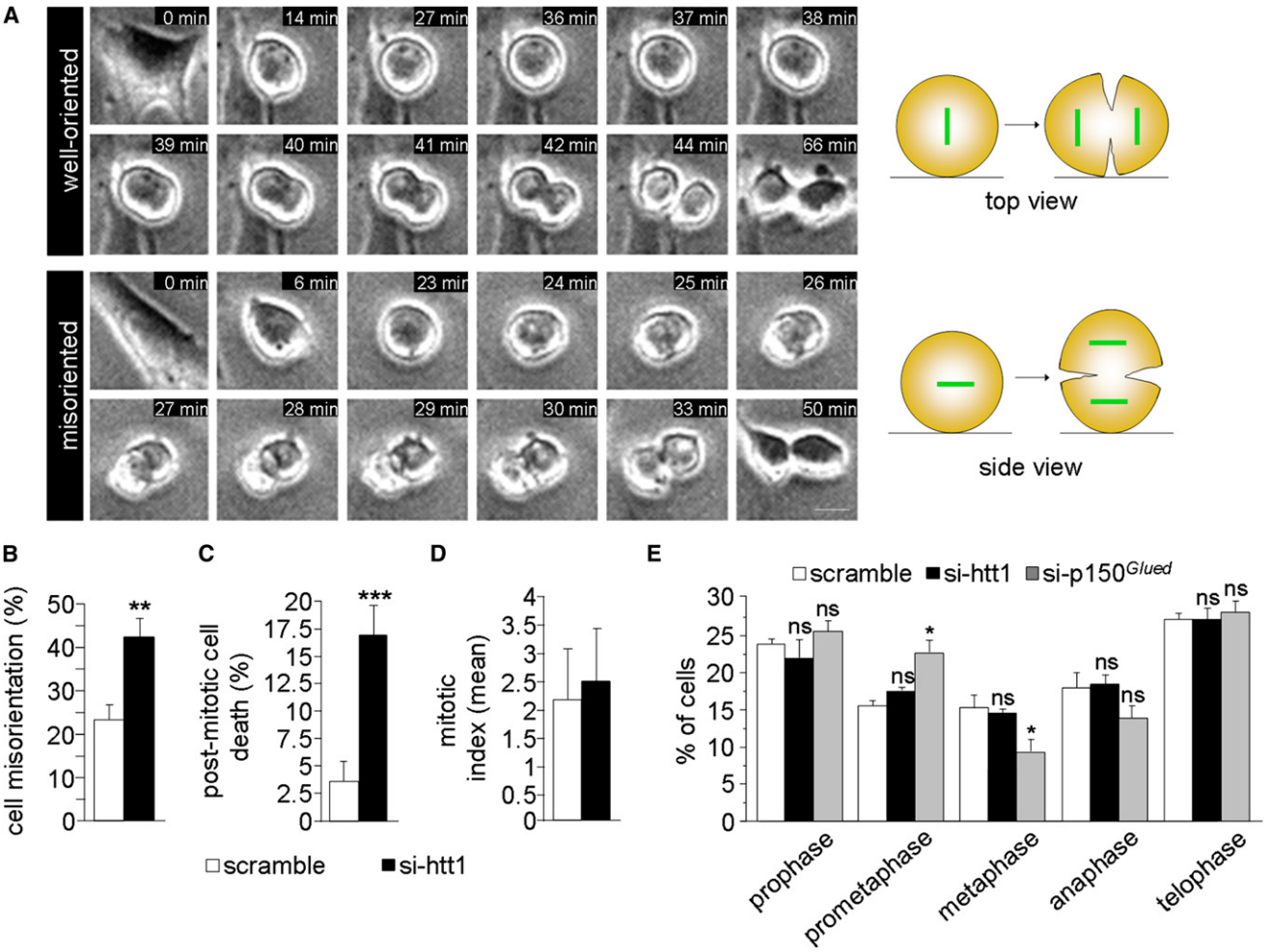

Figure 5. Huntingtin Regulates the Orientation of Division in Cultured Cells

(A) Video recording of mouse neuronal cells reveals two cell populations: cells dividing in (well-oriented) and out of the substratum plane (misoriented). Scale bar, 10 μm.

(B) Cells transfected with scramble or si-htt1 RNAs are video-recorded for 20 hr. Cells are classified as in (A).

(C and D) Cells are treated as in (B) and the dividing cells are assessed for death after mitosis (C) or for mitotic index (D).

(E) Distribution of mouse neuronal cell transfected with scramble, si-htt1 or si-p150^{Glued} RNAs in each phase of cell cycle.

All graphs ns: not significant, *$p < 0.05$, **$p < 0.01$ and ***$p < 0.001$. Error bars, SEM.

with a mitotic angle below 54° (27.5% versus 6.3% in scramble condition). We also classified the dividing progenitors into three groups according to the orientation of the cleavage plane to the apical surface: vertical (60°–90°), horizontal (0°–30°), and intermediate (30°–60°) (Figure S3A). As expected (Farkas and Huttner, 2008; Konno et al., 2008), the majority of GFP-labeled dividing cells displayed vertical cleavage planes (Figure S3B). In comparison, a smaller percentage of dividing progenitors transfected with si-htt1 exhibited vertical cleavage planes. To confirm the absence of any off target effects, we performed the same experiment with si-htt2 (Figures 6B, 6C, and S3B). si-htt2 resulted in a statistically significant smaller percentage of dividing progenitors displaying angles of the mitotic cleavage plane between 72° and 90° (51.8% versus 68.8% in scramble condition) and a greater proportion of cells with angles below 54° (21.5% versus 6.3% in scramble condition). Furthermore, introducing the htt-1301 fragment with si-htt2 led to a distribution of mitotic angles comparable to that of the control situation (scramble RNA, Figures 6B, 6C, and S3B). These results demonstrate that depletion of htt by RNA interference in neuronal progenitors in vivo leads to spindle misorientation with an increase in the proportion of progenitors with intermediate and horizontal cleavage planes.

Apical progenitors, produce neurons and glia (Gonczy, 2008; Knoblich, 2008; Siller and Doe, 2009). A second type of progenitors, the basal progenitors, is generated from apical progenitors, divides away from the VZ and generates neurons. The cleavage plane of dividing progenitors may regulate cell fate of daughter cells (Gauthier-Fisher et al., 2009; Marzesco et al., 2009). Thus, spindle misorientation that results from the silencing of htt in apical progenitors could impair such process. We electroporated apical progenitors from E14.5 mouse embryos with

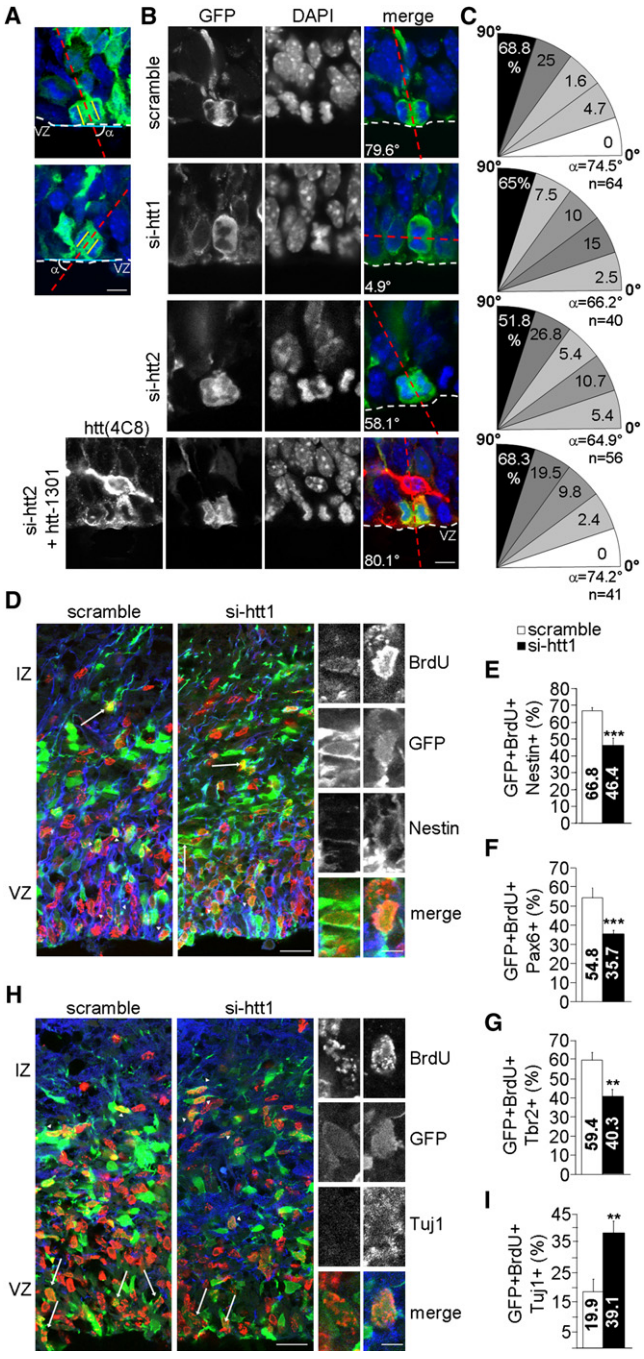

Figure 6. In Vivo Silencing of Huntingtin Modifies Spindle Orientation and Cell Fate of Mouse Cortical Progenitors

(A and B) pCAGGS-NLS-GFP is cotransfected with scramble, si-htt1, si-htt2 + empty vector (pCAGGS-LB-IRES-NLS-GFP), or si-htt2 + htt-1301 (pCAGGS-htt-1301-IRES-NLS-GFP) in E14.5 embryos and brains are fixed at E16.5. Coronal brain sections of E16.5 embryos are stained with antibodies for GFP and nuclei are counterstained with DAPI. (A) Method of measurement of mitotic spindle angle (α) in anaphase cortical progenitors. Orientation of the sister chromatids and the ventricular zone (dashed white line, VZ) are shown, respectively, by yellow and blue lines. Cleavage plane is determined to be positioned such that the distance between the two chromatids is halved (dashed red line). The smallest angle between the cleavage plane and the apical surface is calculated. (B) Progenitors are stained for GFP and htt (4C8). Representative examples of each condition are shown. Scale bars, 10 μm.

(C) Mitotic progenitors are distributed in five 18° intervals according to their cleavage plane angle relative to the apical surface. Values are expressed as a percentage of cortical progenitors within each interval. Mean angle (α) and number of measures (n) are shown.

(D and H) pCAGGS-NLS-GFP is electroporated with scramble or si-htt1 RNAs in cortical progenitors from E14.5 mouse embryos. An intraperitoneal injection of BrdU is performed at E15.5 and brains are analyzed at E16.5. Coronal brain sections are stained with antibodies for BrdU, GFP (green), Nestin (D) and Tuj1 (H). Scale bars, 20 for two large left panels in both (D) and (H) and 10 μm for eight panels on right in both (D) and (H).

(E, F, G, and I) Quantification of the GFP-BrdU-Nestin (E), GFP-BrdU-Pax6 (F), GFP-BrdU-Tbr2 (G), and GFP-BrdU-Tuj1 (I) -positive cells among the GFP-BrdU-positive cells.

All graphs $^{**}p < 0.01$ and $^{***}p < 0.001$. Error bars, SEM.

GFP-expressing vectors and a scramble or si-htt1 RNA. Intraperitoneal injections of BrdU were performed 1 day later to follow the fate of cycling progenitors. BrdU and GFP-labeled cells were then analyzed at E16.5 by immunohistochemistry using progenitor cells (Nestin, Pax6, Tbr2) and neuronal (Tuj1) markers (Figures 6D–6I). Electroporation of si-htt1 decreased the pool of cycling progenitors (BrdU+/GFP+/Nestin+ cells: 46.4% versus 66.8% in control), including apical (BrdU+/GFP+/Pax6+ cells: 35.7% versus 54.8% in control) and basal (BrdU+/GFP+/Tbr2+ cells: 40.3% versus 59.4% in control) progenitors as compared with the control condition (Figures 6D–6G). The decrease in cycling progenitors was not associated with an increased cell death as determined by a cleaved caspase 3 staining (Figure S3D). Instead, we observed a strong increase in the proportion of newborn postmitotic neurons with 39.1% of BrdU- and GFP-labeled cells also positive for Tuj1 in si-htt1-electroporated cells, as compared with 19.9% in the scramble-electroporated cells (Figures 6H and 6I). We also determined the proportion of BrdU- and GFP-labeled cells in different layers of the E16.5 cortical coronal sections (Figure S3E). There was no difference between the scramble RNA and the si-htt1 situations suggesting that htt depletion does not interfere with neuronal migration. In summary, loss of htt expression in cortical progenitors favors their neuronal differentiation at the expense of their proliferation and maintenance in the VZ.

Inactivation of the Mouse Huntingtin Gene in Nestin Cell Lineages Alters Cell Division and Cell Fate of Cortical Progenitors

To unequivocally address the role of htt in the control of spindle orientation of mouse progenitors, we inactivated the mouse *Hdh* gene in Nestin cell lineages. *Nestin-Cre*/+ mice (Tronche et al., 1999) were crossed with *Hdh*+/− mice (Zeitlin et al., 1995) and double heterozygous *Nestin-Cre*/+; *Hdh*+/− males were then crossed with *Hdhflox/flox* females (Dragatsis et al., 2000). We then analyzed spindle orientation of dividing apical progenitors in E14.5 wild-type and *Nestin-Cre*/+;*Hdhflox*/- mouse embryos by measuring the cleavage plane orientation as before (Figures 7A–7C). In wild-type embryos, 65.1% of the progenitors divided with angles of the mitotic cleavage plane ranging from 72° to 90° (Figure 7C). In contrast, the lack of htt expression in Nestin cells

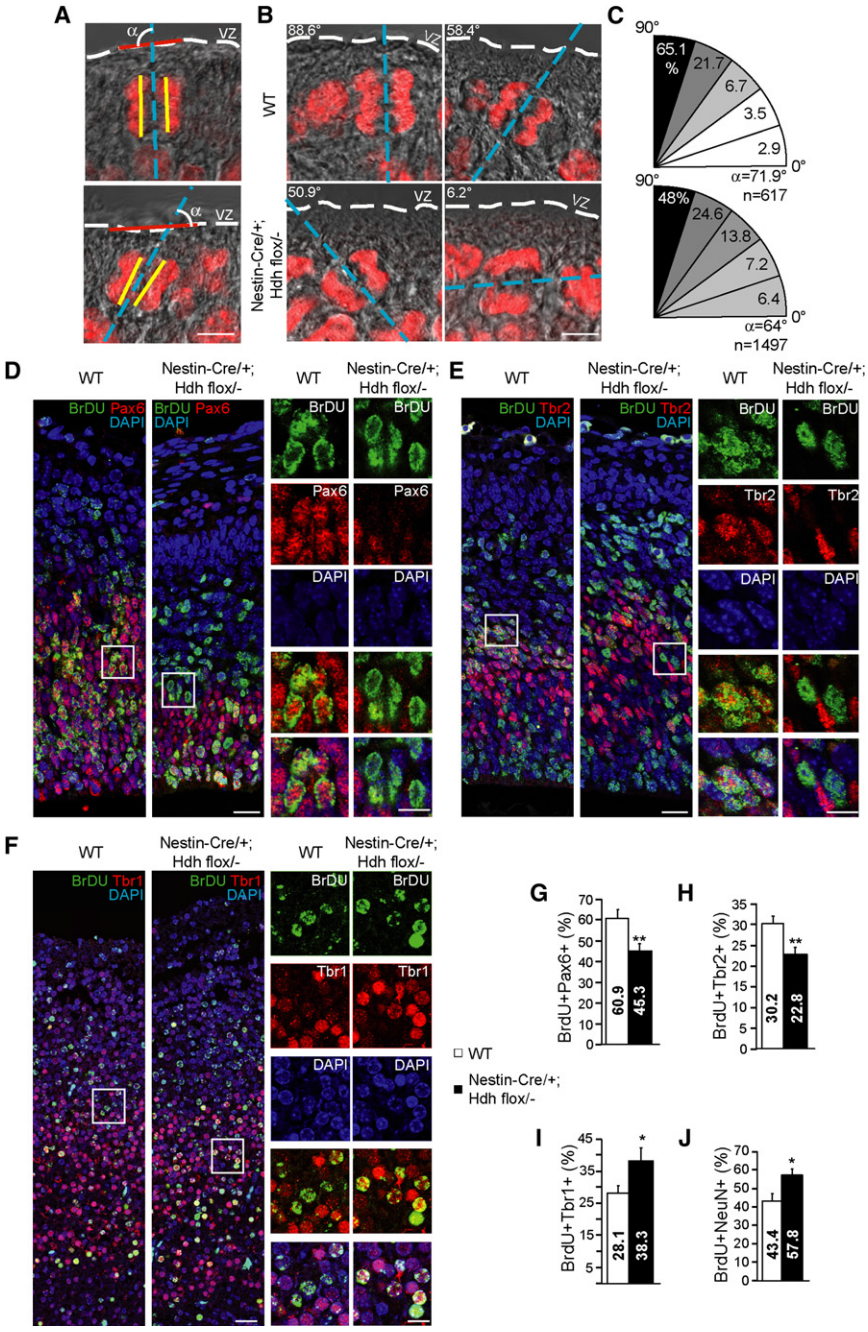

Figure 7. Nestin Progenitors Lacking Huntingtin Show Altered Cleavage Plane Orientation and Cell Fate

(A) Method of spindle angle (α) measurement in apical progenitor. Sections of E14.5 embryo are stained for DNA using DAPI. Orientation of the sister chromatids and the ventricular zone (dashed white line, VZ) are shown, respectively, by yellow and red lines. VZ border is shown by differential interference contrast microscopy. Cleavage plane is shown by dashed blue line. The smallest angle between the cleavage plane and the apical membrane is calculated. Scale bar, 5 μm.

(B) Coronal brain sections of wild-type (WT) and *Nestin-Cre/+;Hdhflox/-* E14.5 embryos are stained with DAPI. Representative examples are shown. Scale bar, 5 μm.

(C) Dividing progenitors at E14.5 are distributed in five 18° intervals according to their cleavage plane angle relative to the apical surface. Values are expressed as a percentage of cortical progenitors within each interval. Mean angle (α) and number of measures (n) are shown.

(D–I) An intraperitoneal injection of BrdU is performed at E13.5 and wild-type (WT) and *Nestin-Cre/+;Hdhflox/-* brains are analyzed at E14.5 (D, E, G, and H) or E18.5 (F, I, and J). Coronal brain sections are stained with antibodies for BrdU, pax6 (D), Tbr2 (E), or Tbr1 (F) and counterstained with DAPI. Scale bars, 10 μm (D and E) or 20 μm (F) (left) and 5 μm (D and E) or 10 μm (F) (enlargements, right).

(G–J) Quantifications of the BrdU-Pax6 (G), BrdU-Tbr2 (H), BrdU-Tbr1 (I), and BrdU-NeuN (J) -positive cells among the BrdU-positive cells.

All graphs *p < 0.05, **p < 0.01. Error bars, SEM.

resulted in 48.0% of progenitors displaying angles above 72° while an increased proportion had angles below 54° (27.4% versus 13.1% in wild-type progenitors). When classifying the progenitors according to their cleavage planes (Figure S3A), we observed less vertical cleavage plane in dividing progenitors in *Nestin-Cre/+;Hdhflox/-* embryos compared with the wild-type embryos (Figure S3C). Thus, knock-down of htt in Nestin progenitors increases the proportion of progenitors with a misalignment of the cleavage planes relative to the apical surface. This recapitulates the phenotype observed after acute depletion of htt in cortical progenitors using in utero electroporation (Figures 6A–6C and S3B).

To investigate the consequences of the lack of htt on neuronal differentiation of cortical progenitors, we performed intraperitoneal injections of BrdU at E13.5. Wild-type and *Nestin-Cre/+;Hdhflox/-* brains were then analyzed by immunohistochemistry using antibodies against BrdU and markers of progenitor cells (Pax6 and Tbr2) at E14.5 (Figures 7D and 7E) or markers of postmitotic neurons (Tbr1 and NeuN) at E18.5 (Figures 7F). The pool of cycling apical (BrdU+/Pax6+ cells: 45.3% versus 60.9% in control) (Figures 7D and 7G) and basal progenitors (BrdU+/Tbr2+ cells: 22.8% versus 30.2% in control) (Figures 7E and 7H) was decreased in *Nestin-Cre/+;Hdhflox/-* brains as compared with the wild-type condition. Quantification of the BrdU+/Tbr1+ and BrdU+/NeuN+ newborn neurons revealed that depleting htt increased the proportion of differentiated neurons as compared with the wild-type condition (BrdU+/Tbr1+ cells: 38.3% versus 28.1% in control; BrdU+/NeuN+ cells: 57.8% versus 43.4% in control) (Figures 7F, 7I, and 7J). These

effects were not accompanied by an increased cell death or migration defects (data not shown).

Collectively, our results demonstrate that htt ensures proper spindle orientation and controls the fate of progenitors in the developing mouse neocortex.

Drosophila melanogaster Huntingtin Regulates Spindle Orientation in Larval Neuroblasts

To further establish the role of htt in spindle orientation, we analyzed the function of htt in *D. melanogaster* neuroblasts, the neuronal precursors of the central nervous system. Their mode of division is a well-studied model for investigating the molecular mechanisms involved in asymmetric cell division (Knoblich, 2008). Neuroblasts have apical/basal polarity and they align their mitotic spindle with this axis giving rise to a larger apical cell, which divides in a stem cell-like way, and to a smaller basal cell (ganglion mother cell, GMC), which divides only once more to ultimately generate differentiated neurons. This process involves the differential sorting of several proteins to the apical neuroblast (such as atypical protein kinase C, aPKC) and to the basal daughter cells (such as Miranda) (Siller and Doe, 2009). Apical/basal spindle orientation is determined by centrosome anchoring and migration (Rebollo et al., 2007, 2009; Rusan and Peifer, 2007). Proteins such as Mud are essential for spindle orientation by binding to PINS and to microtubules therefore linking cortical polarity proteins to the mitotic spindle (Bowman et al., 2006; Izumi et al., 2006; Siller et al., 2006).

We used the expression of two independent *D. melanogaster* htt (dHtt) dsRNA under the control of the inscuteable-Gal4 (*insc*) driver, which expresses Gal4 expression in neuroblasts (hereafter referred to as dHttRNAi(1) or dHttRNAi(2)) (Figures 8A–8C). We analyzed the effects of reducing htt on neuroblast spindle orientation by immunostaining for Miranda and Centrosomin in third instar larval brains. In *insc*-Gal4 neuroblasts, Miranda was distributed at the basal cortex forming a crescent at metaphase, the spindle bisecting the Miranda crescent (Figure 8A). In dHttRNAi(1) and dHttRNAi(2) neuroblasts, Miranda was still located at the basal cortical crescent at metaphase. However, the mitotic spindle failed to bisect the Miranda crescent in these cells. We quantified this defect by measuring the angle between a line connecting the two centrosomes and a line bisecting the Miranda crescent in metaphase neuroblasts (Figures 8B and 8C). As observed in mud^2 mutant neuroblasts (Figures 8A and 8C), decreased levels of htt in neuroblasts led to an increase in the percentage of neuroblasts that display abnormally positioned spindles with angles higher than 15° (25%, n = 40; 16%, n = 44 for dHttRNAi(1) and dHttRNAi(2), respectively, and 0%, n = 54 for *insc*-Gal4).

To ensure that the phenotype observed in dHttRNAi(1) and dHttRNAi(2) neuroblasts is due to the specific loss of htt and does not reflect off-target effects, we investigated spindle orientation in neuroblasts of a recently generated *Drosophila* htt knock-out model (Zhang et al., 2009) (Figures 8D and 8E). In wild-type w^{1118} animals, the measured angle was in majority less than 15° (89%, n = 56). However in the *dhtt-ko* mutant flies, spindles showed more oblique orientations with only 57% of spindles with measured angles of 15° or less (n = 40). Also, the spindle length was decreased in *dhtt-ko* dividing neuroblasts compared with w^{1118} and mud^2 neuroblasts (Figures 8F and 8G). This agrees with our observations in mammalian neuronal cells (Figures 3A and 3B).

Given the spindle orientation defect in metaphase neuroblasts depleted for htt, we analyzed the positioning of Miranda during telophase. We did not observe a missegregation of Miranda in *dhtt-ko* flies (data not shown). We next investigated whether depleting htt affected the number of neuroblasts. For this, we immunostained larval brains with neuronal (Elav) and neuroblast (Miranda) markers (Figure 8H). As expected, mud^2 mutants showed excess neuroblasts in the posterior half of the larval brain hemisphere and an increased brain size (Bowman et al., 2006; Peng et al., 2000), while the number of neuroblasts in this region was similar in the *dhtt-ko* and control flies (Figures 8H and 8I). We propose that *dhtt*-ko neuroblasts divide asymmetrically by repositioning the spindle during telophase. A similar correcting phenomenon was previously described for other mutants (Bowman et al., 2006; Peng et al., 2000).

We also tested whether *Drosophila* htt could rescue the spindle orientation defect in mammalian htt-depleted cells. We expressed a construct encoding the N-terminal 620 amino acid fragment of the *Drosophila* htt protein in mouse cells treated with scramble or si-htt1 RNA (Figure 8J). Expression of *Drosophila* htt significantly rescued spindle misorientation defects in htt-depleted mammalian cells but had no effect in control cells (Figure 8K). Overall, our data demonstrate that htt controls spindle orientation in *Drosophila* and that this function is evolutionarily conserved.

DISCUSSION

Huntingtin as a Scaffold Protein for the Dynein/Dynactin Complex in Dividing Cells

Previous studies have established a role for htt in the regulation of molecular motors. Htt forms a complex with dynein and dynactin in neurons (Caviston et al., 2007; Gauthier et al., 2004; Goehler et al., 2004; Li et al., 1998). Htt is required for efficient axonal transport, with decrease in htt levels leading to a reduced microtubule-dependent transport of vesicles (Caviston et al., 2007; Gauthier et al., 2004). The role of htt in the control of the dynein/dynactin complex could extend beyond a role in axonal transport as suggested by the fact that proper organization of the Golgi apparatus requires htt (Caviston et al., 2007; Strehlow et al., 2007). We now show that impairing the function of htt or dynactin results in similar phenotypes during mitosis.

While the dynein/dynactin complex is required for the assembly of spindle, it is also essential at the cell cortex to exert pulling forces on astral microtubules (Busson et al., 1998; Carminati and Stearns, 1997; Farkasovsky and Kuntzel, 2001; Nguyen-Ngoc et al., 2007; O'Connell and Wang, 2000; Skop and White, 1998). The exact mechanisms by which dynein/dynactin complexes are delivered to the cell cortex are not completely understood, but the location of dynein/dynactin at the astral microtubules plus ends involves at least the Bik1p/CLIP-170 and Pac1p/NudF/Lis1 proteins (Coquelle et al., 2002; Faulkner et al., 2000; Lee et al., 2003; Sheeman et al., 2003). Consistent with previous studies showing a reduction in dynein/dynactin-dependent transport in the absence of htt (Caviston et al.,

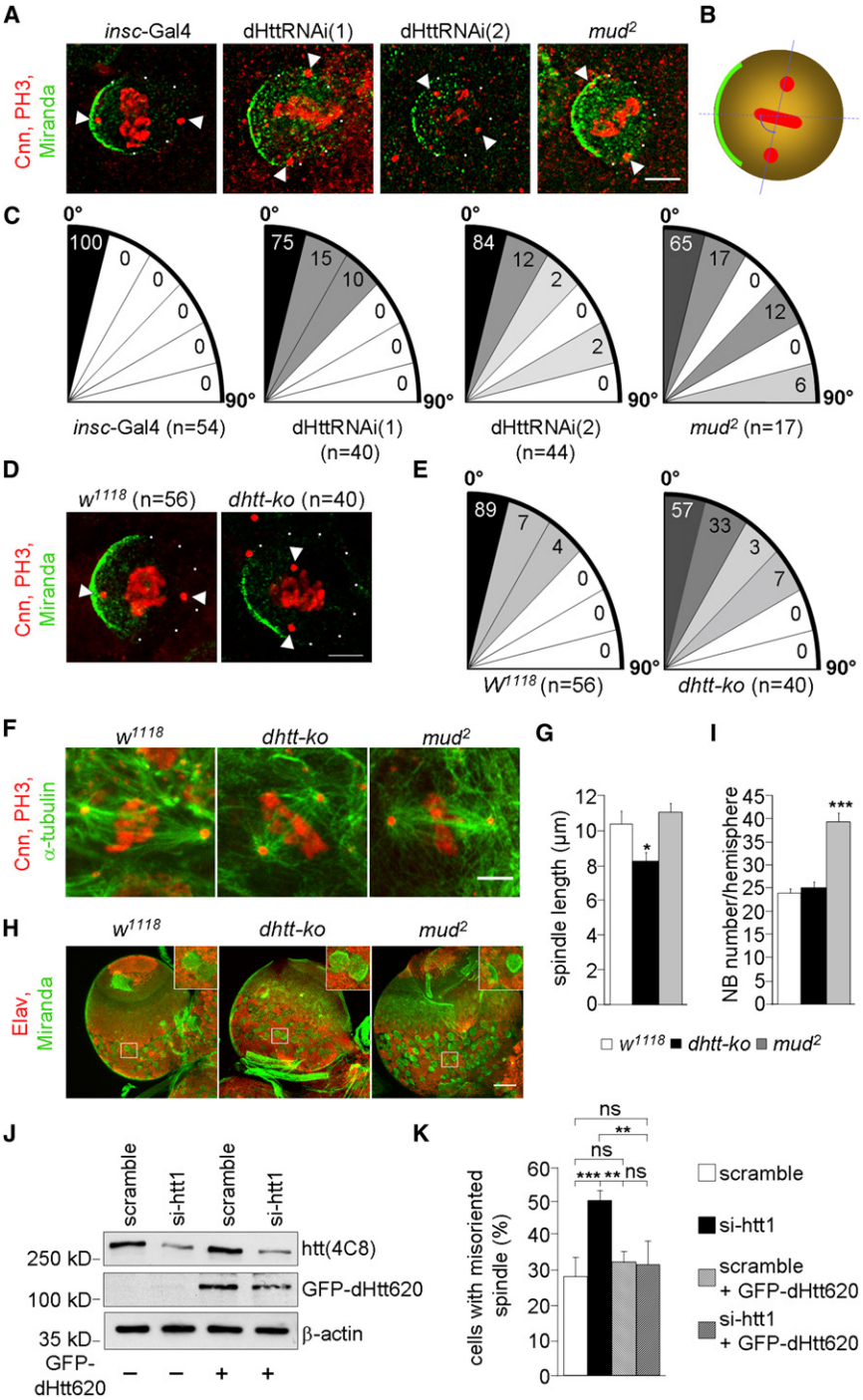

Figure 8. The Function of Huntingtin during Mitosis Is Conserved in *D. melanogaster* Neuroblasts

(A) *insc*-Gal4, dHttRNAi(1), dHttRNAi(2), and *mud*^{2} mutant neuroblasts of third instar larvae are stained with Centrosomin (Cnn, arrowhead), the mitotic marker phosphohistone H3 (PH3), and Miranda. Scale bar, 5 μm.

(B) Schematic representation of spindle poles (red) and Miranda crescent (green). The angle (line arc) between the spindle pole (solid line) and the middle of Miranda crescent (dashed line) is measured for each metaphase.

(C) Quantification of spindle orientation relative to Miranda crescent. Values are expressed as a percentage of neuroblasts within each angle intervals.

(D) *w*^{1118} and *dhtt-ko* neuroblasts of third instar larvae are stained as described in (A). Scale bar, 5 μm.

(E) Quantification of spindle orientation in *w*^{1118} and *dhtt-ko* neuroblasts as in (C).

(F and G) *w*^{1118}, *dhtt-ko*, and *mud*^{2} neuroblasts of third instar larvae are stained with Centrosomin (Cnn), the mitotic marker phosphohistone H3 (PH3), and α-tubulin. Scale bar, 5 μm. (G) Quantifications of spindle length in *w*^{1118}, *dhtt-ko*, and *mud*^{2} neuroblasts.

(H and I) *w*^{1118}, *dhtt-ko*, and *mud*^{2} brains of third instar larvae are stained with Elav and Miranda. Scale bar, 50 μm. (I) Quantification of neuroblasts (NB) number in the posterior brain hemisphere of third instar larvae.

(J) Western blot analysis showing the expression of a GFP-tagged N-terminal fragment of *Drosophila* htt (GFP-dHtt620) in mouse neuronal cells treated with scramble or si-htt1 RNAs.

(K) Mouse neuronal cells are treated as in (J).

All graphs ns: not significant, *p < 0.05, **p < 0.01, and ***p < 0.001. Error bars, SEM.

2007; Colin et al., 2008; Gauthier et al., 2004), our data suggest that the microtubule-dependent transport of the dynein/dynactin complex to the spindle is also reduced in htt-depleted cells. Therefore, it is tempting to speculate that htt could participate to the distribution of this complex at the cell cortex.

One attractive hypothesis is that htt functions as a scaffold molecule that orchestrates the assembly of the dynein/dynactin complex for distinct cellular functions (Caviston et al., 2007; Gauthier et al., 2004). During cell division, this could extend to a complex also containing NuMA (the *D. melanogaster* Mud and *C. elegans* LIN-5 homolog) (Radulescu and Cleveland, 2010). Indeed, NuMA was reported to interact with htt by yeast two-hybrid screening (Kaltenbach et al., 2007) and its localization is modified in the absence of htt. In mammalian cells, NuMA by assembling with dynein/dynactin is essential for the organization of microtubules at the spindle pole (Fant et al., 2004; Merdes et al., 1996). Furthermore, NuMA and the Goloco-containing protein LGN form a complex that regulates the interaction of astral microtubules with the cell cortex (Du and Macara, 2004).

Huntingtin, an Evolutionary Conserved Protein that Regulates Spindle Orientation

The precise spindle orientation is crucial for neuroepithelial stem cell proliferation (NESC). This mechanism is tightly regulated by

proteins such as *Lis1* (Yingling et al., 2008). In utero electroporation was performed at E14.5, and we observed the same phenotype in spindle orientation in acute and genetic depletion conditions. Thus, we can exclude that the phenotypes analyzed in mouse primarily derived from a defect during NESC divisions. However, htt could also participate to spindle orientation in NESC and therefore regulate neuronal development.

Although we show in this study that the function of htt in spindle orientation is conserved between flies and mammals, the phenotypes of flies and mice deleted for htt are different as $Hdh^{-/-}$ mice die during early embryogenesis (Duyao et al., 1995; Nasir et al., 1995; Zeitlin et al., 1995), whereas *dhtt-ko* flies show no obvious developmental defects (Zhang et al., 2009). As proposed by Zhang and colleagues (Zhang et al., 2009), this discrepancy might be due to intrinsic differences between mouse and fly embryogenesis as early lethality in mouse is likely to result from the absence of htt in extraembryonic tissues (Dragatsis et al., 1998). In agreement with this hypothesis is the observation that mice deleted for htt in adult stages show neurodegeneration (Dragatsis et al., 2000) and, *dhtt-ko* adult flies show a compromised mobility and reduced viability (Zhang et al., 2009). Moreover, as in mouse models, absence of htt in fly increases the vulnerability to the presence of mutant htt (Leavitt et al., 2001; Zhang et al., 2009) suggesting that crucial functions are conserved between fly and mouse htt.

Asymmetric cell division is a key cellular event generating cell diversity. It is tightly regulated through proper spindle orientation and segregation of cue determinants. Most of our understanding of the mechanisms that control spindle orientation is based on studies of *D. melanogaster*, *C. elegans*, and mice (Gonczy, 2008; Knoblich, 2008; Siller and Doe, 2009). Many of the proteins involved in spindle orientation and symmetric/asymmetric divisions are conserved in these species, including those that regulate cell polarity, cell fate, and spindle alignment. For example, LIN-5 in worms, Mud in *Drosophila*, and NuMA in mammals use similar mechanisms to regulate spindle assembly (Bowman et al., 2006; Knoblich, 2008). We demonstrate here that htt is a key regulator of spindle orientation in mammals and in flies. Is the role of htt in the regulation of the dynein/dynactin complex also conserved in *C. elegans*? A putative *C. elegans* ortholog of htt was recently identified (Palidwor et al., 2009). However, mammalian and worm htt sequences show only a low degree of similarity and there are no functional data available for worm htt demonstrating such a conserved function.

Role of Huntingtin in Determining Cell Fate

A direct link between the regulation of spindle orientation during neural progenitors division and the fate of the daughter cells is still under debate. Several proteins involved in spindle orientation control the subsequent generation and distribution of neurons in the brain. Lfc, a Rho-specific guanine nucleotide exchange factor, and its negative regulator Tctex-1 control the genesis of neurons from cortical precursor cells by regulating mitotic spindle orientation (Gauthier-Fisher et al., 2009; Marzesco et al., 2009). One study has also found that *adenomatous polyposis coli* APC is essential for the maintenance of radial glial polarity and the correct generation and migration of cortical neurons in mouse (Yokota et al., 2009). This could be linked to its function in spindle pole orientation. Indeed, APC localizes to kinetochores, spindles, and centrosomes and acts downstream of Akt in *Drosophila* to ensure correct chromosome segregation and mitotic spindle orientation (Buttrick et al., 2008). Studies on Nde1 have suggested a link between spindle orientation and the proper construction of mouse brain (Feng and Walsh, 2004). Nde1 is a lissencephaly gene 1 LIS1-interacting protein. Ablation of Nde1 in mice causes a small cerebral cortex resulting from mitotic defects and altered neuronal cell fate. Finally, $G\beta\gamma$ subunits of heterotrimeric G proteins and AGS3, a nonreceptor activator of $G\beta\gamma$, regulate spindle orientation in cortical progenitor cells; impairing this signaling enhances neuronal differentiation (Sanada and Tsai, 2005). In contrast, ablating LGN results in randomized spindle orientation of mouse cortical apical progenitors with little effect on neurogenesis (Konno et al., 2008). As shown in the study by Konno et al. and in our study, most of all cleavages of ventricular zone progenitors are vertical. However, vertical cleavages can result in either symmetric or asymmetric cell division. We show that removing htt changes the nature of the division cleavages, decreases the pool of cycling progenitors and increases neuronal differentiation. A crucial determining factor of symmetric versus asymmetric divisions is the distribution of the polarity and adhesion membrane proteins of the apical complex (Konno et al., 2008; Kosodo et al., 2004; Marthiens and ffrench-Constant, 2009; Yingling et al., 2008). Further studies are required to establish whether htt plays a role in such distribution between daughter cells.

Htt is widely expressed in the early developing embryo where it plays an essential role in several processes including cell differentiation and neuronal survival. Inactivation of the mouse gene results in developmental retardation and embryonic lethality at E7.5 (Duyao et al., 1995; Nasir et al., 1995; Zeitlin et al., 1995). Null homozygous embryos display abnormal gastrulation associated with increased apoptosis. Additionally, htt is essential for the early patterning of the embryo during the formation of the anterior region of the primitive streak (Woda et al., 2005). Finally, specific inactivation of htt in Wnt1 cell lineages leads to congenital hydrocephalus in mice further establishing a role for htt in brain development (Dietrich et al., 2009). Our data specifically show that htt is involved in neurogenesis. We observed similar phenotype when decreasing htt levels by RNA interference in VZ progenitors by electroporation at E14.5, or by genetic conditional removal of htt in these progenitors at early steps of cerebral cortical neurogenesis. The altered spindle orientation lowers the pools of both apical and basal progenitors and promotes neuronal differentiation of daughter cells. This may explain previous observations showing that lowering the levels of htt in mouse results, in addition to severe anatomical brain abnormalities, in ectopic masses of differentiated neurons near the striatum (White et al., 1997).

In conclusion, we demonstrate a function for htt protein in flies and mammals. These results not only open new lines of investigation for elucidating the pathogenic mechanisms in Huntington's disease, but also identify htt as a crucial player in spindle orientation and neurogenesis.

EXPERIMENTAL PROCEDURES

Statistical Analyses

Statview 4.5 software (SAS Institute Inc., Cary, NC) was used for statistical analysis. Data are expressed as mean ± SEM. Complete statistical analyses may be found in Supplemental Information.

Cell Lines and Transfection

Mouse neuronal cells and HeLa cells stably expressing GFP–tubulin and H2B–mCherry were cultured as previously described (Steigemann et al., 2009; Trettel et al., 2000). See Supplemental Information for culture and transfection details.

Videomicroscopy Experiments and Analyses

Videomicroscopy was performed 48 hr after electroporation. Images were collected in phase contrast using a coolSnap HQ camera (Ropper Scientific) every min during 20 hr (33°C, 5% CO_2). For determination of misorientation percentage, films were visualized with Metamorph, and dividing cells were classified into two groups: well-oriented or misoriented and numbered using a special plug-in.

To quantify microtubule polymerization velocity, mouse neuronal cells were grown on glass coverslips and mounted in a Ludin's chamber. The microscope and the chamber were kept at 33°C. Images with a Z-step of 0.3 μm were acquired with a X100 PlanApo N.A. 1.4 oil immersion objective coupled to a piezo device (PI). Images were collected in stream mode using a Micromax camera (Ropper Scientific) set at 2 × 2 binning with an exposure time of 150 ms (frequency of one stack/s). All stacks were treated by automatic batch deconvolution using the PSF of the optical system. Projections, animations, and analyses were generated using ImageJ software. Dynamics were characterized by tracking positions of EB3 comets in cells as a function of time with a special plug-in (F.P. Cordelières, IC, http://rsb.info.nih.gov/ij/plugins/track/track.html).

To quantify mitosis duration and spindle oscillation during mitosis, images of HeLa stably expressing GFP-tubulin and H2B-mCherry were collected every minute during 2 hr with xyzt acquisition mode using a Leica SP5 laser scanning confocal microscope equipped with a ×40 oil-immersion objective. Analysis was done using ImageJ. Dividing cells were resliced at the z axis. To quantify the duration from the beginning of the prophase until the beginning of anaphase, the number of frames between chromatin condensation and chromosome separation (1 frame = 1 min) were scored. To quantify spindle oscillation, the angle formed between the substratum plane and the virtual line passing through spindle poles was measured. Spindle oscillation analysis was performed during the 15 min previous to anaphase.

Cell Cycle Analysis

Mouse neuronal cells were electroporated with scramble, si-htt1, and si-p150^{Glued} RNAs. After 48 hr, cells were fixed in cold methanol at −20°C for 5 min, washed in PBS, stained with anti-γ-tubulin antibody and counterstained with DAPI. Cells were qualitatively assessed and binned into five categories: prophase, prometaphase, metaphase, anaphase, and telophase.

In Utero Electroporation

In utero electroporation was performed as described previously (Nguyen et al., 2006) with minor modifications. See Supplemental Information for details.

SUPPLEMENTAL INFORMATION

Supplemental Information includes Experimental Procedures, complete statistical analyses, four figures, and one movie and can be found online at doi:10.1016/j.neuron.2010.06.027.

ACKNOWLEDGMENTS

We greatly acknowledge J. Briscoe, D. Devys, N. Fabien, D.W. Gerlich, L.S.B. Goldstein, T.C. Kaufman, C.A. Martin, F. Maschat, F. Matsuzaki, N. Perrimon, M. Piel, and S. Zhang, Bloomington *Drosophila* stock center, *Drosophila* Genomics Resource Center, Vienna *Drosophila* RNAi Center (VDRC) stock center for reagents, flies and/or discussions; J.P. Dompierre for initial observations; F.P. Cordelières and the Institut Curie Imaging Facility for help in image acquisition and treatment; members of the Saudou and Humbert's laboratories for helpful comments. This work was supported by grants from Agence Nationale pour la Recherche (ANR-07-BLAN-3-207540, Y.B.; ANR-09-BLAN-0080, S.H.; ANR-08-MNP-039, F.S.), Association pour la Recherche sur le Cancer (ARC 4830, Y.B.; 3665, S.H.), Fondation pour la Recherche Médicale (FRM) and Fondation BNP Paribas (F.S.), F.R.S.-F.N.R.S. (L.N. and M.-L.V.), Fonds Léon Fredericq (L.N. and M.-L.V.), Fondation Médicale Reine Elisabeth (L.N.), CNRS, INSERM and ERC Starting Grants (CePoDro 209718, Y.B.) and the Curie Institute (Y.B., S.H., F.S.). J.D.G. was supported by Region Ile de France and ARC; K.C. by Ligue Nationale contre le Cancer and EMBO (Long Term Fellowship); M.M.-C. by an Institut Curie Foreign Student Ph.D. fellowship; D.Z. by FRM and Swiss National Science Foundation postdoctoral fellowships; B.C.C. by HighQ foundation and ARC; G.K. is a CNRS investigator; F.S. and S.H. are INSERM and INSERM/AP-HP investigators, respectively.

Accepted: June 17, 2010
Published: August 11, 2010

REFERENCES

Anne, S.L., Saudou, F., and Humbert, S. (2007). Phosphorylation of huntingtin by cyclin-dependent kinase 5 is induced by DNA damage and regulates wild-type and mutant huntingtin toxicity in neurons. J. Neurosci. *27*, 7318–7328.

Borrell-Pages, M., Zala, D., Humbert, S., and Saudou, F. (2006). Huntington's disease: from huntingtin function and dysfunction to therapeutic strategies. Cell. Mol. Life Sci. *63*, 2642–2660.

Bowman, S.K., Neumuller, R.A., Novatchkova, M., Du, Q., and Knoblich, J.A. (2006). The Drosophila NuMA Homolog Mud regulates spindle orientation in asymmetric cell division. Dev. Cell *10*, 731–742.

Busson, S., Dujardin, D., Moreau, A., Dompierre, J., and De Mey, J.R. (1998). Dynein and dynactin are localized to astral microtubules and at cortical sites in mitotic epithelial cells. Curr. Biol. *8*, 541–544.

Buttrick, G.J., Beaumont, L.M., Leitch, J., Yau, C., Hughes, J.R., and Wakefield, J.G. (2008). Akt regulates centrosome migration and spindle orientation in the early Drosophila melanogaster embryo. J. Cell Biol. *180*, 537–548.

Carminati, J.L., and Stearns, T. (1997). Microtubules orient the mitotic spindle in yeast through dynein-dependent interactions with the cell cortex. J. Cell Biol. *138*, 629–641.

Cattaneo, E., Zuccato, C., and Tartari, M. (2005). Normal huntingtin function: an alternative approach to Huntington's disease. Nat. Rev. Neurosci. *6*, 919–930.

Caviston, J.P., Ross, J.L., Antony, S.M., Tokito, M., and Holzbaur, E.L. (2007). Huntingtin facilitates dynein/dynactin-mediated vesicle transport. Proc. Natl. Acad. Sci. USA *104*, 10045–10050.

Colin, E., Zala, D., Liot, G., Rangone, H., Borrell-Pages, M., Li, X.J., Saudou, F., and Humbert, S. (2008). Huntingtin phosphorylation acts as a molecular switch for anterograde/retrograde transport in neurons. EMBO J. *27*, 2124–2134.

Coquelle, F.M., Caspi, M., Cordelieres, F.P., Dompierre, J.P., Dujardin, D.L., Koifman, C., Martin, P., Hoogenraad, C.C., Akhmanova, A., Galjart, N., et al. (2002). LIS1, CLIP-170's key to the dynein/dynactin pathway. Mol. Cell. Biol. *22*, 3089–3102.

Dietrich, P., Shanmugasundaram, R., Shuyu, E., and Dragatsis, I. (2009). Congenital hydrocephalus associated with abnormal subcommissural organ in mice lacking huntingtin in Wnt1 cell lineages. Hum. Mol. Genet. *18*, 142–150.

Dragatsis, I., Efstratiadis, A., and Zeitlin, S. (1998). Mouse mutant embryos lacking huntingtin are rescued from lethality by wild-type extraembryonic tissues. Development *125*, 1529–1539.

Dragatsis, I., Levine, M.S., and Zeitlin, S. (2000). Inactivation of hdh in the brain and testis results in progressive neurodegeneration and sterility in mice. Nat. Genet. *26*, 300–306.

Du, Q., and Macara, I.G. (2004). Mammalian Pins is a conformational switch that links NuMA to heterotrimeric G proteins. Cell *119*, 503–516.

Duyao, M.P., Auerbach, A.B., Ryan, A., Persichetti, F., Barnes, G.T., McNeil, S.M., Ge, P., Vonsattel, J.P., Gusella, J.F., Joyner, A.L., et al. (1995). Inactivation of the mouse Huntington's disease gene homolog Hdh. Science *269*, 407–410.

Echeverri, C.J., Paschal, B.M., Vaughan, K.T., and Vallee, R.B. (1996). Molecular characterization of the 50-kD subunit of dynactin reveals function for the complex in chromosome alignment and spindle organization during mitosis. J. Cell Biol. *132*, 617–633.

Fant, X., Merdes, A., and Haren, L. (2004). Cell and molecular biology of spindle poles and NuMA. Int. Rev. Cytol. *238*, 1–57.

Farkas, L.M., and Huttner, W.B. (2008). The cell biology of neural stem and progenitor cells and its significance for their proliferation versus differentiation during mammalian brain development. Curr. Opin. Cell Biol. *20*, 707–715.

Farkasovsky, M., and Kuntzel, H. (2001). Cortical Num1p interacts with the dynein intermediate chain Pac11p and cytoplasmic microtubules in budding yeast. J. Cell Biol. *152*, 251–262.

Faulkner, N.E., Dujardin, D.L., Tai, C.Y., Vaughan, K.T., O'Connell, C.B., Wang, Y., and Vallee, R.B. (2000). A role for the lissencephaly gene LIS1 in mitosis and cytoplasmic dynein function. Nat. Cell Biol. *2*, 784–791.

Feng, Y., and Walsh, C.A. (2004). Mitotic spindle regulation by Nde1 controls cerebral cortical size. Neuron *44*, 279–293.

Gauthier, L.R., Charrin, B.C., Borrell-Pages, M., Dompierre, J.P., Rangone, H., Cordelieres, F.P., De Mey, J., MacDonald, M.E., Lessmann, V., Humbert, S., et al. (2004). Huntingtin controls neurotrophic support and survival of neurons by enhancing BDNF vesicular transport along microtubules. Cell *118*, 127–138.

Gauthier-Fisher, A., Lin, D.C., Greeve, M., Kaplan, D.R., Rottapel, R., and Miller, F.D. (2009). Lfc and Tctex-1 regulate the genesis of neurons from cortical precursor cells. Nat. Neurosci. *12*, 735–744.

Goehler, H., Lalowski, M., Stelzl, U., Waelter, S., Stroedicke, M., Worm, U., Droege, A., Lindenberg, K.S., Knoblich, M., Haenig, C., et al. (2004). A protein interaction network links GIT1, an enhancer of huntingtin aggregation, to Huntington's disease. Mol. Cell *15*, 853–865.

Gonczy, P. (2008). Mechanisms of asymmetric cell division: flies and worms pave the way. Nat. Rev. Mol. Cell Biol. *9*, 355–366.

Gutekunst, C.A., Levey, A.I., Heilman, C.J., Whaley, W.L., Yi, H., Nash, N.R., Rees, H.D., Madden, J.J., and Hersch, S.M. (1995). Identification and localization of huntingtin in brain and human lymphoblastoid cell lines with anti-fusion protein antibodies. Proc. Natl. Acad. Sci. USA *92*, 8710–8714.

Hoffner, G., Kahlem, P., and Djian, P. (2002). Perinuclear localization of huntingtin as a consequence of its binding to microtubules through an interaction with beta-tubulin: relevance to Huntington's disease. J. Cell Sci. *115*, 941–948.

Izumi, Y., Ohta, N., Hisata, K., Raabe, T., and Matsuzaki, F. (2006). Drosophila Pins-binding protein Mud regulates spindle-polarity coupling and centrosome organization. Nat. Cell Biol. *8*, 586–593.

Kaltenbach, L.S., Romero, E., Becklin, R.R., Chettier, R., Bell, R., Phansalkar, A., Strand, A., Torcassi, C., Savage, J., Hurlburt, A., et al. (2007). Huntingtin interacting proteins are genetic modifiers of neurodegeneration. PLoS Genet. *3*, e82.

Kegel, K.B., Meloni, A.R., Yi, Y., Kim, Y.J., Doyle, E., Cuiffo, B.G., Sapp, E., Wang, Y., Qin, Z.H., Chen, J.D., et al. (2002). Huntingtin is present in the nucleus, interacts with the transcriptional corepressor C-terminal binding protein, and represses transcription. J. Biol. Chem. *277*, 7466–7476.

Knoblich, J.A. (2008). Mechanisms of asymmetric stem cell division. Cell *132*, 583–597.

Konno, D., Shioi, G., Shitamukai, A., Mori, A., Kiyonari, H., Miyata, T., and Matsuzaki, F. (2008). Neuroepithelial progenitors undergo LGN-dependent planar divisions to maintain self-renewability during mammalian neurogenesis. Nat. Cell Biol. *10*, 93–101.

Kosodo, Y., Roper, K., Haubensak, W., Marzesco, A.M., Corbeil, D., and Huttner, W.B. (2004). Asymmetric distribution of the apical plasma membrane during neurogenic divisions of mammalian neuroepithelial cells. EMBO J. *23*, 2314–2324.

Leavitt, B.R., Guttman, J.A., Hodgson, J.G., Kimel, G.H., Singaraja, R., Vogl, A.W., and Hayden, M.R. (2001). Wild-type huntingtin reduces the cellular toxicity of mutant huntingtin in vivo. Am. J. Hum. Genet. *68*, 313–324.

Lee, W.L., Oberle, J.R., and Cooper, J.A. (2003). The role of the lissencephaly protein Pac1 during nuclear migration in budding yeast. J. Cell Biol. *160*, 355–364.

Li, S.H., Gutekunst, C.A., Hersch, S.M., and Li, X.J. (1998). Interaction of huntingtin-associated protein with dynactin P150Glued. J. Neurosci. *18*, 1261–1269.

Lunkes, A., Lindenberg, K.S., Ben-Haiem, L., Weber, C., Devys, D., Landwehrmeyer, G.B., Mandel, J.L., and Trottier, Y. (2002). Proteases acting on mutant huntingtin generate cleaved products that differentially build up cytoplasmic and nuclear inclusions. Mol. Cell *10*, 259–269.

Marthiens, V., and ffrench-Constant, C. (2009). Adherens junction domains are split by asymmetric division of embryonic neural stem cells. EMBO Rep. *10*, 515–520.

Marzesco, A.M., Mora-Bermudez, F., and Huttner, W.B. (2009). Neurogenesis in G minor. Nat. Neurosci. *12*, 669–671.

McGuire, J.R., Rong, J., Li, S.H., and Li, X.J. (2006). Interaction of Huntingtin-associated protein-1 with kinesin light chain: implications in intracellular trafficking in neurons. J. Biol. Chem. *281*, 3552–3559.

Merdes, A., Ramyar, K., Vechio, J.D., and Cleveland, D.W. (1996). A complex of NuMA and cytoplasmic dynein is essential for mitotic spindle assembly. Cell *87*, 447–458.

Merdes, A., Heald, R., Samejima, K., Earnshaw, W.C., and Cleveland, D.W. (2000). Formation of spindle poles by dynein/dynactin-dependent transport of NuMA. J. Cell Biol. *149*, 851–862.

Moore, J.K., Li, J., and Cooper, J.A. (2008). Dynactin function in mitotic spindle positioning. Traffic *9*, 510–527.

Nasir, J., Floresco, S.B., O'Kusky, J.R., Diewert, V.M., Richman, J.M., Zeisler, J., Borowski, A., Marth, J.D., Phillips, A.G., and Hayden, M.R. (1995). Targeted disruption of the Huntington's disease gene results in embryonic lethality and behavioral and morphological changes in heterozygotes. Cell *81*, 811–823.

Nguyen, L., Besson, A., Heng, J.I., Schuurmans, C., Teboul, L., Parras, C., Philpott, A., Roberts, J.M., and Guillemot, F. (2006). p27kip1 independently promotes neuronal differentiation and migration in the cerebral cortex. Genes Dev. *20*, 1511–1524.

Nguyen-Ngoc, T., Afshar, K., and Gonczy, P. (2007). Coupling of cortical dynein and G alpha proteins mediates spindle positioning in Caenorhabditis elegans. Nat. Cell Biol. *9*, 1294–1302.

O'Connell, C.B., and Wang, Y.L. (2000). Mammalian spindle orientation and position respond to changes in cell shape in a dynein-dependent fashion. Mol. Biol. Cell *11*, 1765–1774.

Palidwor, G.A., Shcherbinin, S., Huska, M.R., Rasko, T., Stelzl, U., Arumughan, A., Foulle, R., Porras, P., Sanchez-Pulido, L., Wanker, E.E., et al. (2009). Detection of alpha-rod protein repeats using a neural network and application to huntingtin. PLoS Comput. Biol. *5*, e1000304.

Peng, C.Y., Manning, L., Albertson, R., and Doe, C.Q. (2000). The tumour-suppressor genes lgl and dlg regulate basal protein targeting in Drosophila neuroblasts. Nature *408*, 596–600.

Radulescu, A.E., and Cleveland, D.W. (2010). NuMA after 30 years: the matrix revisited. Trends Cell Biol. *20*, 214–222.

Rebollo, E., Sampaio, P., Januschke, J., Llamazares, S., Varmark, H., and Gonzalez, C. (2007). Functionally unequal centrosomes drive spindle orientation in asymmetrically dividing Drosophila neural stem cells. Dev. Cell *12*, 467–474.

Rebollo, E., Roldan, M., and Gonzalez, C. (2009). Spindle alignment is achieved without rotation after the first cell cycle in Drosophila embryonic neuroblasts. Development *136*, 3393–3397.

Rusan, N.M., and Peifer, M. (2007). A role for a novel centrosome cycle in asymmetric cell division. J. Cell Biol. *177*, 13–20.

Sanada, K., and Tsai, L.H. (2005). G protein betagamma subunits and AGS3 control spindle orientation and asymmetric cell fate of cerebral cortical progenitors. Cell *122*, 119–131.

Sathasivam, K., Woodman, B., Mahal, A., Bertaux, F., Wanker, E.E., Shima, D.T., and Bates, G.P. (2001). Centrosome disorganization in fibroblast cultures derived from R6/2 Huntington's disease (HD) transgenic mice and HD patients. Hum. Mol. Genet. *10*, 2425–2435.

Sheeman, B., Carvalho, P., Sagot, I., Geiser, J., Kho, D., Hoyt, M.A., and Pellman, D. (2003). Determinants of S. cerevisiae dynein localization and activation: implications for the mechanism of spindle positioning. Curr. Biol. *13*, 364–372.

Siller, K.H., and Doe, C.Q. (2009). Spindle orientation during asymmetric cell division. Nat. Cell Biol. *11*, 365–374.

Siller, K.H., Serr, M., Steward, R., Hays, T.S., and Doe, C.Q. (2005). Live imaging of Drosophila brain neuroblasts reveals a role for Lis1/dynactin in spindle assembly and mitotic checkpoint control. Mol. Biol. Cell *16*, 5127–5140.

Siller, K.H., Cabernard, C., and Doe, C.Q. (2006). The NuMA-related Mud protein binds Pins and regulates spindle orientation in Drosophila neuroblasts. Nat. Cell Biol. *8*, 594–600.

Skop, A.R., and White, J.G. (1998). The dynactin complex is required for cleavage plane specification in early Caenorhabditis elegans embryos. Curr. Biol. *8*, 1110–1116.

Steigemann, P., Wurzenberger, C., Schmitz, M.H., Held, M., Guizetti, J., Maar, S., and Gerlich, D.W. (2009). Aurora B-mediated abscission checkpoint protects against tetraploidization. Cell *136*, 473–484.

Strehlow, A.N., Li, J.Z., and Myers, R.M. (2007). Wild-type huntingtin participates in protein trafficking between the Golgi and the extracellular space. Hum. Mol. Genet. *16*, 391–409.

Tao, T., and Tartakoff, A.M. (2001). Nuclear relocation of normal huntingtin. Traffic *2*, 385–394.

Toyoshima, F., and Nishida, E. (2007). Spindle orientation in animal cell mitosis: roles of integrin in the control of spindle axis. J. Cell. Physiol. *213*, 407–411.

Trettel, F., Rigamonti, D., Hilditch-Maguire, P., Wheeler, V.C., Sharp, A.H., Persichetti, F., Cattaneo, E., and MacDonald, M.E. (2000). Dominant phenotypes produced by the HD mutation in STHdh(Q111) striatal cells. Hum. Mol. Genet. *9*, 2799–2809.

Tronche, F., Kellendonk, C., Kretz, O., Gass, P., Anlag, K., Orban, P.C., Bock, R., Klein, R., and Schutz, G. (1999). Disruption of the glucocorticoid receptor gene in the nervous system results in reduced anxiety. Nat. Genet. *23*, 99–103.

White, J.K., Auerbach, W., Duyao, M.P., Vonsattel, J.P., Gusella, J.F., Joyner, A.L., and MacDonald, M.E. (1997). Huntingtin is required for neurogenesis and is not impaired by the Huntington's disease CAG expansion. Nat. Genet. *17*, 404–410.

Woda, J.M., Calzonetti, T., Hilditch-Maguire, P., Duyao, M.P., Conlon, R.A., and MacDonald, M.E. (2005). Inactivation of the Huntington's disease gene (Hdh) impairs anterior streak formation and early patterning of the mouse embryo. BMC Dev. Biol. *5*, 17.

Yingling, J., Youn, Y.H., Darling, D., Toyo-Oka, K., Pramparo, T., Hirotsune, S., and Wynshaw-Boris, A. (2008). Neuroepithelial stem cell proliferation requires LIS1 for precise spindle orientation and symmetric division. Cell *132*, 474–486.

Yokota, Y., Kim, W.Y., Chen, Y., Wang, X., Stanco, A., Komuro, Y., Snider, W., and Anton, E.S. (2009). The adenomatous polyposis coli protein is an essential regulator of radial glial polarity and construction of the cerebral cortex. Neuron *61*, 42–56.

Zeitlin, S., Liu, J.P., Chapman, D.L., Papaioannou, V.E., and Efstratiadis, A. (1995). Increased apoptosis and early embryonic lethality in mice nullizygous for the Huntington's disease gene homologue. Nat. Genet. *11*, 155–163.

Zhang, S., Feany, M.B., Saraswati, S., Littleton, J.T., and Perrimon, N. (2009). Inactivation of Drosophila Huntingtin affects long-term adult functioning and the pathogenesis of a Huntington's disease model. Dis Model Mech *2*, 247–266.

Zuccato, C., Ciammola, A., Rigamonti, D., Leavitt, B.R., Goffredo, D., Conti, L., MacDonald, M.E., Friedlander, R.M., Silani, V., Hayden, M.R., et al. (2001). Loss of huntingtin-mediated BDNF gene transcription in Huntington's disease. Science *293*, 493–498.

6.3 Discussion

Although some of HTT functions are linked to transcriptional activities in health and disease, HTT is principally a cytoplasmic protein that associates with MTs and vesicles. HTT regulates intracellular trafficking of various organelles, including vesicles, by interacting with the dynein/dynactin complex. In the article **"Huntingtin is required for mitotic spindle orientation and mammalian neurogenesis"** we unravel a novel HTT function during cell division.

We showed that HTT is localized at spindle poles and regulates proper localization of dynein, $p150^{Glued}$ and NuMa. Using video-microscopy in HTT depleted cells, we revealed that positioning of the mitotic spindle parallel to the substrate plane is less efficient. As a result, cells are oriented perpendicular to the substrate and post-mitotic cell death is increased. However, neither mitotic index is affected nor the cell cycle by HTT silencing. Because HTT localization at spindle poles is MT-dependent (Keryer et al., 2011), it is tempting to speculate that HTT is the protein responsible for the distribution of the dynein/dynactin complex at spindle poles.

What is the underlying mechanism? HAP1 could play an important function given the fact that it physically interacts with HTT, kinesin and $p150^{Glued}$ (Engelender et al., 1997; S.H. Li et al., 1998; X. J. Li et al., 1995; McGuire et al., 2006). Thus, the dynein/dynactin complex can be transport along astral MT to the cell cortex by a HTT-HAP1 dependent transport. The use of the already described construct pARIS-htt-ΔHAP1 could help to answer this question.

+TIPs are important effectors for the recruitment of dynein/dynactin to MT plus-ends (Coquelle et al., 2002; Kardon & Vale, 2009; Watson & Stephens, 2006) as well as MT PTMs (Janke & Bulinski, 2011; Peris et al., 2006, 2009). Future work is needed to elucidate the interplay between +TIPs, dynein/dynactin localization and HTT.

Consistent with the results obtain *in cellulo*, silencing of HTT in AP at E14.5 resulted in a modified cleavage plane. During cortical development, AP can divide in a symmetric fashion to expand the pool of cycling progenitors, or asymmetrically to generate post-mitotic neurons. We found a correlation between the cleavage plane and the neurogenic fate of the newly generated cells. By removal of HTT from the system, the cleavage plane was shifted from mostly symmetric to asymmetric, and a large number of +Tbr1, +βIIItub and +NeuN cells were found. Same results were observed either by *in utero* electroporation of siRNAs against HTT or genetic ablation. Our data specifically show that HTT is involved in neurogenesis. However, a direct association between the regulation of spindle orientation during neural progenitors division and the fate of the daughter cells is still under debate.

Another interesting finding of this work is that whereas the function of HTT in spindle regulation is conserved, its role in progenitor fate control might be tissue context dependent. Depletion of *D. melanogaster* HTT results in altered mitotic spindle orientation in NBs. Although *D. melanogaster* HTT could rescue the spindle defect in mammalian cells depleted for HTT, the removal of HTT was

surprisingly not sufficient to induce neurogenesis defects in NBs. These findings suggest that the mechanism of HTT in mammalian neurogenic control may be mediated through a regulatory module that has changed through evolution.

In conclusion, we demonstrate a conserved function for HTT in flies and mammals. These results not only open new lines of investigation for elucidating the pathogenic mechanisms in HD, but also identify HTT as a crucial player in spindle orientation and neurogenesis.

7 Mutant HTT and mitosis

7.1 Study presentation

Identifying regulators of spindle orientation during cortical neurogenesis remains essential to understand brain development and diseases. Huntingtin (HTT), the protein mutated in Huntington's disease (HD), interacts with dynein and regulates spindle orientation by ensuring the proper localization of dynein and the p150^{Glued} subunit of dynactin at the spindle pole. We found here that HTT also regulates the localization of a CLIP170-dynein-p150^{Glued} complex at microtubule (MT) plus-ends. In HD, CLIP170, dynein and p150^{Glued} are delocalized from the MT plus-ends and the integrity of the CLIP170-dynein-p150^{Glued} complex is affected. Interestingly, in the presence of Akt the HTT-dynein interaction and the CLIP170-dynein-p150^{Glued} complex are as in wild-type situation resulting in the proper location of the CLIP170-dynein-p150^{Glued} complex at MT plus-ends. As a physiological consequence of these observations, spindle orientation is altered in HD cultured cells. As for the CLIP170-dynein-p150^{Glued} complex, Akt rescues the defective spindle orientation induced by mutant HTT and this effect occurs specifically through mutant HTT phosphorylation at serine 421 (S421). Moreover, expressing mutant HTT in *Drosophila melanogaster* neuroblasts leads to spindle misorientation that is restored by phosphorylation at S421.

7.2 Article III

This study is part of a manuscript in preparation

Maria Molina-Calavita[1]; Matthieu Piel[2]; Frédéric Saudou[1] and Sandrine Humbert[1,3]

A mutant huntingtin/dynein/dynactin/CLIP170 pathway induces defective spindle orientation and is regulated by Akt

[1]Institut Curie; CNRS UMR 3306; INSERM U1005; Université Paris Sud XI. Orsay, France. [2]Institut Curie; CNRS UMR 144. Paris, France. [3]Correspondence should be addressed to S.H. (e-mail: sandrine.humbert@curie.fr)

RESULTS

Huntingtin localization at spindle poles and at MT plus-ends is altered in HD during mitosis

We have previously shown that HTT localizes at spindle poles during mitosis (Godin, Colombo, et al., 2010). Here, we aimed to address whether the presence of an abnormal polyglutamine expansion in HTT would influence its localization. We analyzed the localization of endogenous wild-type and mutant HTT using a polyclonal antibody, pAb SE3619. We transfected ST*Hdh*$^{+/+}$ and ST*Hdh*$^{Q109/Q109}$ striatal mouse cells derived from *Hdh*$^{Q7/Q7}$ and mutant *Hdh*$^{Q111/Q111}$ mice with the MT plus-ends protein EB3-GFP (Trettel et al., 2000). Wild-type and mutant HTT were found at the spindles poles during mitosis (Figure 1A). Strikingly, we also observed HTT and mutant HTT at a location that could coincides with MT plus-ends as co-localization with EB3-GFP was observed. Furthermore, quantification of HTT signal at spindle poles revealed that in mutant cells this signal was increased compared to wild-type, and localization at MT plus-ends was highly decreased (Figure 1A).

We also addressed the distribution of dynein (DIC) and of the large subunit of the dynactin complex p150^{Glued} (Figures 1B and 1C) in ST*Hdh*$^{+/+}$ and ST*Hdh*$^{Q109/Q109}$ cells. Decreased DIC and p150^{Glued} levels were measured in polyQ-HTT expressing cells at spindle poles. This is consistence with previous results obtained in HTT depleted cells (Godin, Colombo, et al., 2010).

Taken together, these results suggest that the abnormal polyQ expansion in HTT not only modifies HTT distribution during mitosis, but distribution of motor proteins involved in cell division as well.

MT dynamic instability is impaired in mouse embryonic fibroblasts from HD mutant mice

EB proteins, $p150^{Glued}$ and CLIP170 accumulate around the MT plus-ends, thereby forming a cap structure that favours filament growth, reduces catastrophe frequencies and recruits further proteins (Akhmanova & Steinmetz, 2010; Steinmetz & Akhmanova, 2008). This allows MTs to be dynamic filaments that undergo successive cycles of growth and shrinkage, called dynamic instability. Here, we compared MT dynamics in the presence of wild-type and mutant HTT (Figure 2A). We used mouse embryonic fibroblasts (MEFs) generated from wild-type $Hdh^{Q7/Q7}$ and mutant $Hdh^{Q111/Q111}$ mice (Wheeler et al. 1999). The measurement of EB3 comets velocity provides MTs growth rate. We individually tracked MT plus-ends decorated with EB3-GFP in wild-type and mutant fibroblasts using live cell imaging. No differences were found in EB3 comet velocity in wild-type (0.44 µm/sec) or mutant MEFs (0.42 µm/sec; $p = 0.8024$, *t* test) (Figure 2B).

Next, we analyzed the time spent by MTs exploring the area near the leading edge (persistence time) by live imaging. MEFs were transfected with EB3-GFP and mCherry-α-tubulin. In wild-type MEFs, most MTs depolymerized upon contact with the membrane (Figure 2B; 17.76 sec). In contrast, many MTs continued to grow tangential to the leading edge after touching the membrane in MEFs expressing mutant HTT (64.75 sec; $p<0.001$, *t*

test). The time spent by MTs close to the membrane (persistence time) was markedly increased in HD MEFs as compared with wild-type MEFs.

Together these findings show that, while mutant HTT does not affect MT growth, it reduces MT dynamics instability and leads to an abnormal MT persistence after membrane contact.

p150^{Glued} and CLIP170 Proteins Recruitment to MT plus-ends is Altered in HD

Prominent examples of +TIPs are the large subunit of the dynactin complex p150^{Glued}, the CLIP170 (cytoplasmic linker protein 170) and EB3 proteins. We addressed whether the localization of +TIPs was modified in HD. We first transfected ST*Hdh*$^{+/+}$ and ST*Hdh*$^{Q109/Q109}$ striatal mouse cells with EB3-GFP to identify MT ends (Figure 3) and used specific antibodies to label endogenous CLIP170 (Figure 3A) and p150^{Glued} (Figure 3B). In ST*Hdh*$^{+/+}$ cells endogenous CLIP170 and p150^{Glued} colocalized with EB3 in comet-like structures at MT plus-ends as reaveled by linescan analysis. In contrast, mutant cells were essentially devoided of CLIP170 (Figure 3A) and p150^{Glued} (Figure 3B) comets. We quantified this effect by selecting EB3-decorated MT ends and examining CLIP-170 and p150^{Glued} labeling. The percentage of CLIP170 and p150^{Glued} per EB3 positive MT ends was determined (Figure 2, graphs). In ST*Hdh*$^{+/+}$, 83.1% of the MT plus-ends positive for EB3 were positive for endogenous CLIP170 and 78% for p150^{Glued}. In contrast, in mutant ST*Hdh*$^{Q109/Q109}$ cells, the EB3/+TIPs ratio lowered drastically for CLIP170 (39.4%) as well as for p150^{Glued} (52%).

We then conclude that the localization of dynein, p150^{Glued} and CLIP170 at MT plus-ends during mitosis is modified in HD context. These mislocalizations are not due to impaired MT growth in mutant cells and likely reflects an influence of polyQ-HTT by itself.

The Dynein-p150^{Glued} Complex is Altered in HD

Since Dynein, p150^{Glued} and CLIP170 are mislocalized in HD context, we tested the possibility that these proteins complex would be altered when HTT carries an abnormal polyQ expansion (Figure 4A). We thus performed immunoprecipitations from protein extracts of ST*Hdh*$^{+/+}$ and ST*Hdh*$^{Q109/Q109}$ mouse cells. Immunoprecipitation of endogenous DIC led to the co-immunoprecipitation of p150^{Glued} and, to a smaller extent of CLIP170. The levels of immunoprecipitated p150^{Glued} were markedly decreased in mutant cells compared to wild-type, while the levels of CLIP170 were similar.

HTT interacts directly with the dynein intermediate chain (DIC) and indirectly with p150^{Glued} through HAP1 (Caviston et al. 2007; Pardo et al. 2010; Li et al. 1995). HTT was also present in the dynein, p150^{Glued} and CLIP170 complex (Figure 4A). However, given that the levels of wild-type and mutant HTT in ST*Hdh*$^{+/+}$ and ST*Hdh*$^{Q109/Q109}$ cells was not comparable, we could not evaluate the relative level of HTT and mutant HTT pulled-down by the anti-dynein antibody. To address this point, we exogenously expressed wild-type and mutant HTT using a construct encoding the first 480 amino acids of HTT with a 17Q non pathological expansion or a 68Q pathological expansion (Figure 4B). These HTT-480-17Q and HTT-480-68Q constructs are tagged with GFP. HeLa cells were transfected and immunoprecipitations experiments were done using an anti-GFP antibody. HTT and

dynein were present in the same complex. Furthermore, the levels of endogenous dynein, co-immunoprecipitated with htt480-68Q-GFP were lowered as compared to the wild-type situation.

Together these data show that the dynein-p150^{Glued} complex is modified when HTT is mutated. This may be linked to the altered interaction of HTT with dynein when HTT carries an abnormal polyQ expansion.

Akt Regulates the Dynein-p150^{Glued}-CLIP170 Complex assembly and localization in HD

HTT binds to dynein and dynactin through HAP1 to promote vesicular transport along MTs. In HD, alteration of the HTT-p150^{Glued} complex is accompanied by its detachment from the MTs and a decreased vesicular transport (Zala et al., 2008). Interestingly, this mechanism is regulated by phosphorylation of mutant HTT at serine 421 (S421) by Akt. S421-phophorylated mutant HTT is as efficient as wild-type HTT to promote transport as it rescues p150^{Glued} binding to MTs. We thus determine the effect of Akt on the DIC-p150^{Glued}-CLIP170 complex (Figure 4A). We expressed a constitutively active form of Akt (Akt c.a.) in ST*Hdh*$^{+/+}$ and ST*Hdh*$^{Q109/Q109}$ cells. We then immunoprecipitated DIC from protein extracts of these cells. Strikingly, the presence of Akt c.a. led to an increased recruitment of CLIP170 in the DIC immunoprecipitates in both ST*Hdh*$^{+/+}$ and ST*Hdh*$^{Q109/Q109}$ cells. This recruitment was enhanced in mutant cells. Furthermore, in contrast to the situation in ST*Hdh*$^{Q109/Q109}$ cells that do not express Akt c.a., we found similar levels of p150^{Glued} immunoprecipitated with DIC in wild-type and polyQ conditions when Akt c.a. was expressed.

We also exogenously expressed mutant HTT with a S421 to acid aspartic substitution (S421D, HTT-480-68Q-S421D) in HeLa cells (Figure 4B). This substitution micmics constitutive phosphorylation at this site. We immunoprecipitated DIC from cells expressing the variants of HTT. Mutant HTT showed a lower interaction with DIC as compared to wild-type HTT. However, the interaction of polyQ-HTT carrying the S421D mutation was similar to that of the wild-type HTT. This shows that the altered interaction of HTT with dynein when HTT carries an abnormal polyQ expansion is rescued when S421 is phosphorylated. This rescued interaction could participate to the rescued dynein-p150^{Glued}-CLIP170 assembly in HD in the presence of Akt (Figure 4A).

We also determined the effect of Akt on the localization of dynein, p150^{Glued} and CLIP170 at MT plus-ends during. We cotransfected ST*Hdh*$^{+/+}$ and ST*Hdh*$^{Q109/Q109}$ cells with EB3-GFP and Akt c.a. and immunostained for the presence of endogenous CLIP170 (Figure 3A) and p150^{Glued} (Figure 3B). In ST*Hdh*$^{+/+}$ cells the MT plus-ends mislocalization of CLIP170and p150^{Glued} was rescued by Akt c.a. with this situation ressembling the wild-type situation (ST*Hdh*$^{+/+}$ cells).

We conclude that Akt rescues the altered DIC-p150^{Glued}-CLIP170 complex and the mislocalization of dynein, p150^{Glued} and CLIP170 at MT plus-ends in HD.

PolyQ-HTT Leads to Mitotic Spindle Misorientation

We then asked whether the mutant HTT-induced modifications observed could impact on mitotic spindle orientation (Figure 5). We first examined the position of the spindle pole axis with respect to the substrate plane in ST*Hdh*$^{+/+}$ and ST*Hdh*$^{Q109/Q109}$ cells (Figure 5A). Z-

series stacks were acquired using 3D microscopy from cells immunostained for □-tubulin and counterstained for DAPI. We measured the angle α formed between the pole-pole axis and the substrate plane. Most of wild-type cells oriented their spindle axis parallel to the substratum plane with angle smaller than 10° (8° ± 1.1, n = 109). PolyQ-HTT expressing cells showed a defective spindle positioning, with an higher average angle (17.8° ± 1.5, n = 117). A significant proportion of mutant cells had spindle angles greater than 40°. We also analyzed spindle orientation in HeLa cells expressing exogenously a wild-type or mutant 480 amino acid fragment of HTT (Figure 5B). Cells transfected with a pcDNA empty vector or with 480-17Q-HTT behaved similarly with most of the spindle angles smaller than 10° (control: 11.5° ± 0.9, n = 107°; HTT-480-17Q: 11.3° ± 1.2, n = 74). In HD conditions, the mean angle a was markedly increased (HTT-480-68Q: 16.2° ± 1.16, n = 89).

We confirmed these findings using printed micropatterns of fibronectin (Figure 6). Indeed, cells *in situ* are sensitive to geometrical and mechanical constraints from their microenvironment. While, these parameters are uncontrolled under classic culture conditions, the so-called micropatterns approach allows to restrict the location and shape of the substrate regions, in which cells can attach (Théry et al., 2005). We studied spindle positioning in histone2B–mCherry transfected ST*Hdh*$^{+/+}$ and ST*Hdh*$^{Q109/Q109}$ cell lines plated on printed [L]-shaped patterns of fibronectin. The majority of mitotic spindles of wild-type cells grown on [L]-shaped patterns divided with an angle of 45°, showing a constrained cell division axis (Figure 6A). In contrast, there was a wider dispersion of spindle angles in polyQ-HTT containing cells indicating an impaired control of spindle positioning. In ST*Hdh*$^{Q109/Q109}$ cells approximately 60% of spindles deviated by more than 15° from the

mean angle compared with only 35% in ST*Hdh*$^{+/+}$ cells (Figure 6B), indicating an impaired control of spindle positioning in polyQ-HTT expressing cells.

These results show that the function of HTT as a regulator of spindle orientation during mitosis is modified by the presence of a pathological polyQ expansion.

PolyQ-HTT-induced Spindle Misorientation is Rescued by Akt Phosphorylation of S421

As Akt impacts on the Dynein-p150^{Glued}-CLIP170 Complex assembly and localization, we investigated the consequence of this kinase on mutant HTT-induced spindle misorientation (Figure 7). We first transfected Akt c.a. in ST*Hdh*$^{Q109/Q109}$ cells (Figure 7A) and analyzed spindle orientation as before in the different conditions (Figure 5). While the mean spindle angle was 16.63° ± 1.27 in ST*Hdh*$^{Q109/Q109}$ cells (n = 28), it was similar in ST*Hdh*$^{+/+}$ and ST*Hdh*$^{Q109/Q109}$/Akt c.a. cells (ST*Hdh*$^{+/+}$: 7.35° ± 1.43, n = 21; ST*Hdh*$^{Q109/Q109}$/Akt c.a.: 6.5° ± 0.7, n = 48) (Figure 7A). Similarly, co-expressing Akt with HTT-480-68Q in HeLa cells rescued the defect observed in the presence of HTT-480-68Q alone (Figure 7B). Thus expression of Akt is sufficient to rescue the spindle misorientation defect observed in HD.

Akt phosphorylates HTT at S421 and this phosphorylation rescues the alteration of the HTT/dynein interaction when HTT encompasses an abnormal polyQ mutation (Figures 3 and 4). We aimed to specifically investigate whether the effect of Akt on spindle misorientation induced by mutant HTT involves HTT phosphorylation at S421. We expressed mutant HTT with S421 to alanine (alanine is an unphosphorylatable amino acid, S421A, (Humbert et al. 2002) and to aspartic acid (S421D) substitutions in HeLa cells

(Figure 7B). In HTT-480-68Q-S421A cells spindle was not properly oriented parallel to the substratum plane. In sharp contrast, expressing HTT-480-68Q-S421D behaved as the wild-type HTT-480-17Q with most of the cells showing a spindle aligned with the substratum plane.

To unequivocally demonstrate that Akt mediates its effect on spindle orientation through HTT S421 phosphorylation, we expressed Akt c.a. and mutant HTT or mutant HTT carrying a S421 to alanine (S421A) mutation (Figure 7B). As seen before, spindle orientation was altered in cells expressing mutant HTT and this was rescued to wild-type situation by expression of Akt c.a.. However, Akt c.a. had no effect in cells expressing an unphosphorylatable form of mutant HTT, showing that the effect of Akt occurs, at least in part, through mutant HTT S421 phosphorylation.

Together our data demonstrate that Akt rescues spindle misorientation in HD by phosphorylating polyQ-HTT at S421.

The conserved function of HTT during mitosis is lost when HTT is mutated in *D. melanogaster* neuroblasts

To establish a physiological relevance of the role of HTT in spindle orientation, we analyzed the effect of mutant HTT in *D. melanogaster* neuroblasts (NBs), the neuronal precursors of the central nervous system. Their mode of division is a well-studied model for investigating the molecular mechanisms involved in asymmetric cell division (Siller & Doe, 2009). In asymmetric division, cells create an internal polarity axis and localize cell fate determinants to one pole. Alignment of the mitotic spindle along the axis of polarity

causes the determinants to segregate into one of the two daughter cells, making it different from its sibling. NBs undergo repeated rounds of asymmetric division, generating a larger apical cell that retains NB characteristics and a smaller, basal ganglion mother cell (GMC) that divides only once more to generate two neurons (Siller & Doe 2009; Morin & Bellaïche 2011). We have previously shown that HTT function during mitosis is evolutionarily conserved in *D. melanogaster* NBs (Godin, Colombo, et al., 2010). Absence of HTT in NBs increased the percentage of NBs that display abnormally positioned spindles.

We used transgenic flies that express the first 548 amino acids of the human *HTT* gene with either a pathogenic polyQ tract of 128 repeats (Htt^{548aa}-Q128) or a non-pathogenic tract of 0 repeats (Htt^{548aa}-Q0) (W.C. M. Lee et al., 2004). This N-terminal motif contains regions of strong homology between HTT isoforms from *D. melanogaster* to humans and is more likely to faithfully mimic endogenous HTT. As a control we used wild-type (W^{1118}) flies. In order to analyse spindle orientation in NBs, we performed immunostaining for Miranda, a multi-domain adaptor protein localized in the basal NB cortex, Centrosomin (Cnn) a spindle pole marker and phospho-histone 3 (PH3) in third instar larval brains. We quantified mitotic spindle alignment by measuring the angle between the line connecting the two centrosomes (Cnn) and the line bisecting the Miranda crescent in metaphase NBs (Figure 8A). In W^{1118} and Htt^{548aa}-Q0 NBs, Miranda was distributed at the basal cortex forming a crescent at metaphase, the line connecting the pole-to-pole axis bisecting the Miranda crescent. In Htt^{548aa}-Q128 NBs, Miranda was still located at the basal cortical crescent at metaphase. However, mitotic spindle

alignment failed to bisect the Miranda crescent in polyQ NBs. W^{1118} (10.54° ± 2.4, n=20) and Htt^{548aa}-Q0 (11.71° ± 1.4, n=37) NBs mean angles were statistically different from Htt^{548aa}-Q128 (18.7° ± 3, n=35) (Figure 8B).

We generated transgenic flies that express Htt^{548aa}-Q128 with a S421D substitution (Htt^{548aa}-Q128-S421D). Mitotic spindle alignment in Htt^{548aa}-Q128-S421D (12.15° ± 1.6, n=41) NBs was similar to the observed in W^{1118} and Htt^{548aa}-Q0 (Figures 8A and 8B).

Overall, our data demonstrate that HTT function in spindle orientation in *D. melanogaster* NBs is altered in the presence of mutant HTT. As observed *in cellulo*, S421 phosphorylation of mutant HTT rescues the mitotic spindle misalignment phenotype observed in mutant HTT expressing NBs.

EXPERIMENTAL PROCEDURES

Statistical Analyses

Statview 4.5 software (SAS Institute Inc., Cary, NC) was used for statistical analysis. All data herein described were performed in duplicate or triplicate. Data are expressed as mean ± S.E.M. *P < 0.05; **P < 0.01; ***P < 0.001. P values ≥ 0.05 were considered non-significant.

Cell lines and Transfection

Mouse neuronal cells derived from immortalized striatal progenitor cells, ST*Hdh*$^{+/+}$ and ST*Hdh*$^{Q109/Q109}$ were grown at 33°C with 5% CO_2 as previously described including 400 µg/ml geneticin (Trettel et al., 2000) and electroporated using cell line nucleofector kit L (Amaxa) according to the manufacturer's instructions. Experiments were performed 48h after transfection.

Mouse embryonic fibroblasts (MEFs) were prepared from E14.5 embryos following standard procedures and cultured in Dulbeco's modified Eagle's medium (DMEM, Gibco) supplemented with 10% bovine calf serum, 1% non-essential amino acids, 1M β-mercaptoethanol, 1% L-glutamine and antibiotics (50 units/ml penicillin and 50 µg/ml streptomycin). MEFs were maintained at 37°C with 5% CO_2. MEFs were electroporated using cell line nucleofector kit L (Amaxa) according to the manufacturer's instructions. Experiments were performed 24h to 48h after transfection.

HeLa cells were grown at 37°C in 5% CO_2 in DMEM (Gibco) supplemented with 10% bovine calf serum, 1% L-glutamine and antibiotics (50 units/ml penicillin and 50 µg/ml streptomycin). Cells were transfected using Lipofectamine 2000 (Invitrogen) according to the manufacturer's instructions. Experiments were performed 48h after transfection.

DNA Constructs and siRNAs

Constructs encoding HTT-480-17Q, HTT-480-68Q, HTT-480-17Q-S421A, HTT-480-17Q-S421D, HTT-480-68Q-S421A, HTT-480-68Q-S421D have been described previously (Humbert et al. 2002; Saudou et al. 1998). These plasmids encode the first 480 amino acids fragment of HTT with 17 or 68 glutamines and a serine-to-alanine mutation (S421A) or a serine to aspartic acid mutation (S421D) at position 421. HTT-480-17Q-HA and HTT-480-68Q-HA were previously described (Pardo et al., 2006). Constructs GFP-HTT-480-17Q, GFP-HTT-480-68Q and GFP-HTT-480-68Q-S421D were previously described (Zala et al., 2008). Constitutively active Akt (Akt c.a.; myristylated-DPH) tagged HA have been described previously (Datta et al. 1997).

End-binding protein 3 (EB3)-GFP was described previously (Stepanova et al., 2003). mCherry-α-tubulin was kindly provided by C. Janke (Institut Curie, France) and pBOS-histone2B–mCherry–IRES–hygromycin by M. Piel (Institut Curie, France).

The siRNA targeting Akt (Akt1 and Akt2) was purchased from Cell Signaling Technology.

Antibodies and Immunostaining procedures

The following antibodies were used: mouse anti-dynein intermediate chain (1:1000 for immunoblotting and 1:100 for immunocytochemistry; Chemicon), anti-p150^{Glued} (1:1000 for Western blotting and 1:100 for immunocytochemistry; BD Transduction Laboratories), rabbit anti-CLIP170 (1:3000 for Western blotting and 1:300 for immunocytochemistry; (Coquelle et al., 2002), kindly provived by C Janke, Institut Curie, France), mouse anti-HTT 4C8 (1:4000 for Western blotting; Euromedex), mouse anti-polyQ expansion-HTT 1C2 (1:500 for Western blotting; Euromedex), mouse anti-α-tubulin (1:500 for Western blotting and 1:1000 for immunocytochemistry; kindly provided by C. Janke; Institut Curie, France), human anti-CREST (1:1000 for immunocytochemistry; Antibody Incorporated), mouse anti-γ-tubulin, GTU88 (1:1000 for immunocytochemistry; Sigma), mouse anti-γ-tubulin, GTU88 (1:100 for immunocytochemistry; Abcam), rabbit anti-γ-tubulin, AK-15 (1:300 for immunocytochemistry; Sigma), mouse anti-Akt (1:1000 for Western blotting; Cell Signaling Technology), rat anti-HA (1:1000 for Western blotting and 1:200 for immunocytochemistry; Roche), rabbit anti-GFP (1:500 for Western blotting; Proteins and Antibodies Laboratory; Institut Curie, France). Rabbit anti-phospho-HTT SE3619 antibody was previously described (Godin et al., 2010). Briefly, SE3619 antibody was generated by synthesis, coupling to keyhole limpet hemocyanin (Eurogentec) and injection into rabbits of the following respective peptide: CGGRSRSGS[PO3H2]IVE (mouse huntingtin sequence amino acid 414 to 424). Polyclonal antibody was obtained by affinity-purification of serum using the appropriate peptide columns. The serum was filtered (0.22 μm filter) and after addition of 1 M tris (pH 8.0) up to a final concentration of 100 mM, it was applied to a

sulfolink column (Pierce) coupled to the appropriate peptide. Retained antibody was eluted with 100 mM glycine buffer (pH 2.7) and pH was neutralised with 1 M tris pH 9. Antibody was concentrated (Vivaspin concentrator 10 000 MW, VivaScience) and stored in 50% glycerol. Anti-rat, anti-rabbit or anti-mouse HRP-conjugated secondary antibodies were purchased from Jackson laboratories. AlexaFluor conjugated secondary antibodies were purchased from Molecular Probes (Invitrogen).

In order to analyze +TIP localization at MT plus-end, ST*Hdh*$^{+/+}$and ST*Hdh*$^{Q109/Q109}$ cell were electroporated with EB3-GFP and grown on glass coverslips for 48h. Cells were first fixed using 1mM EGTA diluted in cold methanol (-20°C) for 10min and then in 4% paraformaldehyde in PBS for 10 min at room temperature. Coverslips were washed in PBS 0,5% Triton X-100 (PBT 0.5%) for 5min, blocked 1h in 3% BSA, 0.1% Triton X-100 in PBS (PBT 0.1%), and incubated with mouse anti-p150^{Glued} and rabbit anti-CLIP170 at room temperature diluted in PBT 0.1% for 1h or over-night at 4°C. Anti-mouse AlexaFluor-555 and anti-rabbit AlexaFluor-555 were used as secondary antibodies.

To analyze phospho-HTT localization during mitosis, ST*Hdh*$^{+/+}$and ST*Hdh*$^{Q109/Q109}$ cells were electroporated with Akt c.a. HA-tagged and grown in glass coverslips for 48h. Cells were pre-lyzed 2 min in pre-warmed 0.5% Triton X-100-PHEM buffer before being fixed in cold methanol (-20°C) for 5 min. Coverslips were incubated with rabbit anti-phospho-HTT SE3619 and mouse anti-γ-tubulin and rat anti-HA. Secondary antibodies used were anti-rabbit AlexaFluor-555, anti-mouse AlexaFluor-488 and anti-rat AlexaFluor-647.

To visualize p150^{Glued} and dynein at spindle poles ST*Hdh*$^{+/+}$and ST*Hdh*$^{Q109/Q109}$ cells were first permeabilized 1 min in PHEM buffer containing 1% Triton X-100 and then fixed with

4% paraformaldehyde in PHEM buffer for 20 minutes. Then cells were fixed for 5 min in cold methanol (-20°C) and washed in PBT 0.1%. Cells were double immunostained with mouse anti-p150^{Glued} or mouse anti-dynein and rabbit anti-γ-tubulin. Anti-mouse AlexaFluor-555 and anti-rabbit AlexaFluor-488 were used as secondary antibodies.

To measure spindle orientation, ST*Hdh*$^{+/+}$and ST*Hdh*$^{Q109/Q109}$ cells were fixed 5 min with cold methanol (-20°C) and washed twice with PBT before immunostaining. The cells were incubated with mouse anti-γ-tubulin and human anti-CREST antibodies for 1 hr. Secondary antibodies used were anti-mouse AlexaFluor-488 and anti-human AlexaFluor-647. HeLa cells were transfected with HTT-480 plasmids and grown on glass coverslips for 48h. Cells were fixed in 4% paraformaldehyde and permeabilized for 5 min using PBT 0.5%. Coverslips were incubated with mouse anti-HTT 4C8 and rabbit anti-γ-tubulin. Secondary antibodies used were anti-mouse AlexaFluor-555 and anti- AlexaFluor-647.

For all immunostainings, cells were counterstained with DAPI (Roche). The mounting medium was 0.1 g/ml Mowiol 4-88 (Calbiochem, Darmstadt, Germany) in 20% glycerol.

Immunoblotting

Cells were harvested and lyzed in 50 mM Tris-HCl, containing 0.1% Triton X-100, 2 mM EDTA, 2 mM EGTA, 50 mM sodium fluoride, 10 mM β-glycerophosphate, 5 mM sodium pyrophosphate, 1 mM sodium orthovanadate, 0.1% (v/v) β-mercaptoethanol, 250 µM PMSF, 10 mg/ml aprotinin and leupeptin, pH 7.5. Cell lysates were centrifuged at 20,000 g for 15 min at 4°C. Equal amounts of protein were subjected to SDS-PAGE on polyacrylamide gels and transferred to nitrocellulose membranes (Whatman, Dassel,

Germany). Blocked membranes (5% milk in TBS-0.1% Tween-20 or 3% BSA in TBS-0.1% Tween-20) were incubated with the following antibodies: mouse anti-HTT 4C8, mouse anti-polyQ expansion-HTT 1C2, mouse anti-p150^{Glued}, rabbit anti-CLIP170, mouse anti-dynein, rat anti-HA, rabbit anti-Akt, mouse anti-GFP, mouse anti-b-actin or mouse anti-α-tubulin and washed with TBS-0.1% Tween-20. Membranes were then labelled with secondary IgG-HRP antibodies raised against each corresponding primary antibody. After three washes, the membranes were incubated with SuperSignal West Pico Chemiluminescent Substrate (Pierce, Erembodegem, Belgium) according to the instructions of the supplier. Membranes were exposed to Amersham Hyperfilm™ MP (GE Healthcare, Buckinghamshire, UK) films and developed.

Immunoprecipitation

ST*Hdh*$^{+/+}$, ST*Hdh*$^{Q109/Q109}$ and HeLa cells were lyzed in 20mM Tric-HCl, containing 2mM EDTA, 100mM NaCl, 10mM sodium fluoride, 50mM potassium phosphate dibasic, 2.5 sodium pyrophosphate, 0.25% Triton X-100, pH 7,5 on ice. Lysates at the concentration of 500 µg/ml were pre-cleared for 30min at 4°C using protein G-Sepharose beads (25µl; Sigma) and next incubated over-night at 4°C with a preformed complex of protein G-Sepharose beads (100 µl; Sigma) + antibody (1 µg). Beads were washed 3 times with lysis buffer and boiled 10 min at 95°C in SDS loading buffer to be denaturated and Western blot was performed as described.

Images Acquisition and Analysis

Images were acquired using a Leica DM RXA microscope with a HCL PL APO CS oil 63 × NA of 1.4-0.60 objective or a PL APO oil 100 × NA of 1.4 objective coupled to a piezzo and a CoolSNAP HQ camera controlled by Metamorph software (Molecular Devices, Sunnyvale, CA). Z-stack step was of 0.2 µm. All stacks were treated by automatic batch deconvolution using the PSF of the optical system, Meinel algorithm with parameters set at 8 iterations, 0.8 sigma and 3 frequencies.

Spindle orientation in ST*Hdh*$^{+/+}$, ST*Hdh*$^{Q109/Q109}$ and HeLa cells stained for γ-tubulin was quantified using ImageJ software (http://rsb.info.nih.gov/ij/, NIH, USA). A line crossing both spindle poles was drawn on the Z projection pictures and repositioned along the Z-axis using the stack of Z-sections. The angle between the pole-pole axis and the substratum plane was calculated using a home-made ImageJ plug-in (Godin, Colombo, et al., 2010).

For quantification of phospho-HTT, dynein and p150^{Glued} at spindle poles, cells were double-stained for the protein of interest and γ-tubulin. Quantification was achieved using using 3D object counter plug-in (Bolte & Cordelières 2006); available at http://imagejdocu.tudor.lu/doku.php?id=plugin:analysis:3d_object_counter:start. Total volume and intensity of the particles were retrieved for further analysis.

Neuronal progenitors were imaged using a Leica SP5 laser scanning confocal microscope equipped with a 63 × oil-immersion objective.

Micropattern fabrication and analysis

L-shaped fibronectin micropatterns of 33 µm long and 7 µm thickness were made as described previously (Carpi et al. , 2012). Briefly, glass coverslips of 25mm Ø (Marienfeld, GmBH) were illuminated with deep UVs lamp (UVO cleaner, model 342-220, Jetlight) for 5 minutes followed by 1h RT incubation with 0.1 mg/mL of poly-L-lysine-g-poly(ethyleneglycol) (PLL(20)-g[3.5]-PEG(2), Surface Solutions GmbH, Zurich). Pegylated coverslips were washed 2 min in PBS, then rinsed twice 2 min in H_2O. Synthetic quartz mask bearing the motifs (Delta Mask, Toppan, Selba Tech) was illuminated for 5 min using deep UVs lamp. Coverslips were next placed with the pegilated side towards the activated face of the quartz mask and illuminated for 5 min using deep UVs lamp. Finally, coverslips were incubated for 1h at RT with 25 µg/mL of fibronectin (Sigma) and fibrinogen-647 (Invitrogen).

ST*Hdh*$^{Q109/Q109}$ and ST*Hdh*$^{+/+}$ cells were electroporated with histone2B–mCherry and positive cells were selected with Hygromycin B (50 µg/ml) and subsequent fluorescence-activated cell sorting (FACS). 150.000 to 250.000 ST*Hdh*$^{+/+}$ and ST*Hdh*$^{Q109/Q109}$ cells were deposited on printed coverslips 1 to 3 hours before video recording.

Individual cells on micropatterns were used to analyze the positioning of the metaphasic plate. The angle was measured using Metamorph software (Molecular Devices, Sunnyvale, CA).

Live-cell imaging

Cell recordings on fibronectin micropatterns were done using a Leica DM IRB microscope with a N PLAN 10 × NA of 0.25 objective coupled to a moving stage and a Photometric CoolSNAP *fx* camera controlled by Metamorph software (Molecular Devices, Sunnyvale, CA). Images were acquired every 3 min during 20h. Controlled temperature (37°C) and CO_2 conditions (5%) were keep along the acquisition time.

For MT dynamics experiments, MEFs were transiently transfected with EB3-GFP and m-Cherry-α-tubulin. Confocal video microscopy experiments were performed on a Nikon Ti Eclipse inverted microscope (Nikon S.A, France) equipped with a CSU-X1 spinning-disk head (Yokogawa, Japan) under controlled environment (regulated temperature and CO2 conditions; LIS, Switzerland). Images were collected with a 60x/1.4 objective. eGFP and m-Cherry were respectively excited with a 491 and 561 nm laser, both being part of the iLAS2 illumination device (Roper Scientific, France). Fluorescent emissions were selected with a dual-band filter (ET GFP/mCherry, ref. 244375, Chroma Technology Corp.) and captured on an Evolve 512x512 EM-CCD camera (Photometrics). A set of GFP and mCherry images was acquired sequentially, each second.

Flies and Immunohistochemistry

D. melanogaster were maintained on standard medium at 18°C. Control W^{1118} flies are a kind gift from S Zhang and N Perrimon (Harvard Medical School, USA; Zhang et al. 2009). UAS-Htt^{548aa}-Q0 and UAS-Htt^{548aa}-Q128 were generously provided by JT Littleton (Massachusetts Institute of Technology, USA; Lee et al. 2004). UAS-Htt^{548aa}-Q128-S421D

flies were generated from the cDNA for human Htt-Q128 kindly provided by F Maschat (Institute of Human Genetics, France) where a point mutation at S421 was inserted using PCR and subsequently subcloned into pUAST vectors.

The expression of Htt^{548aa}-Q0, Htt^{548aa}-Q128 and Htt^{548aa}-Q128-S421D in *D. melanogaster* was done under the control of the inscuteable-Gal4 (*insc*) driver, which drives Gal4 expression in neuroblasts. Flies were maintained at 25°C for the experiments.

For immunohistochemistry on *D. melanogaster* brains, third instar larvae were dissected in PBS. The brains were collected and fixed in PBS containing 4% paraformaldehyde, 0.1% triton X-100 for 20 min at room temperature and processed as described (Betschinger et al. 2006). Briefly, brains were incubated overnight with mAb anti-Miranda (1:20; a kind gift of F. Matsuzaki), pAb anti-centrosomin (1:500; a kind gift of T. Kaufman) and pAb anti-phospho-histone H3 (1:2000; Upstate Biotechnology). After three washes in PBS Triton X-100 0.1% (PBT), brains were incubated with mouse AlexaFluor-488, rabbit AlexaFluor-555 and DAPI for 1-2 hr at room temperature, washed again three times in PBT, incubated in PBS/glycerol for 30 min and mounted in Glycerol/PBS-N-propylgalate. The pictures were captured with a Leica SP5 laser scanning confocal microscope equipped with an X63 oil-immersion objective. The spindle orientation was quantified using an home-built macro in ImageJ software (Godin, Colombo, et al., 2010), by measuring the angle between a line connecting the two spindle poles and a line bisecting Miranda crescent.

FIGURE LEGENDS

Figure 1. Huntingtin and molecular motor distributions are modified in HD

(A) Metaphase ST*Hdh*$^{+/+}$ and ST*Hdh*$^{Q109/Q109}$ cells transfected with EB3-GFP are immunostained using a a polyclonal antibody, pAb SE3619 against HTT.

(B, C) Immunostainings of metaphase ST*Hdh*$^{+/+}$ and ST*Hdh*$^{Q109/Q109}$ cells with **(B)** anti-γ-tubulin and anti-p150^{Glued} antibodies and **(C)** anti-γ-tubulin and anti-dynein (DIC) antibodies.

The left graphs corresponds to the quantification of **(A)** HTT, **(B)** p150^{Glued} and **(C)** DIC intensities at spindle poles. Results are shown as mean values ± SEM. *p<0.05; ***p<0.001, *t* test. Scale bar 10µm.

Figure 2. Impaired MT dynamics in polyQ MEFs

(A) Videomicroscopy examination of MTs in *Hdh*$^{Q7/Q7}$ and *Hdh*$^{Q111/Q111}$ MEFs expressing mCherry-α-tubulin and EB3-GFP close to the leading edge of lamellipodial extensions. Colored arrowheads indicate localization of the MT plus-ends at different time points. Time is expressed as minutes:seconds.

(B) Measurement of the time spent by MTs exploring the area near the leading edge (persistence time, right, ***p<0.001, *t* test) and EB3-comets velocity (mean velocity, left, NS is p=0.8024, *t* test.) in *Hdh*$^{Q7/Q7}$ and *Hdh*$^{Q111/Q111}$ MEFs. Results are shown as mean values ± SEM. Scale bar 10µm.

Figure 3. CLIP-170 and p150^{Glued} localization at MT plus-ends is modified by mutant HTT and regulated by Akt

(A, right) CLIP170 immunostainings of ST*Hdh*$^{+/+}$ and ST*Hdh*$^{Q109/Q109}$ cells transfected with EB3-GFP and Akt c.a. when indicated. High magnification of a region of interest from ST*Hdh*$^{+/+}$ and ST*Hdh*$^{Q109/Q109}$ cells. Merged images show CLIP-170 in red and EB3 in green. **(A, middle)** Graph of the line scan of fluorescence intensity (arbitrary units) of CLIP170 (red) and EB3 (green), starting at the end of the MT (distance 0) to 2.5 µm inwards. **(A, left)** Quantitative analysis of CLIP170 localization at MT plus-ends in ST*Hdh*$^{+/+}$ and ST*Hdh*$^{Q109/Q109}$ cells.

(B) p150^{Glued} immunostainings of ST*Hdh*$^{+/+}$ and ST*Hdh*$^{Q109/Q109}$ cells transfected with EB3-GFP and Akt c.a. when indicated. High magnification of a region of interest from ST*Hdh*$^{+/+}$ and ST*Hdh*$^{Q109/Q109}$ cells. Merged images show p150^{Glued} in red and EB3 in green. **(B, middle)** Graph of the line scan of fluorescence intensity (arbitrary units) of p150^{Glued} (red) and EB3 (green), starting at the end of the MT (distance 0) to 2.5 µm inwards. **(B, left)** Quantitative analysis of p150^{Glued} localization in ST*Hdh*$^{+/+}$ and ST*Hdh*$^{Q109/Q109}$ cells.

Results are shown as mean values ± SEM. ***p<0.001, *t* test. Scale bar 10µm.

Figure 4. Mutant HTT affects CLIP170/p150^{Glued} /dynein complex affinity, an effect that is regulated by Akt

(A, left) Dynein immunoprecipitation (IP) (anti-DIC antibody) experiments from ST*Hdh*$^{+/+}$ and ST*Hdh*$^{Q109/Q109}$ cell lysates. Endogenous levels of HTT, CLIP170, p150^{Glued}, DIC and α-tubulin are shown in the input. Decreased interaction of dynein with p150^{Glued} was

observed in ST*Hdh*$^{Q109/Q109}$ cells compared to ST*Hdh*$^{+/+}$ while CLIP170 levels were bearly detectable. **(A, right)** Dynein immunoprecipitation (IP) (anti-DIC antibody) experiments from ST*Hdh*$^{+/+}$ and ST*Hdh*$^{Q109/Q109}$ cells transfected with Akt c.a. Endogenous levels of HTT, CLIP170, p150^{Glued}, DIC, α-tubulin and transfected Akt c.a. HA tagged are shown in the input. Equal interaction of dynein with p150^{Glued} in ST*Hdh*$^{Q109/Q109}$ cells was observed compared to ST*Hdh*$^{+/+}$. CLIP170 levels were highly increased.

(B) Dynein immunoprecipitation (IP) (anti-DIC antibody) experiments from lysates of HeLa cells expressing HTT-480-17Q, HTT-480-68Q, HTT-480-68Q-S421D or GFP alone. Endogenous HTT, DIC, β-actin and transfected levels of GFP-constructs are shown in the input. Decreased interaction of DIC with HTT-480-68Q are restored when the mutant point version was expressed HTT-480-68Q-S421D.

Figure 5. Mutant huntingtin causes spindle misorientation

(A, left) Immunoblotting of ST*Hdh*$^{+/+}$ and ST*Hdh*$^{Q109/Q109}$ cells extracts using anti-HTT (htt-4C8), anti-polyQ-HTT (htt-1C2) and anti-α-tubulin antibodies. Z-X projections of ST*Hdh*$^{+/+}$ and ST*Hdh*$^{Q109/Q109}$ cells stained with anti-γ-tubulin antibody (green) and DAPI. **(A, right)** Distribution and average of spindle angles of ST*Hdh*$^{+/+}$ and ST*Hdh*$^{Q109/Q109}$ metaphase cells.

(B, left) HeLa cells transfected with HTT-480-17Q, HTT-480-68Q and the corresponding empty vector are analyzed by immunoblotting for the presence of endogenous and transfected HTT (htt-4C8) and α-tubulin. **(B, right)** Distribution and average of spindle angles. Z-X projections of HeLa cells stained with anti-γ-tubulin antibody (green) and DAPI.

Results are shown as mean values ± SEM. ***p<0.001, *t* test; **p<0.01, one way ANOVA followed by Fisher's *Post-hoc* test.

Figure 6. Mitotic spindle positioning is altered in ST*Hdh*$^{Q109/Q109}$ cells

(A, left) The distribution of mitotic angles in ST*Hdh*$^{+/+}$ and ST*Hdh*$^{Q109/Q109}$ cell population. **(A, right)** Examples of time-lapse acquisition of ST*Hdh*$^{+/+}$ and ST*Hdh*$^{Q109/Q109}$ cells during mitosis. Time-lapse pictures were used to measure the positioning of the metaphasic plate (H2B-mCherry).

(B) Percentages of misaligned spindles (spindle angle deviating by >15° from the mean value) in ST*Hdh*$^{+/+}$ and ST*Hdh*$^{Q109/Q109}$ cells. Results are shown as mean values ± SEM. *p<0.05, *t* test. Scale bar 10µm.

Figure 7. Akt phosphorylation at S421 rescue the mutant phenotype in spindle orientation

(A, left) ST*Hdh*$^{+/+}$ and ST*Hdh*$^{Q109/Q109}$ cells transfected with an empty vector or HA tagged Akt c.a. are analyzed by immunoblotting using anti-HTT (htt-4C8), anti-HA and anti-β-actin antibodies. Mean spindle angle measured at metaphase, of ST*Hdh*$^{+/+}$ and ST*Hdh*$^{Q109/Q109}$ cells transfected with Akt c.a. or an empty vector. **(A, right)** Z-X projections of ST*Hdh*$^{+/+}$ and ST*Hdh*$^{Q109/Q109}$ cells stained with γ-tubulin (green) and DAPI.

(B) Mean spindle angle measured at metaphase, of HeLa cells transfected with several HTT constructs with or without Akt c.a.: HTT-480-17Q, HTT-480-17QA, HTT-480-17Q-S421D, HTT-480-68Q, HTT-480-68Q + Akt c.a., HTT-480-68Q-S421A, HTT-480-68Q-S421A + Akt c.a. and HTT-480-68Q-S421D.

Results are shown as mean values ± SEM. **p<0.05, *t* test. *p<0.05, one way ANOVA followed by Fisher's *Post-hoc* test.

Figure 8. HTT function during mitosis is affected by polyQ expansion in *D. melanogaster* neuroblasts

(A, left) Schematic representation of spindle poles (red) and Miranda crescent (green). The angle between the spindle pole (solid line) and the middle of Miranda crescent (dashed line) is measured for each NB in metaphase. **(A, right)** NBs of third instar larvae from W^{1118}, htt^{548aa}-0Q, htt^{548aa}-128Q and htt^{548aa}-128Q-S421D flies are stained with Centrosomin (Cnn, white arrowhead), the mitotic marker phosphohistone H3 (PH3), and Miranda. Quantification of spindle positioning angles relative to Miranda crescent. Values are expressed as a percentage of NBs within each angle intervals.

(B) Mean of spindle positioning angle from W^{1118}, htt^{548aa}-0Q, htt^{548aa}-128Q and htt^{548aa}-128Q-S421D NBs.

Results are shown as mean values ± SEM. *p<0.05, one way ANOVA followed by Fisher's *Post-hoc* test. Scale bar 5µm.

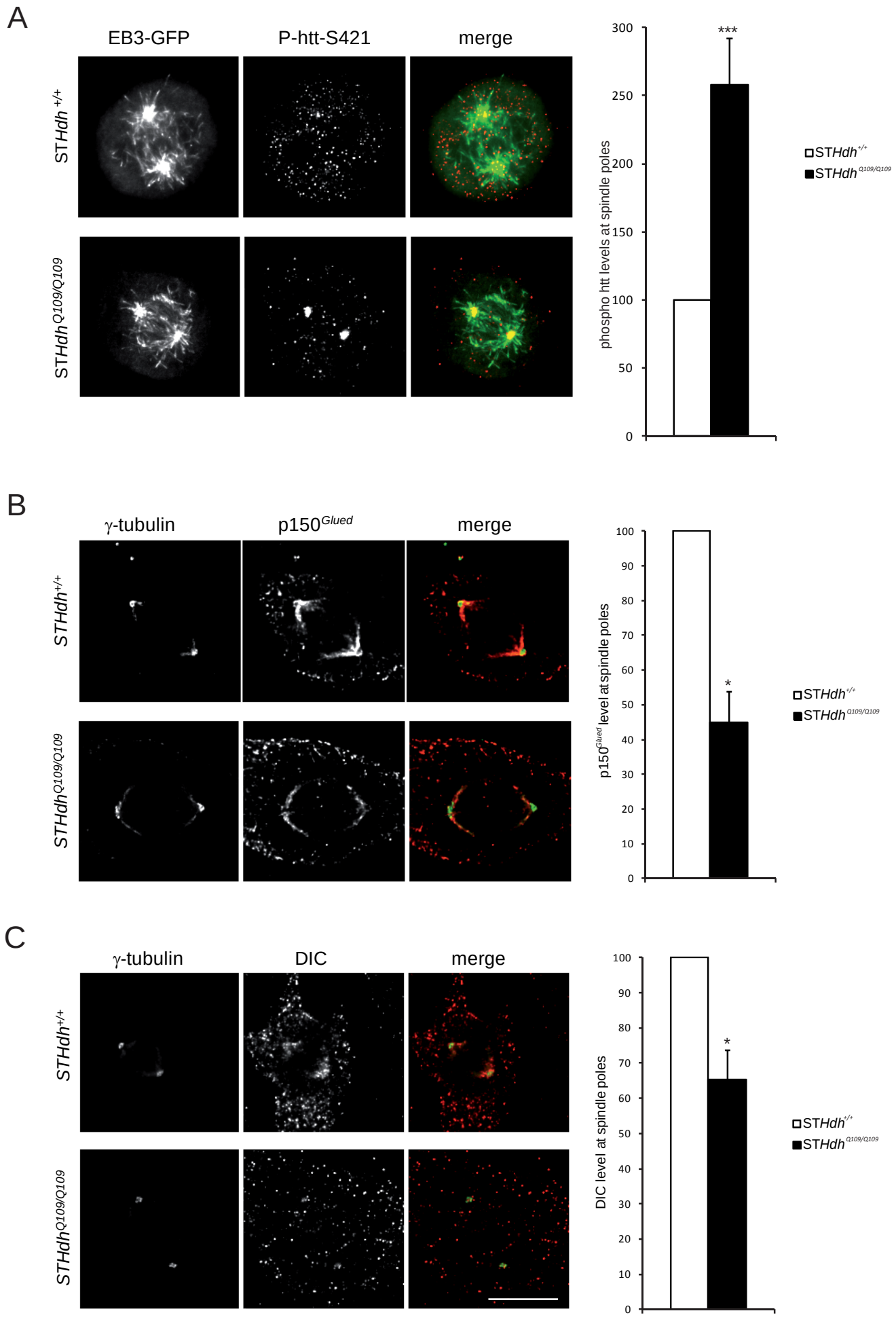
A
EB3-GFP
P-htt-S421
merge
STHdh+/+
STHdhQ109/Q109
phospho htt levels at spindle poles
300
250
200
150
100
50
0
***
STHdh+/+
STHdhQ109/Q109
B
γ-tubulin
p150Glued
merge
STHdh+/+
STHdhQ109/Q109
p150Glued level at spindle poles
100
90
80
70
60
50
40
30
20
10
0
*
STHdh+/+
STHdhQ109/Q109
C
γ-tubulin
DIC
merge
STHdh+/+
STHdhQ109/Q109
DIC level at spindle poles
100
90
80
70
60
50
40
30
20
10
0
*
STHdh+/+
STHdhQ109/Q109

FIGURE 1

A

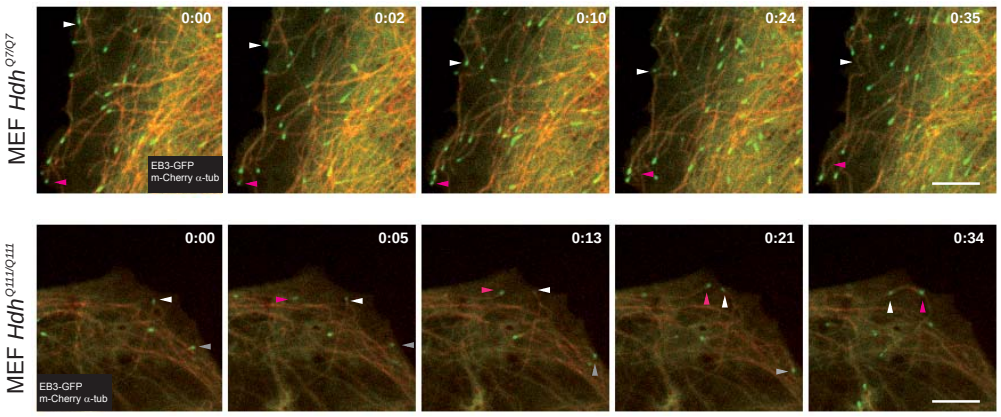
MEF Hdh Q7/Q7
0:00
0:02
0:10
0:24
0:35
EB3-GFP
m-Cherry α-tub
MEF Hdh Q111/Q111
0:00
0:05
0:13
0:21
0:34
EB3-GFP
m-Cherry α-tub

B

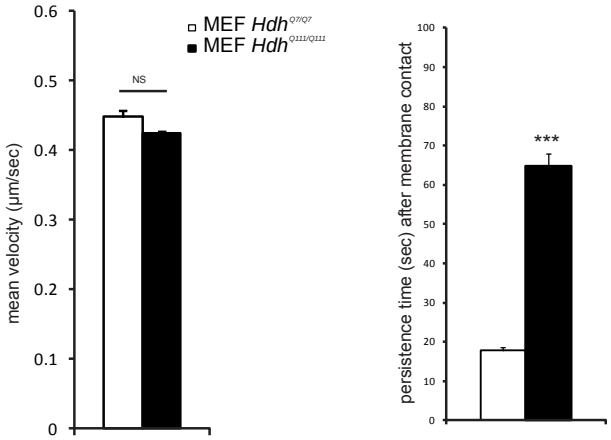
MEF Hdh Q7/Q7
MEF Hdh Q111/Q111
mean velocity (μm/sec)
0.6
0.5
0.4
0.3
0.2
0.1
0
NS
persistence time (sec) after membrane contact
100
90
80
70
60
50
40
30
20
10
0
***

FIGURE 2

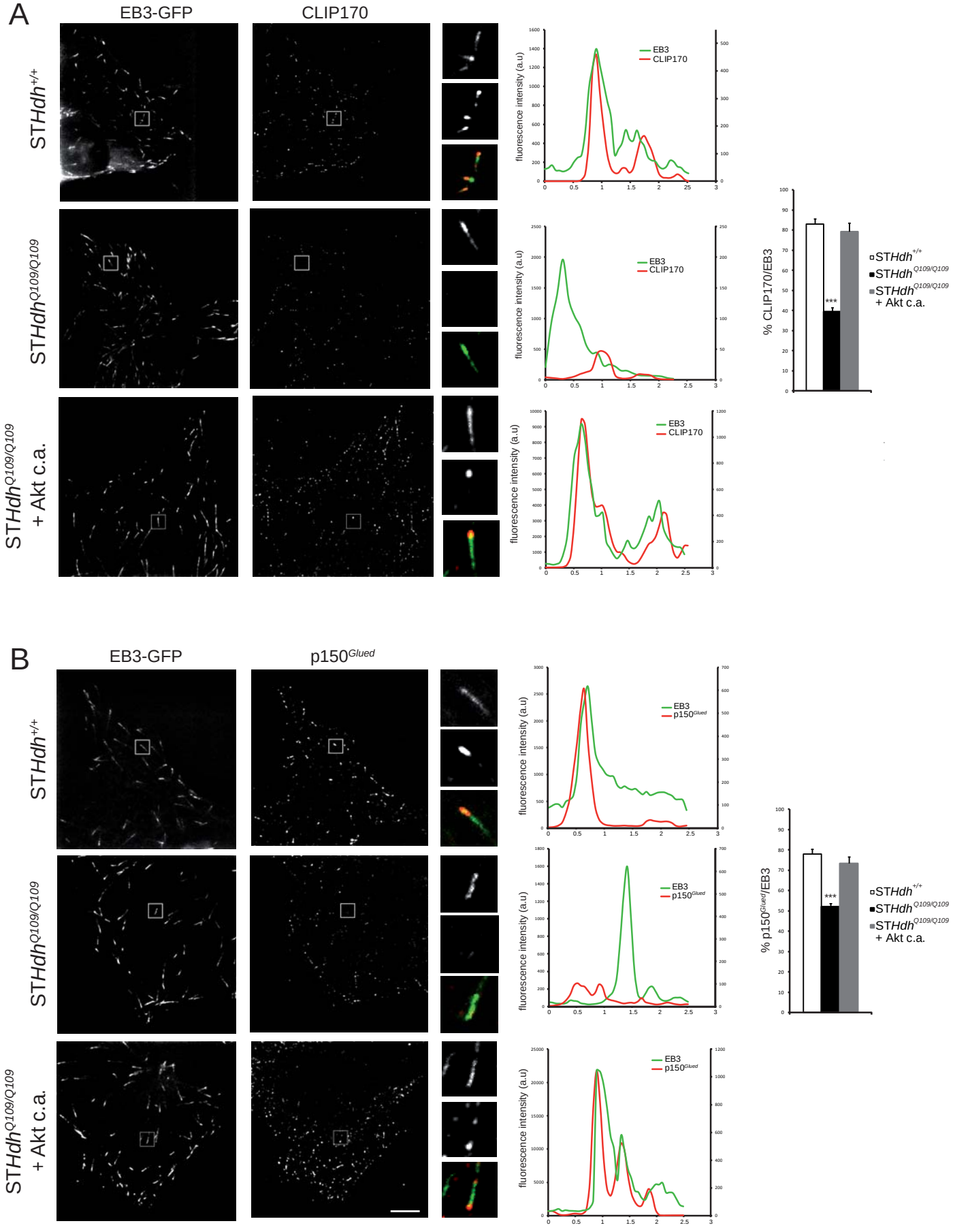
A
EB3-GFP
CLIP170
STHdh+/+
STHdhQ109/Q109
STHdhQ109/Q109 + Akt c.a.
fluorescence intensity (a.u)
EB3
CLIP170
% CLIP170/EB3
***
STHdh+/+
STHdhQ109/Q109
STHdhQ109/Q109 + Akt c.a.
B
EB3-GFP
p150Glued
STHdh+/+
STHdhQ109/Q109
STHdhQ109/Q109 + Akt c.a.
fluorescence intensity (a.u)
EB3
p150Glued
% p150Glued/EB3
***
STHdh+/+
STHdhQ109/Q109
STHdhQ109/Q109 + Akt c.a.

FIGURE 3

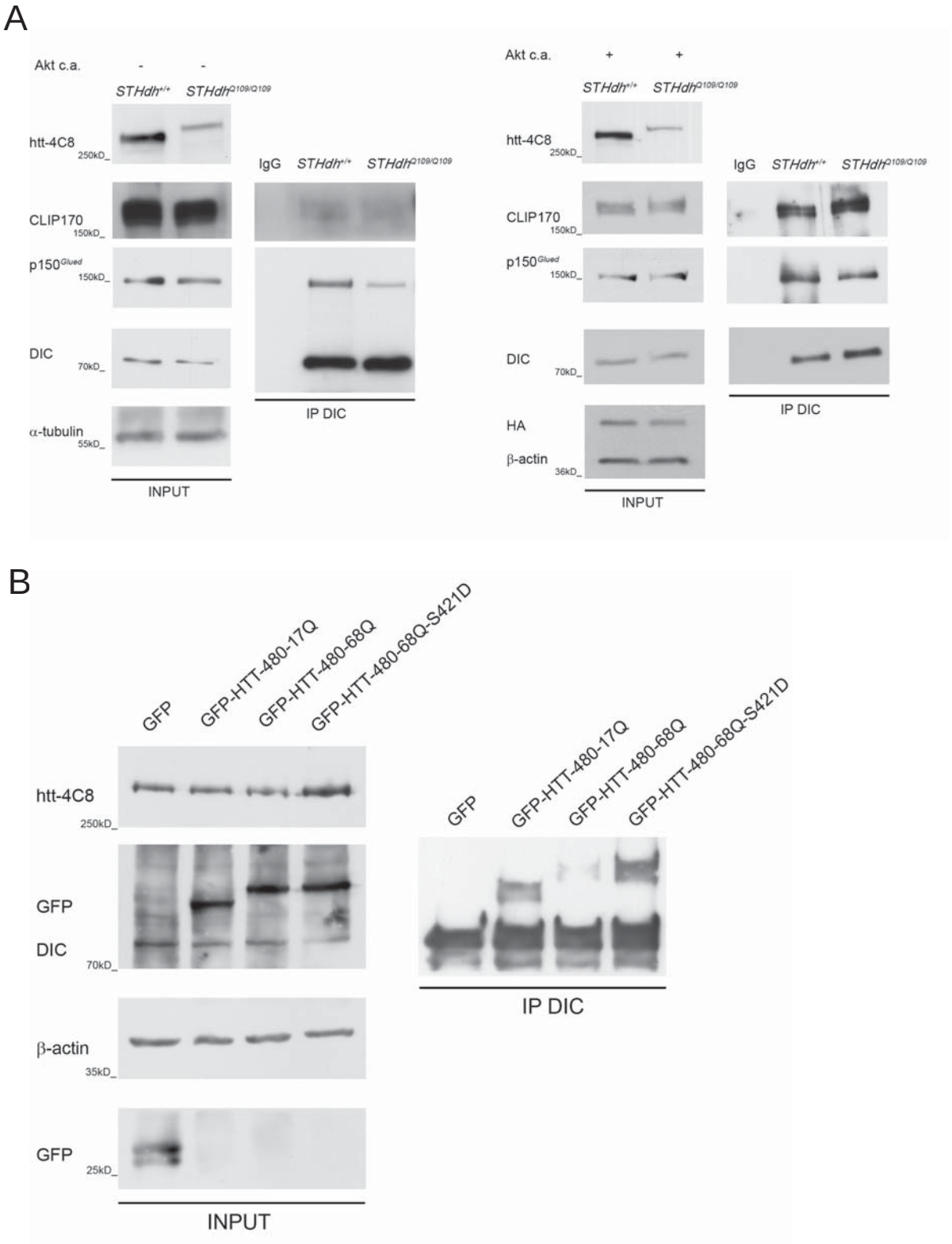
A
Akt c.a.
-
-
STHdh+/+
STHdhQ109/Q109
htt-4C8
250kD
CLIP170
150kD
p150Glued
150kD
DIC
70kD
α-tubulin
55kD
INPUT
IgG
STHdh+/+
STHdhQ109/Q109
IP DIC
Akt c.a.
+
+
STHdh+/+
STHdhQ109/Q109
htt-4C8
250kD
CLIP170
150kD
p150Glued
150kD
DIC
70kD
HA
β-actin
36kD
INPUT
IgG
STHdh+/+
STHdhQ109/Q109
IP DIC
B
GFP
GFP-HTT-480-17Q
GFP-HTT-480-68Q
GFP-HTT-480-68Q-S421D
htt-4C8
250kD
GFP
DIC
70kD
β-actin
35kD
GFP
25kD
INPUT
GFP
GFP-HTT-480-17Q
GFP-HTT-480-68Q
GFP-HTT-480-68Q-S421D
IP DIC

FIGURE 4

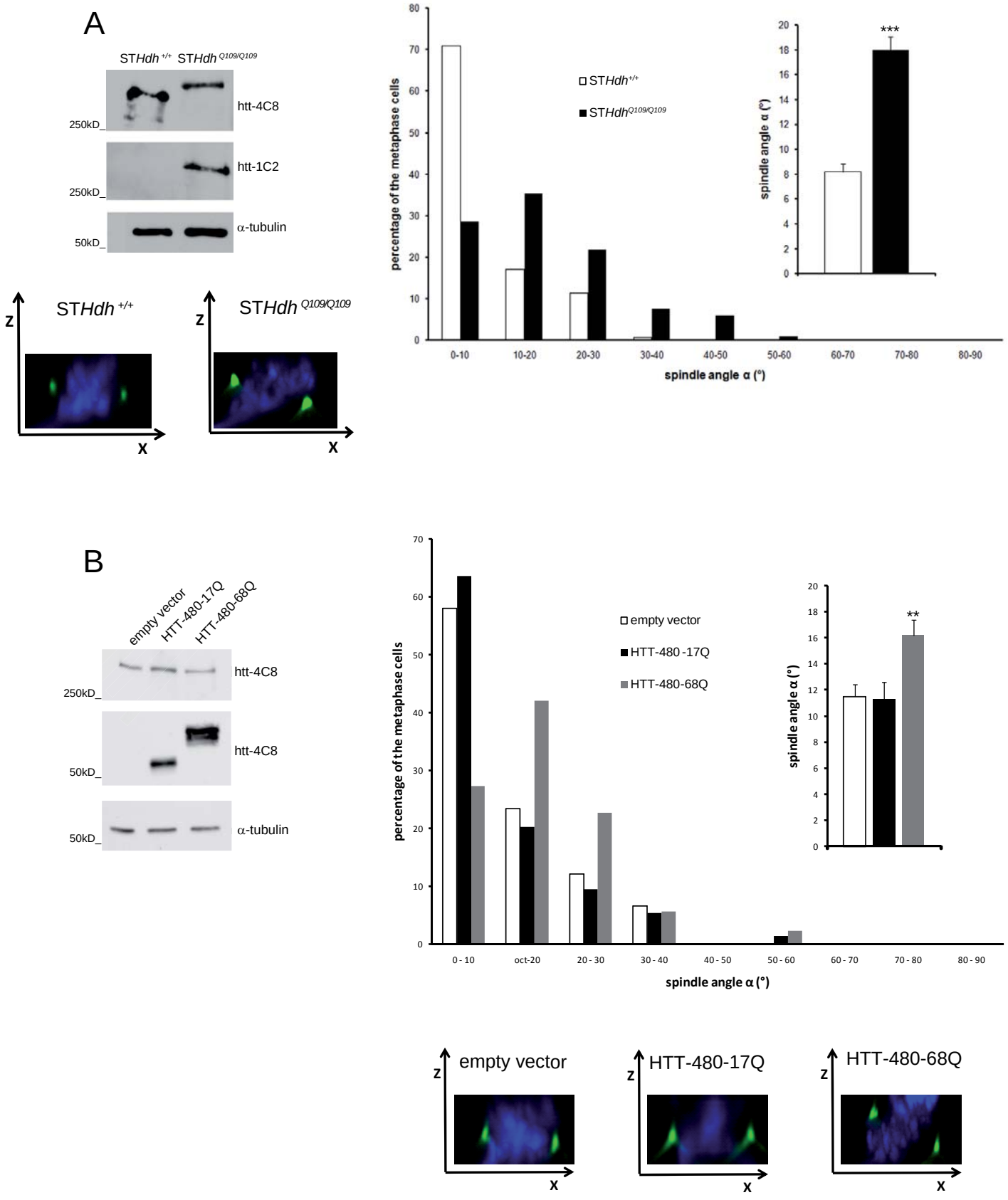
A
STHdh +/+
STHdh Q109/Q109
250kD_
htt-4C8
250kD_
htt-1C2
50kD_
α-tubulin
STHdh +/+
STHdh Q109/Q109
Z
X
percentage of the metaphase cells
spindle angle α (°)
0-10
10-20
20-30
30-40
40-50
50-60
60-70
70-80
80-90
***
B
empty vector
HTT-480-17Q
HTT-480-68Q
250kD_
htt-4C8
50kD_
htt-4C8
50kD_
α-tubulin
0 - 10
oct-20
20 - 30
30 - 40
40 - 50
50 - 60
60 - 70
70 - 80
80 - 90
**

FIGURE 5

A

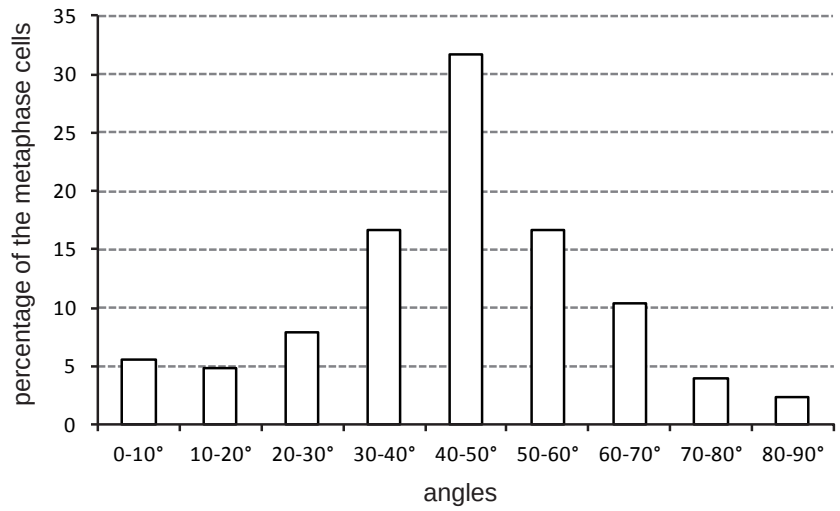
ST*Hdh*$^{+/+}$
percentage of the metaphase cells
35
30
25
20
15
10
5
0
0-10°
10-20°
20-30°
30-40°
40-50°
50-60°
60-70°
70-80°
80-90°
angles

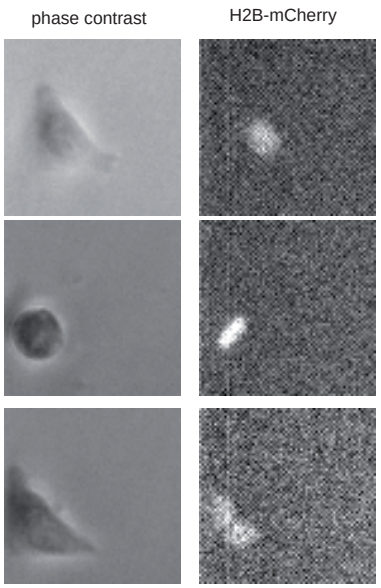
phase contrast
H2B-mCherry

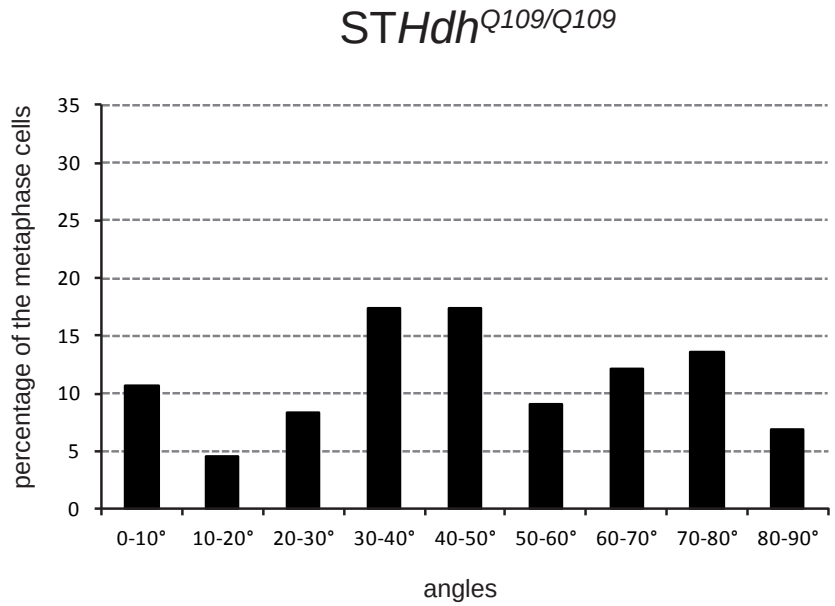
ST*Hdh*$^{Q109/Q109}$
percentage of the metaphase cells
35
30
25
20
15
10
5
0
0-10°
10-20°
20-30°
30-40°
40-50°
50-60°
60-70°
70-80°
80-90°
angles

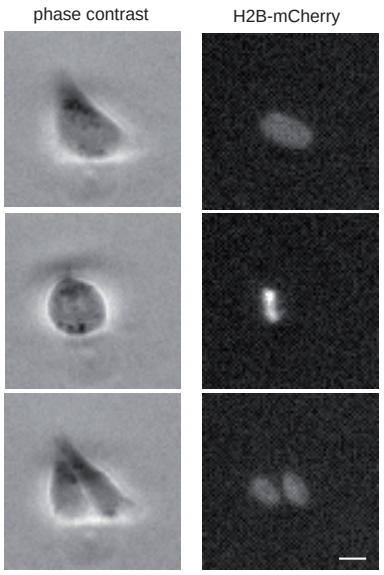
phase contrast
H2B-mCherry

B

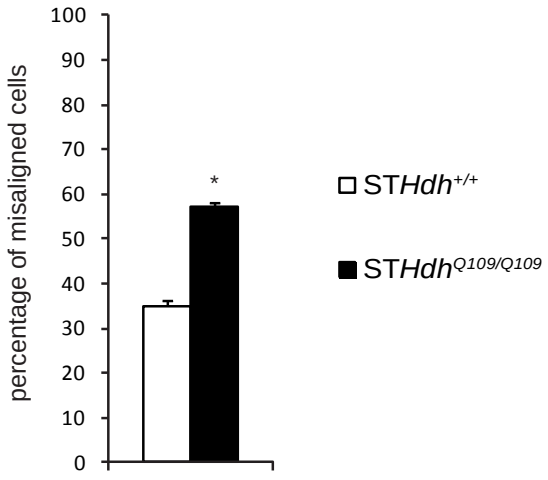
percentage of misaligned cells
100
90
80
70
60
50
40
30
20
10
0
*
ST*Hdh*$^{+/+}$
ST*Hdh*$^{Q109/Q109}$

FIGURE 6

A

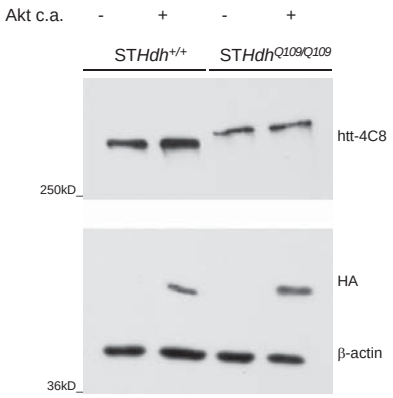
Akt c.a. - + - +
STHdh+/+
STHdhQ109/Q109
htt-4C8
250kD
HA
β-actin
36kD

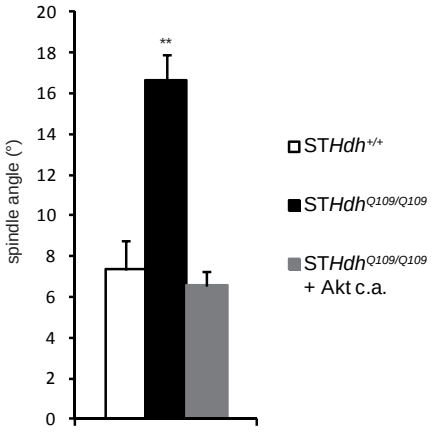
spindle angle (°)
**
STHdh+/+
STHdhQ109/Q109
STHdhQ109/Q109 + Akt c.a.

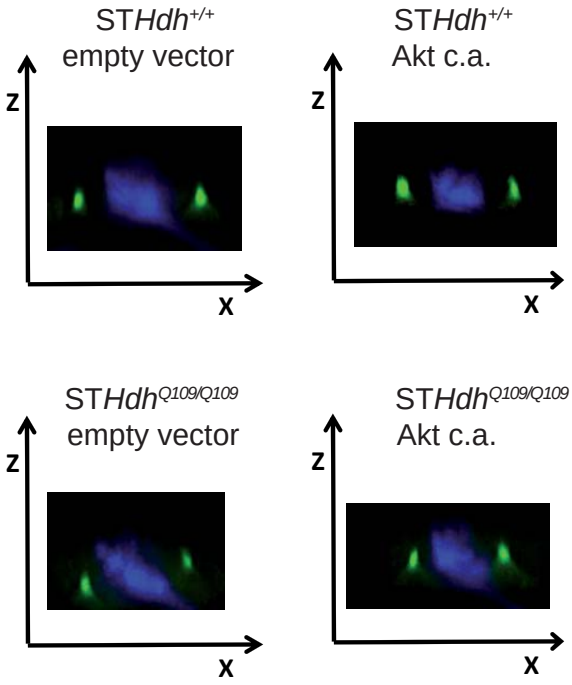
STHdh+/+ empty vector
STHdh+/+ Akt c.a.
STHdhQ109/Q109 empty vector
STHdhQ109/Q109 Akt c.a.
Z
X

B

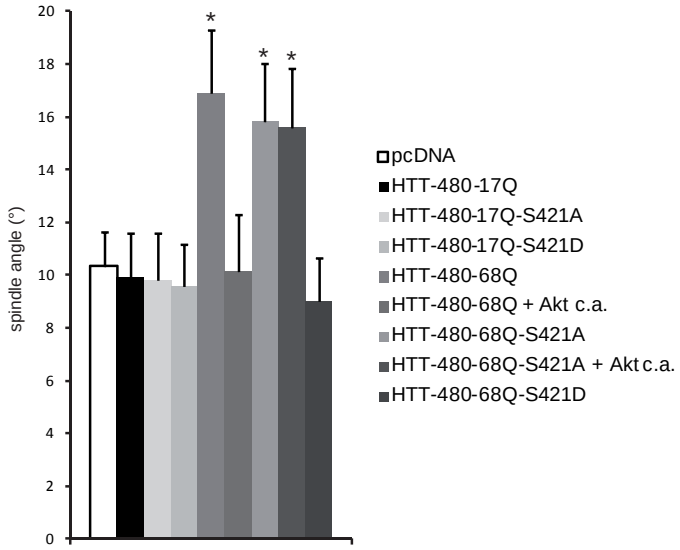
spindle angle (°)
*
pcDNA
HTT-480-17Q
HTT-480-17Q-S421A
HTT-480-17Q-S421D
HTT-480-68Q
HTT-480-68Q + Akt c.a.
HTT-480-68Q-S421A
HTT-480-68Q-S421A + Akt c.a.
HTT-480-68Q-S421D

FIGURE 7

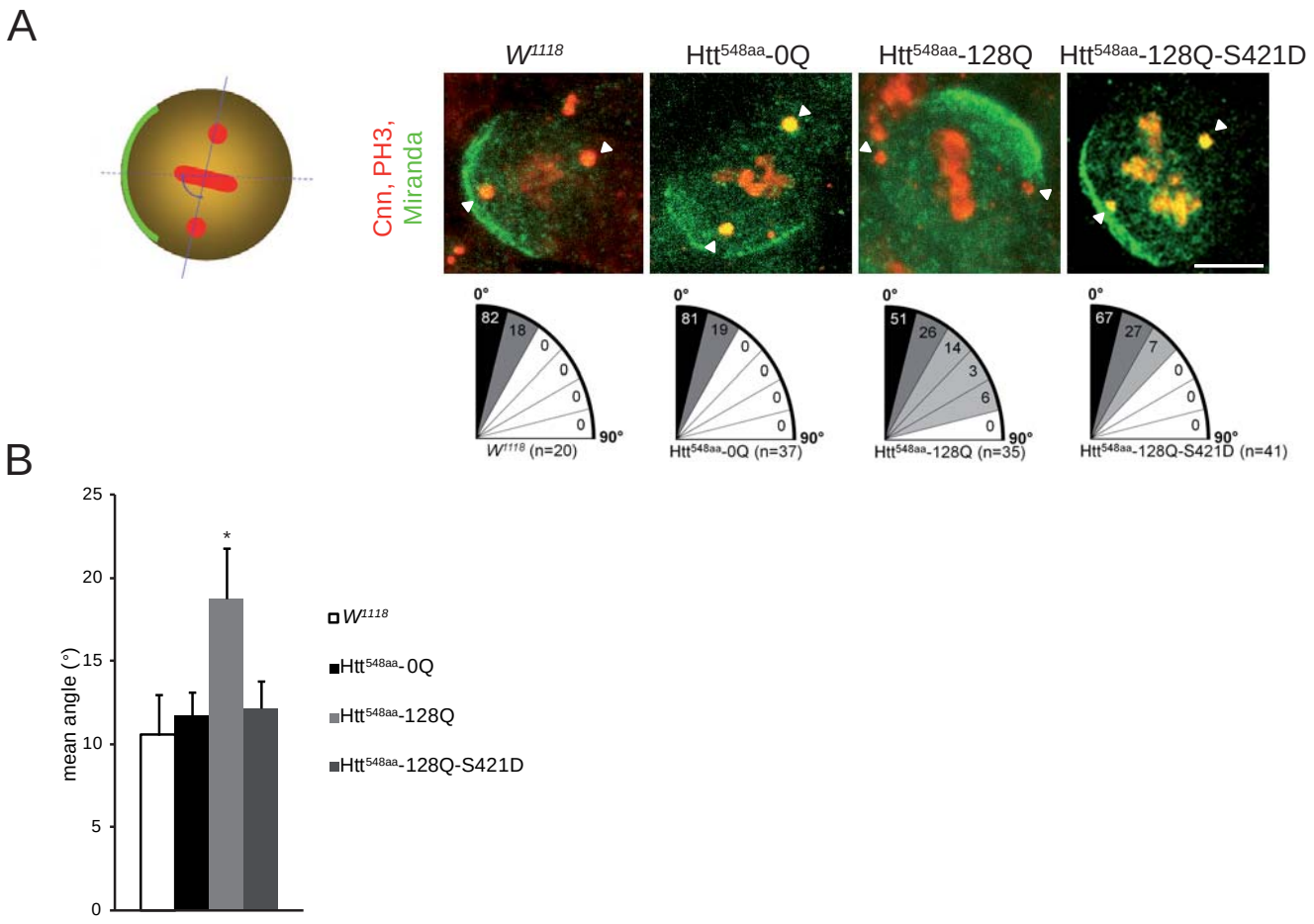
A
W1118
Htt548aa-0Q
Htt548aa-128Q
Htt548aa-128Q-S421D
Cnn, PH3, Miranda
0°
82
18
0
0
0
0
90°
W1118 (n=20)
0°
81
19
0
0
0
0
90°
Htt548aa-0Q (n=37)
0°
51
26
14
3
6
0
90°
Htt548aa-128Q (n=35)
0°
67
27
7
0
0
0
90°
Htt548aa-128Q-S421D (n=41)
B
mean angle (°)
25
20
15
10
5
0
*
W1118
Htt548aa-0Q
Htt548aa-128Q
Htt548aa-128Q-S421D

FIGURE 8

Akhmanova, A. & Steinmetz, M.O., 2010. Microtubule +TIPs at a glance. *Journal of cell science*, 123(Pt 20), pp.3415–9. Available at: http://www.ncbi.nlm.nih.gov/pubmed/20930136 [Accessed June 28, 2011].

Betschinger, J., Mechtler, K. & Knoblich, J., 2006. Asymmetric segregation of the tumor suppressor Brat regulates self-renewal in Drosophila neural stem cells. *Cell*, 124, pp.1241–1253.

Bolte, S. & Cordelières, F P, 2006. A guided tour into subcellular colocalization analysis in light microscopy. *Journal of microscopy*, 224(Pt 3), pp.213–32. Available at: http://www.ncbi.nlm.nih.gov/pubmed/17210054 [Accessed August 21, 2012].

Bowman, S.K. et al., 2006. The Drosophila NuMA Homolog Mud regulates spindle orientation in asymmetric cell division. *Developmental cell*, 10(6), pp.731–42. Available at: http://www.ncbi.nlm.nih.gov/pubmed/16740476.

Buttrick, G.J. et al., 2008. Akt regulates centrosome migration and spindle orientation in the early Drosophila melanogaster embryo. *The Journal of cell biology*, 180(3), pp.537–48. Available at: http://www.ncbi.nlm.nih.gov/pubmed/18268102.

Carpi, N. et al., 2012. Micropatterning on glass with deep UV. *PROTOCOL EXCHANGE*, pp.1–9.

Caviston, J.P. et al., 2007. Huntingtin facilitates dynein/dynactin-mediated vesicle transport. *Proc. Natl Acad. Sci. USA*, 104, pp.10045–10050.

Colin, E et al., 2005. Akt is altered in an animal model of Huntington's disease and in patients. *Eur. J. Neurosci.*, 21, pp.1478–1488.

Colin, Emilie et al., 2008. Huntingtin phosphorylation acts as a molecular switch for anterograde/retrograde transport in neurons. *The EMBO journal*, 27(15), pp.2124–34. Available at: http://www.ncbi.nlm.nih.gov/pubmed/18615096.

Coquelle, F.M. et al., 2002. LIS1 , CLIP-170 ' s Key to the Dynein / Dynactin Pathway. *Molecular and Cellular Biology*, 22(9), pp.3089–3102.

Datta, S R et al., 1997. Akt phosphorylation of BAD couples survival signals to the cell-intrinsic death machinery. *Cell*, 91(2), pp.231–41. Available at: http://www.ncbi.nlm.nih.gov/pubmed/9346240 [Accessed July 16, 2012].

Galjart, N., 2005. CLIPs and CLASPs and cellular dynamics. *Nature reviews. Molecular cell biology*, 6(6), pp.487–98. Available at: http://www.ncbi.nlm.nih.gov/pubmed/15928712 [Accessed July 14, 2011].

Gauthier, L.R. et al., 2004. Huntingtin Controls Neurotrophic Support and Survival of Neurons by Enhancing BDNF Vesicular Transport along Microtubules. *Cell*, 118, pp.127–138.

Godin, J.D. et al., 2010. Huntingtin Is Required for Mitotic Spindle Orientation and Mammalian Neurogenesis. *Neuron*, 67(3), pp.392–406. Available at: http://www.ncbi.nlm.nih.gov/pubmed/20696378 [Accessed August 11, 2010].

Humbert, S et al., 2002. The IGF-1/Akt pathway is neuroprotective in Huntington's disease and involves Huntingtin phosphorylation by Akt. *Dev Cell*, 2, pp.831–7.

Johnston, C. a et al., 2009. Identification of an Aurora-A/PinsLINKER/Dlg spindle orientation pathway using induced cell polarity in S2 cells. *Cell*, 138(6), pp.1150–63. Available at: http://www.ncbi.nlm.nih.gov/pubmed/19766567.

Knoblich, J.A., 2001. Asymmetric cell division during animal development. *Nat. Rev. Mol. Cell Biol.*, 2, pp.11–20.

Lee, W.-C.M., Yoshihara, M. & Littleton, J.T., 2004. Cytoplasmic aggregates trap polyglutamine-containing proteins and block axonal transport in a Drosophila model of Huntington's disease. *Proceedings of the National Academy of Sciences of the United States of America*, 101(9), pp.3224–9. Available at: http://www.ncbi.nlm.nih.gov/pubmed/14978262.

Li, S.-H. et al., 1998. Interaction of Huntingtin-Associated Protein with Dynactin P150 Glued. *The Journal of Neuroscience*, 18(4), pp.1261–1269.

Li, X.J. et al., 1995. A huntingtin-associated protein enriched in brain with implications for pathology. *Nature*, 378(6555), pp.398–402. Available at: http://www.ncbi.nlm.nih.gov/pubmed/7477378 [Accessed August 7, 2012].

Mitsushima, M., Toyoshima, F. & Nishida, E., 2009. Dual Role of Cdc42 in Spindle Orientation Control of. *Molecular and Cellular Biology*, 29(10), pp.2816–2827.

Morin, X. & Bellaïche, Y., 2011. Mitotic Spindle Orientation in Asymmetric and Symmetric Cell Divisions during Animal Development. *Developmental cell*, 21(1), pp.102–19. Available at: http://www.ncbi.nlm.nih.gov/pubmed/21763612 [Accessed July 19, 2011].

Pardo, R. et al., 2006. Inhibition of calcineurin by FK506 protects against polyglutamine-huntingtin toxicity through an increase of huntingtin phosphorylation at S421. *The Journal of neuroscience : the official journal of the Society for Neuroscience*, 26(5), pp.1635–45. Available at: http://www.ncbi.nlm.nih.gov/pubmed/16452687.

Pardo, R. et al., 2006. Inhibition of calcineurin by FK506 protects against polyglutamine-huntingtin toxicity through an increase of huntingtin phosphorylation at S421. *The Journal of neuroscience : the official journal of the Society for Neuroscience*, 26(5), pp.1635–45. Available at: http://www.ncbi.nlm.nih.gov/pubmed/16452687.

Pardo, R. et al., 2010. pARIS-htt: an optimised expression platform to study huntingtin reveals functional domains required for vesicular trafficking. *Molecular brain*, 3, p.17. Available at: http://www.pubmedcentral.nih.gov/articlerender.fcgi?artid=2887845&tool=pmcentrez&rendertype=abstract.

Saudou, F et al., 1998. Huntingtin acts in the nucleus to induce apoptosis but death does not correlate with the formation of intranuclear inclusions. *Cell*, 95, pp.55–66.

Schroer, T. a, 2004. Dynactin. *Annual review of cell and developmental biology*, 20, pp.759–79. Available at: http://www.ncbi.nlm.nih.gov/pubmed/15473859 [Accessed June 29, 2010].

Siller, K.H., Cabernard, C. & Doe, C Q, 2006. The NuMA-related Mud protein binds Pins and regulates spindle orientation in Drosophila neuroblasts. *Nature cell biology*, 8, pp.594–600.

Siller, K.H. & Doe, Chris Q, 2008. Lis1/dynactin regulates metaphase spindle orientation in Drosophila neuroblasts. *Dev. Biol.*, 319, pp.1–9.

Siller, K.H. & Doe, Chris Q, 2009. Spindle orientation during asymmetric cell division. *Nature cell biology*, 11(4), pp.365–374.

Steinmetz, M.O. & Akhmanova, A., 2008. Capturing protein tails by CAP-Gly domains. *Trends in biochemical sciences*, 33(October), pp.535–545.

Stepanova, T. et al., 2003. Visualization of microtubule growth in cultured neurons via the use of EB3-GFP (end-binding protein 3-green fluorescent protein). *The Journal of neuroscience : the official journal of the Society for Neuroscience*, 23(7), pp.2655–64. Available at: http://www.ncbi.nlm.nih.gov/pubmed/12684451 [Accessed August 22, 2012].

Tanenbaum, M.E. et al., 2006. CLIP-170 facilitates the formation of kinetochore-microtubule attachments. *The EMBO journal*, 25(1), pp.45–57. Available at: http://www.pubmedcentral.nih.gov/articlerender.fcgi?artid=1356359&tool=pmcentrez&rendertype=abstract [Accessed July 1, 2010].

Théry, M. et al., 2005. The extracellular matrix guides the orientation of the cell division axis. *Nature cell biology*, 7(10), pp.947–53. Available at: http://www.ncbi.nlm.nih.gov/pubmed/16179950.

Toyoshima, F. et al., 2007. PtdIns(3,4,5)P3 regulates spindle orientation in adherent cells. *Developmental cell*, 13(6), pp.796–811. Available at: http://www.ncbi.nlm.nih.gov/pubmed/18061563.

Trettel, F. et al., 2000. Dominant phenotypes produced by the HD mutation in STHdh(Q111) striatal cells. *Hum. Mol. Genet*, 9, pp.2799–2809.

Wheeler, V C et al., 1999. Length-dependent gametic CAG repeat instability in the Huntington's disease knock-in mouse. *Human molecular genetics*, 8(1), pp.115–22. Available at: http://www.ncbi.nlm.nih.gov/pubmed/9887339 [Accessed August 23, 2012].

Yingling, J. et al., 2008. Supplemental Data Neuroepithelial stem cell proliferation requires LIS1 for precise spindle orientation and symmetric division. *Cell*, 132(3), pp.474–86. Available at: http://www.pubmedcentral.nih.gov/articlerender.fcgi?artid=2265303&tool=pmcentrez&rendertype=abstract.

Zala, D. et al., 2008. Phosphorylation of mutant huntingtin at S421 restores anterograde and retrograde transport in neurons. *Human molecular genetics*, 17(24), pp.3837–46. Available at: http://www.ncbi.nlm.nih.gov/pubmed/18772195.

7.3 Discussion and perspectives

We described that HTT plays a role in spindle orientation and mitosis (Godin, Colombo, et al., 2010). Depletion of endogenous HTT leads to post-mitotic cell death in cultured cells and affects the fate of neural progenitors *in vivo*. Moreover, HTT role is conserved in *D. melanogaster*.

The rational of this study **"A mutant huntingtin/dynein/dynactin/CLIP170 pathway induces defective spindle orientation and is regulated by Akt"** was to elucidate the effect of HTT poly-glutamine expansion during cell division. We have shown that HTT poly-glutamine expansion, the cause of HD, leads to deficits in spindle positioning in dividing cells. This phenotype is linked to a decreased localization of important proteins involved in mitosis at spindle poles and MT plus-ends. Moreover, a diminution in the affinity of the complex formed by CLIP170/p150^{Glued}/dynein was observed in a mutant context. Phosphorylation at S421 by Akt rescues the observed phenotype.

HTT has been proved to be a scaffold protein, required for diverse cellular functions, including various intracellular trafficking processes. In particular, HTT physically interacts with HAP-1 (X. J. Li et al., 1995; Pardo et al., 2010) and dynein (J P Caviston et al., 2007; Pardo et al., 2010). Dynein associates with the multiprotein dynactin complex, through the p150^{Glued} subunit (Schroer, 2004). Under HD pathological conditions, the HAP1-p150^{Glued} interaction is altered, leading to the molecular motors being depleted from the MTs (Gauthier et al. 2004; S.H. Li et al. 1998). Moreover, abnormal increased interaction of HTT with p150^{Glued} has been observed in cells, leading to detachment of HTT and p150^{Glued} from MT (Zala et al., 2008).

Astral MTs are actively pulled towards the cortex by motor proteins. These pulling forces drive spindle positioning in yeast, worms, insect and mammalian cells (Knoblich, 2001; Siller & Doe, 2009). Emerging data from diverse model systems have led to the prevailing view that, during mitotic spindle positioning, polarity cues at the cell cortex leads to the recruitment of NuMA and cytoplasmic dynein/dynactin complex. The dynein/dynactin complex and its regulators are essential for mitotic spindle positioning (Siller & Doe, 2008, 2009). CLIP170 participates in the plus-end recruitment of dynein: CLIP170 associates with MT and EB through its CAP-Gly motifs and p150^{Glued} binds to the C-terminal of CLIP170 and is recruited to the plus-ends (Coquelle et al., 2002; Galjart, 2005). Together with dynein, CLIP170 is also present at the kinetochores of mitotic cells, where it might participate in MT capture (Tanenbaum et al., 2006). We studied MT dynamics in wild-type and polyQ-HTT expressing fibroblasts (MEF). While MT polymerization rate is not altered in mutant fibroblasts as revealed by the measure of EB3-comets velocity, the time spent by individuals MT exploring the cell cortex was markedly longer (persistence time). In addition, the co-localization of p150^{Glued} and CLIP170 with EB3 is diminished. We found the colocalization ratio of +TIP/EB3 at MT plus-ends significative lower in polyQ fibroblast compared to wild-type. Furthermore, biochemical assays in which we pulled-down endogenous dynein revealed a decreased affinity in the CLIP170/p150^{Glued}/dynein complex in ST*Hdh*$^{Q109/Q109}$ cells. We thus suggest that normal localization of dynein, CLIP170 and p150^{Glued} is altered when HTT is mutated, affecting MT persistence time and anchoring to the cell cortex. We proposed a dynamic and transient

CLIP170/p150^{Glued}/dynein complex at MT plus-ends, which integrity and affinity is regulated by HTT. Mutant HTT would in turn detach HTT and p150^{Glued} from MT, hampering the recruitment of CLIP170 and dynein to plus-ends.

In order to study the consequences of +TIPs mislocalization in polyQ-HTT expressing cells, we next analyzed spindle orientation in cultured cells. The angle formed between the pole-to-pole axis and the substrate plane was measured. ST*Hdh*$^{Q109/Q109}$ divided with a misorientated spindle compared to ST*Hdh*$^{+/+}$ cells. Same result was observed in HeLa cells transfected with a construct encoding for a mutant form of HTT. These observations would indicate that the mechanism underlying spindle misorientation in ST*Hdh*$^{Q109/Q109}$ cells is the delocalization of +TIPs from MT plus-ends and from spindle poles provoked by HTT mutation. Similarly, LIS1 is important for localization of its binding partners NDEL1, dynein, and CLIP170 and this localization impacts on MT stability and capture at the cell cortex (Yingling et al., 2008b). Futures studies will determine whether HTT and LIS1 act through the same pathways to regulate spindle positioning.

HTT is phosphorylated at S421 upon IGF1/Akt pathway activation (Humbert et al. 2002) and a progressive alteration of Akt has been shown during the pathological progression of HD (Colin et al. 2005). S421 phosporylation plays a key role in vesicular transport. When phosphorylated, HTT recruits kinesin-1 to the dynactin complex on vesicles and MTs (Colin et al. 2008). In particular, HTT phosphorylation restores HTT-p150^{Glued} interaction and modulates the HTT–p150^{Glued} association with MTs *in vitro* and in cells (Zala et al., 2008). We tested whether Akt phosphorylation at S421 could rescue the phenotype observed in dividing cells in polyQ conditions. In ST*Hdh*$^{Q109/Q109}$ cells expressing Akt, +TIPs and EB3 have the same level of colocalization than in wild-type cells. In addition, in a biochemical assay where endogenous dynein was pulled-down, comparable levels of CLIP170/p150^{Glued}/dynein complex was obtained in ST*Hdh*$^{Q109/Q109}$ cells expressing Akt and wild-type cells. We confirmed these results in HeLa cells transfected to HTT contructs with point-mutations at S421. We can postulate that Akt plays a role during mitotic spindle orientation through HTT phosphorylation at S421. Concordantly, Akt regulates centrosome migration and spindle orientation in *D. melanogaster* embryos (Buttrick et al., 2008). In cells, the phosphatidylinositol-3,4,5-triphosphate (PtdIns(3,4,5)P3) plays a crucial role in the control of spindle orientation in a β1 integrin-dependent manner (Toyoshima et al., 2007). Cdc42, a Rho family of small GTPases, is responsible for the activation of PI(3)K during mitosis and distribution of cortical dynactin (Mitsushima et al., 2009). Akt is activated downstream PI(3)K. Cell treatment with LY294002 and Wortmannin, two selective inhibitors of PI(3)K, induce spindle misorientation (Toyoshima et al., 2007). All these observations draw a picture in which HTT, and its phosphorylation at S421 by Akt, could act as key regulator of spindle orientation.

Previous studies in *D. melanogaster* NBs have shown the importance of certain proteins in the correct alignment of the mitotic spindle and the distribution of apical/basal polarity cues. For instance, NuMA holomog Mud regulates spindle orientation and cell fate of daughter cells (Bowman et al. 2006; Siller et al. 2006). Moreover, Partner of Inscuteable (Pins; LGN in mammals) have been show to regulate spindle orientation in S2 *D. melanogaster* cells in a Mud/dynein/dynactin/LIS1 dependent manner (Johnston et al., 2009). We have proved HTT

function in mitosis to be conserved in *D. melanogaster* NBs (Godin, Colombo, et al., 2010) as absence of *htt* in NBs alters spindle orientation. Transgenic flies expressing an N-terminal fragment of human HTT with a polyQ expansion recapitulates the same phenotype. Moreover, Akt phosphorylation at S421 rescues the mitotic spindle misalignment. Further studies are necessary to elucidate if this change in spindle positioning also affects the apico-basal axis of polarity.

We propose to further analyse the physiological relevance of our study using mouse models. As discussed before (results section 5), work in a HTT full-length context is crucial. We started to analyse cortical neurogenesis in $Hdh^{Q111/Q111}$ knock-in mouse in which the mouse exon 1 of HTT was replaced by human exon 1 (Wheeler et al. 1999). We measured the cleavage plane of ventricular dividing cells at E9.5 and E14.5. At both stages, we observed an increased number of NESC and RGCs dividing with a horizontal cleavage compared to wild-type condition. These observations suggest that mutant HTT not only alters spindle orientation in cells in culture and in NBs from *D. melanogaster*, but induces a shift in the mode of division of neural progenitors. Cell fate analysis at E16.5 showed a reduction in the number of positive cells for Nestin and Tbr2, with a subsequent increase in the number of βIII-tubulin positive cells in HD mice. These preliminary results indicate that the presence of mutant HTT increases the proportion of progenitors with horizontal cleavage planes and favours their differentiation. In parallel, we are currently performing *in utero* electroporation experiments of E14.5 embryos with different constructs encoding wild-type and mutant HTT. In particular, this approach will allow us to address the *in vivo* effect of phosphorylating S421. We will express mutant HTT constructs with a single point mutation and determine spindle orientation of dividing progenitors and the cell fate of the generated daughter cells.

In conclusion, we confirmed the function of HTT during mitosis and showed that the presence of an abnormal polyQ expansion alters this function. These results open new lines of investigation for elucidating the pathogenic mechanisms in HD. Indeed, the understanding of wild-type HTT function and the study of the consequences of the polyQ mutation on this function will help to elucidate the complex molecular mechanisms leading to this devastating disorder.

8 GENERAL DISCUSSION

8.1 The importance of studying full-length HTT

Expression of HTT short polyQ N-terminal fragments, for example the 89 amino acid fragment corresponding to the exon 1, are sufficient to generate a neurological phenotype in mice and to induce the death of various cell types (Mangiarini et al., 1996). For this reason, most of the studies in HD have been performed with a truncated form of HTT.

We described and functionally validated pARIS-htt, an innovative tool to facilitate HTT cloning and analysis. We designed a cellular model to silence endogenous HTT and over-express pARIS-htt. Shortly, we have shown that mutant form of HTT, as well as deletion forms for HAP1 and dynein, failed to transport Golgi or BDNF-containing vesicles (Pardo et al., 2010).

BDNF vesicular trafficking is disrupted when HTT is mutated (Gauthier et al., 2004) by detachment of molecular motor from MTs (Gauthier et al., 2004; Zala et al., 2008). HTT interacts with the dynein intermediate chain (DIC) via a minimal interaction region mapping to amino acid positions 536-698 of HTT (J P Caviston et al., 2007) and with dynactin via HAP1 (Engelender et al., 1997; S.H. Li et al., 1998; X. J. Li et al., 1995) with a minimal interacting region corresponding to amino acids 171-230 of HTT (Bertaux et al., 1998). We have show for the first time that HTT lacking dynein or HAP1 interaction domains affects vesicular transport.

Does pARIS-htt-Δdynein favour anterograde transport and pARIS-htt-ΔHAP1 retrograde transport? Dynein is an evolutionary conserved motor protein complex that moves towards MTs minus-end (Schliwa & Woehlke, 2003; Schroer, 2004). HAP1 has been shown to interact with the C-terminal part of the kinesin light chain (KLC) (McGuire et al., 2006) and with $p150^{Glued}$ and the heavy chain of kinesin-1 through its coiled-coil domain (Engelender et al., 1997; S.H. Li et al., 1998). Futures studies will be necessary to elucidate the effect of pARIS-htt-Δdynein and pARIS-htt-ΔHAP1 in vesicles directionality.

The role of HTT in the regulation of vesicular trafficking is not limited to its association with dynein or HAP1. Indeed, the contribution of HTT to different membrane trafficking events involves other protein partners, such as HIP-1 (Wanker et al., 1997), HAP40 (Pal et al., 2006), Rab8/optineurin (Hattula & Peränen, 2000) or Rab11 (X. Li et al., 2009). Rab5 specifically associates with early endosomes and regulates its motility along MTs. HTT forms a complex with a Rab5 effector that induces a change in the cytoskeletal affinity of early endosomes (Pal et al., 2006). Actin-based transport is most often used for short-range transport, and MTs are used for long-distance transport. HTT promotes a change in endosome association from MTs to actin through an interaction with HAP40. When there is an increase in cytoplasmic levels of HAP40, the early endosome positive for Rab5 is able to associate with actin. When HAP40 levels are decreased, Rab5-positive early endosomes bind to the MTs. Nevertheless, it remains unclear how the HTT–HAP40 complex enhances the affinity of Rab5-positive vesicles for actin filament. Optineurin is a

good candidate as it links HTT to the actin-based motor myosin VI (Sahlender et al., 2005). N-terminal of HTT directly interacts with optineurin (Sahlender et al., 2005) and HAP40 binds to the C-terminal region of HTT (Pal et al., 2006). Generation of HTT deletion mutants for the interaction domain of optineurin and HAP40 would be of valuable interest to understand HTT role as a global coordinator of cytoskeletal vesicular transport.

HTT is the substrate of various PTMs, such as phosphorylation, SUMOylation, ubiquitination, acetylation and palmitoylation (discussed in the section 1.8) as well as calpains and caspases cleavage (discussed in 1.7.1). Furthermore, HTT sequence has been conserved through evolution. N-terminal fragment is the most recently evolved part of HTT, while the C-terminal part represents the most conserved portion among all animals, from sea urchin to insects and mammals (Tartari et al., 2008). In agreement, more than one hundred interactors have been reported in yeast-two-hybrid screens using various HTT fragments as baits (Goehler et al., 2004; Kaltenbach et al., 2007). Under these premises, the need of study HTT in a full-length context is essential.

8.2 HTT and mitosis

We have proved that HTT have a major role during cell division acting at spindle orientation level (Godin et al., 2010; Molina-Calavita et al., in preparation) and that this function is altered in HD (Molina-Calavita et al., in preparation).

8.2.1 HTT dynamic localization during cell division

HTT is present in the cytoplasm where it associates with MTs and with proteins of the molecular motor machinery including dynein and HAP1 that interacts with p150^{Glued} and kinesin-1 (Caviston et al., 2007; Engelender et al., 1997; Gauthier et al., 2004; S.H. Li et al., 1998; McGuire et al., 2006). As well, HTT localizes at spindle poles in dividing (Godin, Colombo, et al., 2010) and non-dividing cells (Keryer et al., 2011). This localization is MT dependent (Keryer et al., 2011) as shown by nocodazol treatment and FRAP experiments. This dynamic shuttling might be essential in transporting protein complexes to the centrosome. For example, absence of wild-type HTT or polyQ mutation delocalized dynein and p150^{Glued} from the spindle poles (Godin et al., 2010; Molina-Calavita et al., in preparation).

+TIPs accumulate at MT plus-ends and can be classified according to their structure (Akhmanova & Steinmetz, 2010). EB protein represents the core components of +TIP networks. This small molecule can individually track growing MTs (Akhmanova & Steinmetz, 2008; Bieling et al., 2008; Dixit et al., 2009). CLIPs (CLIP115 and CLIP170) and p150^{Glued} shares a globular CAP-Gly domain. CLIPs stabilize MTs by preventing catastrophes or by stimulating rescues. In addition, CLIP170

participates in the plus-end recruitment of dynein: CLIP170 associates with MT and EB through its CAP-Gly motifs, p150^{Glued} binds to the C-terminal of CLIP170 and is recruited to the plus ends, and dynein associates with dynactin (Coquelle et al., 2002; Galjart, 2005). We found that in polyQ condition, EB3 localization and MTs growth rate, calculated by following EB3 positive comets, was unchanged compared to wild-type. However, CLIP170 and p150^{Glued} were delocalized from MT plus-ends. The affinity of the complex formed by CLIP170/p150^{Glued}/dynein is perturbed in a mutant context. These observations draw a general picture in which HTT would be critical to the recruitment of +TIPs.

We speculate that HTT could be also found at the cell cortex of dividing cells. In favour of this hypothesis we found the complex linking astral MT plus-ends and cell cortex: NuMA and dynein. HTT interacts with dynein (Caviston et al., 2007; Pardo et al., 2010) and NuMA (Kaltenbach et al., 2007). In the absence of HTT, NuMA delocalizes from the spindle poles (Godin, Colombo, et al., 2010). NuMA links the dynein/dynactin-LIS1 complex to the cortically polarized LGN protein. NuMA couples therefore dynein motor activity to cortex polarity cues (Du & Macara, 2004; Siller & Doe, 2009). Whether HTT participates to this coupling remains to be established. So far, in the experimental conditions used in our study, I did not observed HTT at the cell cortex. This could be linked to the fixation protocols for HTT maintenance at the cortex, or a rapid and highly dynamic of HTT to and from the cortex. Futures studies will be necessary to investigate whether HTT co-localized and interact with NuMA and LIS1 at the cell cortex during cell division.

8.2.2 HTT as a transport-mediator during mitosis

HTT function in vesicular transport has been the object of several studies. In particular, HTT controls trafficking of vesicles via a dynein/dynactin-dependent pathway (Caviston et al., 2007; Colin et al., 2008; Gauthier et al., 2004; Zala et al., 2008). HTT could mediate the transport of the dynein/dynactin complex along astral MTs in a HTT-HAP1 dependent manner. In a mutant context, HTT and molecular motors are detached from MT (Gauthier et al., 2004; Zala et al., 2008). Thus, the absence of HTT or its polyQ mutation would then lead to a loss of dynein/dynactin from the MT plus-ends and cell cortex.

Another potential interactor of HTT that could mediate its function during mitosis is Cdc42-interacting protein 4 (CIP4). CIP4 is a Wiskott–Aldrich syndrome protein (WASp) interactor and Cdc42 effector protein involved in cytoskeletal organization (Tian et al., 2000). CIP4 appears to be involved in the binding of WASp to MTs (Tian et al., 2000). In fact, CIP4 interacts with the N-terminal domain of HTT (Holbert et al., 2003). In this context, HTT could be involved in the regulation of actin dynamics at the cell cortex, cell polarization and proper localization of the dynein/dynactin complex. In favour of this hypothesis, it has been shown that Cdc42-PAK/βPix modulates spindle orientation (Mitsushima et al., 2009) and p21-activated kinase 1 (PAK1) localized at centrosomes during mitosis (Zhao et al., 2005). Interestingly, PAK1 interacts with HTT

in vivo and *in vitro* (Luo et al., 2008). Hence, Cdc42 might regulate actin remodeling during mitosis through PAK, βPix and HTT.

Finally in favor of a transport role for HTT during mitosis, it has been proposed that HTT controls transport to the centrosome of proteins required for ciliogenesis. In the absence of HTT, dynein/dynactin-dependent transport would be altered, leading to a reduction of PCM proteins at the centrosome. In disease, the increased concentration of pericentriolar proteins is caused by the loss of the dynamics of pericentriolar satellites that remain closely localized to the centrosome (Keryer et al., 2011). Thus, HTT would be a transport-mediator in several cellular processes.

8.3 HTT and neurogenesis

8.3.1 HTT and corticogenesis

During mammalian corticogenesis, NESC proliferate symmetrically to expand. Progenitors then undergo symmetric or asymmetric divisions. When the division is symmetric, the cells self-renew and there is an expansion of progenitors. Conversely, during asymmetric division, there is production of a progenitor cell and a neuron, which migrates to integrate into the future cortex. The direction of the division depends on proper spindle orientation and segregation of cue determinants (Konno et al., 2008; Kosodo et al., 2004; Marthiens and ffrench-Constant, 2009; Yingling et al., 2008).

We have shown that inactivation of HTT in murine cortical progenitors changes the nature of the division cleavages, thereby decreasing the pool of cycling progenitors and increasing neuronal differentiation (Godin, Colombo, et al., 2010).

Several arguments support that mutant HTT impairs cell division and neurogenesis. In fibroblast from a murine model of HD and in cell lines from HD patients a disorganization of the centrosome and a subsequent disruption of the cell cycle leading to aneuploidy, micronuclei and dysmorphic cells was reported (Sathasivam et al., 2001). Impaired adult neurogenesis was revealed in the DG of HD mouse models (Phillips et al., 2005; Simpson et al., 2010). In contrast, embryonic neurogenesis in HD condition has been poorly addressed. However, premanifest HD mutation carriers have smaller intracranial adult brain volume compared with controls that could result from an abnormal development (Nopoulos et al., 2010).

As described before in the results section, preliminary observations in HD mouse models suggest and affected cleavage plane of neural progenitors and a change in the cell fate. Thus, it is tempting to speculate that mutant HTT could induce early developmental deficit.

8.3.2 The role of HTT in cell fate

The link between orientation of cell division and differential fate acquisition has been studied in ACD of *D. melanogaster* embryonic NBs (Bellaiche & Gotta, 2005; Siller & Doe, 2009; Yu et al., 2006). These studies uncovered a role for inhibitory heterotrimeric G proteins (Gαi) and their regulators in controlling mitotic spindle positioning. In particular, Pins interacts with cortical GDP-Gαi (Schaefer et al., 2001). Hence, Pins seems to have a pivotal role in ACD, acting not only as a signal but also as a physical bridge between spindle poles and the cell cortex.

Pins vertebrate homolog, LGN is localized at the cell cortex and at spindle poles (Du & Macara, 2004). *In vivo* studies in chick embryonic trunks showed that LGN is expressed in NECs, and localizes to the cell membrane and spindle poles in metaphase and anaphase (Morin et al., 2007). Removing LGN, NuMA, or Gαi, as well as interfering with the LGN/Gαi interaction, suppress spindle rotation during metaphase and result in defects in final spindle orientation at anaphase *in vivo* (Konno et al., 2008; Morin et al., 2007; Peyre et al., 2011). Indeed, NuMA interacts with HTT by yeast two-hybrid screening and mislocalizes from spindle pole in absence of HTT (Kaltenbach et al., 2007). We can picture that HTT is important to regulate proper localisation of NuMA and dynein/dynactin, and as a consequence, the localisation of LGN. These observations further support the notion of HTT as a regulator of spindle orientation and the balance between asymmetric and symmetric divisions in the developing cortex.

8.3.3 HTT and neuronal migration

Neuronal migration is a fundamental process for the development of laminary structures in the mammalian brain, including the cortex, hippocampus, midbrain, and hindbrain (Feng & Walsh, 2001; J.W. Tsai et al.,2007; L.H. Tsai & Gleeson, 2005; Wynshaw-Boris, 2007).

After the transition of young neurons from multipolar to bipolar shape in the SVZ, they migrate along the radial glial fibers across a long distance toward the pial surface. The leading edge of the neuron extends along the radial glial fiber, and a swelling of the plasma membrane forms in the leading process. The MT network is then pulled forward, and the centrosome moves steadily into the swelling. Next, the nucleus is pulled by MTs toward the centrosome. Finally, the trailing cytoplasmic region follows the nucleus and finishes soma translocation (J.W. Tsai et al., 2007; L.H. Tsai & Gleeson, 2005). LIS1, Ndel1, DCX, and the dynein complex have been shown to have critical roles in coupling microtubules and the nucleus (Feng et al., 2000; J.W. Tsai et al., 2007).

Deletion of Nde1, a LIS1-interacting protein, induced neuronal migration defect and thinning of the superficial cortical layers in mice (Feng & Walsh, 2004). Single *Lis1* and *Dcx* mutants and double *Lis1 Dcx* mutants showed neuronal migration defects during corticogenesis (Pramparo et al., 2010).

Given HTT interactors (as discussde before), HTT could be involved at several steps during the migration process. As shown recently, *Htt* deletion disrupts migration of neurons in the developing cortex (Tong et al., 2011). In particular, *Htt* shRNA abolishes normal cell migration from the ventricular zone to the cortical plate and this effect is time-dependent. Interestingly, knockdown of *Htt* in the cerebellum did not affect cell migration.

The mechanism underlying this phenotype has not been fully described yet. However, is tempting to speculate that the dynein/dynactin complex and other +TIPs are involved.

We have shown that HTT is necessary to properly localize dynein, p150^{Glued} and CLIP170, and when HTT is mutated, these proteins are mislocalized (Godin et al., 2010; Molina-Calavita et al., in preparation). Futures studies to address the effect of HTT mediated delocalization of +TIPs and neuronal migration are necessary. For instance, delocalization of CLIP170 from the growth cones in TTL-null mice induce a disruption of the cortico-thalamic loop and reduced cell numbers in the cortical plate zone (Erck et al., 2005).

8.3.4 Is HD a cortical developmental disorder?

Disorders of cerebral cortical development are generally categorized by the developmental stage that is disrupted (Barkovich et al., 1996). For example, impaired neurogenesis affects brain size and results in “microcephaly” (small brain), and defective neuronal migration results in cortical lamination defects.

Lissencephaly (smooth brain) is considered to be neuronal migration disorder (Dobyns & Truwit, 1995). Mutations in two genes, *LIS1* (Lo Nigro et al., 1997; O. Reiner et al., 1993) and *DCX* (Gleeson et al., 1998; des Portes et al., 1998), are responsible for most cases of classical lissencephaly (Kato & Dobyns, 2003).

Heterozygous loss or mutation of *LIS1* is sufficient to cause neuronal migration defect, characterized by a smooth cortical surface, abnormal cortical layering, and enlarged ventricles (Gupta et al., 2002). Mitotic spindle orientation in both NESCs and RGCs has been show to be regulated by *Lis1* (Yingling et al., 2008). The underlying mechanism is an impaired cortical MT capture via loss of cortical dynein. Nde1 is essential for mitotic spindle assembly and function and is required for determining the mode and speed of cortical neural progenitor cell mitosis (Feng & Walsh, 2004). Moreover, *Nde1* homozygous mutation results in a reduction in the size of the cerebral cortex.

Loss of *Dcx* does not affect spindle positioning during NESCs expansion but does have effects on RGCs, randomizing spindle orientation. Although the final cortical organization is preserved in *Dcx* mutants, neuronal migration is slower with a multidirectional pattern of migration (Pramparo et al., 2010). DCX binds ubiquitously to MTs in non-neuronal cells and its activity is essential for their

bundling and stabilization (Gleeson et al., 1999). This function could be impaired in *Dcx* mutants resulting in abnormal branching and change of direction during migration (Pramparo et al., 2010).

Lis1 and *Dcx* double mutants displayed a more severe randomization of the spindle during radial glial mitotic divisions with abventricular divisions leading to increased cell-cycle exit and depletion of the progenitor pool at the ventricular surface (Pramparo et al., 2010). Neuronal migration and proliferation defects lead to a severe disorganization of the cortex.

For HD, it has been published that premanifest HD mutation carriers have smaller intracranial adult brain volume compared with controls (Nopoulos et al., 2010). Furthermore, abnormal brain structure has been documented in prodromal HD subjects decades prior to the onset of disease (Paulsen et al., 2010). A difference in intracranial volume is unlikely to be caused by degenerative process as intracranial volume, once determined by maximal brain growth in childhood, does not change over time. Instead, an alternative explanation for this finding is that, in the subjects with prodromal HD, the brain did not grow to its full capacity, raising the possibility of a global abnormality in the process of brain development.

In a recent study, basic anthropometric measures of height, weight, body mass index (BMI), and head circumference in children at risk for HD were evaluated (J. K. Lee et al., 2012). The head of preHD children is disproportionately small and therefore, showing an abnormality of brain growth. Furthermore, the significant association between longer CAG repeat length and smaller head circumference highlights the direct genetic impact of expanded CAG repeat on this measure (J. K. Lee et al., 2012).

We have shown *in vivo* that removal of *Htt* from progenitors cells at E14.5 leads to a change in the cleavage plane with an increase in the proportion of progenitors with intermediate and horizontal cleavage planes (Godin, Colombo, et al., 2010). This shift in the cleavage plane of progenitors lowers the pools of both apical and basal progenitors and promotes neuronal differentiation of daughter cells. Knockdown of *Htt* in neurons of the neuroepithelium at E12.5 impairs normal cell migration in cerebral cortex and leads to caspase-mediated cell apoptosis (Tong et al., 2011). This may explain previous observations showing that lowering the levels of *Htt* in mouse results, in addition to severe anatomical brain abnormalities, in ectopic masses of differentiated neurons near the striatum (White et al., 1997).

Using HD knock-in mouse models, we observed at E14.5 an increased number of RGCs dividing with a horizontal cleavage compared to wild-type condition. Same results were obtained at E9.5 in NESCs. Cell fate analysis showed a reduction in the number of positive cells for progenitors markers such as Nestin and Tbr2, with a subsequent increase in the number of post-mitotic neurons (βIII-tub+) (Molina-Calavita et al., in preparation). These preliminary results would suggest an alteration in corticogenesis in mutant HTT condition. More work is needed to be done to explain the consequences of this phenotype and how it contributes to HD pathogenesis.

9 Annexe I: Rodent HD models

	General features			Neuropathology and Symptoms			
	Animal, Construct	**Promoter, CAG**	**Onset of symptoms, survival**	**Nuclear inclusions, cell pathology**	**Brain atrophy and cell loss**	**Neuronal dysfunction**	**Motor and cognitive problems**
R6/1 (Mangiarini et al., 1996)	Transgenic mouse 1.9-kb fragment from the 5' of human *HTT* gene	Human *HTT* 113	15–21 wk 32–40 wk	Nuclear inclusions and neuropil aggregates throughout the brain	Overall brain atrophy, reduced brain volume No evidence of massive cell death	Aberrant synaptic plasticity, Reduced expression of mGLURs, D1-D2 and CB1 receptors	Clasping behaviour (onset 20 wk) Rotarod deficit Decrease anxiety
R6/2 (Mangiarini et al., 1996)	Transgenic mouse 1.9-kb fragment from the 5' of human HTT	Human *HTT* 114	5–6 wk 12–15 wk	Nuclear inclusions and neuropil aggregates throughout the brain	Overall brain atrophy, reduced brain and striatal volume at 12 wk No evidence of massive cell death	Aberrant synaptic plasticity, reactive astrogliosis. Decrease in D1-D2, mGLURII, AMPA, kainate and A2A receptors	Clasping behaviour (onset 8 wk) Rotarod deficit (5 wk) Rigidity in cognitive process, increased exploratory behaviour at 4 wk that declines and ends by 8.5 wk
N171-82Q (Schilling et al., 1999)	Transgenic mouse First 171 amino acids of human *HTT* gene	Mouse prion protein promoter 82	10 wk 10-24 wk	nuclear inclusions in cortex, hippocampus, amigdala and striatum	Overall brain atrophy, cells with degenerative morphology at 20 wk	Reactive astrogliosis	Clasping behaviour (onset 15 wk) Rotarod deficit (15 wk) Deficit in working memory, ridigity in cognitive process
YAC128 (Slow et al., 2005)	Transgenic mouse Yeast artificial chromosome expressing full-length human *HTT* gene	Human *HTT* 128	8-12 wk Normal life span	EM48 positive inclusions in striatal cells, no nuclear inclusions detected	Reduced striatal and cortical volume at 48 wk, reduced striatal and cortical neuron number at 48 wk	Increase in NMDA, AMPA, mGLURI and II receptor binding. No change in striatal dopamine, GABAA/B or adenosine receptor binding	Clasping behaviour, Rotarod deficit (24 wk) Depressive behaviour (12 wk)
BACHD (Gray et al., 2008)	Transgenic mouse BAC expressing full-length human *HTT* gene	Human *HTT* 97	12 wk Normal life span	mHtt inclusions in neuropil and few in cortex and striatum (48 and 72 wk)	Brain atrophy Degenerating darkly stained neurons in striatum	Reduced excitatory neurotransmission mediated by AMPA receptors	Clasping behavior not reported, Rotarod deficit (by 8 wk and progressed by 24 wk)

Transgenic HD rat (Von Horsten et al., 2003)	Transgenic rat 1962-bp rat *Htt* fragment	Endogenous rat *Htt* promoter 51	40–50 wk 98 wk	Neuropil aggregates and nuclear inclusion in striatum and less extent in cortex (72 wk)	Enlarged lateral ventricles Focal lesions in the striatum	Reduced brain glucose metabolism	Progressive impairment of coordination and balance Reduced anxiety-like behaviour, emotional and cognitive decline
HdhQ92-111 (Wheeler et al., 1999)	Knock-in mouse Replacing exon 1 of mouse *Htt* with a mutant human exon 1	Mouse *Htt* promoter 92-111	96 wk Normal life span	Nuclear inclusions and striatal neuropil aggregates (68 wk)	No brain atrophy observed No cell loss observed	Striatal gliosis	No clasping behaviour No rotarod deficit No cognitive symptoms
HdhQ140 (Menalled et al., 2003)	Knock-in mouse polyQ sequence inserted into the endogenous mouse *Htt* gene	Mouse *Htt* promoter 140	12 mo Normal life span	Nuclear and neuropil inclusion bodies in striatum, cortex, hippocampus, and cerebellum (16–24 wk)	No brain atrophy observed No cell loss observed		Decrease in locomotor activity No cognitive symptoms
Hdh(CAG)150 (Lin et al., 2001)	Knock-in mouse polyQ sequence inserted into the endogenous mouse *Htt* gene	Mouse *Htt* promoter 150	4 mo Normal life span	Striatal Nuclear inclusions in striatum (37 wk)	Cellular dysfunction revealed by dark bodies surrounding cytoplasmic vacuoles	Striatal gliosis Axons degeneration	Clasping behaviour Rotarod deficit (100 wk) No cognitive symptoms

10 Annexe II: Other HD models

	General features			Neuropathology and Symptoms		
	Animal, Construct	**Promoter, CAG**	**Nuclear inclusions**	**Cell loss**	**Neuronal dysfunction**	**Motor problems**
Htn-Q150 (Faber et al., 1999)	Transgenic worm, first 171 amino acids of human HTT	*osm-10* 150	Cytoplasmic inclusions	Cell death	Progressive neuronal degeneration, Dye-Filling defect neurons	Impaired ability to respond in the nose touch assay
Htt57Q128::GFP (Parker et al., 2001)	Transgenic worm, first 57 amino acids of human HTT fused to GFP	*mec-3* 128	Cytoplasmic inclusions	No evidence of cell death	Swelling of axonal processes	Mechanosensory defect at the tail (Mec phenotype)

	General features				Neuropathology and Symptoms		
	Animal, Construct	**Promoter, CAG**	**Onset of symptoms, survival**	**Nuclear inclusions**	**Cell loss**	**Neuronal dysfunction**	**Motor problems**
Q120 (Jackson et al., 1998)	Transgenic fly, first 170 amino acids of human HTT	pGMR (eye-specific promoter) 120	Onset of degeneration is determined by the length of the polyglutamine tract	Multiple small aggregates	Cell death shares morphological features with apoptosis	Degeneration of photoreceptor neurons	
httex1-93Q (Steffan et al., 2001)	Transgenic fly, exon 1 of human *HTT* gene	GAL4-UAS system 93	70% lethality and early adult death	Nuclear, cytoplasmic and neuritic aggregates	Neuronal Cell Death	Progressive neuronal degeneration, progressive loss of rhabdomeres (eye)	
Htt-Q128 (Lee at al., 2004)	Transgenic fly, first 548 amino acids of the human *HTT* gene	GAL4-UAS system 128	Decreased lifespan	Cytoplasmic and neuritic aggregates		Photoreceptor degeneration, defects in membrane excitability and brain activity	Loss of motor coordination

	General features			Neuropathology and Symptoms		
	Animal, Construct	**Promoter, CAG**	**Onset of symptoms, survival**	**Nuclear inclusions**	**Cell loss**	**Neuronal dysfunction**
Q102-GFP (Schiffer et al., 2007)	Zebrafish transiently expressing exon 1 of human HTT fused to GFP	102	Reduced viability of embryos	Inclusion body-like aggregates throughout the body of embryos	Apoptosis	"cyclopic" phenotype
EGFP-HDQ71 (Williams et al., 2008)	Transgenic zebrafish, exon 1 of human HTT fused to GFP	Rhodopsin 71		Aggregates		Rod photoreceptor degeneration

11 Annexe III: Huntington's disease signalling

Huntington's Disease Signaling

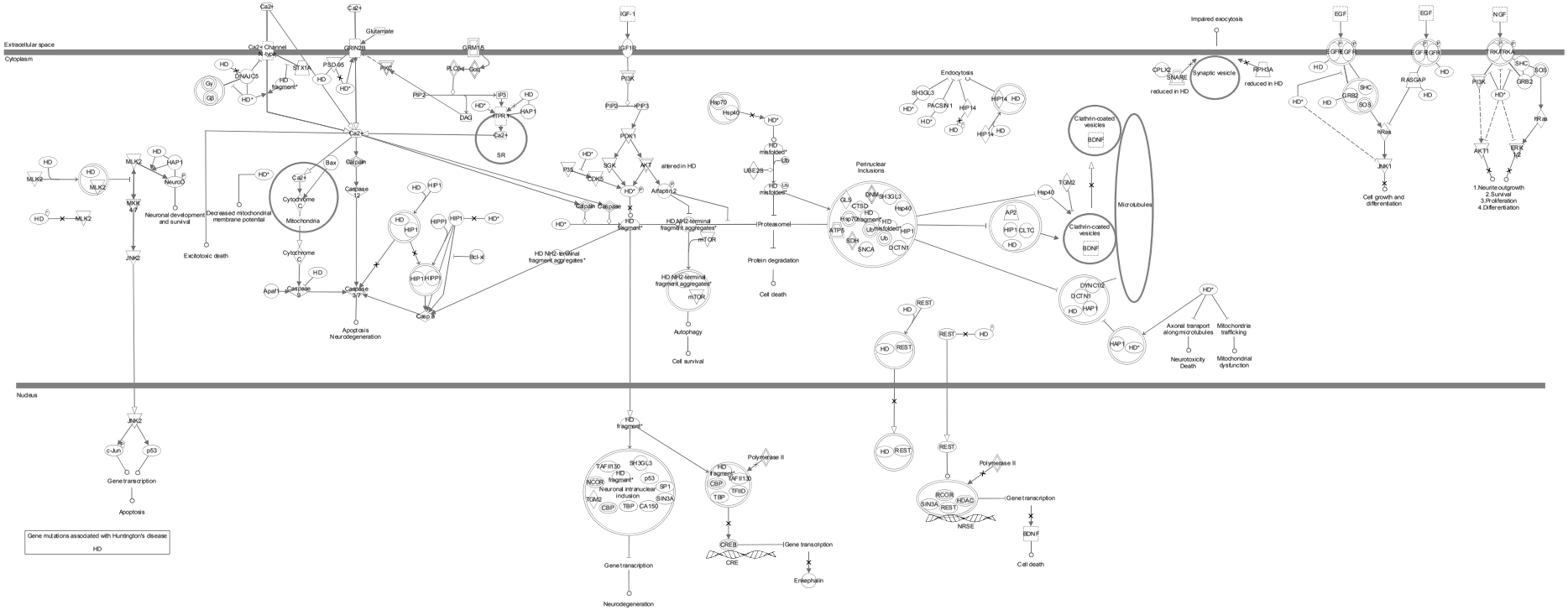

12 Annexe IV: HD therapeutic strategies and biomarkers

THERAPEUTIC STRATEGIES				
Target	**Deficiency**	**Strategy or drug used**	**Effect**	**Clinical trial**
Excitotoxicity	Increased glutamate release and increased NMDAR activity, impaired calcium signalling and cell death	Riluzole	Inhibitor of glutamate neurotransmission	Phase II
		Memantine	Block NMDAR	Phase II
		Tetrabenazine	Dopamine pathway inhibitor	Available
BDNF	Reduced levels of BDNF	Recombinant BDNF	Methionyl human BDNF infused subcutaneously or intrathecally	Basic Research
		BDNF gene therapy	BDNF delivered locally to neurons	Basic Research
		BDNF-releasing cell grafts	Intrastriatal graft of cells engineered to stably express BDNF	Basic Research
		BDNF mimetics	Small molecules directed specifically to the BDNF receptors	Basic Research
		Diet and environment	Dietary restriction regimens, intermittent fasting, and environmental enrichment	Preclinical
		Enrichment BDNF inducers	Compounds that will increase endogenous BDNF levels	Basic Research
Caspase activities and HTT proteolysis	Production of toxic fragments through the cleavage of HTT by caspases	Minocycline	Inhibit caspase 1 and 3	Phase II
		R1–R4 compounds	Caspase 6 inhibitors	Basic Research
Aggregation	Large inclusions of mutant HTT	Trehalose	prevent nuclear inclusion formation	Preclinical
		C2-8	antiaggregation compound upregulate autophagy and	Preclinical

		Drugs stimulating HTT clearance	enhance the clearance of mutant HTT	Basic Research
Mitochondrial dysfunction	impaired mitochondrial energy production and cellular respiration	Creatine	stimulates mitochondrial respiration	Phase II
		Coenzyme Q10	stimulate mitochondrial activity	Phase II
		Eicosapentaenoic acid (EPA)	promoting mitochondrial fitness	Phase II
		Cysteamine	inhibit oxidative damage	Preclinical
Gene transcription	downregulation of gene expression	Sodium phenylbutyrate	HDAC inhibitor	Phase I
		HDACi 4b	HDAC inhibitor	Preclinical
Mutant HTT		RNA interference	Block the production of mutant HTT mRNA by the use of RNA interference	Preclinical
		Artificial peptides and intrabodies	Block mutant HTT at the posttranslational level using small synthetic peptides or antibodies	Preclinical
Cell loss		Intrastriatal transplantation of fetal cells	Cell replacement	Phase I
		Cell replacement using embryonic/neural stem cells	Cell replacement	Basic Research

BIOMARKERS		
Imaging Studies	**Metabolomic, Proteomic and Transcriptomic Approaches**	**Biomarkers Built on Hypothesis-Driven Experiments**
Structural magnetic resonance imaging (MRI) *Decline in striatal volume, white matter abnormalities, atrophy in frontal, temporal, parietal, and cortical areas in HD patients*	Branched chain amino acid (BCAA) *Reduced levels in HD samples*	A2A receptor; endocannabinoid system (ECS) *Changes in A2A receptor expression, binding activity, signalling and abnormalities in the ECS observed in HD patients*
Functional magnetic resonance imaging (fMRI) and positron emission tomography (PET) *Changes in brain metabolism and striatal function in HD patients*	Interleukin-6 (IL-6), interleukin-8 (IL-8), tumor necrosis factor-alpha (TNF-α) *Increased interleukin levels in HD gene carriers*	24-hydroxycholesterol (24OHC) *Lower levels of 24OHC in HD patients*
Diffusion tensor imaging (DTI) *White matter degeneration observed in HD patients*	Subset of transcripts *Changes in gene expression in blood samples from HD patients*	BDNF *BDNF is reduced in HD brains*
		8-OH-2'-dG (indicator of oxidative injury to DNA) *Elevated levels in HD patients*

13 Annexe V: Huntingtin is required for mitotic spindle orientation and mammalian neurogenesis (supplemental information)

Supplemental Information Neuron, Volume 67

Huntingtin is Required for Mitotic Spindle Orientation and Mammalian Neurogenesis

Juliette D. Godin, Kelly Colombo, Maria Molina-Calavita, Guy Keryer, Diana Zala, Bénédicte C. Charrin, Paula Dietrich, Marie-Laure Volvert, François Guillemot, Ioannis Dragatsis, Yohanns Bellaiche, Frédéric Saudou, Laurent Nguyen and Sandrine Humbert

SUPPLEMENTAL FIGURES LEGENDS

Supplemental Figure S1, related to Figure 1. Huntingtin Distribution during Mitosis using Different Huntingtin Antibodies Targeted against Distinct Regions. Immunostaining of mouse neuronal cells with anti-γ-tubulin (green), anti-htt 812 (red) (A), anti-htt 4E6 (red) (B) antibodies and DAPI (blue) counterstaining. Huntingtin localizes at the spindle poles during mitosis. Scale bar 5 μm.

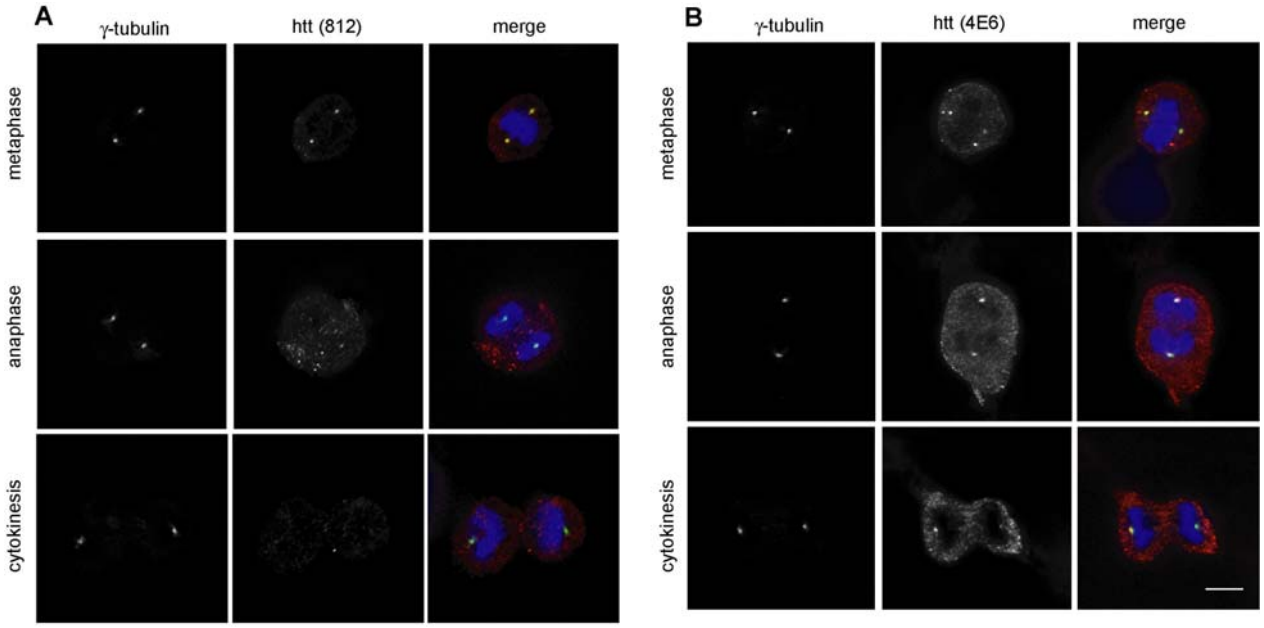

Figure S1 Godin et al.

Supplemental Figure S2, related to Figure 2. Huntingtin Regulates Spindle Orientation during Mitosis in Mouse Neuronal and HeLa Cells.

(A) Quantification of spindle orientation defect in mouse neuronal cells treated with scramble, si-htt1 and si-p150^{Glued} RNAs. Results are expressed as the percentage of cells with misoriented spindle (more than 9 stacks of 0.2μm between the two poles, $\Delta Z > 1.8\mu m$).

(B) Spindle angles in metaphase cells are plotted as a function of cell area at midsection showing no correlation between spindle angle and size of the mouse neuronal cells treated as in (A).

(C) Immunostaining of HeLa cells with anti-γ-tubulin (green) and anti-htt SE3619 (red) antibodies and DAPI (blue) counterstaining reveals that huntingtin localizes at the spindle poles.

(D) Lysates from si-ctrl and si-Huhtt RNAs treated HeLa cells are analyzed by immunoblotting using anti-htt 4C8 and anti-α-tubulin antibodies. Huntingtin levels are severely diminished in si-Huhtt treated cells.

(E) Z-X projections of immunostaining of si-ctrl or si-Huhtt RNAs treated HeLa cells with γ-tubulin (green) and DAPI counterstaining (blue). Z-X projections reveal a striking misorientation of the mitotic spindle in metaphase cells depleted for huntingtin.

(F) Quantification of HeLa cells with a misoriented spindle orientation, defined as in (A). (*$P<0.05$, ***$P<0.001$; see below for detailed statistical analyses and number of measures). Scale bar 5 μm.

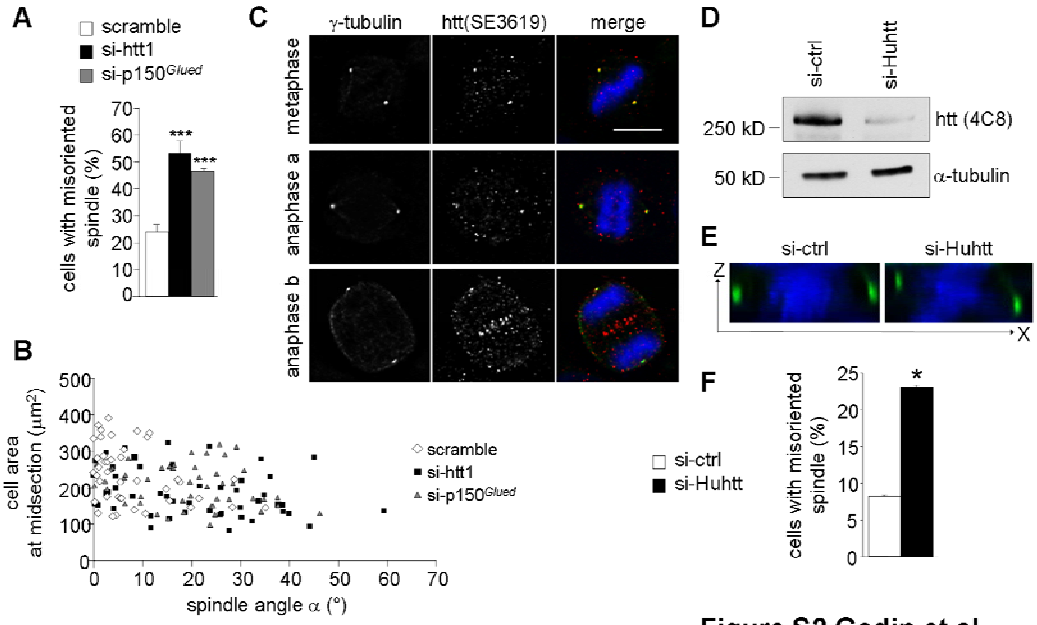

Figure S2 Godin et al.

Supplemental Figure S3, related to Figures 6 and 7. Huntingtin Regulates Spindle Orientation of Dividing Mouse Cortical Progenitors *in vivo*.

(A) Schemes representing dividing progenitors cells within three groups according to the orientation of the cleavage plane to the ventricular zone (VZ): vertical (0-30°, left), horizontal (60-90°, middle) and intermediate (30-60°, right).

(B and C) Analysis of the percentage of vertical, horizontal and intermediate cleavage planes reveal an increase in the fraction of neuronal progenitors that show horizontal cleavage in absence of huntingtin. This is restored to the control situation when re-expressing huntingtin (htt-1301). Analyses are performed either in neuronal progenitors from (B) E14.5 embryos electroporated with scramble RNA, si-htt1 RNA, si-htt2 RNA + empty vector or si-htt2 RNA+ htt-1301 (pCAGGS- htt-1301-IRES-NLS-GFP) or (C) from wild-type and *Nestin-Cre/+;Hdh flox/-* E14.5 embryos.

(D) Cleaved-caspase3 immunostaining of coronal sections of E14.5 embryos electroporated with scramble or si-htt1 RNAs reveal that huntingtin depletion in neuronal progenitors does not induce cell death. Scale bar 20μm.

(E) Distribution of GFP positive cells in subventricular (SVZ) and intermediate (IZ) zones of E14.5 embryos co-electroporated with pCAGGS-NLS-GFP and scramble or si-htt1 RNAs. GFP positive cells are scored in SVZ and IZ, each divided in three equal bins. Huntingtin-depleted cells are distributed as the control cells.

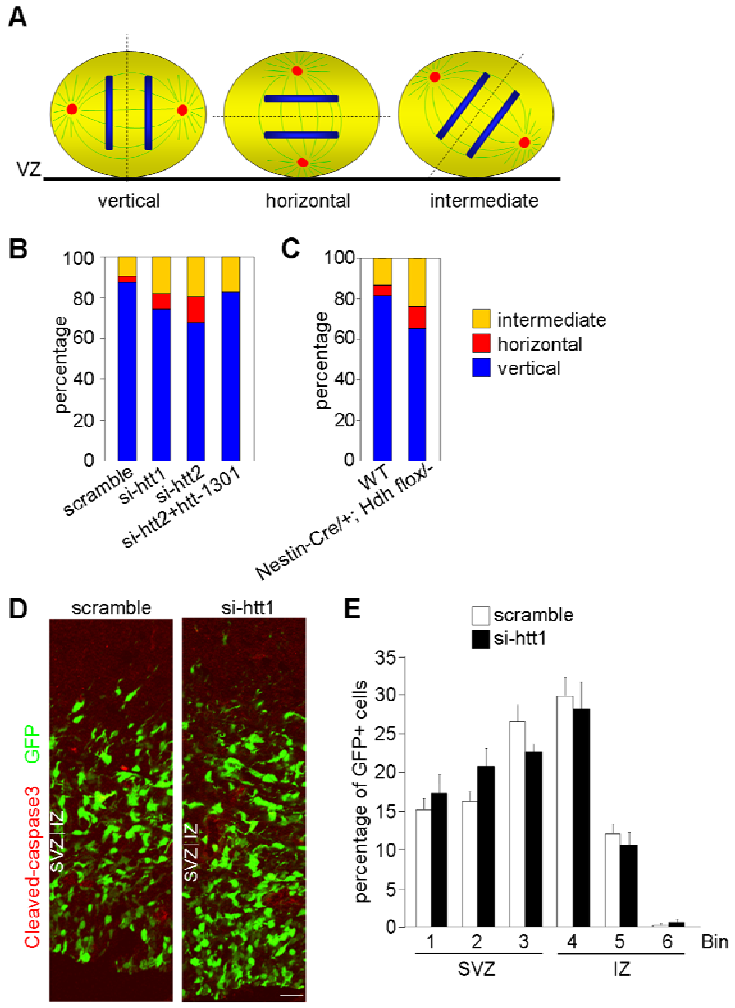

Figure S3 Godin et al.

Supplemental Figure S4, related to Figure 7. Cortical (co) and Striatal (st) cells are Extensively Recombined in *Nestin-Cre/+;R26R/+* embryos. X-gal staining with an eosin counterstaining of E14.5 section of a representative *Nestin-Cre/+;R26R/+* embryo.

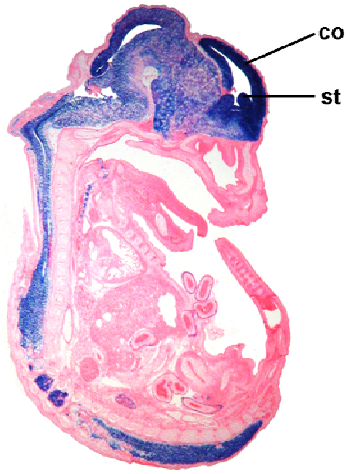

Figure S4 Godin et al.

SUPPLEMENTAL MOVIE LEGEND

Supplemental Movie S1, **related to Figure 4.** Video-recording of HeLa cells stably expressing GFP-tubulin (green) and H2B-mCherry (red) treated with si-ctrl (left panel) or si-Huhtt RNAs (right panel). Time acquisition: 1 image/min. Playing 4 frames per second. Pole-pole axis is represented by a white line (middle panel). Position of the pole-pole axis at each time point shows an increased variability in huntingtin-depleted cells. t=0min corresponds to the beginning of anaphase.

STATISTICAL ANALYSES

Figure 1D
Data are from three independent experiments: scramble: 29 cells, si-htt1: 31 cells
ANOVA F[1,58] = 22.811; T test ***p<0.0001

Figure 2E
Data are from four independent experiments: scramble: 42 cells, si-htt1: 48 cells, si-p150: 48 cells
ANOVA F[2,135] =14.551; p***<0.0001
Fisher's PLSD:

	p-value
scramble, si-htt1	<0.0001
scramble, si-p150	<0.0001
si-htt1, si-p150	0.5626

Figure 2F
Data are from three independent experiments: scramble: 55 cells, si-htt2: 184 cells, scramble + htt-1301: 73 cells, si-htt2 + htt-1301: 64 cells
ANOVA F[3,372] =58.252; p***<0.0001
Fisher's PLSD:

	p-value
scramble, si-htt2	<0.0001
scramble, scramble+htt	0.9883
scramble, si-htt2+htt	0.1802
si-htt2, scramble+htt	<0.0001
si-htt2, si-htt2+htt	<0.0001
scramble+htt, si-htt2+htt	0.1461

Figure 3B
Data are from four independent experiments: scramble: 42 cells, si-htt1: 48 cells, si-p150: 48 cells
ANOVA F[2,135] = 7.686; ***p = 0.0007
Fisher's PLSD:

	p-value
scramble, si-htt1	0.0013
scramble, si-p150	0.0005
si-htt1, si-p150	0.7839

Figure 3C
Data are from four independent experiments: scramble: 42 cells, si-htt1: 48 cells, si-p150: 48 cells
ANOVA F[2,135] = 0.338; p = 0.7137
Fisher's PLSD:

	p-value
scramble, si-htt1	0.5522
scramble, si-p150	0.4268
si-htt1, si-p150	0.8355

Figure 4E
Data are from 3 independent experiments: scramble: 20 cells, si-htt1: 44 cells,
ANOVA F[1,6] = 6.312; T test *p = 0.0325

Figure 4F
Data are from two independent experiments: scramble: 15 cells, si-p150: 9 cells
ANOVA F[1,29] = 8.291; T test *p = 0.0427

Figure 4G
Data are from three independent experiments: scramble: 37 cells, si-htt1: 55 cells
ANOVA F[1,90] = 5.953; T test *p = 0.0167

Figure 4H
Data are from three independent experiments: scramble: 116 cells, si-htt1: 81 cells
ANOVA F[1,195] = 8.816; T test **p = 0.0034

Figure 4K
Data are from three independent experiments: scramble: 6 cells, si-Huhtt: 23 cells
ANOVA F[1,27] = 4.982; T test *p = 0.0341

Figure 5B
Data are from four independent experiments: scramble: 731 cells, si-htt1: 673 cells
ANOVA F[1,31] = 12.267; T test **p = 0.0014

Figure 5C
Data are from three independent experiments: scramble: 338 cells, si-htt1: 271 cells

ANOVA F[1,24] = 22.05; T test ***p<0.0001

Figure 5D
Data are from four independent experiments: scramble: 340 cells, si-htt1: 398 cells
ANOVA F [1,6] = 0.229; T test p = 0.6492

Figure 5E
Data are from three independent experiments: scramble: 1284 cells, si-htt1: 1143 cells, si-p150: 1135 cells
ANOVA F[14,30] = 17.693; ***p<0.0001
Fisher's PLSD:

	p-value
prophase	
scramble, si-htt1	0.5327
scramble, si-p150	0.5618
si-htt1, si-p150	0.9647
prometaphase	
scramble, si-htt1	0.1468
scramble, si-p150	0.0008
si-htt1, si-p150	0.0343
metaphase	
scramble, si-htt1	0.2632
scramble, si-p150	0.0955
si-htt1, si-p150	0.5656
anaphase	
scramble, si-htt1	0.9772
scramble, si-p150	0.9875
si-htt1, si-p150	0.9898
telophase	
scramble, si-htt1	0.8019
scramble, si-p150	0.1659
si-htt1, si-p150	0.1057

Figure 6C
Data are from: scramble: 6 embryos (64 cells), si-htt1: 2 embryos (40 cells), si-htt2: 5 embryos (56 cells), si-htt2 + htt-1301: 4 embryos (41 cells)
ANOVA F[3,197] = 4.006; **p = 0.0085
Fisher's PLSD:

	p-value
scramble, si-htt1	0.0253
scramble, si-htt2	0.0044
scramble, si-htt2+htt-1301	0.8946
si-htt2, si-htt2+htt-1301	0.0157

Figure 6E
Data are from: scramble: 3 embryos (378 cells), si-htt1: 3 embryos (503 cells)
ANOVA F[1,14] = 22.429; T test ***p = 0.0003

Figure 6F
Data are from: scramble: 3 embryos (477 cells), si-htt1: 6 embryos (508 cells)
ANOVA F[1,20] = 16.762; T test ***p = 0.0006

Figure 6G
Data are from: scramble: 3 embryos (200 cells), si-htt1: 6 embryos (543 cells)
ANOVA F[1,20] = 8.556; T test **p = 0.0083

Figure 6I
Data are from: scramble: 3 embryos (262 cells), si-htt1: 5 embryos (798 cells)
ANOVA F[1,16] = 10.665; T test **p = 0.0049

Figure 7C
Data are from: WT: 2 embryos (341 cells), Nestin-Cre/+;Hdh flox/-: 2 embryos (471 cells)
ANOVA F[1,810] = 28.759; T test ***p< 0.0001

Figure 7G
Data are from: WT: 2 embryos (3457 cells), Nestin-Cre/+;Hdh flox/-: 2 embryos (4884 cells)
ANOVA F[1,1] = 10.066; T test **p = 0.0056

Figure 7H
Data are from: WT: 2 embryos (4216 cells), Nestin-Cre/+;Hdh flox/-: 2 embryos (6275 cells)
ANOVA F[1,18] = 9.914; T test **p = 0.0056

Figure 7I
Data are from: WT: 2 embryos (2085 cells), Nestin-Cre/+;Hdh flox/-: 2 embryos (3239 cells)
ANOVA F[1,13] = 5.335; T test *p = 0.04

Figure 7J
Data are from: WT: 2 embryos (617 cells), Nestin-Cre/+;Hdh flox/-: 2 embryos (1497 cells)
ANOVA F[1,15] = -2.935; T test *p = 0.0102

Figure 8C
Data are from two independent experiments: *insc*-Gal4: 54 NBs, RNAi(1): 40 NBs, RNAi(2): 44 NBs, *mud*^{2}:17 NBs
ANOVA F[3,151] = 7.720; ***p<0.0001
Fisher's PLSD :

	p-value
insc-Gal4, RNAi(1)	0.0139
insc-Gal4, RNAi(2)	0.0568
insc-Gal4, *mud*^{2}	<0.0001
mud^{2}, RNAi (1)	0.0073

mud^2, RNAi(2)	0.0016
RNAi(1), RNAi(2)	0.5550

Figure 8E
Data are from three independent experiments: w^{1118} : 56 NBs, *dhtt-ko*: 40 NBs
ANOVA F[1,94] = 5.536; T test *p=0.0207

Figure 8G
Data are from three independent experiments: w^{1118}: 18 NBs, *dhtt-ko*: 29 NBs, mud^2:18 NBs
ANOVA F[2,62] = 7.192; **p=0.0016
Fisher's PLSD :

	p-value
w^{1118}, *dhtt-ko*	0.4375
w^{1118}, mud^2	0.0101
dhtt-ko, mud^2	0.0008

Figure 8I
Data are from three independent experiments: w^{1118}: 18 NBs, *dhtt-ko*: 27 NBs, mud^2:19 NBs
ANOVA F[2,61] = 39.059; ***p<0.0001
Fisher's PLSD :

	p-value
w^{1118}, *dhtt-ko*	0.5459
w^{1118}, mud^2	<0.0001
dhtt-ko, mud^2	<0.0001

Figure 8K
Data are from three independent experiments: scramble: 86 cells, si-htt1: 90 cells, scramble +dHtt620: 90 cells, si-htt1 + dHtt620: 88 cells
ANOVA F[3,8] = 12.737; **p=0.0021
Fisher's PLSD :

	p-value
scramble, si-htt1	0.0005
scramble, scramble+dHtt620	0.3464
scramble, si-htt1+dHtt620	0.4020
si-htt1, scramble+dHtt620	0.0018
si-htt1, si-htt1+dHtt620	0.0015
scramble+dHtt620, si-htt1+dHtt260	0.9109

Supplemental Figure 2A
Data are from four independent experiments: scramble: 93 cells, si-htt1: 89 cells, si-p150:101 cells
ANOVA F[2,11] = 28.195; ***p<0.0001
Fisher's PLSD:

	p-value
scramble, si-htt1	<0.0001
scramble, si-p150	0.0001

si-htt1, si-p150 0.1404

Supplemental Figure S2F
Data are from three independant experiments: si-ctrl: 240 cells, si-Huhtt: 259 cells
ANOVA F[1,4] =19.828 ; T test *p=0.0112

SUPPLEMENTAL EXPERIMENTAL PROCEDURES

Constructs and siRNAs. The *Drosophila* Dm-620-huntingtin fragment (Dm-620-htt) was provided by *Drosophila* Genomics Resource Center (DGRC, Indiana, USA). This fragment was amplified by PCR using the following primers: Dm-620-htt-s (5' cgcggatccgacaaatccaggtccagtgc 3') and Dm-620-htt-as (5' cgcggatccggctgctgctgctctttgctg 3'). PCR product was digested by BamHI, ligated to pEGFP-C1 (Invitrogen) and sequenced. YFP-htt-1301-17Q and EB3-GFP constructs were previously described (Anne et al., 2007; Stepanova et al., 2003). pEYFPC1 (BD Biosciences Clontech, Palo Alto, CA) was used as control. To obtain pCAGGS-htt-1301-17Q IRES-NLS-GFP construct, a PCR was done in order to insert a SmaI site in YFP-htt-1301-17Q construct, using it as a template with the following primers (Eurofins, MWG Operon): YFP-1301 mut Sma1 Cter-sens (5' gaaatcctgcaggcatcccgggagggcgaattc 3') and YFP-1301 mut Sma1 Cter-antisens (5' cagattcgccctcccgggatgccgtcaggattt 3') The PCR product was inserted (SacI/SmaI; Biolabs) in pCAGGS-LB-IRES-NLS-GFP vector and sequenced.

The RNA oligonucleotides for siRNA (Eurogentec) were annealed and used at 2 μM in neuronal cells and at 8μM in HeLa cells. The following pairs of oligonucleotides were used: Mohtt361-sens (5' ggaacucucagccaccaag 3') and Mohtt361-antisens (5' cuugguggcugagaguucc 3') for siRNA against mouse huntingtin (si-htt1); Mohtt 4325-sens (5' uuacugucuacuggauuc 3') and Mohtt 4325-antisens (5' ugaauccaguagacagua 3') for siRNA againt mouse huntingtin (si-htt2); si-p150^{Glued}-sens (5' agaagucacucaagauuaa 3'), si-p150^{Glued}-antisens (5' uuaaucuugagugacuucu 3')

for siRNA against mouse/rat/human $p150^{Glued}$ (si-$p150^{Glued}$) and Huhtt585-sens (5' aacuuucagcuaccaagaaag 3') and Huhtt585-antisens (5' cuuucuugguagcugaaaguu 3') for siRNA against human huntingtin (si-Huhtt); scramble-sens (5' aucgagcuaccacgaacgc 3') and scramble-antisens (5' gcguucgugguagcucgau 3') for negative control siRNA (scramble). siRNA negative control (si-ctrl) from Eurogentec (OR-0030-neg05) was used for HeLa cells experiments. The huntingtin siRNAs were extensively used to target huntingtin function in dynein/dynactin dependent transport along microtubules in cells without off-target effects, as shown in rescue experiments and by the use of other siRNAs (Colin et al., 2008).

Cell lines and Transfection. Mouse neuronal cells derived from immortalized striatal progenitor cells were grown as previously described including 400 μg/ml geneticin (Trettel et al., 2000) and electroporated using cell line nucleofactor kit (Amaxa). Cells were spread in 10 cm^2 plate and in glass coverslips for immunoblotting and immunofluorescence experiments respectively. For rescue experiments, expression of fragment of human (YFP-htt-1301) or *Drosophila* huntingtin (GFP-dHtt620) in mouse neuronal cells was achieved by co-electroporation of the YFP-htt-1301 or GFP-dHtt620 construct with scramble or si-htt. After 48 hr, cells were lyzed or fixed and immunoprocessed. For microtubule polymerization analysis, mouse neuronal cells were first electroporated with si-htt1 or scramble RNA and transfected the following day with Lipofectamine2000 (Invitrogen) with EB3-GFP. Videomicroscopy was performed 48 hr after electroporation.

HeLa cells stably expressing GFP–tubulin (green) and H2B–mCherry (red) were cultured as previously described (Steigemann et al., 2009), plated on glass coverslips and transfected using

Lipofectamin2000 with scramble or si-Huhtt. After 48 hr, transfected cells were analyzed by confocal videomicroscopy.

Antibodies and Immunostaining Procedures. Anti-huntingtin (anti-htt) antibodies used in this study have been either previously described: mAb 2B4 (epitope 49-64, clone HU 2B4, Euromedex) (Lunkes et al., 2002), mAb 4C8 (epitope 445-456, clone HU-4C8-As, Euromedex) or generated for this study (pAbs 812 and SE3619). The pAbs 812 and SE3619 antibodies were generated by synthesis, coupling to keyhole limpet hemocyanin (Eurogentec) and injection into rabbits of the following respective peptides: MATLEKLMKAFESLKSF (mouse/human huntingtin amino acid sequence 1 to 18) and CGGRSRSGS[PO_3H_2]IVE (mouse huntingtin sequence amino acid 414 to 424). Polyclonal antibodies were obtained by affinity-purification of serum using the appropriate peptide columns. Briefly, the serum was filtered (0.22 μm filter) and after addition of 1 M tris (pH 8.0) up to a final concentration of 100 mM, it was applied to a sulfolink column (Pierce) coupled to the appropriate peptide. Retained antibodies were eluted with 100 mM glycine buffer (pH 2.7) and pH was neutralised with 1 M tris pH 9. Antibodies were concentrated (Vivaspin concentrator 10 000 MW, VivaScience) and stored in 50% glycerol. For immunofluorescence, the primary mouse antibodies used were: anti-α-tubulin DM1A (1:100; Sigma), anti-α-tubulin-FITC conjugated (1:30; Sigma), anti-huntingtin 4C8 (1:500), anti-p150^{Glued} (1:100; BD bioscience), anti-intermediary chain 74.1 of mammalian cytoplasmic dynein (1:200; MAB1618, Chemicon) and anti-γ-tubulin GTU88 (1:100; Sigma). The primary polyclonal antibodies used were: anti-huntingtin SE3619 (1:100), anti-huntingtin 812 (1:100), and anti-γ-tubulin (1:100; Sigma). Secondary antibodies used were goat anti-mouse and anti-rabbit conjugated to AlexaFluor-488 or AlexaFluor-555 (Molecular Probes) at 1:200. Cells were

grown on glass coverslip transfected with various constructs or siRNA. To analyze huntingtin localization during mitosis, cells were prelyzed 2 min in prewarmed 0.5% Triton X-100-PHEM buffer before being fixed in anhydrous methanol at -20°C for 5 min and incubated with anti-huntingtin 4C8, anti-huntingtin 4E6 or anti-huntingtin SE3619 and γ-tubulin.

To visualize spindles, mouse neuronal cells were fixed with cold methanol with 5mM EGTA at -20°C for 5 min, and then in 4% formaldehyde in PHEM for 10 min at room temperature, washed in PBS, blocked in 1% BSA, 0.1% Triton X-100 in PBS, and incubated with an anti-α-tubulin antibody. To visualize astral microtubules, mouse neuronal cells were fixed in a solution of 3% paraformaldehyde, 0.25% glutaraldehyde, 0.2% Nonidet P-40 in BRB80 for 10 min, treated with 0.1M sodium borohydride in BRB80 for 10 min, washed in BRB80, blocked in 0.2% Nonidet P-40, 3% BSA in BRB80 and incubated with an anti-α-tubulin antibody.

p150^{Glued} and dynein at spindle poles were visualized as follow: cells were first permeabilized 1 min in PHEM buffer containing 1% Triton X-100 and then fixed with 4% PAF in PHEM buffer for 20 minutes. Then cells were fixed for 5 minutes in cold methanol (-20°C) and washed 3 times before immunostaining (adapted from (Busson et al., 1998)). Cells were double immunostained with anti-huntingtin antibodies (SE3619) and anti-p150^{Glued} or anti-dynein for 1 hr and then with anti-mouse AlexaFluor-555 and anti-rabbit AlexaFluor-488.

For NuMA staining cells were fixed 5 min with cold methanol (-20°C) and washed with PBS before immunostaining. The cells were triple labeled with anti-NuMA (1:4000, human autoimmune serum provided by N.Fabien), anti-htt (SE3619) and anti-γ-tubulin antibodies for 1 hr, washed three times 10 min in PBS and incubated with Cy5 anti-human, anti-rabbit AlexaFluor-555 and anti-mouse AlexaFluor-488 secondary labeled antibodies for 1 hr at room temperature.

To assess microtubule re-growth, microtubules were completely depolymerized by treating cells with 5 mM nocodazole for 1 hr at 37°C and 30 min on ice. After treatment, cells were washed twice with $C0_2$ equilibrated medium. Microtubules were allowed to re-grow for different times (4, 8, 12, 18 minutes). Cells were permeabilized in PHEM buffer containing 1% triton X-100 for 1 min and fixed with 4% PAF in PHEM buffer containing 0.025% glutaraldehyde, washed twice with PBS and immunostained with anti-htt SE3619 and anti-α-tubulin for 1 hr.

For all immunostainings, the slides were counterstained with DAPI (Roche) and mounted in Mowiol. The pictures were captured either with a three-dimensional deconvolution imaging system as previously described (Gauthier et al., 2004) or with a Leica DM RXA microscope equipped with a 63x oil-immersion objective coupled to a piezzo and a Micromax RTE/CDD-1300-Y/HS camera controlled by Methamorph software (Molecular Devices). Z-stack steps were of 0.2 µm. Images were treated with ImageJ (http://rsb.info.nih.gov/ij/, NIH, USA).

For western blot analysis, mouse neuronal cell extracts were prepared by scrapping cells in 1% NP40 buffer supplemented with 1 mM vanadate, 5% aprotinin, 100 µM PMSF and 2 mM DTT, sonicated, spinned at 10 000 rpm for 10 min at 4°C. Finally, the soluble fraction was collected for immunoblotting analyses. The primary monoclonal anti-huntingtin 4C8, anti-p150^{Glued}, anti-α-tubulin (DM1A), anti-GFP (Roche) and anti-β-actin antibodies were used at 1:5000, 1:1000, 1:1000 and 1:2000 respectively and the secondary HRP-conjugated goat anti-mouse antibody (Amersham) at 1:10 000.

Spindle Orientation Quantification and Image Analyses. The quantification of huntingtin or p150^{Glued} at the spindle poles was achieved by drawing a circle of constant size around the

spindle poles. Signal corresponds to the average pixel intensities detected within the area substracted from the background and cytoplasmic pixel average intensities.

The quantification of NuMA at spindle pole was done using a home-built macro (ImageJ software, see below for details). In order to analyze each pole separately, their coordinates were determined using γ-tubulin staining. On the NuMA image, a circle (radius equal to half of pole-pole distance) was drawn around the pole position, and image was cleared outside the circle. Quantification of NuMA was performed on the resulting z-stacks (one for each pole) using 3D object counter plugin (Bolte and Cordelieres, 2006); available at http://imagejdocu.tudor.lu/doku.php?id=plugin:analysis:3d_object_counter:start. Total volume and intensity of the particles were retrieved for further analysis.

Quantification of dynein at spindle pole was performed with ImageJ software using Circular3DProfiler plugin (in house developed ImageJ plugin, available on request at fabrice.cordelieres@curie.u-psud.fr). Briefly, on each z-stacks, intensities were retrieved within spindle pole centered spheres of increasing radii. The differences of intensities between two successive radii accounts for the dynein signal at a certain distance from the pole. Once normalized, the latter parameter is plotted as a function of the distance. The plot being Gaussian-like, the experimental curve was numerically adjusted to the theoretical one. The full-width at half maximum was subsequently used as an estimator of the dynein signal spread.

Spindle orientation in mouse neuronal metaphase cells stained for γ-tubulin and DAPI to visualize the spindle poles and chromatin was quantified using ImageJ software (http://rsb.info.nih.gov/ij/, NIH, USA). A line crossing both spindle poles was drawn on the Z projection pictures and repositioned along the Z-axis using the stack of Z-sections. The angle

between the pole-pole and the substratum plane was calculated by the ImageJ Plug-in. Spindle lengths and cell lengths were quantified along the line that crosses both spindle poles.

In *Drosophila* neuroblasts, the spindle orientation was quantified using an home-built macro in ImageJ software (see below for details), by measuring the angle between a line connecting the two spindle poles and a line bisecting the crescent of Miranda.

In mouse neural progenitors, the spindle orientation was quantified using an especially developed macro (ImageJ software, see below for details). Orientation of sister chromatids was first defined by drawing a line connecting the top and the bottom of each chromatids. The cleavage plane was defined as the line bisecting both chromatids orientation lines. The plane of the apical surface was determined as a tangent line to the ventricular zone. Finally, the angle between the cleavage plane and the apical surface was measured. Only the smallest angle was recorded.

Flies. *D. melanogaster* flies were maintained at 18°C. *insc*-Gal4 flies are from Bloomington *Drosophila* Stock Center (Indiana, USA). mud^{2} strain has been previously described (Siller et al., 2006). UAS-dHttRNAi(1) flies are from Lawrence S.B. Goldstein (Gunawardena et al., 2003) and UAS-dHttRNAi(2) (transformant ID29532) strain was provided by Vienna Drosophila RNAi Center (VDRC) stock center. *dhtt-ko* flies are a gift of S. Zhang and N. Perrimon (Zhang et al., 2009). For the experiments assessing spindle orientation in *dhtt-ko* flies, we used, as previously described (Zhang et al., 2009), w^{1118} flies as controls, and both control and *dhtt-ko* flies were maintained at 25°C.

For immunohistochemistry on *D. melanogaster* brains, third instar larvae were dissected in PBS. The brains were collected and fixed in PBS containing 4% paraformaldehyde, 0.1% triton X-100 for 20 min at room temperature and processed as described (Betschinger et al., 2006). Briefly, brains were incubated overnight with mAb anti-Miranda (1:20; a kind gift of F. Matsuzaki), pAb

anti-centrosomin (1:500; a kind gift of T. Kaufman) and pAb anti-phospho-histone H3 (1:2000; Upstate Biotechnology). After three washes in PBS Triton X-100 0.1% (PBT), brains were incubated with mouse AlexaFluor-488, rabbit AlexaFluor-555 and DAPI for 1-2 hr at room temperature, washed again three times in PBT, incubated in PBS/glycerol for 30 min and mounted in Glycerol/PBS-N-propylgalate. The pictures were captured with a three-dimensional deconvolution imaging system as previously described (Gauthier et al., 2004) or with a Leica SP5 laser scanning confocal microscope equipped with a X63 oil-immersion objective and analyzed using ImageJ.

For *D. melanogaster* spindle length measure, larval brains were dissected and incubated overnight using pAb anti-centrosomin (1:500, a kind gift of T. Kaufman), pAb anti-phospho-histone H3 (1:2000, Update Biotechnology) and mAb anti-α-tubulin (1:1000, clone DM1A, Sigma) and stained for 1-2 hr with anti-mouse AlexaFluor-555, anti-rabbit AlexaFluor-488 and DAPI. Images were adquired using a Leica SP5 laser scanning confocal microscope equipped with a 63x oil-immersion objective. Spindle-spindle lengths in metaphasic neuroblasts were measured using ImageJ.

For quantification of *D. melanogaster* neuroblasts, brains were dissected and incubated overnight using pAb anti-miranda (1:1000; a kind gift of F. Matsuzaki), mAb anti-elav (1:100, DSHB, University of Iowa) and stained for 1-2 hr with anti-rabbit AlexaFluor-488 (Molecular Probes), anti-mouse-Cy3 (Interchim) and DAPI (Roche). Images were acquired using a Zeiss LSM 710 laser scanning confocal microscope equipped with a 40x/1,3 OIL DICII PL APO. Miranda-positive and elav-negatives neuroblasts in the posterior half of the larva brain hemisphere were quantified using ImageJ.

Immunohistochemistry. For immunohistochemistry on electroporated mouse brain, 10 μM sections of E16.5 brain were permeabilized in 0.1% Triton X-100 in PBS (PBT), blocked in PBT-10% goat serum (Sigma) for 20 min at room temperature and incubated with anti-htt (4C8) and polyclonal anti-GFP (Invitrogen, 1:1000) antibodies in PBT-10% goat serum overnight at 4°C. The slices were washed in PBT and incubated with a rabbit AlexaFluor-488 as secondary antibody. To define the identity of electroporated cells, mouse brain sections were incubated with polyclonal anti-GFP serum and monoclonal anti-nestin (Rat401, BD Pharmingen, 1:200) or monoclonal anti-Tuj1 (Class III β-tubulin, MAB 1637, Chemicon; 1:50) overnight at 4°C in the blocking solution. The slices were washed in PBT and incubated with AlexaFluor-488-conjugated anti-rabbit IgG and AlexaFluor-555-conjugated anti-mouse IgG antibodies. For analysis of Pax6 and Tbr2 distribution, mouse brain sections were briefly (1 min) boiled in 10mM sodium citrate solution, pH6.0, for antigen enhancement. Sections were then permeabilized in PBS Triton X-100 0.3% (PBT3), blocked as above, incubated with a primary chicken anti-GFP antibody (ab16901, Chemicon; 1:300) and polyclonal anti-Pax6 (PRB-278-0100, Eurogentec, 1:300) or Tbr2 (ab23345, Abcam, 1:300) antibodies overnight at 4°C. The slices were washed in PBT3 and incubated with AlexaFluor-488-conjugated anti-chicken IgG and AlexaFluor-555-conjugated anti-rabbit IgG antibodies. The brain sections were washed in PBT or PBT3 and postfixed for 20 min in 4% paraformaldehyde in PBS (pH 7) at room temperature, washed in PBS and incubated with HCl 2N for 30 min at room temperature followed by three washes in PBT. The brain sections were then incubated with the blocking solution for 20 min at room temperature and incubated with rat anti-BrdU (OBT0030, AbD Serotec, 1:300) for 1 hr in the blocking solution. The sections were subsequently incubated with a Cy5-conjugated anti-rat IgG antibody.

For cell fate analysis in wild-type and *Nestin-Cre/+; Hdh flox/-* E14.5 or E18.5 embryos, 7 μm paraffin sections were boiled in 10 mM sodium citrate solution, pH6, for 10 min. Sections were then permeabilized in PBT3, blocked as above, incubated with polyclonal anti-Pax6 (PRB-278-0100, Eurogentec, 1:300), Tbr2 (ab23345, Abcam, 1:300), Tbr1 (ab31940, Abcam, 1:300) or anti-NeuN (MAB377, Chemicon; 1:200) and rat anti-BrdU (OBT0030, AbD Serotec; 1:300) antibodies overnight at 4°C. The slices were washed in PBT3 and incubated with AlexaFluor-555-conjugated anti-mouse IgG and Cy5-conjugated anti-rat IgG antibodies.

The cell nuclei were stained with DAPI. All the slices were mounted in Mowiol. Neuronal progenitors were imaged using a Leica SP5 laser scanning confocal microscope equipped with a X63 oil-immersion objective.

In Utero **Electroporation.** *In utero* electroporation was performed as described previously (Nguyen et al., 2006) with minor modifications. Briefly, uteri of anaesthetized timed-pregnant mothers (14 days) with isoflurane in oxygen carrier (Abbot Laboratories Ltd, Kent, UK) were exposed through a 1.5 cm incision in the ventral peritoneum. Embryos were carefully lifted using ring forceps through the incision and placed on humidified gauze pads. pCAGGS-NLS-GFP (2 μg/μl) (gift from J. Briscoe, National Institute for Medical Research, London), prepared using EndoFree plasmid purification kit (Qiagen Benelux B.V.) was mixed with 0.05% Fast Green (Sigma) and scramble or si-htt1 RNAs (10μM) and, injected through the uterine wall into the telencephalic vesicle using pulled borosilicate needles and a Femtojet microinjector (VWR International). For rescue experiments, pCAGGS-NLS-GFP (1 μg/μl) and pCAGGS-htt-1301-17Q-IRES-NLS-GFP (3 μg/μl) were mixed with 0.05% Fast Green and si-htt2 RNA (10 μM) and, injected as described above. For control experiment, pCAGGS-NLS-GFP (2 μg/μl) and

pCAGGS-LB-IRES-NLS-GFP (2 μg/μl) were used. Five electrical pulses were applied at 35V (50 ms duration) across the uterine wall at 1s intervals using 5 mm platinum tweezers electrodes (CUY650P5, Sonidel, Ireland) and an ECM-830 BTX square wave electroporator (VWR International). The uterine horns were then replaced in the abdominal cavity and the abdomen wall and skin were sutured using surgical needle and thread. Pregnant mice were injected with buprenorphine (Temgesic®, Schering-Plough, Brussels, Belgium) and warmed on heating pad until it woke up. The whole procedure was complete within 30 min. Two days following the surgery, pregnant mice were sacrificed by neck dislocation and E16.5 embryos were collected and fixed with 4% paraformaldehyde in PBS for 45 min at 4°C followed by a cryoprotection in PBS containing 20% sucrose for 18 hr. 10 μm coronal sections were cut on a cryostat (Leica CM 3050S) at -20°C and processed for immunohistochemistry. To analyze neurogenesis, E14.5 embryos were electroporated with GFP encoding plasmid and scramble or si-htt RNAs as described above followed by an intraperitoneal injection of BrdU to the mother (100 mg/Kg body weight) at E15. 24 hr after BrdU injection, E16.5 brains were collected, fixed, and prepared for immunohistochemistry as described above.

Mice. The line of Nestin-Cre mice used in our experiments has been used successfully for neuronal ablation (Tronche et al., 1999) and was purchased from The Jackson Laboratory (strain name B6.Cg(SJL)-TgN(NesCre)1Kln). To evaluate the efficiency of the Nestin-Cre expression and recombination in neuronal tissues, we characterized the Nestin-Cre transgene activity during embryogenesis using the R26R reporter mouse strain (Soriano, 1999). In *Nestin-Cre/+;R26R/+* embryos, LacZ expression throughout the embryonic neural tube was detected as early as E10.5 by whole-mount X-gal staining (data not shown). Analysis of X-gal stained sections at E14.5

confirmed that most cells of the cortex and striatum had recombined (Figure S4). Counts for efficiency of recombination (recombined versus unrecombined cells; blue-stained versus non-stained) were then performed at high magnification (40X) on sections derived from two E14.5 embryos. These analyses revealed that the frequency of recombined cells was in average 80-95% in the developing cortex (data not shown).

For routine genotyping of progeny we used PCR analysis (30 cycles consisting of 45 sec denaturation at 94˚C, 45 sec annealing at 61˚C, and 1 min extension at 72˚C). The *Hdh* null allele was detected using the primers Neo 3 (Neo reverse) 5'- AGAGCAGCCGATTGTCTGTTGT-3' and Neo 6 (MC1 forward) 5'- AACACCGAGCGACCCTGCAG-3', which generated a 130 bp product. The *cre* transgene was detected using the primers Cre 1 (Cre forward): 5´-CTGCCACGACCAAGTGACAGC-3´ and Cre 2 (Cre reverse): 5´-CTTCTCTACACCTGCGGTGCT-3´ to generate a 325 bp product corresponding to a portion of the *cre* coding region. The Hdh floxed allele was detected using the primers pgk (pgk promoter sequence): 5'-GCCCGGCATTCTGCACGCTT-3' and Hdhpr13 (Hdh promoter sequence): 5'-CTGTCTGGAGGTGATCCATGC-3', which generated a 150 bp PCR product. For detection of the R26R allele, the primers Lac 1 (LacZ forward) 5'-CGGCGGTGAAATTATCGATGAG-3'and Lac 2 (LacZ reverse): 5'-ATCAGCAGGATATCCTGCACCA-3'were used to generate a 315 bp PCR product.

BrdU Injections and Paraffin Embedding. *Hdhflox/flox* females were crossed with *Nestin-Cre/+;Hdh+/-* males, and checked for vaginal plug in the morning after the mating. Pregnant females were given a single intraperitoneal injection of 100 mg/Kg BrdU at E13.5, and embryos were dissected at E14.5 or E18.5 and processed for paraffin embedding. Briefly, embryos were

fixed in 4% paraformaldehyde in PBS, incubated for 24 hrs at 4˚C in PBS containing 0.25 M sucrose, 0.2 M glycine, dehydrated, cleared with toluene and embedded in paraffin.

Supplemental Experimental Procedures for Supplemental Figures

HeLa cells were maintained in Dulbecco Modified Eagle Medium (DMEM) with 10% bovine calf serum and 1% glutamine. Oligofectamine (Invitrogen) was used to transfect si-ctrl and si-Huhtt into Hela cells. Cells were spread in 10 cm^2 plate and in glass coverslips, lyzed or fixed after 48-72 hours and processed for immunoblotting and immunofluorescence experiments. Imunoblotting, immunostaining and spindle orientation quantification were performed as described for mouse neuronal cells.

Mouse neuronal cells were grown on glass coverslip, prelyzed 2 minutes in prewarmed 0.5% Triton X-100-PHEM buffer before being fixed in anhydrous methanol at -20°C for 5 minutes and incubated with anti-huntingtin 4E6 (epitope 1354-456, clone HU-4E6-As, Euromedex) (1:100) or anti-huntingtin 812 and γ-tubulin. Secondary antibodies used were goat anti-mouse and anti-rabbit conjugated to AlexaFluor-488 or AlexaFluor-555 (Molecular Probes) at 1:200.

Staining of sections to visualize lacZ expression was performed as described (Hogan et al., 1994). Embryos were first fixed overnight at 4˚C in 0.1 M PIPES pH 6.9, 2 mM $MgCl_2$, 5 mM EGTA containing 0.2% paraformaldehyde, and then cryopreserved in PBS containing 30% sucrose and 2 mM $MgCl_2$. They were then embedded in OCT compound (TissueTek), and frozen at -80˚C. Specimens were sectioned on a sagital plane (9 μm thickness) in a cryostat and mounted on superfrost slides (Fisher). Sections were stained with X-gal at 37˚C overnight, washed with PBS, and counterstained with eosin.

MACROS

Macro "spindle orientation in mouse neuronal progenitors". This macro was developed on site by J.D.Godin.

```
w=getWidth;
leftButton=16;
rightButton=4;
run("RGB Color");
setOption("DisablePopupMenu", true);
	while (!isKeyDown("space")){
	roiManager("reset");
	flags=0;
	while (flags!=leftButton){
		getCursorLoc(n1topx, n1topy, n1topz, flags);
		showStatus("ADN1 top (Click left)");
}
flags=0;
	while (flags!=rightButton){
		getCursorLoc(n1bottomx, n1bottomy, n1bottomz, flags);
		showStatus("ADN1 bottom (Click right)");
			}
setForegroundColor(0, 255, 0);
	drawLine(n1topx, n1topy, n1bottomx, n1bottomy);
	flags=0;
	while (flags!=leftButton){
		getCursorLoc(n2topx, n2topy, n2topz, flags);
		showStatus("ADN1 top (Click left)");
}
flags=0;
	while (flags!=rightButton){
		getCursorLoc(n2bottomx, n2bottomy, n2bottomz, flags);
		showStatus("ADN1 bottom (Click right)");
			}
setForegroundColor(255, 0, 0);
	drawLine(n2topx, n2topy, n2bottomx, n2bottomy);
pente1=(n1topy-n1bottomy)/(n1topx-n1bottomx);
pente2=(n2topy-n2bottomy)/(n2topx-n2bottomx);
oao1=n1topy- (n1topx * pente1);
oao2=n2topy- (n2topx * pente2);
intersectiony=pente1*((oao2-oao1)/(pente1-pente2))+oao1;
intersectionx=(intersectiony-oao1)/pente1;
pentebissectrice=tan((atan(pente1)+atan(pente2))/2);
oaobissectrice=intersectiony- (intersectionx*pentebissectrice);
setForegroundColor(0, 0, 255);
	drawLine(0, oaobissectrice, w, pentebissectrice*w+oaobissectrice);
```

```
flags=0;
	while (flags!=leftButton){
		getCursorLoc(nv1x, nv1y, nv1z, flags);
		showStatus("ventricule point 1 (Click left)");
}
flags=0;
	while (flags!=rightButton){
		getCursorLoc(nv2x, nv2y, nv2z, flags);
		showStatus("ventricule point 2 (Click right)");
			}
setForegroundColor(255, 255, 0);
	drawLine(nv1x, nv1y, nv2x, nv2y);
penteVZ=(nv1y-nv2y)/(nv1x-nv2x);
angle=abs((atan(pentebissectrice)-atan(penteVZ))*180/PI);
setResult("angle", nResults, angle);
	updateResults();
	wait(250);
```

Macro "spindle orientation in *Drosophila* neuroblasts". This macro was developed on site by

F.P. Cordelières at the Institut Curie Imaging Facility.

```
radius=4;
deb=false;

in=getDirectory("where are the images?");
files=getFileList(in);

out=getDirectory("Where do you save the images?");

for (i=0; i<files.length; i++){
	if(endsWith(files[i], "lif")){
		open(in+files[i]);
		getAngle();
		close();
	}

}

function getAngle(){
	row=nResults;
	title=getTitle();
	setResult("Label", row, title);
	w=getWidth();
	h=getHeight();
	Stack.getDimensions(width, height, channels, slices, frames);
```

```
run("Z Project...", "start=1 stop="+slices+" projection=[Max Intensity]");
Stack.setChannel(2);
setAutoThreshold();
setTool(8);
run("Threshold...");
waitForUser("(Option: Ajust the threshold)\nClick on the cell\nwith magic wand");

resetThreshold();

//Fit ellipse
List.setMeasurements;
x = List.getValue("X");
y = List.getValue("Y");
a = List.getValue("Major");
b = List.getValue("Minor");
angle = List.getValue("Angle");
getVoxelSize(w, h, d, unit);

x=x/w;
y=y/h;
a=a/w;
b=b/h;

makeRectangle(0,0,0,0);
setTool(7);
modifiers=0;
while (modifiers!=48){
        showStatus("click on the left of the crescent (Miranda staining)");
        getCursorLoc(xg, yg, z, modifiers);
}
wait(250);

modifiers=0;
while (modifiers!=48){
        showStatus("click on the right of the crescent (Miranda staining) ");
        getCursorLoc(xd, yd, z, modifiers);
}
wait(250);

Stack.setChannel(1);

modifiers=0;
while (modifiers!=48){
        showStatus("Click on the upper spindle pole");
        getCursorLoc(xh, yh, z, modifiers);
}
wait(250);
```

```
modifiers=0;
while (modifiers!=48){
	showStatus("Click on the lower spindle pole ");
	getCursorLoc(xb, yb, z, modifiers);
}
wait(250);

Stack.setDisplayMode("composite");
run("RGB Color");
setForegroundColor(0, 0, 255);

drawEllipse(x, y, a/2, b/2, angle);

drawOval(x-radius, y-radius, 2*radius, 2*radius);
drawOval(xg-radius, yg-radius, 2*radius, 2*radius);
drawOval(xd-radius, yd-radius, 2*radius, 2*radius);
drawOval(xh-radius, yh-radius, 2*radius, 2*radius);
drawOval(xb-radius, yb-radius, 2*radius, 2*radius);


makeSelection("angle", newArray(xg, x, xd), newArray(yg, y, yd));
setForegroundColor(0, 255, 0);
run("Draw");

List.setMeasurements;
angleArc=List.getValue("Angle")/2;
if (deb) setResult("Angle_arc", row, 2*angleArc);

makeSelection("angle", newArray(xd, x, w), newArray(yd, y, y));
List.setMeasurements;
angleTmp=180-List.getValue("Angle");
if (deb) setResult("Angle_tmp", row, angleTmp);

if (yd<y){
	angleArc=(angleArc-angleTmp);
}else{
	angleArc=(angleArc+angleTmp);
}

if (deb) setResult("Angle_arc_apres", row, angleArc);

a=tan(angleArc*PI/180);
b=y-x*a;

setForegroundColor(0, 255, 0);
drawLine(0, b, getWidth(), a*getWidth()+b);
```

```
        c=(yb-yh)/(xb-xh);
        d=yb-xb*c;

        setForegroundColor(255, 0, 0);
        drawLine(0, d, getWidth(), c*getWidth()+d);

        xInter=(d-b)/(a-c);
        yInter=a*xInter+b;
        setForegroundColor(255, 255, 255);
        drawOval(xInter-radius, yInter-radius, 2*radius, 2*radius);

        x1=(w-b)/a;
        x2=(w-d)/c;

        makeSelection("angle", newArray(x1, xInter, x2), newArray(h, yInter, h));

        List.setMeasurements;
        angleAxe =List.getValue("Angle");
        setForegroundColor(255, 255, 255);
        run("Draw");
        setResult("Angle_axe", row, angleAxe);

        drawString(title+", "+(floor(angle*100)/100)+"Á", 5, 25);

        saveAs("Tiff", out+getTitle());
        close();
        close();
        updateResults();
}

function drawEllipse(x, y, a, b, angle) {
    autoUpdate(false);
    setLineWidth(1);
    beta = -angle * (PI/180);
    for (i=0; i<=360; i+=2) {
       alpha = i*(PI/180) ;
       X = x + a*cos(alpha)*cos(beta) - b*sin(alpha)*sin(beta);
       Y = y + a*cos(alpha)*sin(beta) + b*sin(alpha)*cos(beta);
       if (i==0) moveTo(X, Y); else lineTo(X,Y);
       if (i==0) {ax1=X; ay1=Y;}
       if (i==90) {bx1=X; by1=Y;}
       if (i==180) {ax2=X; ay2=Y;}
       if (i==270) {bx2=X; by2=Y;}
    }
    updateDisplay;
 }
```

Macro “quantification at poles”. This macro was developed on site by J.D.Godin.

```
index=0;
limVol=50;
dir=getDirectory("Choose a Directory");
dest=getDirectory("Choose the output Directory");
dirAnalyseNuma=dest+"analyseNuma"+File.separator;
File.makeDirectory(dirAnalyseNuma);
dirAnalyseHtt=dest+"analyseHtt"+File.separator;
File.makeDirectory(dirAnalyseHtt);
dirResults=dest+"Results"+File.separator;
File.makeDirectory(dirResults);
obj=newArray("63x", "100x", "Without calibration");

Dialog.create("macro quantif at poles");
Dialog.addNumber("number of canals", 4);
Dialog.addString("gammaTub", "_w3FITC");
Dialog.addString("Htt", "_w2RHOD");
Dialog.addString("NuMa", "_w1CY5");
Dialog.addString("Nucleus", "_w4DAPI");
Dialog.addChoice("Objectif", obj);
Dialog.show();
n=Dialog.getNumber();
canalGammaTub=Dialog.getString();
canalHtt=Dialog.getString();
canalNuma=Dialog.getString();
canalDapi=Dialog.getString();
nObj=Dialog.getChoice();

pixX=1;
pixY=1;
pixZ=1;

if(nObj==obj[0]){
        pixX=0.1024;
        pixY=0.1024;
        pixZ=0.2;
}

if(nObj==obj[1]){
        pixX=0.0645;
        pixY= 0.0645;
        pixZ=0.2;
}
```

```
imgList=getFileList(dir);
ExpNumber=0;
for(i=0; i<imgList.length; i++) if(endsWith(imgList[i], "stk")) ExpNumber++;
ExpNumber=ExpNumber/n;

// to divide an image into two image - to work on half image
SpindlePole();
//to decide which half images to analyse based on htt downregulation
GoForAnalysis();
//to apply 3D object counter to Numa Images
listImagesNuma=getFileList(dirAnalyseNuma);
AnalyseProteinAtPole(listImagesNuma, dirAnalyseNuma);

selectWindow("Results");
run("Close");
TransferResult();

function SpindlePole(){
for(i=1;i<=ExpNumber; i=i+1){
	titleNuma="Experiment"+i+canalNuma+".stk";
	titleGammaTub="Experiment"+i+canalGammaTub+".stk";
	titleHtt="Experiment"+i+canalHtt+".STK";
	titleNumaSp1="Experiment"+i+canalNuma+"_sp1.stk";
	titleNumaSp2="Experiment"+i+canalNuma+"_sp2.stk";
	titleGammaTubSp1="Experiment"+i+canalGammaTub+"_sp1.stk";
	titleGammaTubSp2="Experiment"+i+canalGammaTub+"_sp2.stk";
	titleHttSp1="Experiment"+i+canalHtt+"_sp1.stk";
	titleHttSp2="Experiment"+i+canalHtt+"_sp2.stk";

	whereisthefileNuma=dir+titleNuma;
	open(whereisthefileNuma);
	whereisthefileTub=dir+titleGammaTub;
	open(whereisthefileTub);
	whereisthefileHtt=dir+titleHtt;
	open(whereisthefileHtt);

	w=getWidth;
	h=getHeight;

	selectWindow(titleGammaTub);
	run("Duplicate...", "title="+titleGammaTubSp1+" duplicate range=1-numberSlices");
	selectWindow(titleGammaTub);
	run("Duplicate...", "title="+titleGammaTubSp2+" duplicate range=1-numberSlices");
	selectWindow(titleNuma);
	run("Duplicate...", "title="+titleNumaSp2+" duplicate range=1-"+nSlices+" ");
	selectWindow(titleHtt);
```

```
run("Duplicate...", "title="+titleHttSp2+" duplicate range=1-"+nSlices+" ");

selectWindow(titleGammaTub);
tmp=FindSpindle3D();
sp1x=tmp[0];
sp1y=tmp[1];
sp1z=tmp[2];
sp2x=tmp[3];
sp2y=tmp[4];
sp2z=tmp[5];

Xpp=(sp2x+sp1x)/2;
Ypp=(sp2y+sp1y)/2;
setBackgroundColor(0, 0, 0);
a1=abs(sp1x-Xpp);
b1=abs(sp1y-Ypp);
r1=sqrt(a1*a1+b1*b1);
selectWindow(titleNuma);
makeOval(sp1x-r1,sp1y-r1,2*r1,2*r1);
run("Clear Outside", "stack");
wherewillbeSp1=dest+titleNumaSp1;
saveAs("tiff", wherewillbeSp1);
selectWindow(titleGammaTubSp1);
makeOval(sp1x-r1,sp1y-r1,2*r1,2*r1);
run("Clear Outside", "stack");
wherewillbeTubSp1=dest+titleGammaTubSp1;
saveAs("tiff", wherewillbeTubSp1);

selectWindow(titleHtt);
makeOval(sp1x-r1,sp1y-r1,2*r1,2*r1);
run("Clear Outside", "stack");
wherewillbeHttSp1=dest+titleHttSp1;
saveAs("tiff", wherewillbeHttSp1);

setBackgroundColor(0, 0, 0);
a2=abs(sp2x-Xpp);
b2=abs(sp2y-Ypp);
r2=sqrt(a2*a2+b2*b2);
selectWindow(titleNumaSp2);
makeOval(sp2x-r2,sp2y-r2,2*r2,2*r2);
run("Clear Outside", "stack");
wherewillbeSp2=dest+titleNumaSp2;
saveAs("tiff", wherewillbeSp2);
selectWindow(titleGammaTubSp2);
makeOval(sp2x-r2,sp2y-r2,2*r2,2*r2);
run("Clear Outside", "stack");
wherewillbeTubSp2=dest+titleGammaTubSp2;
```

```
	saveAs("tiff", wherewillbeTubSp2);

	selectWindow(titleHttSp2);
	makeOval(sp2x-r2,sp2y-r2,2*r2,2*r2);
	run("Clear Outside", "stack");
	wherewillbeHttSp2=dest+titleHttSp2;
	saveAs("tiff", wherewillbeHttSp2);

	run("Close All Without Saving");
	run("Close");

function FindSpindle3D(){

	run("Set Measurements", "volume integrated_density centre_of_mass
	close_original_images_while_processing_(saves_memory) dots_size=5 font_size=10
	redirect_to=none");
	run("3D object counter...");
	nParticules=nResults;
	tableau=newArray(nParticules);
		for(j=0; j<nParticules; j++){
			tableau[j]=getResult("IntDen", j);
			}
	Array.sort(tableau);
	max1=tableau[tableau.length-2];
	max2=tableau[tableau.length-1];


	for(j=0; j<nParticules; j++){
		Int=getResult("IntDen", j);
		if(Int==max1){
			sp1x=getResult("XM", j);
			sp1y=getResult("YM", j);
			sp1z=getResult("ZM", j);
			}
		if(Int==max2){
			sp2x=getResult("XM", j);
			sp2y=getResult("YM", j);
			sp2z=getResult("ZM", j);
			}
		}
	Tab=newArray(sp1x,sp1y,sp1z,sp2x,sp2y,sp2z);
	return Tab;
}

function GoForAnalysis(){
	for(j=1;j<=ExpNumber; j=j+1){
```

```
		titleNumaSp1="Experiment"+j+canalNuma+"_sp1.tif";
		titleNumaSp2="Experiment"+j+canalNuma+"_sp2.tif";
		titleHttSp1="Experiment"+j+canalHtt+"_sp1.tif";
		titleHttSp2="Experiment"+j+canalHtt+"_sp2.tif";


		wherewillbeSp1=dest+titleNumaSp1;
		open(wherewillbeSp1);
		wherewillbeSp2=dest+titleNumaSp2;
		open(wherewillbeSp2);
		wherewillbeHttSp1=dest+titleHttSp1;
		open(wherewillbeHttSp1);
		wherewillbeHttSp2=dest+titleHttSp2;
		open(wherewillbeHttSp2);
		selectWindow(titleHttSp1);
		waitForUser("downregulation htt");
		Dialog.create("analyse");
		Dialog.addCheckbox("Yes, I want to analyse this set of images", true);
		Dialog.show();
		analyseChoice=Dialog.getCheckbox();
		if(analyseChoice==1){
			selectWindow(titleNumaSp1);
			saveAs("tiff", dirAnalyseNuma+titleNumaSp1);
			selectWindow(titleHttSp1);
			saveAs("tiff", dirAnalyseHtt+titleHttSp1);
			}

		selectWindow(titleHttSp2);
		waitForUser("downregulation htt");
		Dialog.create("analyse");
		Dialog.addCheckbox("Yes, I want to analyse this set of images", true);
		Dialog.show();
		analyseChoice=Dialog.getCheckbox();
			if(analyseChoice==1){
			selectWindow(titleNumaSp2);
			saveAs("tiff", dirAnalyseNuma+titleNumaSp2);
			selectWindow(titleHttSp2);
			saveAs("tiff", dirAnalyseHtt+titleHttSp2);
			}
	run("Close All Without Saving");
	}
}

function AnalyseProteinAtPole(listImages, dir){
	numberImagesToAnalyse=listImages.length;
		for (i=0; i<numberImagesToAnalyse; i++) {
```

```
		run("Set Measurements", "volume integrated_density bounding_box dots_size=5
		font_size=10 redirect_to=none");

		if(i==0){
			setBatchMode(false);
			whereisthefile=dir+listImages[i];
			open(whereisthefile);
			selectWindow(listImages[i]);
			title=File.nameWithoutExtension;
			waitForUser("please note the threshold value");
			run("3D object counter...");
			thrNuma=getNumber("threshold", 220);
			saveAs("measurements", dirResults+"Results"+title+".xls");
			run("Close All Without Saving");
			}
		else {
			whereisthefile=dir+listImages[i];
			open(whereisthefile);
			selectWindow(listImages[i]);
			title=File.nameWithoutExtension;
			run("3D object counter...");
			saveAs("measurements", dirResults+"Results"+title+".xls");
			run("Close All Without Saving");
			}
		}
}


function TransferResult(){
	list=getFileList(dirResults);
	res=dirResults+"ResultFinal.xls";
	File.saveString("", res);

	for(i=0; i<list.length; i++){
	if(endsWith(list[i], "xls") && list[i]!="ResultFinal.xls"){
		index++;
		table="";
		if(index==1){
			tmp=File.openAsString(dirResults+list[i]);
			lines=split(tmp,"\n");

			splitLine=split(lines[0],"\t");
	table=splitLine[0]+"\t"+splitLine[1]+"\t"+splitLine[5]+"\t"+splitLine[20]+"\t"+splitLine[
	21]+"\t"+splitLine[22]+"\t"+splitLine[23]+"\t"+splitLine[24]+"\n"+removeNumber(list[i],
	tmp);
		}else{
			table="\n"+removeNumber(list[i], File.openAsString(dirResults+list[i]));
```

```
		}
		File.append(table, res);
	}
}


function removeNumber(label, string){
	lines=split(string,"\n");

	for(i=1; i<lines.length; i++){
		splitLine=split(lines[i],"\t");
		volume=parseInt(splitLine[1]);
		if(volume<limVol){
			lines[i]="";
		}else{

		lines[i]=label+"\t"+splitLine[1]+"\t"+splitLine[5]+"\t"+splitLine[20]+"\t"+splitLin
	e[21]+"\t"+splitLine[22]+"\t"+splitLine[23]+"\t"+splitLine[24];
		}
	}

	string="";
	for(i=1; i<lines.length; i++) if(lines[i]!="") string=string+lines[i]+"\n";
	return string;
}
```

SUPPLEMENTAL REFERENCES

Anne, S.L., Saudou, F., and Humbert, S. (2007). Phosphorylation of huntingtin by cyclin-dependent kinase 5 is induced by DNA damage and regulates wild-type and mutant huntingtin toxicity in neurons. J Neurosci *27*, 7318-7328.

Betschinger, J., Mechtler, K., and Knoblich, J.A. (2006). Asymmetric segregation of the tumor suppressor brat regulates self-renewal in Drosophila neural stem cells. Cell *124*, 1241-1253.

Bolte, S., and Cordelieres, F.P. (2006). A guided tour into subcellular colocalization analysis in light microscopy. J Microsc *224*, 213-232.

Busson, S., Dujardin, D., Moreau, A., Dompierre, J., and De Mey, J.R. (1998). Dynein and dynactin are localized to astral microtubules and at cortical sites in mitotic epithelial cells. Curr Biol *8*, 541-544.

Colin, E., Zala, D., Liot, G., Rangone, H., Borrell-Pages, M., Li, X.J., Saudou, F., and Humbert, S. (2008). Huntingtin phosphorylation acts as a molecular switch for anterograde/retrograde transport in neurons. Embo J *27*, 2124-2134.

Gauthier, L.R., Charrin, B.C., Borrell-Pages, M., Dompierre, J.P., Rangone, H., Cordelieres, F.P., De Mey, J., MacDonald, M.E., Lessmann, V., Humbert, S., *et al.* (2004). Huntingtin controls neurotrophic support and survival of neurons by enhancing BDNF vesicular transport along microtubules. Cell *118*, 127-138.

Gunawardena, S., Her, L.S., Brusch, R.G., Laymon, R.A., Niesman, I.R., Gordesky-Gold, B., Sintasath, L., Bonini, N.M., and Goldstein, L.S. (2003). Disruption of axonal transport by loss of huntingtin or expression of pathogenic polyQ proteins in Drosophila. Neuron *40*, 25-40.

Hogan, B., Beddington, R., Costantini, F. and Lacy, E. (1994). Manipulating the mouse embryo: A laboratory manual, Cold Spring Harbor Laboratory Press, Cold Spring Harbor, NY.

Lunkes, A., Lindenberg, K.S., Ben-Haiem, L., Weber, C., Devys, D., Landwehrmeyer, G.B., Mandel, J.L., and Trottier, Y. (2002). Proteases acting on mutant huntingtin generate cleaved products that differentially build up cytoplasmic and nuclear inclusions. Mol Cell *10*, 259-269.

Nguyen, L., Besson, A., Heng, J.I., Schuurmans, C., Teboul, L., Parras, C., Philpott, A., Roberts, J.M., and Guillemot, F. (2006). p27kip1 independently promotes neuronal differentiation and migration in the cerebral cortex. Genes Dev *20*, 1511-1524.

Siller, K.H., Cabernard, C., and Doe, C.Q. (2006). The NuMA-related Mud protein binds Pins and regulates spindle orientation in Drosophila neuroblasts. Nat Cell Biol *8*, 594-600.

Soriano, P. (1999). Generalized lacZ expression with the ROSA26 Cre reporter strain. Nat Genet *21*, 70-71.

Steigemann, P., Wurzenberger, C., Schmitz, M.H., Held, M., Guizetti, J., Maar, S., and Gerlich, D.W. (2009). Aurora B-mediated abscission checkpoint protects against tetraploidization. Cell *136*, 473-484.

Stepanova, T., Slemmer, J., Hoogenraad, C.C., Lansbergen, G., Dortland, B., De Zeeuw, C.I., Grosveld, F., van Cappellen, G., Akhmanova, A., and Galjart, N. (2003). Visualization of microtubule growth in cultured neurons via the use of EB3-GFP (end-binding protein 3-green fluorescent protein). J Neurosci *23*, 2655-2664.

Trettel, F., Rigamonti, D., Hilditch-Maguire, P., Wheeler, V.C., Sharp, A.H., Persichetti, F., Cattaneo, E., and MacDonald, M.E. (2000). Dominant phenotypes produced by the HD mutation in STHdh(Q111) striatal cells. Hum Mol Genet *9*, 2799-2809.

Tronche, F., Kellendonk, C., Kretz, O., Gass, P., Anlag, K., Orban, P.C., Bock, R., Klein, R., and Schutz, G. (1999). Disruption of the glucocorticoid receptor gene in the nervous system results in reduced anxiety. Nat Genet *23*, 99-103.

Zhang, S., Feany, M.B., Saraswati, S., Littleton, J.T., and Perrimon, N. (2009). Inactivation of Drosophila Huntingtin affects long-term adult functioning and the pathogenesis of a Huntington's disease model. Dis Model Mech *2*, 247-266.

14 Annexe VI: pARIS-htt: an optimised expression platform to study huntingtin reveals functional domains required for vesicular trafficking (supplemental information)

Full name : pARIS-htt-N[His-Cherry]Q23-C[HA-TC]
Used name : pARIS-mCherry-httQ23
vector : pENTRY

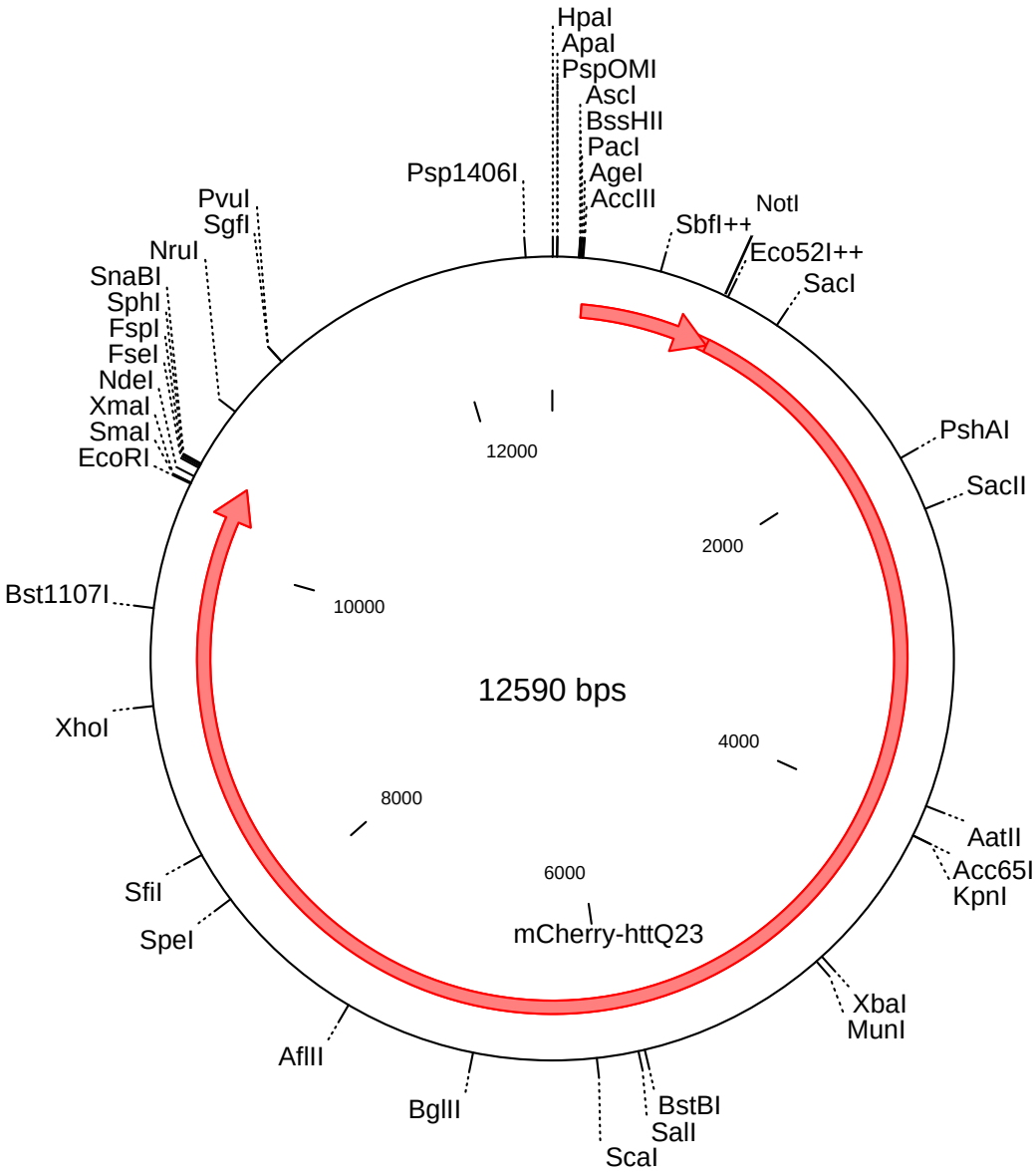

gene : mCherry-httQ23
- start : 165
- end 10451

Molecule: pARIS-mCherry-httQ23, 12590 bps DNA Circular
Description:
File Name: pARIS-mCherry-httQ23.cm5, dated 23 Apr 2010
Printed: List of Sites in bps, sorted by Enzyme name.
Filter ON: cut N <= 1

	#sites	----- Bp position of recognition site -----
AatII	1	3900
Acc65I	1	4061
AccIII	1	155
AflII	1	7361
AgeI	1	149
ApaI	1	24
AscI	1	133
BglII	1	6692
BssHII	1	134
Bst1107I	1	9695
BstBI	1	5829
Ecl136II	1	1188
Eco52I	1	907
EcoRI	1	10344
FseI	1	10434
FspI	1	10443
HpaI	1	3
KpnI	1	4061
MunI	1	4857
NdeI	1	10386
NotI	1	906
NruI	1	10767
PacI	1	141
PshAI	1	2102
Psp1406I	1	12457
PspOMI	1	24
PvuI	1	11109
SacI	1	1188
SacII	1	2383
SalI	1	5862
SbfI	1	548
ScaI	1	6072
SfiI	1	8420
SgfI	1	11108
SgrAI	1	878
SmaI	1	10350
SnaBI	1	10458
SpeI	1	8156
SphI	1	10452
XbaI	1	4821
XhoI	1	9206
XmaI	1	10350

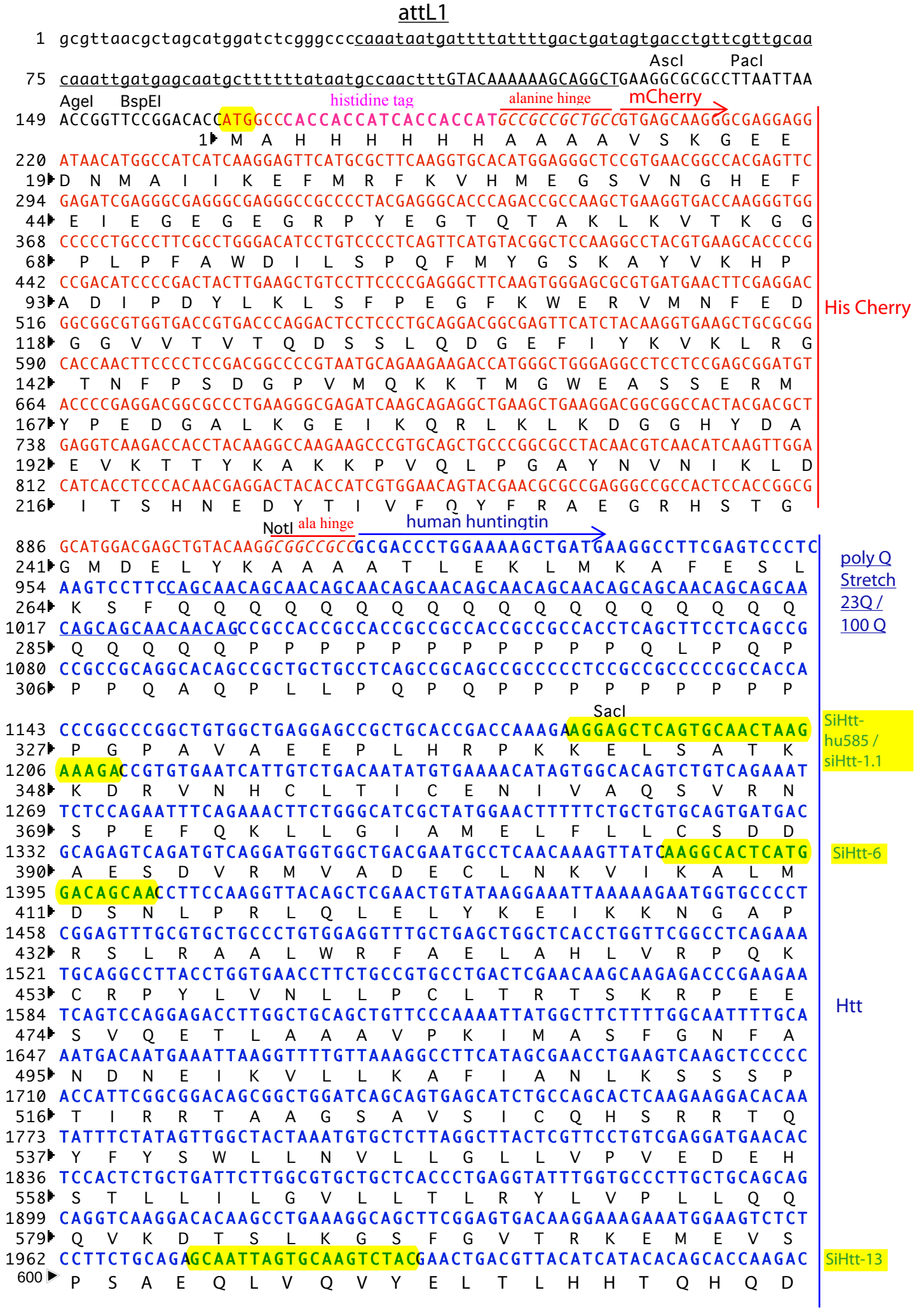
attL1
AscI
PacI
AgeI
BspEI
histidine tag
alanine hinge
mCherry
His Cherry
NotI
ala hinge
human huntingtin
poly Q Stretch 23Q / 100 Q
SacI
SiHtt-hu585 / siHtt-1.1
SiHtt-6
Htt
SiHtt-13

```
2025 CACAATGTTGTGACCGGAGCCCTGGAGCTGTTGCAGCAGCTCTTCAGAACGCCTCCACCCGAG
 621  H  N  V  V  T  G  A  L  E  L  L  Q  Q  L  F  R  T  P  P  P  E
2088 CTTCTGCAAACCCTGACCGCAGTCGGGGGCATTGGGCAGCTCACCGCTGCTAAGGAGGAGTCT
 642  L  L  Q  T  L  T  A  V  G  G  I  G  Q  L  T  A  A  K  E  E  S
2151 GGTGGCCGAAGCCGTAGTGGGAGTATTGTGGAACTTATAGCTGGAGGGGGTTCCTCATGCAGC
 663  G  G  R  S  R  S  G  S  I  V  E  L  I  A  G  G  G  S  S  C  S
2214 CCTGTCCTTTCAAGAAAACAAAAAGGCAAAGTGCTCTTAGGAGAAGAAGAAGCCTTGGAGGAT
 684  P  V  L  S  R  K  Q  K  G  K  V  L  L  G  E  E  E  A  L  E  D
2277 GACTCTGAATCGAGATCGGATGTCAGCAGCTCTGCCTTAACAGCCTCAGTGAAGGATGAGATC
 705  D  S  E  S  R  S  D  V  S  S  S  A  L  T  A  S  V  K  D  E  I
                                                    SacII
2340 AGTGGAGAGCTGGCTGCTTCTTCAGGGGTTTCCACTCCAGGGTCCGCGGGGCATGACATCATC
 726  S  G  E  L  A  A  S  S  G  V  S  T  P  G  S  A  G  H  D  I  I
2403 ACAGAACAGCCACGGTCACAGCACACACTGCAGGCGGACTCAGTGGATCTGGCCAGCTGTGAC
 747  T  E  Q  P  R  S  Q  H  T  L  Q  A  D  S  V  D  L  A  S  C  D
2466 TTGACAAGCTCTGCCACTGATGGGGATGAGGAGGATATATTGAGCCACAGCTCCAGCCAGGTC
 768  L  T  S  S  A  T  D  G  D  E  E  D  I  L  S  H  S  S  S  Q  V
2529 AGCGCCGTCCCATCTGACCCTGCCATGGACCTGAATGATGGGACCCAGGCCTCGTCGCCCATC
 789  S  A  V  P  S  D  P  A  M  D  L  N  D  G  T  Q  A  S  S  P  I
2592 AGCGACAGCTCCCAGACCACCACCGAAGGGCCTGATTCAGCTGTTACCCCTTCAGACAGTTCT
 810  S  D  S  S  Q  T  T  T  E  G  P  D  S  A  V  T  P  S  D  S  S
2655 GAAATTGTGTTAGACGGCACCGACAACCAGTATTTGGGCCTGCAGATTGGACAGCCCCAGGAT
 831  E  I  V  L  D  G  T  D  N  Q  Y  L  G  L  Q  I  G  Q  P  Q  D
2718 GAAGATGAGGAAGCCACAGGTATTCTTCCTGATGAAGCCTCGGAGGCCTTCAGGAACTCTTCC
 852  E  D  E  E  A  T  G  I  L  P  D  E  A  S  E  A  F  R  N  S  S
2781 ATGGCCCTTCAACAGGCACATTTATTGAAAAACATGAGTCACTGCAGGCAGCCTTCTGACAGC
 873  M  A  L  Q  Q  A  H  L  L  K  N  M  S  H  C  R  Q  P  S  D  S
2844 AGTGTTGATAAATTTGTGTTGAGAGATGAAGCTACTGAACCGGGTGATCAAGAAAACAAGCCT
 894  S  V  D  K  F  V  L  R  D  E  A  T  E  P  G  D  Q  E  N  K  P
2907 TGCCGCATCAAAGGTGACATTGGACAGTCCACTGATGATGACTCTGCACCTCTTGTCCATTGT
 915  C  R  I  K  G  D  I  G  Q  S  T  D  D  D  S  A  P  L  V  H  C
2970 GTCCGCCTTTTATCTGCTTCGTTTTTGCTAACAGGGGGAAAAAATGTGCTGGTTCCCGACAGG
 936  V  R  L  L  S  A  S  F  L  L  T  G  G  K  N  V  L  V  P  D  R
3033 GATGTGAGGGTCAGCGTGAAGGCCCTGGCCCTCAGCTGTGTGGGAGCAGCTGTGGCCCTCCAC
 957  D  V  R  V  S  V  K  A  L  A  L  S  C  V  G  A  A  V  A  L  H
3096 CCGGAATCTTTCTTCAGCAAACTCTATAAAGTTCCTCTTGACACCACGGAATACCCTGAGGAA
 978  P  E  S  F  F  S  K  L  Y  K  V  P  L  D  T  T  E  Y  P  E  E
3159 CAGTATGTCTCAGACATCTTGAACTACATCGATCATGGAGACCCACAGGTTCGAGGAGCCACT
 999  Q  Y  V  S  D  I  L  N  Y  I  D  H  G  D  P  Q  V  R  G  A  T
3222 GCCATTCTCTGTGGGACCCTCATCTGCTCCATCCTCAGCAGGTCCCGCTTCCACGTGGGAGAT
1020  A  I  L  C  G  T  L  I  C  S  I  L  S  R  S  R  F  H  V  G  D
3285 TGGATGGGCACCATTAGAACCCTCACAGGAAATACATTTTCTTTGGCGGATTGCATTCCTTTG
1041  W  M  G  T  I  R  T  L  T  G  N  T  F  S  L  A  D  C  I  P  L
3348 CTGCGGAAAACACTGAAGGATGAGTCTTCTGTTACTTGCAAGTTAGCTTGCACAGCTGTGAGG
1062  L  R  K  T  L  K  D  E  S  S  V  T  C  K  L  A  C  T  A  V  R
3411 AACTGTGTCATGAGTCTCTGCAGCAGCAGCTACAGTGAGTTAGGACTGCAGCTGATCATCGAT
1083  N  C  V  M  S  L  C  S  S  S  Y  S  E  L  G  L  Q  L  I  I  D
3474 GTGCTGACTCTGAGGAACAGTTCCTATTGGCTGGTGAGGACAGAGCTTCTGGAAACCCTTGCA
1104  V  L  T  L  R  N  S  S  Y  W  L  V  R  T  E  L  L  E  T  L  A
3537 GAGATTGACTTCAGGCTGGTGAGCTTTTTGGAGGCAAAAGCAGAAAACTTACACAGAGGGGCT
1125  E  I  D  F  R  L  V  S  F  L  E  A  K  A  E  N  L  H  R  G  A
3600 CATCATTATACAGGGCTTTTAAAACTGCAAGAACGAGTGCTCAATAATGTTGTCATCCATTTG
1146  H  H  Y  T  G  L  L  K  L  Q  E  R  V  L  N  N  V  V  I  H  L
3663 CTTGGAGATGAAGACCCCAGGGTGCGACATGTTGCCGCAGCATCACTAATTAGGCTTGTCCCA
1167  L  G  D  E  D  P  R  V  R  H  V  A  A  A  S  L  I  R  L  V  P
3726 AAGCTGTTTTATAAATGTGACCAAGGACAAGCTGATCCAGTAGTGGCCGTGGCAAGAGATCAA
1188  K  L  F  Y  K  C  D  Q  G  Q  A  D  P  V  V  A  V  A  R  D  Q
3789 AGCAGTGTTTACCTGAAACTTCTCATGCATGAGACGCAGCCTCCATCTCATTTCTCCGTCAGC
1209  S  S  V  Y  L  K  L  L  M  H  E  T  Q  P  P  S  H  F  S  V  S
3852 ACAATAACCAGAATATATAGAGGCTATAACCTACTACCAAGCATAACAGACGTCACTATGGAA
1230  T  I  T  R  I  Y  R  G  Y  N  L  L  P  S  I  T  D  V  T  M  E
3915 AATAACCTTTCAAGAGTTATTGCAGCAGTTTCTCATGAACTAATCACATCAACCACCAGAGCA
1251  N  N  L  S  R  V  I  A  A  V  S  H  E  L  I  T  S  T  T  R  A
```

Htt

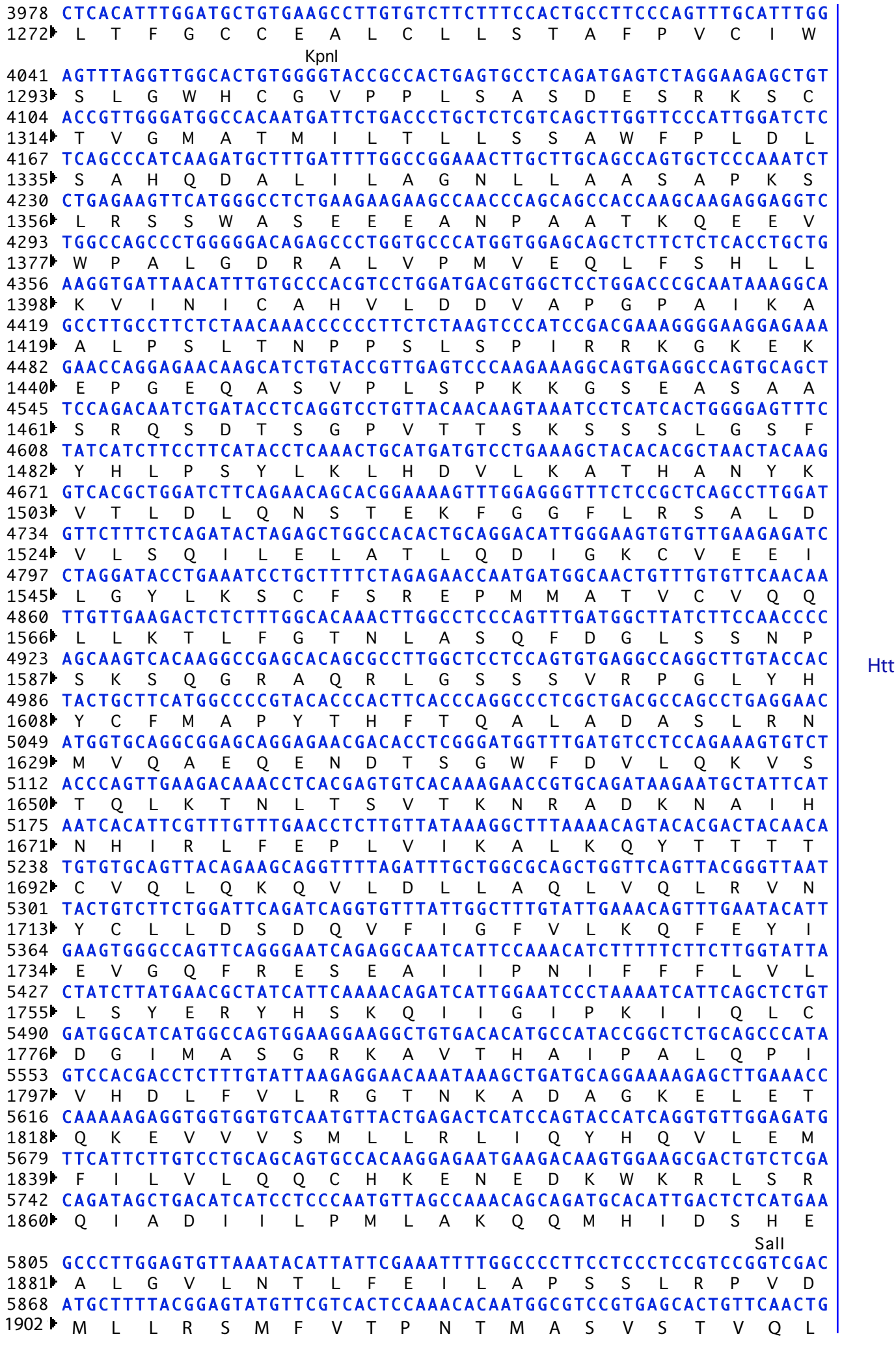
3978 CTCACATTTGGATGCTGTGAAGCCTTGTGTCTTCTTTCCACTGCCTTCCCAGTTTGCATTTGG
1272 L T F G C C E A L C L L S T A F P V C I W
KpnI
4041 AGTTTAGGTTGGCACTGTGGGGTACCGCCACTGAGTGCCTCAGATGAGTCTAGGAAGAGCTGT
1293 S L G W H C G V P P L S A S D E S R K S C
4104 ACCGTTGGGATGGCCACAATGATTCTGACCCTGCTCTCGTCAGCTTGGTTCCCATTGGATCTC
1314 T V G M A T M I L T L L S S A W F P L D L
4167 TCAGCCCATCAAGATGCTTTGATTTTGGCCGGAAACTTGCTTGCAGCCAGTGCTCCCAAATCT
1335 S A H Q D A L I L A G N L L A A S A P K S
4230 CTGAGAAGTTCATGGGCCTCTGAAGAAGAAGCCAACCCAGCAGCCACCAAGCAAGAGGAGGTC
1356 L R S S W A S E E E A N P A A T K Q E E V
4293 TGGCCAGCCCTGGGGGACAGAGCCCTGGTGCCCATGGTGGAGCAGCTCTTCTCTCACCTGCTG
1377 W P A L G D R A L V P M V E Q L F S H L L
4356 AAGGTGATTAACATTTGTGCCCACGTCCTGGATGACGTGGCTCCTGGACCCGCAATAAAGGCA
1398 K V I N I C A H V L D D V A P G P A I K A
4419 GCCTTGCCTTCTCTAACAAACCCCCCTTCTCTAAGTCCCATCCGACGAAAGGGGAAGGAGAAA
1419 A L P S L T N P P S L S P I R R K G K E K
4482 GAACCAGGAGAACAAGCATCTGTACCGTTGAGTCCCAAGAAAGGCAGTGAGGCCAGTGCAGCT
1440 E P G E Q A S V P L S P K K G S E A S A A
4545 TCCAGACAATCTGATACCTCAGGTCCTGTTACAACAAGTAAATCCTCATCACTGGGGAGTTTC
1461 S R Q S D T S G P V T T S K S S S L G S F
4608 TATCATCTTCCTTCATACCTCAAACTGCATGATGTCCTGAAAGCTACACACGCTAACTACAAG
1482 Y H L P S Y L K L H D V L K A T H A N Y K
4671 GTCACGCTGGATCTTCAGAACAGCACGGAAAAGTTTGGAGGGTTTCTCCGCTCAGCCTTGGAT
1503 V T L D L Q N S T E K F G G F L R S A L D
4734 GTTCTTTCTCAGATACTAGAGCTGGCCACACTGCAGGACATTGGGAAGTGTGTTGAAGAGATC
1524 V L S Q I L E L A T L Q D I G K C V E E I
4797 CTAGGATACCTGAAATCCTGCTTTTCTAGAGAACCAATGATGGCAACTGTTTGTGTTCAACAA
1545 L G Y L K S C F S R E P M M A T V C V Q Q
4860 TTGTTGAAGACTCTCTTTGGCACAAACTTGGCCTCCCAGTTTGATGGCTTATCTTCCAACCCC
1566 L L K T L F G T N L A S Q F D G L S S N P
4923 AGCAAGTCACAAGGCCGAGCACAGCGCCTTGGCTCCTCCAGTGTGAGGCCAGGCTTGTACCAC
1587 S K S Q G R A Q R L G S S S V R P G L Y H
4986 TACTGCTTCATGGCCCCGTACACCCACTTCACCCAGGCCCTCGCTGACGCCAGCCTGAGGAAC
1608 Y C F M A P Y T H F T Q A L A D A S L R N
5049 ATGGTGCAGGCGGAGCAGGAGAACGACACCTCGGGATGGTTTGATGTCCTCCAGAAAGTGTCT
1629 M V Q A E Q E N D T S G W F D V L Q K V S
5112 ACCCAGTTGAAGACAAACCTCACGAGTGTCACAAAGAACCGTGCAGATAAGAATGCTATTCAT
1650 T Q L K T N L T S V T K N R A D K N A I H
5175 AATCACATTCGTTTGTTTGAACCTCTTGTTATAAAGGCTTTAAAACAGTACACGACTACAACA
1671 N H I R L F E P L V I K A L K Q Y T T T T
5238 TGTGTGCAGTTACAGAAGCAGGTTTTAGATTTGCTGGCGCAGCTGGTTCAGTTACGGGTTAAT
1692 C V Q L Q K Q V L D L L A Q L V Q L R V N
5301 TACTGTCTTCTGGATTCAGATCAGGTGTTTATTGGCTTTGTATTGAAACAGTTTGAATACATT
1713 Y C L L D S D Q V F I G F V L K Q F E Y I
5364 GAAGTGGGCCAGTTCAGGGAATCAGAGGCAATCATTCCAAACATCTTTTTCTTCTTGGTATTA
1734 E V G Q F R E S E A I I P N I F F F L V L
5427 CTATCTTATGAACGCTATCATTCAAAACAGATCATTGGAATCCCTAAAATCATTCAGCTCTGT
1755 L S Y E R Y H S K Q I I G I P K I I Q L C
5490 GATGGCATCATGGCCAGTGGAAGGAAGGCTGTGACACATGCCATACCGGCTCTGCAGCCCATA
1776 D G I M A S G R K A V T H A I P A L Q P I
5553 GTCCACGACCTCTTTGTATTAAGAGGAACAAATAAAGCTGATGCAGGAAAAGAGCTTGAAACC
1797 V H D L F V L R G T N K A D A G K E L E T
5616 CAAAAAGAGGTGGTGGTGTCAATGTTACTGAGACTCATCCAGTACCATCAGGTGTTGGAGATG
1818 Q K E V V V S M L L R L I Q Y H Q V L E M
5679 TTCATTCTTGTCCTGCAGCAGTGCCACAAGGAGAATGAAGACAAGTGGAAGCGACTGTCTCGA
1839 F I L V L Q Q C H K E N E D K W K R L S R
5742 CAGATAGCTGACATCATCCTCCCAATGTTAGCCAAACAGCAGATGCACATTGACTCTCATGAA
1860 Q I A D I I L P M L A K Q Q M H I D S H E
SalI
5805 GCCCTTGGAGTGTTAAATACATTATTCGAAATTTTGGCCCCTTCCTCCCTCCGTCCGGTCGAC
1881 A L G V L N T L F E I L A P S S L R P V D
5868 ATGCTTTTACGGAGTATGTTCGTCACTCCAAACACAATGGCGTCCGTGAGCACTGTTCAACTG
1902 M L L R S M F V T P N T M A S V S T V Q L
Htt

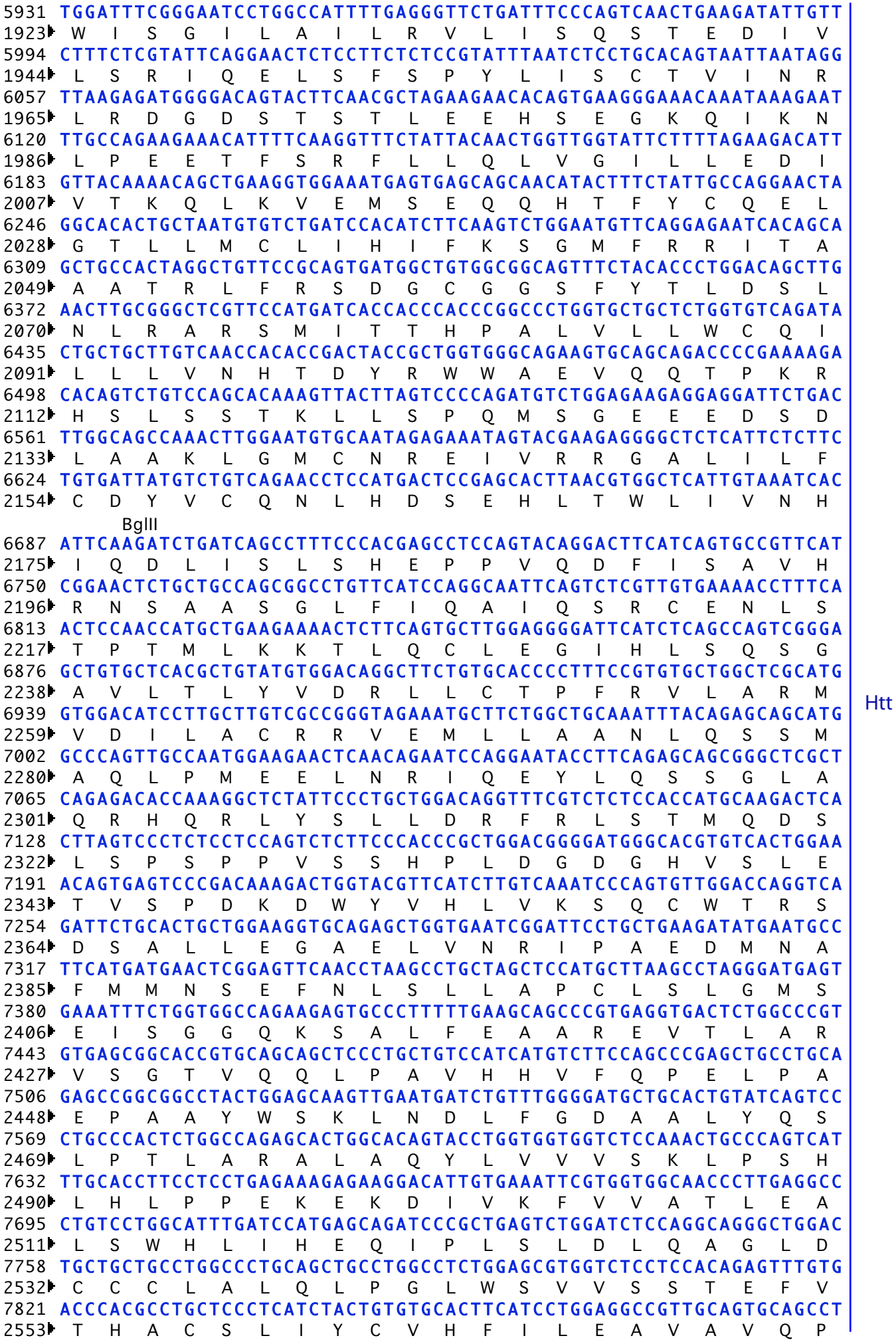
5931 TGGATTTCGGGAATCCTGGCCATTTTGAGGGTTCTGATTTCCCAGTCAACTGAAGATATTGTT
1923 W I S G I L A I L R V L I S Q S T E D I V
5994 CTTTCTCGTATTCAGGAACTCTCCTTCTCTCCGTATTTAATCTCCTGCACAGTAATTAATAGG
1944 L S R I Q E L S F S P Y L I S C T V I N R
6057 TTAAGAGATGGGGACAGTACTTCAACGCTAGAAGAACACAGTGAAGGGAAACAAATAAAGAAT
1965 L R D G D S T S T L E E H S E G K Q I K N
6120 TTGCCAGAAGAAACATTTTCAAGGTTTCTATTACAACTGGTTGGTATTCTTTTAGAAGACATT
1986 L P E E T F S R F L L Q L V G I L L E D I
6183 GTTACAAAACAGCTGAAGGTGGAAATGAGTGAGCAGCAACATACTTTCTATTGCCAGGAACTA
2007 V T K Q L K V E M S E Q Q H T F Y C Q E L
6246 GGCACACTGCTAATGTGTCTGATCCACATCTTCAAGTCTGGAATGTTCAGGAGAATCACAGCA
2028 G T L L M C L I H I F K S G M F R R I T A
6309 GCTGCCACTAGGCTGTTCCGCAGTGATGGCTGTGGCGGCAGTTTCTACACCCTGGACAGCTTG
2049 A A T R L F R S D G C G G S F Y T L D S L
6372 AACTTGCGGGCTCGTTCCATGATCACCACCCACCCGGCCCTGGTGCTGCTCTGGTGTCAGATA
2070 N L R A R S M I T T H P A L V L L W C Q I
6435 CTGCTGCTTGTCAACCACACCGACTACCGCTGGTGGGCAGAAGTGCAGCAGACCCCGAAAAGA
2091 L L L V N H T D Y R W W A E V Q Q T P K R
6498 CACAGTCTGTCCAGCACAAAGTTACTTAGTCCCCAGATGTCTGGAGAAGAGGAGGATTCTGAC
2112 H S L S S T K L L S P Q M S G E E E D S D
6561 TTGGCAGCCAAACTTGGAATGTGCAATAGAGAAATAGTACGAAGAGGGGCTCTCATTCTCTTC
2133 L A A K L G M C N R E I V R R G A L I L F
6624 TGTGATTATGTCTGTCAGAACCTCCATGACTCCGAGCACTTAACGTGGCTCATTGTAAATCAC
2154 C D Y V C Q N L H D S E H L T W L I V N H
BglII
6687 ATTCAAGATCTGATCAGCCTTTCCCACGAGCCTCCAGTACAGGACTTCATCAGTGCCGTTCAT
2175 I Q D L I S L S H E P P V Q D F I S A V H
6750 CGGAACTCTGCTGCCAGCGGCCTGTTCATCCAGGCAATTCAGTCTCGTTGTGAAAACCTTTCA
2196 R N S A A S G L F I Q A I Q S R C E N L S
6813 ACTCCAACCATGCTGAAGAAAACTCTTCAGTGCTTGGAGGGGATTCATCTCAGCCAGTCGGGA
2217 T P T M L K K T L Q C L E G I H L S Q S G
6876 GCTGTGCTCACGCTGTATGTGGACAGGCTTCTGTGCACCCCTTTCCGTGTGCTGGCTCGCATG
2238 A V L T L Y V D R L L C T P F R V L A R M
6939 GTGGACATCCTTGCTTGTCGCCGGGTAGAAATGCTTCTGGCTGCAAATTTACAGAGCAGCATG
2259 V D I L A C R R V E M L L A A N L Q S S M
7002 GCCCAGTTGCCAATGGAAGAACTCAACAGAATCCAGGAATACCTTCAGAGCAGCGGGCTCGCT
2280 A Q L P M E E L N R I Q E Y L Q S S G L A
7065 CAGAGACACCAAAGGCTCTATTCCCTGCTGGACAGGTTTCGTCTCTCCACCATGCAAGACTCA
2301 Q R H Q R L Y S L L D R F R L S T M Q D S
7128 CTTAGTCCCTCTCCTCCAGTCTCTTCCCACCCGCTGGACGGGGATGGGCACGTGTCACTGGAA
2322 L S P S P P V S S H P L D G D G H V S L E
7191 ACAGTGAGTCCCGACAAAGACTGGTACGTTCATCTTGTCAAATCCCAGTGTTGGACCAGGTCA
2343 T V S P D K D W Y V H L V K S Q C W T R S
7254 GATTCTGCACTGCTGGAAGGTGCAGAGCTGGTGAATCGGATTCCTGCTGAAGATATGAATGCC
2364 D S A L L E G A E L V N R I P A E D M N A
7317 TTCATGATGAACTCGGAGTTCAACCTAAGCCTGCTAGCTCCATGCTTAAGCCTAGGGATGAGT
2385 F M M N S E F N L S L L A P C L S L G M S
7380 GAAATTTCTGGTGGCCAGAAGAGTGCCCTTTTTGAAGCAGCCCGTGAGGTGACTCTGGCCCGT
2406 E I S G G Q K S A L F E A A R E V T L A R
7443 GTGAGCGGCACCGTGCAGCAGCTCCCTGCTGTCCATCATGTCTTCCAGCCCGAGCTGCCTGCA
2427 V S G T V Q Q L P A V H H V F Q P E L P A
7506 GAGCCGGCGGCCTACTGGAGCAAGTTGAATGATCTGTTTGGGGATGCTGCACTGTATCAGTCC
2448 E P A A Y W S K L N D L F G D A A L Y Q S
7569 CTGCCCACTCTGGCCAGAGCACTGGCACAGTACCTGGTGGTGGTCTCCAAACTGCCCAGTCAT
2469 L P T L A R A L A Q Y L V V V S K L P S H
7632 TTGCACCTTCCTCCTGAGAAAGAGAAGGACATTGTGAAATTCGTGGTGGCAACCCTTGAGGCC
2490 L H L P P E K E K D I V K F V V A T L E A
7695 CTGTCCTGGCATTTGATCCATGAGCAGATCCCGCTGAGTCTGGATCTCCAGGCAGGGCTGGAC
2511 L S W H L I H E Q I P L S L D L Q A G L D
7758 TGCTGCTGCCTGGCCCTGCAGCTGCCTGGCCTCTGGAGCGTGGTCTCCTCCACAGAGTTTGTG
2532 C C C L A L Q L P G L W S V V S S T E F V
7821 ACCCACGCCTGCTCCCTCATCTACTGTGTGCACTTCATCCTGGAGGCCGTTGCAGTGCAGCCT
2553 T H A C S L I Y C V H F I L E A V A V Q P
Htt

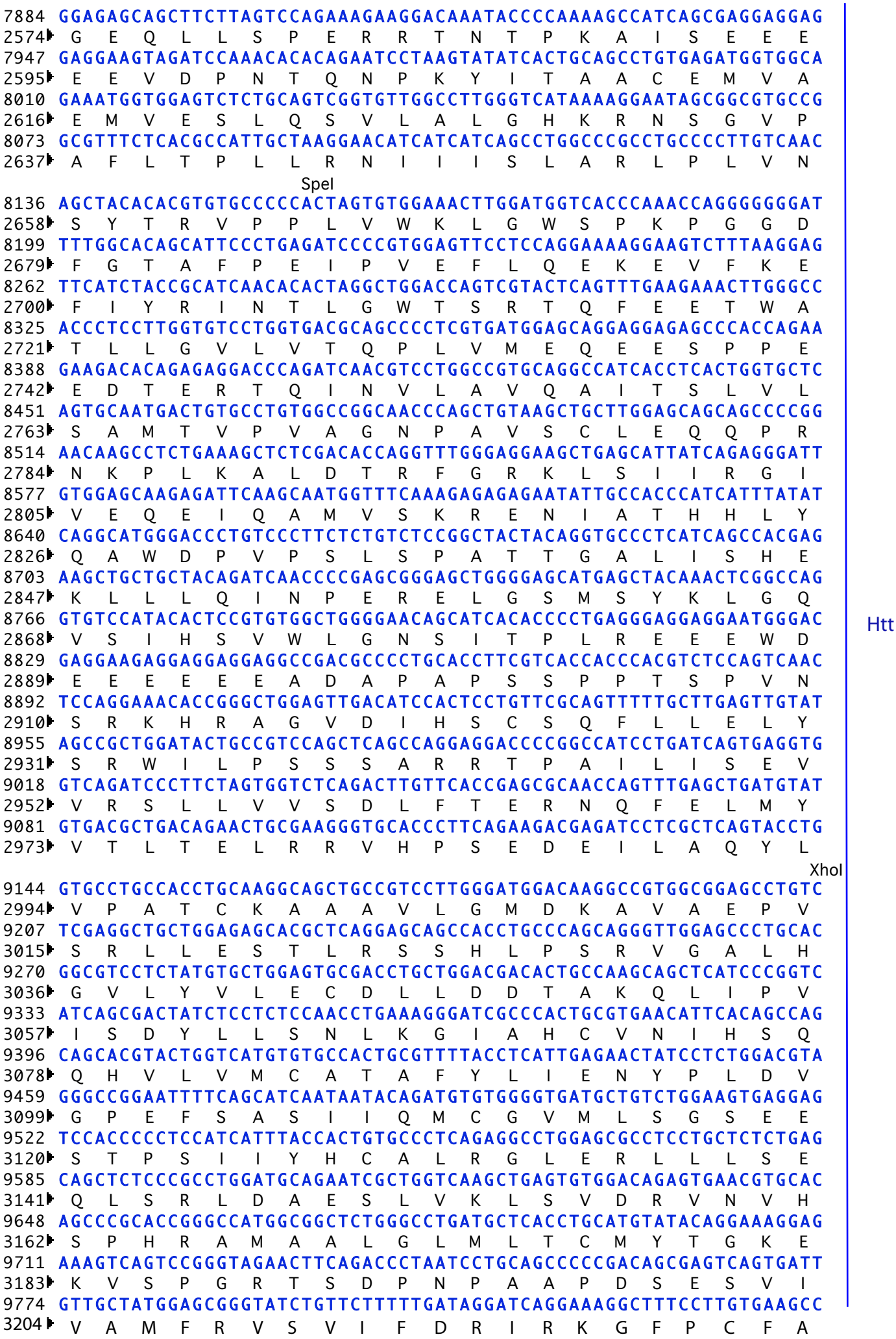
7884 GGAGAGCAGCTTCTTAGTCCAGAAAGAAGGACAAATACCCCAAAAGCCATCAGCGAGGAGGAG
2574 G E Q L L S P E R R T N T P K A I S E E E
7947 GAGGAAGTAGATCCAAACACACAGAATCCTAAGTATATCACTGCAGCCTGTGAGATGGTGGCA
2595 E E V D P N T Q N P K Y I T A A C E M V A
8010 GAAATGGTGGAGTCTCTGCAGTCGGTGTTGGCCTTGGGTCATAAAAGGAATAGCGGCGTGCCG
2616 E M V E S L Q S V L A L G H K R N S G V P
8073 GCGTTTCTCACGCCATTGCTAAGGAACATCATCATCAGCCTGGCCCGCCTGCCCCTTGTCAAC
2637 A F L T P L L R N I I I S L A R L P L V N
SpeI
8136 AGCTACACACGTGTGCCCCCACTAGTGTGGAAACTTGGATGGTCACCCAAACCAGGGGGGGAT
2658 S Y T R V P P L V W K L G W S P K P G G D
8199 TTTGGCACAGCATTCCCTGAGATCCCCGTGGAGTTCCTCCAGGAAAAGGAAGTCTTTAAGGAG
2679 F G T A F P E I P V E F L Q E K E V F K E
8262 TTCATCTACCGCATCAACACACTAGGCTGGACCAGTCGTACTCAGTTTGAAGAAACTTGGGCC
2700 F I Y R I N T L G W T S R T Q F E E T W A
8325 ACCCTCCTTGGTGTCCTGGTGACGCAGCCCCTCGTGATGGAGCAGGAGGAGAGCCCACCAGAA
2721 T L L G V L V T Q P L V M E Q E E S P P E
8388 GAAGACACAGAGAGGACCCAGATCAACGTCCTGGCCGTGCAGGCCATCACCTCACTGGTGCTC
2742 E D T E R T Q I N V L A V Q A I T S L V L
8451 AGTGCAATGACTGTGCCTGTGGCCGGCAACCCAGCTGTAAGCTGCTTGGAGCAGCAGCCCCGG
2763 S A M T V P V A G N P A V S C L E Q Q P R
8514 AACAAGCCTCTGAAAGCTCTCGACACCAGGTTTGGGAGGAAGCTGAGCATTATCAGAGGGATT
2784 N K P L K A L D T R F G R K L S I I R G I
8577 GTGGAGCAAGAGATTCAAGCAATGGTTTCAAAGAGAGAGAATATTGCCACCCATCATTTATAT
2805 V E Q E I Q A M V S K R E N I A T H H L Y
8640 CAGGCATGGGACCCTGTCCCTTCTCTGTCTCCGGCTACTACAGGTGCCCTCATCAGCCACGAG
2826 Q A W D P V P S L S P A T T G A L I S H E
8703 AAGCTGCTGCTACAGATCAACCCCGAGCGGGAGCTGGGGAGCATGAGCTACAAACTCGGCCAG
2847 K L L L Q I N P E R E L G S M S Y K L G Q
8766 GTGTCCATACACTCCGTGTGGCTGGGGAACAGCATCACACCCCTGAGGGAGGAGGAATGGGAC
2868 V S I H S V W L G N S I T P L R E E E E W D
8829 GAGGAAGAGGAGGAGGAGGCCGACGCCCCTGCACCTTCGTCACCACCCACGTCTCCAGTCAAC
2889 E E E E E E A D A P A P S S P P T S P V N
8892 TCCAGGAAACACCGGGCTGGAGTTGACATCCACTCCTGTTCGCAGTTTTTGCTTGAGTTGTAT
2910 S R K H R A G V D I H S C S Q F L L E L Y
8955 AGCCGCTGGATACTGCCGTCCAGCTCAGCCAGGAGGACCCCGGCCATCCTGATCAGTGAGGTG
2931 S R W I L P S S S A R R T P A I L I S E V
9018 GTCAGATCCCTTCTAGTGGTCTCAGACTTGTTCACCGAGCGCAACCAGTTTGAGCTGATGTAT
2952 V R S L L V V S D L F T E R N Q F E L M Y
9081 GTGACGCTGACAGAACTGCGAAGGGTGCACCCTTCAGAAGACGAGATCCTCGCTCAGTACCTG
2973 V T L T E L R R V H P S E D E I L A Q Y L
XhoI
9144 GTGCCTGCCACCTGCAAGGCAGCTGCCGTCCTTGGGATGGACAAGGCCGTGGCGGAGCCTGTC
2994 V P A T C K A A A V L G M D K A V A E P V
9207 TCGAGGCTGCTGGAGAGCACGCTCAGGAGCAGCCACCTGCCCAGCAGGGTTGGAGCCCTGCAC
3015 S R L L E S T L R S S H L P S R V G A L H
9270 GGCGTCCTCTATGTGCTGGAGTGCGACCTGCTGGACGACACTGCCAAGCAGCTCATCCCGGTC
3036 G V L Y V L E C D L L D D T A K Q L I P V
9333 ATCAGCGACTATCTCCTCTCCAACCTGAAAGGGATCGCCCACTGCGTGAACATTCACAGCCAG
3057 I S D Y L L S N L K G I A H C V N I H S Q
9396 CAGCACGTACTGGTCATGTGTGCCACTGCGTTTTACCTCATTGAGAACTATCCTCTGGACGTA
3078 Q H V L V M C A T A F Y L I E N Y P L D V
9459 GGGCCGGAATTTTCAGCATCAATAATACAGATGTGTGGGGTGATGCTGTCTGGAAGTGAGGAG
3099 G P E F S A S I I Q M C G V M L S G S E E
9522 TCCACCCCCTCCATCATTTACCACTGTGCCCTCAGAGGCCTGGAGCGCCTCCTGCTCTCTGAG
3120 S T P S I I Y H C A L R G L E R L L L S E
9585 CAGCTCTCCCGCCTGGATGCAGAATCGCTGGTCAAGCTGAGTGTGGACAGAGTGAACGTGCAC
3141 Q L S R L D A E S L V K L S V D R V N V H
9648 AGCCCGCACCGGGCCATGGCGGCTCTGGGCCTGATGCTCACCTGCATGTATACAGGAAAGGAG
3162 S P H R A M A A L G L M L T C M Y T G K E
9711 AAAGTCAGTCCGGGTAGAACTTCAGACCCTAATCCTGCAGCCCCCGACAGCGAGTCAGTGATT
3183 K V S P G R T S D P N P A A P D S E S V I
9774 GTTGCTATGGAGCGGGTATCTGTTCTTTTTGATAGGATCAGGAAAGGCTTTCCTTGTGAAGCC
3204 V A M F R V S V I F D R I R K G F P C F A
Htt

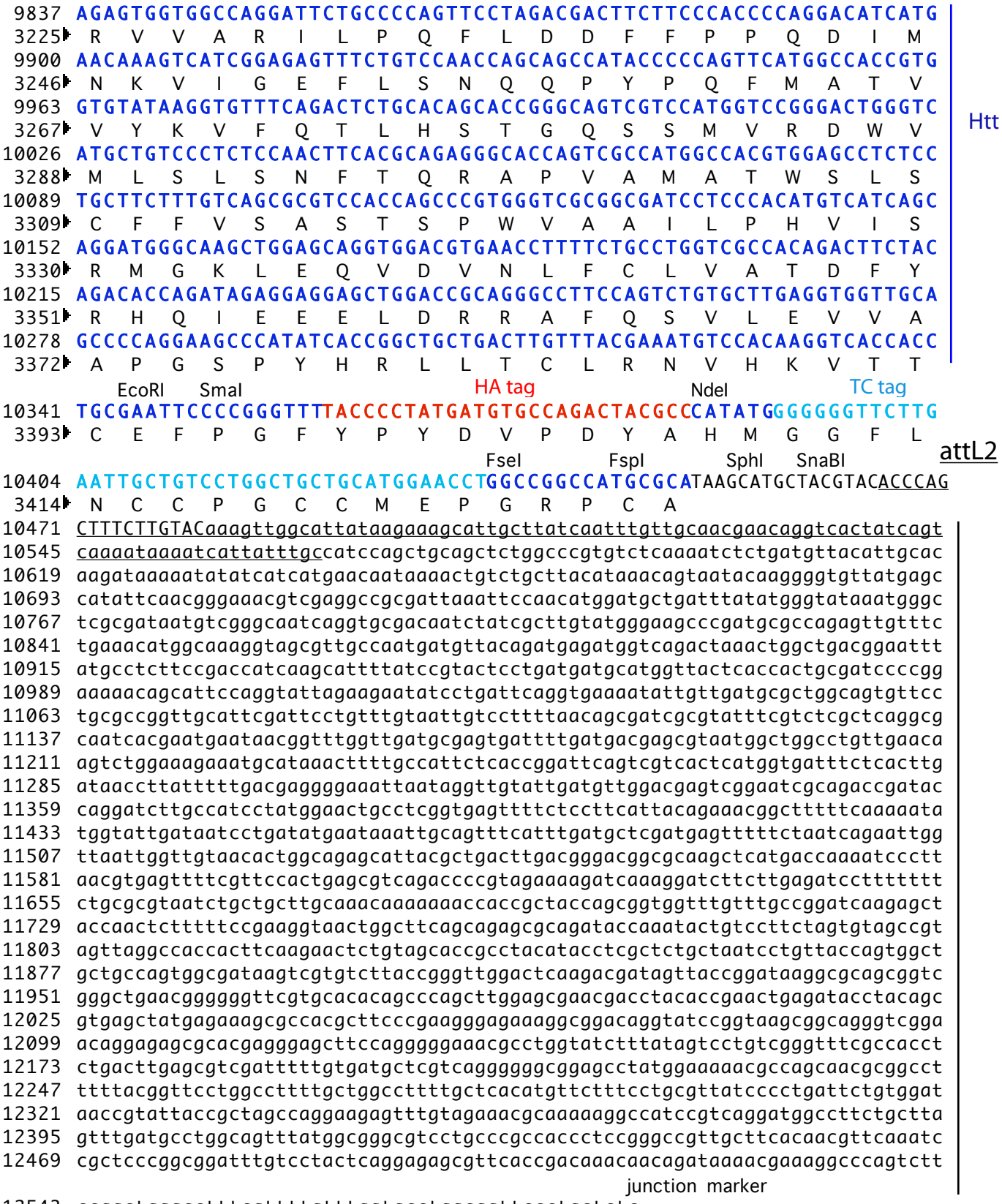
Htt
EcoRI
SmaI
HA tag
NdeI
TC tag
FseI
FspI
SphI
SnaBI
attL2
junction marker

Full name : pARIS-htt-N[His-Cherry]Q100-C[HA-TC]
Used name : pARIS-mCherry-httQ100
vector : pENTRY

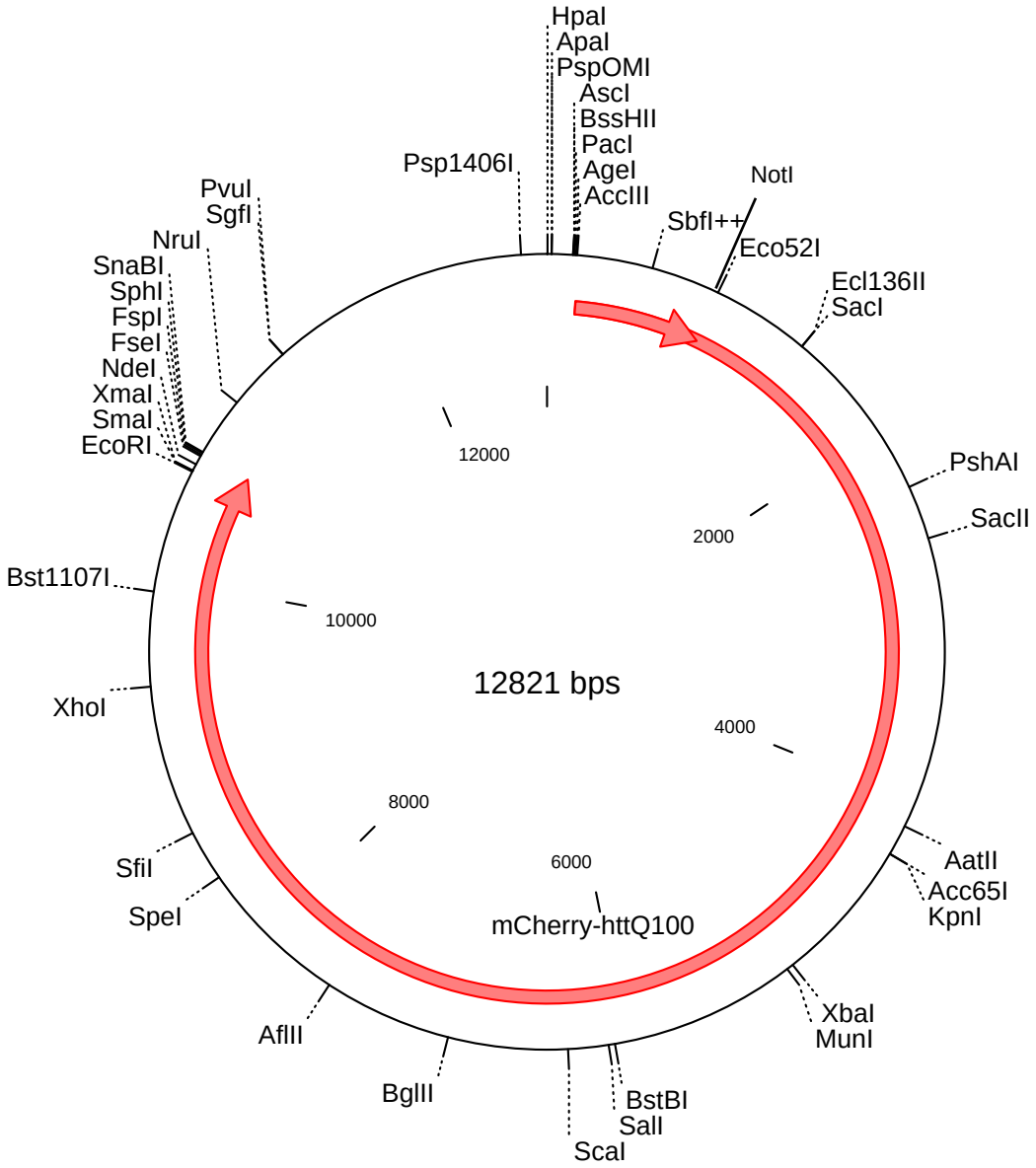

gene : mCherry-httQ100
- start : 165
- end 10682

Molecule: pARIS-mCherry-httQ100, 12821 bps DNA Circular
Description:
File Name: pARIS-mCherry-httQ100.cm5, dated 23 Apr 2010
Printed: List of Sites in bps, sorted by Enzyme name.
Filter ON: cut N <= 1

	#sites	----- Bp position of recognition site -----
AatII	1	4131
Acc65I	1	4292
AccIII	1	155
AflII	1	7592
AgeI	1	149
ApaI	1	24
AscI	1	133
BglII	1	6923
BssHII	1	134
Bst1107I	1	9926
BstBI	1	6060
Ecl136II	1	1419
Eco52I	1	907
EcoRI	1	10575
FseI	1	10665
FspI	1	10674
HpaI	1	3
KpnI	1	4292
MunI	1	5088
NdeI	1	10617
NotI	1	906
NruI	1	10998
PacI	1	141
PshAI	1	2333
Psp1406I	1	12688
PspOMI	1	24
PvuI	1	11340
SacI	1	1419
SacII	1	2614
SalI	1	6093
SbfI	1	548
ScaI	1	6303
SfiI	1	8651
SgfI	1	11339
SgrAI	1	878
SmaI	1	10581
SnaBI	1	10689
SpeI	1	8387
SphI	1	10683
XbaI	1	5052
XhoI	1	9437
XmaI	1	10581

15 Bibliography

Aaku-Saraste, E., Hellwig, A., & Huttner, W. B. (1996). Loss of Occludin and Functional Tight Junctions , but Not ZO-1 , during Neural Tube Closure — Remodeling of the Neuroepithelium Prior to Neurogenesis. *Developmental biology*, *679*(0336), 664–679.

Akhmanova, A., & Hoogenraad, C. C. (2005). Microtubule plus-end-tracking proteins: mechanisms and functions. *Current opinion in cell biology*. doi:10.1016/j.ceb.2004.11.001

Akhmanova, A., & Steinmetz, M. O. (2008). Tracking the ends: a dynamic protein network controls the fate of microtubule tips. *Nature Reviews Molecular Cell Biology*, *9*(April). doi:10.1038/nrm2369

Akhmanova, A., & Steinmetz, M. O. (2010). Microtubule +TIPs at a glance. *Journal of cell science*, *123*(Pt 20), 3415–9. doi:10.1242/jcs.062414

Alberts, B., Alexander, J., Lewis, J., Raff, M., Roberts, K., & Walter, P. (2002). *Molecular Biology of the Cell*. New York: Garland Science. Retrieved from http://www.ncbi.nlm.nih.gov/books/NBK21054/

Albin, R. L., Young, A. B., Penney, J. B., Handelin, B., Balfour, R., Anderson, K. D., Markel, D. S., et al. (1990). Abnormalities of striatal projection neurons and N-methyl-D-aspartate receptors in presymptomatic Huntington's disease. *The New England journal of medicine*, *322*(18), 1293–8. Retrieved from http://www.ncbi.nlm.nih.gov/pubmed/1691447

Alexandre, P., Reugels, A. M., Barker, D., Blanc, E., & Clarke, J. D. W. (2010). Neurons derive from the more apical daughter in asymmetric divisions in the zebrafish neural tube. *Nature neuroscience*, *13*(6), 673–9. doi:10.1038/nn.2547

Ali, N. J., & Levine, M. S. (2006). Changes in Expression of N-Methyl- D -Aspartate Receptor Subunits Occur Early in the R6/2 Mouse Model of Huntington ' s Disease. *Dev Neurosci*, *90095*, 230–238. doi:10.1159/000091921

Anborgh, P. H., Godin, C., Pampillo, M., Dhami, G. K., Dale, L. B., Cregan, S. P., Truant, R., et al. (2005). Inhibition of Metabotropic Glutamate Receptor Signaling by the Huntingtin-binding Protein Optineurin *. *The Journal of biological chemistry*, *280*(41), 34840–34848. doi:10.1074/jbc.M504508200

Andrew, S. E., Goldberg, Y. P., & Hayden, M. R. (1997). Rethinking genotype and phenotype correlations in polyglutamine expansion disorders. *Human molecular genetics*, *6*(12), 90–92.

Anne, S. L., Saudou, F., & Humbert, S. (2007). Phosphorylation of huntingtin by cyclin-dependent kinase 5 is induced by DNA damage and regulates wild-type and mutant huntingtin toxicity in neurons. *The Journal of neuroscience: the official journal of the Society for Neuroscience*, *27*(27), 7318–28. doi:10.1523/JNEUROSCI.1831-07.2007

Arrasate, M., Mitra, S., Schweitzer, E. S., Segal, M. R., & Finkbeiner, S. (2004). Inclusion body formation reduces levels of mutant huntingtin and the risk of neuronal death. *Nature*, *431*(October).

Asami, M., Pilz, G. a, Ninkovic, J., Godinho, L., Schroeder, T., Huttner, W. B., & Götz, M. (2011). The role of Pax6 in regulating the orientation and mode of cell division of progenitors in the mouse cerebral cortex. *Development (Cambridge, England)*, *138*(23), 5067–78. doi:10.1242/dev.074591

Attardo, A., Calegari, F., Haubensak, W., Wilsch-Brauninger, M., & Huttner, W. B. (2008). Live Imaging at the Onset of Cortical Neurogenesis Reveals Differential Appearance of the Neuronal Phenotype in Apical versus Basal Progenitor Progeny. *PloS one*, *3*(6), 14–18. doi:10.1371/journal.pone.0002388

Atwal, R. S., Desmond, C. R., Caron, N., Maiuri, T., Xia, J., Sipione, S., & Truant, R. (2011). Kinase inhibitors modulate huntingtin cell localization and toxicity. *Nature Chemical Biology*, *7*(7), 452–453. doi:10.1038/nchembio.582

Atwal, R. S., & Truant, R. (2008). A stress sensitive ER membrane-association domain in htt protein defines a potential rol for htt in the regulation of autophagy. *Trends in biochemical sciences*, (January), 91–93.

Aylward, E. H. (2007). Change in MRI striatal volumes as a biomarker in preclinical Huntington ' s disease. *Brain research bulletin*, *72*, 152–158. doi:10.1016/j.brainresbull.2006.10.028

Azimzadeh, J., & Bornens, M. (2007). Structure and duplication of the centrosome Structure and Duplication of the Centrosome. *Journal of cell science*, *2*, 2139–2142. doi:10.1242/jcs.005231

Bae, B., Xu, H., Igarashi, S., Fujimuro, M., Agrawal, N., Taya, Y., Hayward, S. D., et al. (2005). p53 Mediates Cellular Dysfunction and Behavioral Abnormalities in Huntington ' s Disease. *Neuron*, *47*, 29–41. doi:10.1016/j.neuron.2005.06.005

Baena-López, L. A., Baonza, A., & García-bellido, A. (2005). The Orientation of Cell Divisions Determines the Shape of Drosophila Organs. *Current biology*, *15*, 1640–1644. doi:10.1016/j.cub.2005.07.062

Ballas, N., Grunseich, C., Lu, D. D., Speh, J. C., & Mandel, G. (2005). REST and Its Corepressors Mediate Plasticity of Neuronal Gene Chromatin throughout Neurogenesis. *Cell*, *121*, 645–657. doi:10.1016/j.cell.2005.03.013

Bamford, N. S., Robinson, S., Palmiter, R. D., Joyce, J. A., Moore, C., & Meshul, C. K. (2004). Dopamine Modulates Release from Corticostriatal Terminals. *The Journal of Neuroscience*, *24*(43), 9541–9552. doi:10.1523/JNEUROSCI.2891-04.2004

Baquet, Z. C., Gorski, J. A., & Jones, K. R. (2004). Early striatal dendrite deficits followed by neuron loss with advanced age in the absence of anterograde cortical brain-derived neurotrophic

factor. *The Journal of neuroscience : the official journal of the Society for Neuroscience*, *24*(17), 4250–8. doi:10.1523/JNEUROSCI.3920-03.2004

Barkovich, A. J., Kuzniecky, R. I., Dobyns, W. B., Jackson, G. D., Becker, L. E., & Evrard, P. (1996). A classification scheme for malformations of cortical development. *Neuropediatrics*, *27*(2), 59–63. doi:10.1055/s-2007-973750

Bates, G. (2003). Rapid review Huntingtin aggregation and toxicity in Huntington ' s disease. *Lancet*, 1642–1644.

Bates, G. P., MacDonald, M. E., Baxendale, S., Youngman, S., Lin, C., Whaley, W. L., Wasmuth, J. J., et al. (1991). Defined physical limits of the Huntington disease gene candidate region. *American journal of human genetics*, *49*(1), 7–16. Retrieved from http://www.pubmedcentral.nih.gov/articlerender.fcgi?artid=1683226&tool=pmcentrez&rendertype=abstract

Baye, L. M., & Link, B. A. (2007). Nuclear migration during retinal development. *Brain Research*, *92*. doi:10.1016/j.brainres.2007.05.021

Beighton, P., & Hayden, M. R. (1981). Huntington's chorea. *South African medical journal = Suid-Afrikaanse tydskrif vir geneeskunde*, *59*(8), 250. Retrieved from http://www.ncbi.nlm.nih.gov/pubmed/6451036

Bellaiche, Y., & Gotta, M. (2005). Heterotrimeric G proteins and regulation of size asymmetry during cell division. *Current Opinion in Cell Biology*, 658–663. doi:10.1016/j.ceb.2005.10.002

Bement, W. M., Benink, H. a, & von Dassow, G. (2005). A microtubule-dependent zone of active RhoA during cleavage plane specification. *The Journal of cell biology*, *170*(1), 91–101. doi:10.1083/jcb.200501131

Benn, C L, Slow, E. J., & Farrell, L. A. (2007). GLUTAMATE RECEPTOR ABNORMALITIES IN THE YAC128 TRANSGENIC MOUSE MODEL OF HUNTINGTON ' S DISEASE. *Neuroscience*, *147*, 354–372. doi:10.1016/j.neuroscience.2007.03.010

Benn, Caroline L, Landles, C., Li, H., Strand, A. D., Woodman, B., Sathasivam, K., Li, S., et al. (2005). Contribution of nuclear and extranuclear polyQ to neurological phenotypes in mouse models of Huntington ' s disease. *Human molecular genetics*, *14*(20), 3065–3078. doi:10.1093/hmg/ddi340

Bennett, E. J., Bence, N. F., Jayakumar, R., & Kopito, R. R. (2005). Global Impairment of the Ubiquitin-Proteasome System by Nuclear or Cytoplasmic Protein Aggregates Precedes Inclusion Body Formation. *Molecular cell*, *17*, 351–365. doi:10.1016/j.molcel.2004.12.021

Bertaux, F., Sharp, A. H., Ross, C. A., Lehrach, H., Bates, G. P., & Wanker, E. (1998). HAP1-huntingtin interactions do not contribute to the molecular pathology in Huntington's disease transgenic mice. *FEBS letters*, *426*(2), 229–32. Retrieved from http://www.ncbi.nlm.nih.gov/pubmed/9599014

Bertrand, N., Castro, D. S., & Guillemot, F. (2002). PRONEURAL GENES AND THE SPECIFICATION OF NEURAL CELL TYPES. *Nature Reviews Neuroscience*, *3*(July). doi:10.1038/nrn874

Betschinger, J., Mechtler, K., & Knoblich, J. (2006). Asymmetric segregation of the tumor suppressor Brat regulates self-renewal in Drosophila neural stem cells. *Cell*, *124*, 1241–1253.

Bett, J. S., Benn, C. L., Ryu, K.-Y., Kopito, R., & Bates, G. P. (2009). The polyubiquitin Ubc gene modulates histone H2A monoubiquitylation in the R6/2 mouse model of Huntington's disease. *J Cell Mol Med*, *13*, 2645–2657. doi:10.1111/j.1582-4934.2008.00543.x.The

Bett, J. S., Cook, C., Petrucelli, L., & Bates, G. P. (2009). The Ubiquitin-Proteasome Reporter GFPu Does Not Accumulate in Neurons of the R6 / 2 Transgenic Mouse Model of Huntington ' s Disease. *PloS one*, *4*(4). doi:10.1371/journal.pone.0005128

Bett, J. S., Goellner, G. M., Woodman, B., Pratt, G., Rechsteiner, M., & Bates, G. P. (2006). Proteasome impairment does not contribute to pathogenesis in R6 / 2 Huntington ' s disease mice: exclusion of proteasome activator REGg as a therapeutic target. *Human molecular genetics*, *15*(1), 33–44. doi:10.1093/hmg/ddi423

Bieling, P., Kandels-Lewis, S., Telley, I. a, van Dijk, J., Janke, C., & Surrey, T. (2008). CLIP-170 tracks growing microtubule ends by dynamically recognizing composite EB1/tubulin-binding sites. *The Journal of cell biology*, *183*(7), 1223–33. doi:10.1083/jcb.200809190

Bobinnec, Y., Khodjakov, A., Mir, L. M., Rieder, C. L., Eddé, B., & Bornens, M. (1998). Centriole disassembly in vivo and its effect on centrosome structure and function in vertebrate cells. *The Journal of cell biology*, *143*(6), 1575–89. Retrieved from http://www.pubmedcentral.nih.gov/articlerender.fcgi?artid=2132987&tool=pmcentrez&rendertype=abstract

Bobinnec, Y., Moudjou, M., Fouquet, J. P., Desbruyères, E., Eddé, B., & Bornens, M. (1998). Glutamylation of centriole and cytoplasmic tubulin in proliferating non-neuronal cells. *Cell motility and the cytoskeleton*, *39*(3), 223–32. Retrieved from http://www.ncbi.nlm.nih.gov/pubmed/9519903

Bolte, S., & Cordelières, F. P. (2006). A guided tour into subcellular colocalization analysis in light microscopy. *Journal of microscopy*, *224*(Pt 3), 213–32. Retrieved from http://www.ncbi.nlm.nih.gov/pubmed/17210054

Boucrot, E., & Kirchhausen, T. (2007). Endosomal recycling controls plasma membrane area during mitosis. *PNAS*, *104*(19), 7939–7944.

Boucrot, E., & Kirchhausen, T. (2008). Mammalian Cells Change Volume during Mitosis. *PLos ONE*. doi:10.1371/journal.pone.0001477

Boutell, J. M., Thomas, P., Neal, J. W., Weston, V. J., Duce, J., Harper, P. S., & Jones, A. L. (1999). Aberrant interactions of transcriptional repressor proteins with the Huntington ' s disease gene product, huntingtin. *Human molecular genetics*, *8*(9), 1647–1655.

Bowman, S. K., Neumüller, R. A., Novatchkova, M., Du, Q., & Knoblich, J. A. (2006). The Drosophila NuMA Homolog Mud regulates spindle orientation in asymmetric cell division. *Developmental cell*, *10*(6), 731–42. doi:10.1016/j.devcel.2006.05.005

Brennan, W. A., Bird, E. D., & Aprille, J. R. (1985). Regional mitochondrial respiratory activity in Huntington's disease brain. *Journal of neurochemistry*, *44*(6), 1948–50. Retrieved from http://www.ncbi.nlm.nih.gov/pubmed/2985766

Bringmann, H., & Hyman, A. A. (2005). A cytokinesis furrow is positioned by two consecutive signals. *Nature*, *436*(August). doi:10.1038/nature03823

Buey, R. M., Sen, I., Kortt, O., Mohan, R., Gfeller, D., Veprintsev, D., Pereda, D., et al. (2012). Sequence determinants of a microtubule tip localization signal (MtLS). *The Journal of cell biology*. doi:10.1074/jbc.M112.373928

Burgess, D. R., & Chang, F. (2005). Site selection for the cleavage furrow at cytokinesis. *Trends in cell biology*, *15*(3). doi:10.1016/j.tcb.2005.01.006

Butterworth, N. J., Williams, L., Bullock, J. Y., Love, D. R., Faull, R. L. M., & Dragunow, M. (1998). TRINUCLEOTIDE (CAG) REPEAT LENGTH IS POSITIVELY CORRELATED WITH THE DEGREE OF DNA FRAGMENTATION IN HUNTINGTON ' S DISEASE STRIATUM. *Neuroscience*, *87*(1), 49–53.

Buttrick, G. J., Beaumont, L. M. a, Leitch, J., Yau, C., Hughes, J. R., & Wakefield, J. G. (2008). Akt regulates centrosome migration and spindle orientation in the early Drosophila melanogaster embryo. *The Journal of cell biology*, *180*(3), 537–48. doi:10.1083/jcb.200705085

Cabernard, C., Prehoda, K. E., & Doe, C. Q. (2010). A spindle-independent cleavage furrow positioning pathway. *Nature*, *467*(7311), 91–94. doi:10.1038/nature09334

Carpi, N., Piel, M., Azioune, A., & Fink, J. (2012). Micropatterning on glass with deep UV. *PROTOCOL EXCHANGE*, 1–9.

Carreno, S., Kouranti, I., Glusman, E. S., Fuller, M. T., Echard, A., & Payre, F. (2008). Moesin and its activating kinase Slik are required for cortical stability and microtubule organization in mitotic cells. *The Journal of cell biology*, *180*(4), 739–746. doi:10.1083/jcb.200709161

Carvalho, P., Gupta, M. L., Hoyt, M. A., & Pellman, D. (2004). Cell cycle control of kinesin-mediated transport of Bik1 (CLIP-170) regulates microtubule stability and dynein activation. *Developmental cell*, *6*(6), 815–29. doi:10.1016/j.devcel.2004.05.001

Carvalho, P., Tirnauer, J. S., & Pellman, D. (2003). Surfing on microtubule ends. *Trends in cell biology*, *13*(5), 229–237. doi:10.1016/S0962-8924(03)00074-6

Cattaneo, E., Zuccato, C., & Tartari, M. (2005). Normal huntingtin function: an alternative approach to Huntington's disease. *Nat. Rev. Neurosci.*, *6*, 919–930.

Caviston, J P, Ross, J. L., Antony, S. M., Tokito, M., & Holzbaur, E. L. (2007). Huntingtin facilitates dynein/dynactin-mediated vesicle transport. *Proc. Natl Acad. Sci. USA*, *104*, 10045–10050.

Caviston, Juliane P, & Holzbaur, E. L. F. (2009). Huntingtin as an essential integrator of intracellular vesicular trafficking. *Trends in cell biology*, *19*(4), 147–55. doi:10.1016/j.tcb.2009.01.005

Cepeda, C., Ariano, M. A., Calvert, C. R., Flores-Hernández, J., Chandler, S. H., Leavitt, B. R., Hayden, M. R., et al. (2001). NMDA receptor function in mouse models of Huntington disease. *Journal of neuroscience research*, *66*(4), 525–39. Retrieved from http://www.ncbi.nlm.nih.gov/pubmed/11746372

Cha, J. J., Kosinski, christoph m, Kerner, julie a, Alsorf, stephen a, Mangiarini, L., Davies, stephen w, Penney, J. B., et al. (1998). Altered brain neurotransmitter receptors in transgenic mice expressing a portion of an abnormal human Huntington disease gene. *PNAS*, *95*(May), 6480–6485.

Chang, D. T. W., Rintoul, G. L., Pandipati, S., & Reynolds, I. J. (2006). Mutant huntingtin aggregates impair mitochondrial movement and trafficking in cortical neurons. *Neurobiology of Disease*, *22*, 388–400. doi:10.1016/j.nbd.2005.12.007

Charrin, B. C., Saudou, F., & Humbert, S. (2005). Axonal transport failure in neurodegenerative disorders: the case of Huntington's disease. *Pathologie Biologie*, *53*, 189–192. doi:10.1016/j.patbio.2004.12.008

Chattopadhyay, B., Ghosh, S., Gangopadhyay, P. K., Das, S. K., Singhal, S., Bhattacharya, A. K., & Bhattacharyya, N. P. (2003). Modulation of age at onset in Huntington ' s disease and spinocerebellar ataxia type 2 patients originated from eastern India. *Neuroscience Letters*, *345*, 93–96. doi:10.1016/S0304-3940(03)00436-1

Che, Y. H., Tamatani, M., & Tohyama, M. (2000). Changes in mRNA for post-synaptic density-95 (PSD-95) and carboxy-terminal PDZ ligand of neuronal nitric oxide synthase following facial nerve transection. *Molecular Brain Research*, 325–335.

Chen, S., Berthelier, V., Hamilton, J. B., Nuallain, B. O., & Wetzel, R. (2002). Amyloid-like Features of Polyglutamine Aggregates and Their Assembly Kinetics. *Biochemistry*, 7391–7399.

Chenn, A., & Walsh, C. A. (2002). Regulation of Cerebral Cortical Size by Control of Cell Cycle Exit in Neural Precursors. *Science*, *297*(2002). doi:10.1126/science.1074192

Chhabra, E. S., & Higgs, H. N. (2007). The many faces of actin : matching assembly factors with cellular structures. *Nature cell biology*, *9*(10).

Colin, E, Regulier, E., Perrin, V., Durr, A., Brice, A., Aebischer, P., Deglon, N., et al. (2005). Akt is altered in an animal model of Huntington's disease and in patients. *Eur. J. Neurosci.*, *21*, 1478–1488.

Colin, Emilie, Zala, D., Liot, G., Rangone, H., Borrell-Pagès, M., Li, X.-J., Saudou, F., et al. (2008). Huntingtin phosphorylation acts as a molecular switch for anterograde/retrograde transport in neurons. *The EMBO journal*, *27*(15), 2124–34. doi:10.1038/emboj.2008.133

Colombo, K., Grill, S. W., Kimple, R. J., Willard, F. S., Siderovski, D. P., & Gönczy, P. (2003). Translation of polarity cues into asymmetric spindle positioning in Caenorhabditis elegans embryos. *Science*, *300*(5627), 1957–61. doi:10.1126/science.1084146

Conde, C., & Cáceres, A. (2009). Microtubule assembly, organization and dynamics in axons and dendrites. *Nature reviews. Neuroscience*, *10*(5), 319–32. doi:10.1038/nrn2631

Connell, J. W., Lindon, C., Luzio, J. P., & Reid, E. (2009). Spastin Couples Microtubule Severing to Membrane Traffic in Completion of Cytokinesis and Secretion. *Traffic*, 42–56. doi:10.1111/j.1600-0854.2008.00847.x

Coquelle, F. M., Caspi, M., Cordelières, F. P., Dompierre, J. P., Dujardin, D. L., Koifman, C., Martin, P., et al. (2002). LIS1 , CLIP-170 ' s Key to the Dynein / Dynactin Pathway. *Molecular and Cellular Biology*, *22*(9), 3089–3102. doi:10.1128/MCB.22.9.3089

Coquelle, F. M., Vitre, B., & Arnal, I. (2009). Structural basis of EB1 effects on microtubule dynamics. *Biochem Soc Trans*, 997–1001. doi:10.1042/BST0370997

Cornett, J., Cao, F., Wang, C., Ross, C. A., Bates, G. P., Li, S., & Li, X. (2005). Polyglutamine expansion of huntingtin impairs its nuclear export. *nature genetics*, *37*(2), 198–204. doi:10.1038/ng1503

Cowan, C. R., & Hyman, A. A. (2007). Acto-myosin reorganization and PAR polarity in C . elegans. *Development*, *1043*, 1035–1043. doi:10.1242/dev.000513

Cui, L., Jeong, H., Borovecki, F., Parkhurst, C. N., Tanese, N., & Krainc, D. (2006). Transcriptional Repression of PGC-1a by Mutant Huntingtin Leads to Mitochondrial Dysfunction and Neurodegeneration. *Cell*, 59–69. doi:10.1016/j.cell.2006.09.015

Datta, S. R., Dudek, H., Tao, X., Masters, S., Fu, H., Gotoh, Y., & Greenberg, M. E. (1997). Akt phosphorylation of BAD couples survival signals to the cell-intrinsic death machinery. *Cell*, *91*(2), 231–41. Retrieved from http://www.ncbi.nlm.nih.gov/pubmed/9346240

DeMali, K. A., & Burridge, K. (2003). Coupling membrane protrusion and cell adhesion. *Journal of Cell Science*. doi:10.1242/jcs.00605

Desai, R. A., Gao, L., Raghavan, S., Liu, W. F., & Chen, C. S. (2009). Cell polarity triggered by cell-cell adhesion via E-cadherin. *Journal of cell science*. doi:10.1242/jcs.028183

Diekmann, H., Anichtchik, O., Fleming, A., Futter, M., Goldsmith, P., Roach, A., & Rubinsztein, D. C. (2009). Decreased BDNF Levels Are a Major Contributor to the Embryonic Phenotype of Huntingtin Knockdown Zebrafish. *The Journal of Neuroscience*, *29*(5), 1343–1349. doi:10.1523/JNEUROSCI.6039-08.2009

Dietrich, P., Shanmugasundaram, R., Shuyu, E., & Dragatsis, I. (2009). Congenital hydrocephalus associated with abnormal subcommissural organ in mice lacking huntingtin in Wnt1 cell lineages. *Human molecular genetics*, *18*(1), 142–150. doi:10.1093/hmg/ddn324

Difiglia, M. (2002). Huntingtin Fragments that Aggregate Go Their Separate Ways. *Molecular cell*, 224–225.

Difiglia, M., Sapp, E., Chase, K., Schwarz, C., Meloni, A., Young, C., Martin, E., et al. (1995). Huntingtin Is a Cytoplasmic Protein Associated with Vesicles in Human and Rat Brain Neurons. *Neuron*, *14*, 1075–1081.

Dikovskaya, D., Zumbrunn, J., Penman, G. A., & Näthke, I. S. (2001). The adenomatous polyposis coli protein : in the limelight out at the edge. *Trends in cell biology*, *11*(9), 378–384.

Dixit, R., Barnett, B., Lazarus, J. E., Tokito, M., Goldman, Y. E., & Holzbaur, E. L. F. (2009). Microtubule plus-end tracking by CLIP-170 requires EB1. *Proceedings of the National Academy of Sciences of the United States of America*, *106*(2), 492–7. doi:10.1073/pnas.0807614106

Djoussé, L., Knowlton, B., Cupples, L. A., & Marder, K. (2002). Weight loss in early stage of Huntington ' s disease. *NEUROLOGY*, 1325–1330.

Dobyns, W. B., & Truwit, C. L. (1995). Lissencephaly and other malformations of cortical development: 1995 update. *Neuropediatrics*, *26*(3), 132–47. doi:10.1055/s-2007-979744

Doherty, G. J., & McMahon, H. T. (2008). Mediation, modulation, and consequences of membrane-cytoskeleton interactions. *Annual review of biophysics*, *37*, 65–95. Retrieved from http://www.ncbi.nlm.nih.gov/pubmed/18573073

Dragatsis, I., Efstratiadis, A., & Zeitlin, S. (1998). Mouse mutant embryos lacking huntingtin are rescued from lethality by wild- type extraembryonic tissues. *Development*, *1539*, 1529–1539.

Dragatsis, I., Levine, M. S., & Zeitlin, S. (2000). Inactivation of Hdh in the brain and testis results in progressive neurodegeneration and sterility in mice. *nature genetics*, *26*(november).

Dragunow, M., Faull, R. L., Lawlor, P., Beilharz, E. J., Singleton, K., Walker, E. B., & Mee, E. (1995). In situ evidence for DNA fragmentation in Huntington's disease striatum and Alzheimer's disease temporal lobes. *Neuroreport*, *6*(7), 1053–7. Retrieved from http://www.ncbi.nlm.nih.gov/pubmed/7632894

Drechsel, D. N., Hyman, A. A., Hall, A., & Glotzer, M. (1996). A requirement for Rho and Cdc42 during cytokinesis in Xenopus embryos. *Current biology*, 12–23.

Du, Q., & Macara, I. G. (2004). Mammalian Pins Is a Conformational Switch that Links NuMA to Heterotrimeric G Proteins. *Cell*, *119*, 503–516.

Dunah, A. W., Jeong, H., Griffin, A., Mouradian, M. M., Young, A. B., & Tanese, N. (2002). Sp1 and TAFII130 Transcriptional Activity Disrupted in Early Huntington ' s Disease. *Science*, *2238*(2002). doi:10.1126/science.1072613

Dunah, A. W., Jeong, H., Griffin, A., Mouradian, M. M., Young, A. B., Tanese, N., & Krainc, D. (2002). Sp1 and TAFII130 Transcriptional Activity Disrupted in Early Huntington ' s Disease. *Science*, *2238*(2002). doi:10.1126/science.1072613

Dupin, I., Camand, E., & Etienne-Manneville, S. (2009). Classical cadherins control nucleus and centrosome position and cell polarity. *The Journal of cell biology*, *185*(5), 779–786. doi:10.1083/jcb.200812034

Duyao, M. P., Auebach, A. B., Ryan, A., Persichetti, F., Barnes, G. T., Mcneil, S. M., Ge, P., et al. (1995). Inactivation of the Mouse Huntington ' s Disease Gene Homolog Hdh. *Science*, (27).

Engelender, S., Sharp, A. H., Colomer, V., Tokito, M. K., Lanahan, A., Worley, P., Holzbaur, E. L. F., et al. (1997). Huntingtin-associated protein 1 (HAP1) interacts with the p150Glued subunit of dynactin. *Human Molecular Genetics*, *6*(13), 2205–2212. doi:10.1093/hmg/6.13.2205

Engler, A. J., Sen, S., Sweeney, H. L., & Discher, D. E. (2006). Matrix Elasticity Directs Stem Cell Lineage Specification. *Cell*, 677–689. doi:10.1016/j.cell.2006.06.044

Erck, C., Peris, L., Andrieux, A., Meissirel, C., Gruber, A. D., Vernet, M., Schweitzer, A., et al. (2005). A vital role of tubulin-tyrosine-ligase for neuronal organization. *Proceedings of the National Academy of Sciences of the United States of America*, *102*(22), 7853–8. doi:10.1073/pnas.0409626102

Estrada-Sánchez, A. M., Montiel, T., Segovia, J., & Massieu, L. (2009). Neurobiology of Disease Glutamate toxicity in the striatum of the R6 / 2 Huntington ' s disease transgenic mice is age-dependent and correlates with decreased levels of glutamate transporters. *Neurobiology of Disease*, *34*(1), 78–86. doi:10.1016/j.nbd.2008.12.017

Etienne-Manneville, S. (2004). Actin and Microtubules in Cell Motility : Which One is in Control ? *Traffic*, (5), 470–477. doi:10.1111/j.1600-0854.2004.00196.x

Etienne-Manneville, S., & Hall, A. (2002). Rho GTPases in cell biology. *Nature Review*, *420*(December), 629–635.

Etienne-Manneville, S., & Hall, A. (2003). Cdc42 regulates GSK-3 b and adenomatous polyposis coli to control cell polarity. *Nature*, *421*(February), 753–756. doi:10.1038/nature01300.1.

Fan, J., Cowan, C. M., Zhang, L. Y. J., Hayden, M. R., & Raymond, L. A. (2009). Interaction of Postsynaptic Density Protein-95 with NMDA Receptors Influences Excitotoxicity in the Yeast Artificial Chromosome Mouse Model of Huntington ' s Disease. *The Journal of Neuroscience*, *29*(35), 10928–10938. doi:10.1523/JNEUROSCI.2491-09.2009

Farkas, L. M., & Huttner, W. B. (2008). The cell biology of neural stem and progenitor cells and its significance for their proliferation versus differentiation during mammalian brain development. *Current opinion in cell biology*, 707–715. doi:10.1016/j.ceb.2008.09.008

Feng, Y, Olson, E. C., Stukenberg, P. T., Flanagan, L. a, Kirschner, M. W., & Walsh, C. a. (2000). LIS1 regulates CNS lamination by interacting with mNudE, a central component of the centrosome. *Neuron*, *28*(3), 665–79. Retrieved from http://www.ncbi.nlm.nih.gov/pubmed/11163258

Feng, Y, & Walsh, C. A. (2001). Protein-protein interactions, cytoskeletal regulation and neuronal migration. *Nature reviews. Neuroscience*, *2*(6), 408–16. doi:10.1038/35077559

Feng, Yuanyi, & Walsh, C. A. (2004). Mitotic Spindle Regulation by Nde1 Controls Cerebral Cortical Size. *Neuron*, *44*, 279–293.

Fernandez-Miñan, A., Martin-Bermudo, M. D., & Gonzalez-Reyes, A. (2007). Integrin Signaling Regulates Spindle Orientation in Drosophila to Preserve the Follicular-Epithelium Monolayer. *Current biology*, *6*, 683–688. doi:10.1016/j.cub.2007.02.052

Ferrante, R. J., Kubilus, J. K., Lee, J., Ryu, H., Beesen, A., Zucker, B., Smith, K., et al. (2003). Histone Deacetylase Inhibition by Sodium Butyrate Chemotherapy Ameliorates the Neurodegenerative Phenotype in Huntington ' s Disease Mice. *The Journal of Neuroscience*, *23*(28), 9418–9427.

Fietz, S. A., Kelava, I., Vogt, J., Wilsch-bräuninger, M., Stenzel, D., Fish, J. L., Corbeil, D., et al. (2010). OSVZ progenitors of human and ferret neocortex are epithelial-like and expand by integrin signaling. *Nature neuroscience*, *13*(6), 690–699. doi:10.1038/nn.2553

Fink, J., Carpi, N., Betz, T., Bétard, A., Chebah, M., Azioune, A., Bornens, M., et al. (2011). External forces control mitotic spindle positioning. *Nature cell biology*, *13*(6), 1–10. doi:10.1038/ncb2269

Fishell, G., & Kriegstein, A. (2005). Cortical Development : New Concepts Overview. *Neuron*, *46*, 361–362. doi:10.1016/j.neuron.2005.04.016

Fishell, G., & Kriegstein, A. R. (2003). Neurons from radial glia : the consequences of asymmetric inheritance. *Current Opinion in Neurobiology*, 34–41. doi:10.1016/S0959-4388(03)00013-8

Foe, V. E., & von Dassow, G. (2008). Stable and dynamic microtubules coordinately shape the myosin activation zone during cytokinetic furrow formation. *The Journal of cell biology*, *183*(3), 457–470. doi:10.1083/jcb.200807128

Frederic Saudou Steven Finkbeiner Didier Devys and Michael E. Greenberg. (1998). Huntingtin acts in the nucleus to induce apoptosis but death does not correlate with the formation of intranuclear inclusions. *Cell*, *95*(1), 55–66. Retrieved from http://www.ncbi.nlm.nih.gov/pubmed/9778247

Fujibuchi, T., Abe, Y., Takeuchi, T., Imai, Y., Kamei, Y., Murase, R., Ueda, N., et al. (2005). AIP1/WDR1 supports mitotic cell rounding. *Biochemical and Biophysical Research Communications*, *327*, 268–275. doi:10.1016/j.bbrc.2004.11.156

Gafni, J., & Ellerby, L. M. (2002). Calpain Activation in Huntington's Disease. *The Journal of Neuroscience*, *22*(12), 4842–4849.

Gafni, J., Hermel, E., Young, J. E., Wellington, C. L., Hayden, M. R., & Ellerby, L. M. (2004). Inhibition of Calpain Cleavage of Huntingtin Reduces Toxicity. *The Journal of biological chemistry*, *279*(19), 20211–20220. doi:10.1074/jbc.M401267200

Gage, F. H. (2000). Mammalian Neural Stem Cells. *Science*, *287*(5457), 1433–1438. doi:10.1126/science.287.5457.1433

Galjart, N. (2005). CLIPs and CLASPs and cellular dynamics. *Nature reviews. Molecular cell biology*, *6*(6), 487–98. doi:10.1038/nrm1664

Gambello, M. J., Darling, D. L., Yingling, J., Tanaka, T., Gleeson, J. G., & Wynshaw-Boris, A. (2003). Multiple Dose-Dependent Effects of Lis1 on Cerebral Cortical Development. *The Journal of Neuroscience*, *23*(5), 1719–1729.

Gatlin, J. C., & Bloom, K. (2010). Microtubule motors in eukaryotic spindle assembly and maintenance. *Seminars in cell & developmental biology*, *21*(3), 248–54. Retrieved from http://www.pubmedcentral.nih.gov/articlerender.fcgi?artid=2927864&tool=pmcentrez&rendertype=abstract

Gauthier, L. R., Charrin, C., Dompierre, J. P., Borrell-page, M., Cordelie, F. P., Mey, J. D., Macdonald, M. E., et al. (2004). Huntingtin Controls Neurotrophic Support and Survival of Neurons by Enhancing BDNF Vesicular Transport along Microtubules. *Cell*, *118*, 127–138.

Gauthier-Fisher, A., Lin, D. C., Greeve, M., Kaplan, D. R., Rottapel, R., & Miller, F. D. (2009). Lfc and Tctex-1 regulate the genesis of neurons from cortical precursor cells. *Nature neuroscience*, *12*(6). doi:10.1038/nn.2339

Ge, X., Frank, C. L., Calderon de Anda, F., & Tsai, L.-H. (2010). Hook3 interacts with PCM1 to regulate pericentriolar material assembly and the timing of neurogenesis. *Neuron*, *65*(2), 191–203. doi:10.1016/j.neuron.2010.01.011

Geiger, B., Spatz, J. P., & Bershadsky, A. D. (2009). Environmental sensing through focal adhesions. *Nature Reviews Molecular Cell Biology*, *10*. doi:10.1038/nrm2593

Gerber, H.-P., Seipel, K., Georgiev, O., Hofferer, M., Hug, M., Rusconi, S., & Schaffner, W. (1994). Transcriptional Activation Modulated by Homopolymeric Glutamine and Proline Stretches. *Science*, (7).

Gervais, F. G., Singaraja, R., Xanthoudakis, S., Gutekunst, C., Leavitt, B. R., Metzler, M., Hackam, A. S., et al. (2002). Recruitment and activation of caspase- 8 by the Huntingtin-interacting

protein Hip-1 and a novel partner Hippi. *Nature cell biology*, *4*(February), 95–105. doi:10.1038/ncb735

Gillies, T. E., & Cabernard, C. (2011). Cell division orientation in animals. *Current biology*, *21*(15), R599–609. doi:10.1016/j.cub.2011.06.055

Gines, S., Seong, I. S., Fossale, E., Ivanova, E., Trettel, F., Gusella, J. F., Wheeler, V. C., et al. (2003). Specific progressive cAMP reduction implicates energy deficit in presymptomatic Huntington ' s disease knock-in mice. *Human molecular genetics*, *12*(5), 497–508. doi:10.1093/hmg/ddg046

Gleeson, J. G., Allen, K. M., Fox, J. W., Lamperti, E. D., Berkovic, S., Scheffer, I., Cooper, E. C., et al. (1998). Doublecortin, a brain-specific gene mutated in human X-linked lissencephaly and double cortex syndrome, encodes a putative signaling protein. *Cell*, *92*(1), 63–72. Retrieved from http://www.ncbi.nlm.nih.gov/pubmed/9489700

Gleeson, J. G., Lin, P. T., Flanagan, L. A., & Walsh, C. A. (1999). Doublecortin is a microtubule-associated protein and is expressed widely by migrating neurons. *Neuron*, *23*(2), 257–71. Retrieved from http://www.ncbi.nlm.nih.gov/pubmed/10399933

Godin, J. D., Colombo, K., Molina-Calavita, M., Keryer, G., Zala, D., Charrin, B. C., Dietrich, P., et al. (2010). Huntingtin Is Required for Mitotic Spindle Orientation and Mammalian Neurogenesis. *Neuron*, *67*(3), 392–406. doi:10.1016/j.neuron.2010.06.027

Godin, J. D., Poizat, G., Hickey, M. a, Maschat, F., & Humbert, S. (2010). Mutant huntingtin-impaired degradation of β-catenin causes neurotoxicity in Huntington's disease. *The EMBO Journal*, 1–13. doi:10.1038/emboj.2010.117

Goehler, H., Lalowski, M., Stelzl, U., Waelter, S., Stroedicke, M., Worm, U., Droege, A., et al. (2004). A protein interaction network links GIT1, an enhancer of huntingtin aggregation, to Huntington's disease. *Molecular cell*, *15*(6), 853–65. doi:10.1016/j.molcel.2004.09.016

Goffredo, D., Rigamonti, D., Zuccato, C., Tartari, M., Valenza, M., & Cattaneo, E. (2005). Prevention of cytosolic IAPs degradation : a potential pharmacological target in Huntington's Disease. *Pharmacological Research*, *52*, 140–150. doi:10.1016/j.phrs.2005.01.006

Goldberg, Y. P., Nicholson, D. W., Rasper, D. M., Kalchman, M. A., Koide, H. B., Graham, R. K., Bromm, M., et al. (1996). Cleavage of huntingtin by apopain, a proapoptotic cysteine protease, is modulated by the polyglutamine tract. *Nature genetics*, *13*(4), 442–9. Retrieved from http://www.ncbi.nlm.nih.gov/pubmed/8696339

Gong, Y., Mo, C., & Fraser, S. E. (2004). Planar cell polarity signalling controls cell division orientation during zebrafish gastrulation. *Nature*, *430*(August), 689–693. doi:10.1038/nature02789.Published

Goodson, H. V., & Folker, E. S. (2006). CLASPing the cell cortex. *Developmental cell*, *11*(1), 4–5. doi:10.1016/j.devcel.2006.06.011

Goranov, A. I., & Amon, A. (2010). Growth and division — not a one-way road. *Current opinion in cell biology*, 7–9. doi:10.1016/j.ceb.2010.06.004

Gotta, M., Abraham, M. C., & Ahringer, J. (2001). CDC-42 controls early cell polarity and spindle orientation in C. elegans. *Current biology*, *11*(7), 482–8. Retrieved from http://www.ncbi.nlm.nih.gov/pubmed/11412997

Gotta, M., Dong, Y., Peterson, Y. K., Lanier, S. M., & Ahringer, J. (2003). Asymmetrically Distributed C . elegans Homologs of AGS3 / PINS Control Spindle Position in the Early Embryo. *Current biology*, *13*, 1029–1037. doi:10.1016/S

Graham, R. K., Deng, Y., Carroll, J., Vaid, K., Cowan, C., Pouladi, M. A., Metzler, M., et al. (2010). Cleavage at the 586 Amino Acid Caspase-6 Site in Mutant huntingtin Influences Caspase-6 Activation In Vivo. *The Journal of Neuroscience*, *30*(45), 15019–15029. doi:10.1523/JNEUROSCI.2071-10.2010

Graham, R. K., Deng, Y., Slow, E. J., Haigh, B., Bissada, N., Lu, G., Pearson, J., et al. (2006). Cleavage at the Caspase-6 Site Is Required for Neuronal Dysfunction and Degeneration Due to Mutant Huntingtin. *cell*, 1179–1191. doi:10.1016/j.cell.2006.04.026

Graham, R. K., Ehrnhoefer, D. E., & Hayden, M. R. (2011). Caspase-6 and neurodegeneration. *Trends in Neurosciences*, *34*(12), 646–656. doi:10.1016/j.tins.2011.09.001

Gu, M., Gash, M. T., Mann, V. M., Javoy-Agid, F., Cooper, J. M., & Schapira, A. H. (1996). Mitochondrial defect in Huntington's disease caudate nucleus. *Annals of neurology*, *39*(3), 385–9. Retrieved from http://www.ncbi.nlm.nih.gov/pubmed/8602759

Guillemot, F. (2005). Cellular and molecular control of neurogenesis in the mammalian telencephalon. *Current opinion in cell biology*, *17*(6), 639–47. doi:10.1016/j.ceb.2005.09.006

Gunawardena, S., Her, L.-S., Brusch, R. G., Laymon, R. a, Niesman, I. R., Gordesky-Gold, B., Sintasath, L., et al. (2003). Disruption of axonal transport by loss of huntingtin or expression of pathogenic polyQ proteins in Drosophila. *Neuron*, *40*(1), 25–40. Retrieved from http://www.ncbi.nlm.nih.gov/pubmed/14527431

Gundersen, G. G., & Bulinski, J. C. (1986). Distribution of tyrosinated and nontyrosinated alpha-tubulin during mitosis. *The Journal of cell biology*, *102*(3), 1118–26. Retrieved from http://www.pubmedcentral.nih.gov/articlerender.fcgi?artid=2114112&tool=pmcentrez&rendertype=abstract

Gupta, A., Tsai, L.-H., & Wynshaw-Boris, A. (2002). Life is a journey: a genetic look at neocortical development. *Nature reviews. Genetics*, *3*(5), 342–55. doi:10.1038/nrg799

Gupta, K. K., Joyce, M. V., Slabbekoorn, A. R., Zhu, Z. C., Paulson, B. a, Boggess, B., & Goodson, H. V. (2010). Probing interactions between CLIP-170, EB1, and microtubules. *Journal of molecular biology*, *395*(5), 1049–62. doi:10.1016/j.jmb.2009.11.014

Gupta, K. K., Paulson, B. a, Folker, E. S., Charlebois, B., Hunt, A. J., & Goodson, H. V. (2009). Minimal plus-end tracking unit of the cytoplasmic linker protein CLIP-170. *The Journal of biological chemistry*, *284*(11), 6735–42. doi:10.1074/jbc.M807675200

Gusella, J. F., Wexler, N. S., Conneally, P. M., Naylor, S. L., Anderson, M. A., Tanzi, R. E., Watkins, P. C., et al. (1983). A polymorphic DNA marker genetically linked to Huntington's disease. *Nature*, *306*(5940), 234–8. Retrieved from http://www.ncbi.nlm.nih.gov/pubmed/6316146

Gutekunst, C., Li, S., Yi, H., Mulroy, J. S., Kuemmerle, S., Jones, R., Rye, D., et al. (1999). Nuclear and Neuropil Aggregates in Huntington ' s Disease : Relationship to Neuropathology. *The Journal of Neuroscience*, *19*(7), 2522–2534.

Götz, M., & Huttner, W. B. (2005). The cell biology of neurogenesis. *Nature reviews. Molecular cell biology*, *6*(10), 777–88. doi:10.1038/nrm1739

Hack, M. A., Sugimori, M., Lundberg, C., Nakafuku, M., & Götz, M. (2004). Regionalization and fate specification in neurospheres : the role of Olig2 and Pax6. *Molecular and Cellular Neuroscience*, *25*, 664–678. doi:10.1016/j.mcn.2003.12.012

Hackam, A. S., Singaraja, R., Wellington, C. L., Metzler, M., Mccutcheon, K., Zhang, T., Kalchman, M., et al. (1998). The Influence of Huntingtin Protein Size on Nuclear Localization and Cellular Toxicity. *The Journal of cell biology*, *141*(5), 1097–1105.

Hansen, D. V., Lui, J. H., Parker, P. R. L., & Kriegstein, A. R. (2010). Neurogenic radial glia in the outer subventricular zone of human neocortex. *Nature*, *464*(7288), 554–561. doi:10.1038/nature08845

Hattula, K., & Peränen, J. (2000). FIP-2 , a coiled-coil protein , links Huntingtin to Rab8 and modulates cellular morphogenesis. *Current Biology*, 1603–1606.

Haubensak, W., Attardo, A., Denk, W., & Huttner, W. B. (2004). Neurons arise in the basal neuroepithelium of the early mammalian telencephalon: a major site of neurogenesis. *Proceedings of the National Academy of Sciences of the United States of America*, *101*(9), 3196–201. doi:10.1073/pnas.0308600100

Havel, L. S., Wang, C., Wade, B., Huang, B., Li, S., & Li, X. (2011). Preferential accumulation of N-terminal mutant huntingtin in the nuclei of striatal neurons is regulated by phosphorylation. *Human molecular genetics*, *20*(7), 1424–1437. doi:10.1093/hmg/ddr023

Hay, D. G., Sathasivam, K., Tobaben, S., Stahl, B., Marber, M., Mestril, R., Mahal, A., et al. (2004). Progressive decrease in chaperone protein levels in a mouse model of Huntington ' s disease and induction of stress proteins as a therapeutic approach. *Human molecular genetics*, *13*(13), 1389–1405. doi:10.1093/hmg/ddh144

Hayashi, I., & Ikura, M. (2003). Crystal Structure of the Amino-terminal Microtubule-binding Domain of End-binding Protein 1 (EB1)*. *The Journal of biological chemistry*, *278*(38), 36430–36434. doi:10.1074/jbc.M305773200

Hedreen, J. C., Peyser, C. E., Folstein, S. E., & Ross, C. A. (1991). Neuronal loss in layers V and VI of cerebral cortex in Huntington's disease. *Neuroscience letters*, *133*(2), 257–61. Retrieved from http://www.ncbi.nlm.nih.gov/pubmed/1840078

Henshall, T. L., Tucker, B., Lumsden, A. L., Nornes, S., Lardelli, M. T., & Ã, R. I. R. (2009). Selective neuronal requirement for huntingtin in the developing zebrafish. *Human molecular genetics*, *18*(24), 4830–4842. doi:10.1093/hmg/ddp455

Hermel, E., Gafni, J., Propp, S. S., Leavitt, B. R., & Wellington, C. L. (2004). Specific caspase interactions and amplification are involved in selective neuronal vulnerability in Huntington ' s disease. *Cell Death and Differentiation*, 424–438. doi:10.1038/sj.cdd.4401358

Hertwig, O. (1893). Ueber den Werth der ersten Furchungszellen für die Organbildung des Embryo Experimentelle Studien am Frosch-und Tritonei. *Archiv für Mikroskopische Anatomie*, *42*(4), 662–807. Retrieved from http://www.springerlink.com/content/j906223pt316j977/

Hilditch-Maguire, P., Trettel, F., Passani, L. A., Auerbach, A., Persichetti, F., & Macdonald, M. E. (2000). Huntingtin : an iron-regulated protein essential for normal nuclear and perinuclear organelles. *Human molecular genetics*, *9*(19), 2789–2798.

Hirabayashi, Y., & Gotoh, Y. (2005). Stage-dependent fate determination of neural precursor cells in mouse forebrain. *Neuroscience Research*, *51*, 331–336. doi:10.1016/j.neures.2005.01.004

Hirabayashi, Y., Itoh, Y., Tabata, H., Nakajima, K., Akiyama, T., Masuyama, N., & Gotoh, Y. (2004). The Wnt/β-catenin pathway directs neuronal differentiation of cortical neural precursor cells. *Development*, 2791–2801. doi:10.1242/dev.01165

Ho, C., Zhou, J., Medina, M., Goto, T., Jacobson, M., Bhide, P. G., & Kosik, K. S. (2000). delta-catenin is a nervous system-specific adherens junction protein which undergoes dynamic relocalization during development. *The Journal of comparative neurology*, *420*(2), 261–76. Retrieved from http://www.ncbi.nlm.nih.gov/pubmed/10753311

Hockly, E., Richon, V. M., Woodman, B., Smith, D. L., Zhou, X., Rosa, E., Sathasivam, K., et al. (2003). Suberoylanilide hydroxamic acid , a histone deacetylase inhibitor , ameliorates motor deficits in a mouse model of Huntington ' s disease. *PNAS*, (11), 2–7.

Hodgson, J. G., Agopyan, N., Gutekunst, C., Leavitt, B. R., Lepiane, F., Singaraja, R., Smith, D. J., et al. (1999). A YAC Mouse Model for Huntington ' s Disease with Full-Length Mutant Huntingtin , Cytoplasmic Toxicity , and Selective Striatal Neurodegeneration. *Neuron*, *23*, 181–192.

Hoffner, G., Kahlem, P., & Djian, P. (2002). Perinuclear localization of huntingtin as a consequence of its binding to microtubules through an interaction with β-tubulin : relevance to Huntington ' s disease. *Journal of cell science*.

Holbert, S., Dedeoglu, A., Humbert, S., Saudou, F., Ferrante, R. J., & Néri, C. (2003). Cdc42-interacting protein 4 binds to huntingtin: neuropathologic and biological evidence for a role in Huntington's disease. *PNAS*, *100*(5), 2712–7. doi:10.1073/pnas.0437967100

Hollenbeck, P. J. (1996). THE PATTERN AND MECHANISM OF MITOCHONDRIAL TRANSPORT IN AXONS. *Frontiers in Bioscience*, (1), 91–102.

Hollenbeck, P. J., & Saxton, W. M. (2005). The axonal transport of mitochondria. *Journal of Cell Science*. doi:10.1242/jcs.02745

Honnappa, S., Gouveia, S. M., Weisbrich, A., Damberger, F. F., Bhavesh, N. S., Jawhari, H., Grigoriev, I., et al. (2009). An EB1-binding motif acts as a microtubule tip localization signal. *Cell*, *138*(2), 366–76. doi:10.1016/j.cell.2009.04.065

Humbert, S, Bryson, E. A., Cordelieres, F. P., Connors, N. C., Datta, S. R., Finkbeiner, S., Greenberg, M. E., et al. (2002). The IGF-1/Akt pathway is neuroprotective in Huntington's disease and involves Huntingtin phosphorylation by Akt. *Dev Cell*, *2*, 831–7.

Humbert, Sandrine, Bryson, E. A., Cordelières, F. P., Connors, N. C., Datta, S. R., Finkbeiner, S., Greenberg, M. E., et al. (2002). The IGF-1/Akt Pathway Is Neuroprotective in Huntington's Disease and Involves Huntingtin Phosphorylation by Akt. *Developmental Cell*, *2*(6), 831–837. doi:10.1016/S1534-5807(02)00188-0

Huntington, G. (2003). On Chorea, *26*(15), 109–112.

Inaba, M., Yuan, H., Salzmann, V., Fuller, M. T., & Yamashita, Y. M. (2010). E-Cadherin Is Required for Centrosome and Spindle Orientation in Drosophila Male Germline Stem Cells. *PloS ONE*, *5*(8), 1–7. doi:10.1371/journal.pone.0012473

Israsena, N., Hu, M., Fu, W., Kan, L., & Kessler, J. A. (2004). The presence of FGF2 signaling determines whether h-catenin exerts effects on proliferation or neuronal differentiation of neural stem cells. *Developmental biology*, *268*, 220–231. doi:10.1016/j.ydbio.2003.12.024

Ito, K., & Hotta, Y. (1992). Proliferation Pattern of Postembryonic Neuroblasts in the Brain of Drosophila melanogaster. *Developmental biology*, 134–148.

Izaki, T., Kamakura, S., Kohjima, M., & Sumimoto, H. (2006). Two forms of human Inscuteable-related protein that links Par3 to the Pins homologues LGN and AGS3. *Biochemical and Biophysical Research Communications*, *341*, 1001–1006. doi:10.1016/j.bbrc.2006.01.050

Jana, N. R., Zemskov, E. A., Wang, G., & Nukina, N. (2001). Altered proteasomal function due to the expression of polyglutamine-expanded truncated N-terminal huntingtin induces apoptosis by caspase activation through mitochondrial cytochrome c release. *Human molecular genetics*, *10*(10), 1049–1059.

Janke, C., & Bulinski, J. C. (2011). Post-translational regulation of the microtubule cytoskeleton: mechanisms and functions. *Nature reviews. Molecular cell biology*, *12*(12), 773–86. doi:10.1038/nrm3227

Jeong, H., Then, F., Jr, T. J. M., Mazzulli, J. R., Cui, L., Savas, J. N., Voisine, C., et al. (2009). Acetylation Targets Mutant Huntingtin to Autophagosomes for Degradation. *Cell*, *137*(1), 60–72. doi:10.1016/j.cell.2009.03.018

Joberty, G., Petersen, C., Gao, L., & Macara, I. G. (2000). The cell-polarity protein Par6 links Par3 and atypical protein kinase C to Cdc42. *Nature cell biology*, *2*(August).

Johnston, C. a, Hirono, K., Prehoda, K. E., & Doe, C. Q. (2009). Identification of an Aurora-A/PinsLINKER/Dlg spindle orientation pathway using induced cell polarity in S2 cells. *Cell*, *138*(6), 1150–63. doi:10.1016/j.cell.2009.07.041

Johri, A., & Beal, M. F. (2012). Mitochondrial dysfunction in Neurodegenerative diseases. *J Pharmacol Exp Ther*. doi:10.1124/jpet.112.192138

Johri, A., Chaturvedi, R. K., & Beal, M. F. (2011). Hugging tight in Huntington's. *Nature Medicine*, *17*(3). doi:10.1093/hmg/ddr024

Kaji, N., Muramoto, A., & Mizuno, K. (2008). LIM Kinase-mediated Cofilin Phosphorylation during Mitosis Is Required for Precise Spindle Positioning. *The Journal of biological chemistry*, *283*(8), 4983–4992. doi:10.1074/jbc.M708644200

Kalchman, M. A., Koide, H. B., McCutcheon, K., Graham, R. K., Nichol, K., Nishiyama, K., Kazemi-Esfarjani, P., et al. (1997). HIP1, a human homologue of S. cerevisiae Sla2p, interacts with membrane-associated huntingtin in the brain. *Nature genetics*, *16*(1), 44–53. Retrieved from http://www.ncbi.nlm.nih.gov/pubmed/9140394

Kaltenbach, L. S., Romero, E., Becklin, R. R., Chettier, R., Bell, R., Phansalkar, A., Strand, A., et al. (2007). Huntingtin Interacting Proteins Are Genetic Modifiers of Neurodegeneration. *plos genetics*, *3*(5). doi:10.1371/journal.pgen.0030082

Kardon, J. R., & Vale, R. D. (2009). Regulators of the cytoplasmic dynein motor. *Nature reviews. Molecular cell biology*, *10*(12), 854–65. doi:10.1038/nrm2804

Karpuj, M. V., Garren, H., Slunt, H., Price, D. L., Gusella, J., Becher, M. W., & Steinman, L. (1999). Transglutaminase aggregates huntingtin into nonamyloidogenic polymers , and its enzymatic activity increases in Huntington ' s disease brain nuclei. *PNAS*, *96*(June), 7388–7393.

Kassubek, J., Juengling, F. D., Kioschies, T., Henkel, K., Karitzky, J., Kramer, B., Ecker, D., et al. (2004). Topography of cerebral atrophy in early Huntington's disease: a voxel based morphometric MRI study. *J Neurol Neurosurg Psychiatry*, *7*, 213–221.

Kato, M., & Dobyns, W. B. (2003). Lissencephaly and the molecular basis of neuronal migration. *Human molecular genetics*, *12 Spec No*, R89–96. Retrieved from http://www.ncbi.nlm.nih.gov/pubmed/12668601

Kegel, K. B., Kim, M., Sapp, E., Mcintyre, C., Castan, G., & Aronin, N. (2000). Huntingtin Expression Stimulates Endosomal-Lysosomal Activity , Endosome Tubulation , and Autophagy. *The Journal of Neuroscience*, *20*(19), 7268–7278.

Kegel, K. B., Meloni, A. R., Yi, Y., Kim, Y. J., Doyle, E., Cuiffo, B. G., Sapp, E., et al. (2002). Huntingtin Is Present in the Nucleus , Interacts with the Transcriptional Corepressor C-terminal Binding Protein , and Represses Transcription *. *the jounal of biological chemistry*, *277*(9), 7466–7476. doi:10.1074/jbc.M103946200

Keryer, G., Pineda, J. R., Liot, G., Kim, J., Dietrich, P., Benstaali, C., Smith, K., et al. (2011). Ciliogenesis is regulated by a huntingtin- HAP1-PCM1 pathway and is altered in Huntington disease. *The Journal of Clinical Investigation*, (13). doi:10.1172/JCI57552.organelle

Kiechle, T., Dedeoglu, A., Kubilus, J., Kowall, N. W., Beal, M. F., Friedlander, R. M., Hersch, S. M., et al. (2002). Cytochrome C and Caspase-9 Expression in Huntington ' s Disease. *NeuroMolecular Medicine*, *1*, 183–195.

Kimura, K., Ito, M., Amano, M., Chihara, K., Fukata, Y., Nakafuku, M., Yamamori, B., et al. (1996). Regulation of Myosin Phosphatase by Rho and Rho-Associated Kinase (Rho-Kinase). *Science*, (February), 10–13.

Knoblich, J. A. (2001). Asymmetric cell division during animal development. *Nat. Rev. Mol. Cell Biol.*, *2*, 11–20.

Knoblich, J. A. (2010). Asymmetric cell division: recent developments and their implications for tumour biology. *Nature Reviews Molecular Cell Biology*, *11*(12), 849–860. doi:10.1038/nrm3010

Kobielak, A., & Fuchs, E. (2004). α-CATENIN : AT THE JUNCTION OF INTERCELLULAR ADHESION AND ACTIN DYNAMICS. *Nature Reviews*, *5*(August), 614–625. doi:10.1038/nrm1433

Komarova, Y., Lansbergen, G., Galjart, N., Grosveld, F., Borisy, G. G., & Akhmanova, A. (2005). EB1 and EB3 Control CLIP Dissociation from the Ends of Growing Microtubules. *Molecular biology of the cell*, *16*(November), 5334–5345. doi:10.1091/mbc.E05

Konno, D., Shioi, G., Shitamukai, A., Mori, A., Kiyonari, H., Miyata, T., & Matsuzaki, F. (2008). Neuroepithelial progenitors undergo LGN-dependent planar divisions to maintain self-renewability during mammalian neurogenesis. *Nature cell biology*, *10*(1), 93–101. doi:10.1038/ncb1673

Kosodo, Y., Röper, K., Haubensak, W., Marzesco, A.-M., Corbeil, D., & Huttner, W. B. (2004). Asymmetric distribution of the apical plasma membrane during neurogenic divisions of mammalian neuroepithelial cells. *The EMBO journal*, *23*(11), 2314–24. doi:10.1038/sj.emboj.7600223

Kriegstein, A., & Alvarez-Buylla, A. (2009). The glial nature of embryonic and adult neural stem cells. *Annual review of neuroscience*, *32*, 149–84. doi:10.1146/annurev.neuro.051508.135600

Kumar, P., & Wittmann, T. (2012). + TIPs : SxIPping along microtubule ends. *Trends in Cell Biology*, 1–11. doi:10.1016/j.tcb.2012.05.005

Kunda, P., & Baum, B. (2009). The actin cytoskeleton in spindle assembly and positioning. *Trends in cell biology*, *19*(4), 174–9. doi:10.1016/j.tcb.2009.01.006

Kunda, P., Pelling, A. E., Liu, T., & Baum, B. (2008). Moesin Controls Cortical Rigidity, Cell Rounding, and Spindle Morphogenesis during Mitosis. *Current biology*, 91–101. doi:10.1016/j.cub.2007.12.051

Laan, L., Pavin, N., Husson, J., Romet-Lemonne, G., van Duijn, M., López, M. P., Vale, R. D., et al. (2012). Cortical Dynein Controls Microtubule Dynamics to Generate Pulling Forces that Position Microtubule Asters. *Cell*, *148*(3), 502–14. doi:10.1016/j.cell.2012.01.007

Lacroix, B., van Dijk, J., Gold, N. D., Guizetti, J., Aldrian-Herrada, G., Rogowski, K., Gerlich, D. W., et al. (2010). Tubulin polyglutamylation stimulates spastin-mediated microtubule severing. *The Journal of cell biology*, *189*(6), 945–54. doi:10.1083/jcb.201001024

Lansbergen, G., Grigoriev, I., Mimori-Kiyosue, Y., Ohtsuka, T., Higa, S., Kitajima, I., Demmers, J., et al. (2006). CLASPs attach microtubule plus ends to the cell cortex through a complex with LL5beta. *Developmental cell*, *11*(1), 21–32. doi:10.1016/j.devcel.2006.05.012

Laurent, M., Kasas, S., Yersin, A., Scha, T. E., Dietler, G., Verkhovsky, A. B., & Meister, J. (2005). Gradient of Rigidity in the Lamellipodia of Migrating Cells Revealed by Atomic Force Microscopy. *Biophysical Journal*, *89*(July). doi:10.1529/biophysj.104.052316

Leavitt, B. R., Raamsdonk, J. M. V., Shehadeh, J., Fernandes, H., Murphy, Z., Graham, R. K., Wellington, C. L., et al. (2006). Wild-type huntingtin protects neurons from excitotoxicity. *Journal of neurochemistry*, 1121–1129. doi:10.1111/j.1471-4159.2005.03605.x

Lechler, T., & Fuchs, E. (2005). Asymmetric cell divisions promote stratification and differentiation of mammalian skin. *Nature*, *437*(September), 275–280. doi:10.1038/nature03922

Lee, J. K., Mathews, K., Schlaggar, B., Perlmutter, J., Paulsen, J. S., Epping, E., Burmeister, L., et al. (2012). Measures of growth in children at risk for Huntington disease. *Neurology*, *79*(7), 668–74. doi:10.1212/WNL.0b013e3182648b65

Lee, J., Ramos, E. M., & Gillis, T. (2012). Repeat expansion in Huntington disease determines age at onset in a fully dominant fashion. *NEUROLOGY*.

Lee, W. C., Yoshihara, M., & Littleton, J. T. (2004). Cytoplasmic aggregates trap polyglutamine-containing proteins and block axonal transport in a Drosophila model of Huntington's disease. *Proc. Natl. Acad. Sci. USA*, *101*, 3224–3229.

Lee, W.-C. M., Yoshihara, M., & Littleton, J. T. (2004). Cytoplasmic aggregates trap polyglutamine-containing proteins and block axonal transport in a Drosophila model of Huntington's

disease. *Proceedings of the National Academy of Sciences of the United States of America*, *101*(9), 3224–9. doi:10.1073/pnas.0400243101

Li, H., Li, S., Yu, Z., Shelbourne, P., & Li, X. (2001). Huntingtin Aggregate-Associated Axonal Degeneration is an Early Pathological Event in Huntington ' s Disease Mice. *The Journal of Neuroscience*, *21*(21), 8473–8481.

Li, H., Li, S.-H., Johnston, H., Shelbourne, P. F., & Li, X. (2000). Amino-terminal fragments of mutant huntingtin show selective accumulation in striatal neurons and synaptic toxicity. *nature genetics*, *25*(august), 385–389.

Li, H., Wyman, T., Yu, Z., Li, S., & Li, X. (2003). Abnormal association of mutant huntingtin with synaptic vesicles inhibits glutamate release. *Human molecular genetics*, *12*(16), 2021–2030. doi:10.1093/hmg/ddg218

Li, Jian-liang, Hayden, M. R., Almqvist, E. W., Brinkman, R. R., Durr, A., Dode, C., Ross, C. A., et al. (2003). A Genome Scan for Modifiers of Age at Onset in Huntington Disease : The HD MAPS Study. *Am. J. Hum. Genet.*, (Hayden 1981), 682–687.

Li, Jun, Lee, W.-L., & Cooper, J. A. (2005). NudEL targets dynein to microtubule ends through LIS1. *Nature cell biology*, *7*(7), 686–90. doi:10.1038/ncb1273

Li, S., & Li, X. (1998). Aggregation of N-terminal huntingtin is dependent on the length of its glutamine repeats, *7*(5).

Li, S.-H., Gutekunst, C.-A., Hersch, S. M., & Li, X.-J. (1998). Interaction of Huntingtin-Associated Protein with Dynactin P150 Glued. *The Journal of Neuroscience*, *18*(4), 1261–1269.

Li, S.-H., Lam, S., Cheng, A. L., & Li, X. (2000). Intranuclear huntingtin increases the expression of caspase-1 and induces apoptosis. *Human molecular genetics*, *9*(19), 2859–2868.

Li, W., Serpell, L. C., Carter, W. J., Rubinsztein, D. C., & Huntington, J. A. (2006). Expression and Characterization of Full-length Human Huntingtin , an Elongated HEAT Repeat Protein. *The Journal of biological chemistry*, *281*(23), 15916–15922. doi:10.1074/jbc.M511007200

Li, X. J., Li, S. H., Sharp, A. H., Nucifora, F. C., Schilling, G., Lanahan, A., Worley, P., et al. (1995). A huntingtin-associated protein enriched in brain with implications for pathology. *Nature*, *378*(6555), 398–402. Retrieved from http://www.ncbi.nlm.nih.gov/pubmed/7477378

Li, X., Standley, C., Sapp, E., Valencia, A., Qin, Z., Kegel, K. B., Yoder, J., et al. (2009). Mutant Huntingtin Impairs Vesicle Formation from Recycling Endosomes by Interfering with Rab11 Activity. *Molecular and cellular biology*. doi:10.1128/MCB.00420-09

Li, X.-J., Orr, A. L., & Li, S. (2010). Impaired mitochondrial trafficking in Huntington's disease. *Biochimica et Biophysica Acta*, *1802*(1), 62–65. doi:10.1016/j.bbadis.2009.06.008

Liu, Y. F. (1998). Expression of polyglutamine-expanded Huntingtin activates the SEK1-JNK pathway and induces apoptosis in a hippocampal neuronal cell line. *The Journal of biological chemistry*, *273*(44), 28873–7. Retrieved from http://www.ncbi.nlm.nih.gov/pubmed/9786889

Lo Nigro, C., Chong, C. S., Smith, A. C., Dobyns, W. B., Carrozzo, R., & Ledbetter, D. H. (1997). Point mutations and an intragenic deletion in LIS1, the lissencephaly causative gene in isolated lissencephaly sequence and Miller-Dieker syndrome. *Human molecular genetics*, *6*(2), 157–64. Retrieved from http://www.ncbi.nlm.nih.gov/pubmed/9063735

Loulier, K., Lathia, J. D., Marthiens, V., Relucio, J., Mughal, M. R., Tang, C., Coksaygan, T., et al. (2009). beta1 Integrin Maintains Integrity of the Embryonic Neocortical Stem Cell Niche. *PLoS biology*, *7*(8). doi:10.1371/journal.pbio.1000176

Lu, B., Roegiers, F., Jan, L. Y., & Jan, Y. N. (2001). Adherens junctions inhibit asymmetric division in the Drosophila epithelium. *Nature*, *409*(January).

Lui, J. H., Hansen, D. V., & Kriegstein, A. R. (2011). Development and Evolution of the Human Neocortex. *Cell*, *146*(1), 18–36. doi:10.1016/j.cell.2011.06.030

Lunkes, A., & Mandel, J. (1998). A cellular model that recapitulates major pathogenic steps of Huntington ' s disease. *Human molecular genetics*, *7*(9), 1355–1361.

Luo, S., Mizuta, H., & Rubinsztein, D. C. (2008). p21-activated kinase 1 promotes soluble mutant huntingtin self-interaction and enhances toxicity. *Human molecular genetics*, *17*(6), 895–905. doi:10.1093/hmg/ddm362

Luo, S., Vacher, C., Davies, J. E., & Rubinsztein, D. C. (2005). Cdk5 phosphorylation of huntingtin reduces its cleavage by caspases: implications for mutant huntingtin toxicity. *The Journal of cell biology*, *169*(4), 647–656. doi:10.1083/jcb.200412071

Luthi-Carter, R., Strand, A., Peters, N. L., Solano, S. M., Hollingsworth, Z. R., Menon, A. S., Frey, A. S., et al. (2000). Decreased expression of striatal signaling genes in a mouse model of Huntington ' s disease. *Human molecular genetics*, *9*(9), 1259–1272.

MacDonald, M. E., Cheng, S. V., Zimmer, M., Haines, J. L., Poustka, A., Allitto, B., Smith, B., et al. (1989). Clustering of multiallele DNA markers near the Huntington's disease gene. *The Journal of clinical investigation*, *84*(3), 1013–6. Retrieved from http://www.pubmedcentral.nih.gov/articlerender.fcgi?artid=329749&tool=pmcentrez&rendertype=abstract

MacDonald, M. E., Haines, J. L., Zimmer, M., Cheng, S. V., Youngman, S., Whaley, W. L., Wexler, N., et al. (1989). Recombination events suggest potential sites for the Huntington's disease gene. *Neuron*, *3*(2), 183–90. Retrieved from http://www.ncbi.nlm.nih.gov/pubmed/2576211

Maglione, V., Cannella, M., Gradini, R., Cislaghi, G., & Squitieri, F. (2006). Huntingtin fragmentation and increased caspase 3 , 8 and 9 activities in lymphoblasts with heterozygous and

homozygous Huntington ' s disease mutation. *Mechanisms of Ageing and Development*, *127*, 213–216. doi:10.1016/j.mad.2005.09.011

Mangiarini, L., Sathasivam, K., Seller, M., Cozens, B., Harper, A., Hetherington, C., Lawton, M., et al. (1996). Exon 1 of the HD gene with an expanded CAG repeat is sufficient to cause a progressive neurological phenotype in transgenic mice. *Cell*, *87*(3), 493–506. Retrieved from http://www.ncbi.nlm.nih.gov/pubmed/8898202

Markus, S. M., & Lee, W.-L. (2011). Microtubule-dependent path to the cell cortex for cytoplasmic dynein in mitotic spindle orientation. *BioArchitecture*, *3*(October), 209–215.

Marthiens, V., & Ffrench-Constant, C. (2009). Adherens junction domains are split by asymmetric division of embryonic neural stem cells. *EMBO reports*, *10*(5), 5–10. doi:10.1038/embor.2009.36

Marthiens, V., Kazanis, I., Moss, L., Long, K., & Ffrench-Constant, C. (2010). Adhesion molecules in the stem cell niche – more than just staying in shape ? *Journal of cell science*. doi:10.1242/jcs.054312

Martinez-Vicente, M., Talloczy, Z., Wong, E., Tang, G., Koga, H., Kaushik, S., Vries, R. D., et al. (2010). Cargo recognition failure is responsible for inefficient autophagy in Huntington ' s disease. *Nature neuroscience*, *13*(5), 567–576. doi:10.1038/nn.2528

Maynard, C. J., Bottcher, C., Ortega, Z., Smith, R., Florea, B. I., Díaz-herna, M., Bo, C., et al. (2009). Accumulation of ubiquitin conjugates in a polyglutamine disease model occurs without global ubiquitin / proteasome system impairment. *PNAS*, 1–6.

McGuire, J. R., Rong, J., Li, S., & Li, X. (2006). Interaction of Huntingtin-associated Protein-1 with Kinesin Light Chain. *the jounal of biological chemistry*, *281*(6), 3552–3559. doi:10.1074/jbc.M509806200

Mccampbell, A., Taylor, J. P., Taye, A. A., Robitschek, J., Li, M., Walcott, J., Merry, D., et al. (2007). CREB-binding protein sequestration by expanded polyglutamine. *Human Molecular Genetics*, *9*(14), 2197–2202.

Mcneil, S. M., Novelletto, A., Srinidhi, J., Barnes, G., Kornbluth, I., Altherr, M. R., Wasmuth, J. J., et al. (1997). Reduced penetrance of the Huntington ' s disease mutation, *6*(5), 775–779.

Mende-Mueller, L. M., Toneff, T., Hwang, S., Chesselet, M., & Hook, V. Y. H. (2001). Tissue-Specific Proteolysis of Huntingtin (htt) in Human Brain : Evidence of Enhanced Levels of N- and C-Terminal htt Fragments in Huntington ' s Disease Striatum. *The Journal of Neuroscience*, *21*(6), 1830–1837.

Merkle, F. T., Tramontin, A. D., Garcia-Verdugo, J.-M., & Alvarez-Buylla, A. (2004). Radial glia give rise to adult neural stem cells in the subventricular zone. *PNAS*.

Meunier, S., & Vernos, I. (2012). Microtubule assembly during mitosis – from distinct origins to distinct functions ? *Journal of Cell Science*, (June). doi:10.1242/jcs.092429

Milnerwood, A. J., Cummings, D. M., Dallerac, G. m, Brown, J. Y., Vatsavayai, S. C., Hirst, M. C., Rezaie, P., et al. (2006). Early development of aberrant synaptic plasticity in a mouse model of Huntington ' s disease. *Human molecular genetics*, *15*(10), 1690–1703. doi:10.1093/hmg/ddl092

Minc, N., & Piel, M. (2012). Predicting division plane position and orientation. *Trends in cell biology*, *22*(4), 193–200. doi:10.1016/j.tcb.2012.01.003

Mitra, S. K., Hanson, D. A., & Schlaepfer, D. D. (2005). FOCAL ADHESION KINASE : IN COMMAND AND CONTROL OF CELL MOTILITY. *Nature Reviews*, *6*(January), 56–68. doi:10.1038/nrm1549

Mitsushima, M., Toyoshima, F., & Nishida, E. (2009). Dual Role of Cdc42 in Spindle Orientation Control of. *Molecular and Cellular Biology*, *29*(10), 2816–2827. doi:10.1128/MCB.01713-08

Miyata, T. (2008). Development of three-dimensional architecture of the neuroepithelium: Role of pseudostratification and cellular "community." *Develop. Growth Differ*. doi:10.1111/j.1440-169x.2007.00980.x

Miyata, T., Kawaguchi, A., Saito, K., Kawano, M., Muto, T., & Ogawa, M. (2004). Asymmetric production of surface-dividing and non-surface- dividing cortical progenitor cells. *Development*, 3133–3145. doi:10.1242/dev.01173

Molnár, Z., Vasistha, N. A., & Garcia-Moreno, F. (2011). Hanging by the tail : progenitor populations proliferate. *Nature neuroscience*, *14*(5), 538–540. doi:10.1038/nn.2817

Morin, X., & Bellaïche, Y. (2011). Mitotic Spindle Orientation in Asymmetric and Symmetric Cell Divisions during Animal Development. *Developmental cell*, *21*(1), 102–19. doi:10.1016/j.devcel.2011.06.012

Morin, X., Jaouen, F., & Durbec, P. (2007). Control of planar divisions by the G-protein regulator LGN maintains progenitors in the chick neuroepithelium. *Nature neuroscience*, *10*(11), 1440–8. doi:10.1038/nn1984

Moseley, J. B., & Nurse, P. (2010). Essay Cell Division Intersects with Cell Geometry. *Cell*, 189–193. doi:10.1016/j.cell.2010.07.004

Moughamian, A. J., & Holzbaur, E. L. F. (2012). Dynactin Is Required for Transport Initiation from the Distal Axon. *Neuron*, *74*(2), 331–343. doi:10.1016/j.neuron.2012.02.025

Murphy, K. P. S. J., Carter, R. J., Lione, L. A., Mangiarini, L., Mahal, A., Bates, G. P., Dunnett, S. B., et al. (2000). Abnormal Synaptic Plasticity and Impaired Spatial Cognition in Mice Transgenic for Exon 1 of the Human Huntington ' s Disease Mutation. *The Journal of Neuroscience*, *20*(13), 5115–5123.

Murthy, K., & Wadsworth, P. (2008). Dual role for microtubules in regulating cortical contractility during cytokinesis. *Journal of cell science*, 2350–2359. doi:10.1242/jcs.027052

Nasir, J., Floresco, S. B., Kusky, J. R. O., Diewert, V. M., Richman, J. M., Zeisler, J., Borowski, A., et al. (1995). Targeted Disruption of the Huntington ' s Disease Gene Results in Embryonic Lethality and Behavioral and Morphological Changes in Heterozygotes. *Cell*, *81*, 811–823.

Nimnual, A. S., Taylor, L. J., & Bar-Sagi, D. (2003). Redox-dependent downregulation of Rho by Rac. *Nature Cell Biology*, *5*(March). doi:10.1038/ncb938

Noctor, S. C., Martínez-Cerdeño, V., Ivic, L., & Kriegstein, A. R. (2004). Cortical neurons arise in symmetric and asymmetric division zones and migrate through specific phases. *Nature neuroscience*, *7*(2), 136–144. doi:10.1038/nn1172

Noctor, S. C., Martínez-Cerdeño, V., & Kriegstein, A. R. (2008). Distinct Behaviors of Neural Stem and Progenitor Cells Underlie Cortical Neurogenesis. *J Comp Neurol*, *508*(1), 28–44. doi:10.1002/cne.21669.Distinct

Nopoulos, P. C., Aylward, E. H., Ross, C. a, Mills, J. a, Langbehn, D. R., Johnson, H. J., Magnotta, V. a, et al. (2010). Smaller intracranial volume in prodromal Huntington's disease: evidence for abnormal neurodevelopment. *Brain*. doi:10.1093/brain/awq280

Norden, C., Young, S., Link, B. A., & Harris, W. A. (2009). Actomyosin Is the Main Driver of Interkinetic Nuclear Migration in the Retina. *Cell*, *138*(6), 1195–1208. doi:10.1016/j.cell.2009.06.032

Nurse, P. (2000). A Long Twentieth Century of the Cell Cycle and Beyond. *Cell*, *100*, 71–78.

Oliferenko, S., Chew, T. G., & Balasubramanian, M. K. (2009). Positioning cytokinesis. *Genes & Development*, 660–674. doi:10.1101/gad.1772009

Ona, V. O., Li, M., Vonsattel, J. P. G., Andrews, L. J., Khan, S. Q., Chung, W. M., Frey, A. S., et al. (1999). Inhibition of caspase-1 slows disease progression in a mouse model of Huntington ' s disease. *nature*, *399*(May), 263–267.

Ou, G., Stuurman, N., D'Ambrosio, M., & Vale, R. D. (2010). Polarized Myosin Produces Unequal-Size Daughters During Asymmetric Cell Division, *677*(2010). doi:10.1126/science.1196112

O'Connell, C. B., & Wang, Y. (2000). Mammalian Spindle Orientation and Position Respond to Changes in Cell Shape in a Dynein- dependent Fashion. *Molecular biology of the cell*, *11*(May), 1765–1774.

Pal, A., Severin, F., Höpfner, S., & Zerial, M. (2008). Regulation of endosome dynamics by Rab5 and Huntingtin-HAP40 effector complex in physiological versus pathological conditions. *Methods in enzymology*, *438*, 239–57. Retrieved from http://www.ncbi.nlm.nih.gov/pubmed/18413253

Pal, A., Severin, F., Lommer, B., Shevchenko, A., & Zerial, M. (2006). Huntingtin–HAP40 complex is a novel Rab5 effector that regulates early endosome motility and is up-regulated in Huntington's disease. *The Journal of cell biology*, *172*(4). doi:10.1083/jcb.200509091

Paluch, E., van der Gucht, J., & Sykes, C. (2006). Cracking up : symmetry breaking in cellular systems. *The Journal of cell biology*, *175*(5), 687–692. doi:10.1083/jcb.200607159

Panov, A. V., Gutekunst, C., Leavitt, B. R., Hayden, M. R., Burke, J. R., Strittmatter, W. J., & Greenamyre, J. T. (2002). Early mitochondrial calcium defects in Huntington ' s disease are a direct effect of polyglutamines. *Nature neuroscience*, 731–736. doi:10.1038/nn884

Paoletti, P., Vila, I., Rife, M., Lizcano, M., Alberch, J., & Gine, S. (2008). Dopaminergic and Glutamatergic Signaling Crosstalk in Huntington ' s Disease Neurodegeneration : The Role of p25 / Cyclin-Dependent Kinase 5. *The Journal of Neuroscience*, *28*(40), 10090–10101. doi:10.1523/JNEUROSCI.3237-08.2008

Pardo, R., Colin, E., Régulier, E., Aebischer, P., Déglon, N., Humbert, S., & Saudou, F. (2006). Inhibition of calcineurin by FK506 protects against polyglutamine-huntingtin toxicity through an increase of huntingtin phosphorylation at S421. *The Journal of neuroscience : the official journal of the Society for Neuroscience*, *26*(5), 1635–45. doi:10.1523/JNEUROSCI.3706-05.2006

Pardo, R., Molina-Calavita, M., Poizat, G., Keryer, G., Humbert, S., & Saudou, F. (2010). pARIS-htt: an optimised expression platform to study huntingtin reveals functional domains required for vesicular trafficking. *Molecular brain*, *3*, 17. doi:10.1186/1756-6606-3-17

Paulsen, J. S., Nopoulos, P. C., Aylward, E., Ross, C. A., Johnson, H., Magnotta, V. A., Juhl, A., et al. (2010). Striatal and white matter predictors of estimated diagnosis for Huntington disease. *Brain research bulletin*, *82*(3-4), 201–7. doi:10.1016/j.brainresbull.2010.04.003

Peris, L., Thery, M., Fauré, J., Saoudi, Y., Lafanechère, L., Chilton, J. K., Gordon-Weeks, P., et al. (2006). Tubulin tyrosination is a major factor affecting the recruitment of CAP-Gly proteins at microtubule plus ends. *The Journal of cell biology*, *174*(6), 839–49. doi:10.1083/jcb.200512058

Peris, L., Wagenbach, M., Lafanechère, L., Brocard, J., Moore, A. T., Kozielski, F., Job, D., et al. (2009). Motor-dependent microtubule disassembly driven by tubulin tyrosination. *The Journal of cell biology*, *185*(7), 1159–66. doi:10.1083/jcb.200902142

Perutz, M. A. X. F., Johnson, T., Suzuki, M., & Finch, J. T. (1994). Glutamine repeats as polar zippers: Their possible role in inherited neurodegenerative diseases. *PNAS*, *91*(June), 5355–5358.

Peters, M. F., & Ross, C. A. (2001). Isolation of a 40-kDa Huntingtin-associated Protein. *the jounal of biological chemistry*, *276*(5), 3188–3194. doi:10.1074/jbc.M008099200

Peterson, L. J., Rajfur, Z., Maddox, A. S., Freel, C. D., Chen, Y., Edlund, M., Otey, C., et al. (2004). Simultaneous Stretching and Contraction of Stress Fibers In Vivo. *Molecular Biology of the Cell*, *15*(July), 3497–3508. doi:10.1091/mbc.E03

Petit, V., & Thiery, J. P. (2000). Focal adhesions: structure and dynamics. *Biology of the cell / under the auspices of the European Cell Biology Organization*, *92*(7), 477–94. Retrieved from http://www.ncbi.nlm.nih.gov/pubmed/11229600

Peyre, E., Jaouen, F., Saadaoui, M., Haren, L., Merdes, A., Durbec, P., & Morin, X. (2011). A lateral belt of cortical LGN and NuMA guides mitotic spindle movements and planar division in neuroepithelial cells. *The Journal of cell biology*, *193*(1), 141–154. doi:10.1083/jcb.201101039

Peyre, E., & Morin, X. (2012). An oblique view on the role of spindle orientation in vertebrate neurogenesis. *Development, growth & differentiation*, *54*(3), 287–305. doi:10.1111/j.1440-169X.2012.01350.x

Phillips, W., Morton, A. J., & Barker, R. A. (2005). Abnormalities of Neurogenesis in the R6/2 Mouse Model of Huntington ' s Disease Are Attributable to the In Vivo Microenvironment. *The Journal of neuroscience*, *25*(50), 11564–11576. doi:10.1523/JNEUROSCI.3796-05.2005

Piel, M., Meyer, P., Khodjakov, A., Rieder, C. L., & Bornens, M. (2000). The Respective Contributions of the Mother and Daughter Centrioles to Centrosome Activity and Behavior in Vertebrate Cells. *The Journal of Cell Biology*, *149*(2), 317–329.

Piel, M., & Tran, P. T. (2009). Cell Shape and Cell Division in Fission Yeast. *Current Biology*, *19*(17), R823–R827. doi:10.1016/j.cub.2009.08.012

Pineda, J. R., Pardo, R., Zala, D., Yu, H., Humbert, S., & Saudou, F. (2009). Genetic and pharmacological inhibition of calcineurin corrects the BDNF transport defect in Huntington's disease. *Molecular brain*, *2*(1), 33. doi:10.1186/1756-6606-2-33

Piperno, G., LeDizet, M., & Chang, X. J. (1987). Microtubules containing acetylated alpha-tubulin in mammalian cells in culture. *The Journal of cell biology*, *104*(2), 289–302. Retrieved from http://www.pubmedcentral.nih.gov/articlerender.fcgi?artid=2114420&tool=pmcentrez&rendertype=abstract

Politis, M., Pavese, N., Tai, F., Tabrizi, S. J., Barker, R. A., & Piccini, P. (2008). Hypothalamic involvement in Huntington ' s disease : an in vivo PET study. *Brain*, 2860–2869. doi:10.1093/brain/awn244

Portera-Cailliau, C., Hedreen, J. C., Price, D. L., & Koliatsos, V. E. (1995). Evidence for Apoptotic Cell Death in Huntington Excitotoxic Animal Models Disease and. *The Journal of Neuroscience*, *15*(May), 3775–3787.

Postiglione, M. P., Jüschke, C., Xie, Y., Haas, G. a, Charalambous, C., & Knoblich, J. a. (2011). Mouse inscuteable induces apical-basal spindle orientation to facilitate intermediate progenitor

generation in the developing neocortex. *Neuron*, *72*(2), 269–84. doi:10.1016/j.neuron.2011.09.022

Poulson, N. D., & Lechler, T. (2010). Robust control of mitotic spindle orientation in the developing epidermis. *The Journal of cell biology*, *191*(5), 915–922. doi:10.1083/jcb.201008001

Powers, W. J., Videen, T. O., Markham, J., Mcgee-minnich, L., Antenor-dorsey, J. V., Hershey, T., & Perlmutter, J. S. (2007). Selective defect of in vivo glycolysis in early Huntington ' s disease striatum. *PNAS*, *104*(8).

Pramparo, T., Youn, Y. H., Yingling, J., Hirotsune, S., & Wynshaw-Boris, A. (2010). Novel embryonic neuronal migration and proliferation defects in Dcx mutant mice are exacerbated by Lis1 reduction. *The Journal of Neuroscience*, *30*(8), 3002–12. doi:10.1523/JNEUROSCI.4851-09.2010

Quyn, A. J., Appleton, P. L., Carey, F. A., Steele, R. J. C., Barker, N., Clevers, H., Ridgway, R. A., et al. (2010). Spindle orientation bias in gut epithelial stem cell compartments is lost in precancerous tissue. *Cell stem cell*, *6*(2), 175–81. Retrieved from http://www.ncbi.nlm.nih.gov/pubmed/20144789

Radulescu, A. E., & Cleveland, D. W. (2010). NuMA after 30 years : the matrix revisited. *Trends in Cell Biology*, *20*(4), 214–222. doi:10.1016/j.tcb.2010.01.003

Ranen, N. G., Stine, C., Abbott, M. H., Sherr, M., Codori, A., Franz, M. L., Chao, N., et al. (1995). Anticipation and Instability of IT- IS (CAG) N Repeats in Parent- Offspring Pairs with Huntington Disease. *Am. J. Hum. Genet.*, 593–602.

Rangone, H., Poizat, G., Troncoso, J., Ross, C. A., Macdonald, M. E., & Humbert, S. (2004). The serum- and glucocorticoid-induced kinase SGK inhibits mutant huntingtin-induced toxicity by phosphorylating serine 421 of huntingtin. *European Journal of Neuroscience*, *19*(October 2003), 273–279. doi:10.1111/j.1460-9568.2003.03131.x

Rappaport, R. (2005). *Cytokinesis in Animal Cells* (Vol. 8, p. 404). Cambridge University Press. Retrieved from http://books.google.com/books?hl=fr&lr=&id=psvR8DxOsRoC&pgis=1

Rauzi, M., Verant, P., Lecuit, T., & Lenne, P.-F. (2008). Nature and anisotropy of cortical forces orienting Drosophila tissue morphogenesis. *Nature cell biology*, *10*(12). doi:10.1038/ncb1798

Ravikumar, B., Vacher, C., Berger, Z., Davies, J. E., Luo, S., Oroz, L. G., Scaravilli, F., et al. (2004). Inhibition of mTOR induces autophagy and reduces toxicity of polyglutamine expansions in fly and mouse models of Huntington disease. *nature genetics*, *36*(6), 585–595. doi:10.1038/ng1362

Raymond, L. a, André, V. M., Cepeda, C., Gladding, C. M., Milnerwood, a J., & Levine, M. S. (2011). Pathophysiology of Huntington's disease: time-dependent alterations in synaptic and receptor function. *Neuroscience*, *198*, 252–73. doi:10.1016/j.neuroscience.2011.08.052

Regnard, C., Desbruyères, E., Denoulet, P., & Eddé, B. (1999). Tubulin polyglutamylase : isozymic variants and regulation during the cell cycle in HeLa cells. *Journal of cell science*, *4289*, 4281–4289.

Reillo, I., Romero, C. D. J., Garcia-Cabezas, M. A., & Borrell, V. (2011). A Role for Intermediate Radial Glia in the Tangential Expansion of the Mammalian Cerebral Cortex. *Cerebral Cortex*, (July). doi:10.1093/cercor/bhq238

Reiner, A., Dragatsis, I., Zeitlin, S., & Goldowitz, D. (2003). Wild-Type Huntingtin Plays a Role in Brain Development and Neuronal Survival. *Molecular neurobiology*, *28*(3), 259–275.

Reiner, A., Mar, N. D., Meade, C. A., Yang, H., Dragatsis, I., Zeitlin, S., & Goldowitz, D. (2001). Neurons Lacking Huntingtin Differentially Colonize Brain and Survive in Chimeric Mice. *The Journal of Neuroscience*, *21*(19), 7608–7619.

Reiner, O., Carrozzo, R., Shen, Y., Wehnert, M., Faustinella, F., Dobyns, W. B., Caskey, C. T., et al. (1993). Isolation of a Miller-Dieker lissencephaly gene containing G protein beta-subunit-like repeats. *Nature*, *364*(6439), 717–21. doi:10.1038/364717a0

Revenu, C., Athman, R., Robine, S., & Louvard, D. (2004). THE CO-WORKERS OF ACTIN FILAMENTS : FROM CELL STRUCTURES TO SIGNALS. *Nature Reviews Molecular Cell Biology*, *5*(August). doi:10.1038/nrm1437

Ridley, A. J., & Hall, A. (1992). The Small GTP-Binding Protein rho Regulates the Assembly of Focal Adhesions and Actin Stress Fibers in Response to Growth Factors. *Cell*, *70*, 389–399.

Rigamonti, D., Bauer, J. H., De-fraja, C., Conti, L., Sipione, S., Sciorati, C., Clementi, E., et al. (2000). Wild-Type Huntingtin Protects from Apoptosis Upstream of Caspase-3. *The Journal of Neuroscience*, *20*(10), 3705–3713.

Rigamonti, D., Sipione, S., Goffredo, D., Zuccato, C., Fossale, E., & Cattaneo, E. (2001). Huntingtin ' s Neuroprotective Activity Occurs via Inhibition of procaspase-9 processing. *The Journal of biological chemistry*, (4), 14545–14548. doi:10.1074/jbc.C100044200

Rong, J., Li, S.-H., & Li, X.-J. (2007). Regulation of intracellular HAP1 trafficking. *Journal of neuroscience research*, *85*(14), 3025–9. Retrieved from http://www.ncbi.nlm.nih.gov/pubmed/17474105

Rosas, H. D., Liu, A. K., Hersch, S., Glessner, M., Ferrante, R. J., Salat, D., van der Kouwe, A., et al. (2002). Regional and progressive thinning of the cortical ribbon in Huntington ' s disease. *NEUROLOGY*, *05886*, 695–701.

Rosenblatt, A. (2007). Neuropsychiatry of Huntington's disease. *Dialogues in Clinical Neuroscience*, 191–197.

Roszko, I., Afonso, C., Henrique, D., & Mathis, L. (2006). Key role played by RhoA in the balance between planar and apico-basal cell divisions in the chick neuroepithelium. *Developmental biology*, *298*, 212–224. doi:10.1016/j.ydbio.2006.06.031

Rotsch, C., & Radmacher, M. (2000). Drug-Induced Changes of Cytoskeletal Structure and Mechanics in Fibroblasts : An Atomic Force Microscopy Study. *Biophysical Journal*, *78*(January), 520–535.

Rubinsztein, D. C., Leggo, J., Coles, R., Almqvist, E., Biancalana, V., Cassiman, J., Chotai, K., et al. (1996). Phenotypic Characterization of Individuals with 30-40 CAG Repeats in the Huntington Disease (HD) Gene Reveals HD Cases with 36 Repeats and Apparently Normal Elderly Individuals with 36-39 Repeats. *Am. J. Hum. Genet.*, 16–22.

Sahlender, D. A., Roberts, R. C., Arden, S. D., Spudich, G., Taylor, M. J., Luzio, J. P., Kendrick-jones, J., et al. (2005). Optineurin links myosin VI to the Golgi complex and is involved in Golgi organization and exocytosis. *The Journal of cell biology*, *169*(2), 285–295. doi:10.1083/jcb.200501162

Sanchez, I., Xu, C., Juo, P., Kakizaka, A., Blenis, J., & Yuan, J. (1999). Caspase-8 Is Required for Cell Death Induced by Expanded Polyglutamine Repeats. *Neuron*, *22*, 623–633.

Sathasivam, K., Woodman, B., Mahal, A., Bertaux, F., Wanker, E. E., Shima, D. T., & Bates, G. P. (2001). Centrosome disorganization in fibroblast cultures derived from R6 / 2 Huntington ' s disease (HD) transgenic mice and HD patients. *Human molecular genetics*, *10*(21), 2425–2436.

Saudou, F., Finkbeiner, S., Devys, D., & Greenberg, M. E. (1998). Huntingtin acts in the nucleus to induce apoptosis but death does not correlate with the formation of intranuclear inclusions. *Cell*, *95*, 55–66.

Schaefer, M., Petronczki, M., Dorner, D., Forte, M., & Knoblich, J. A. (2001). Heterotrimeric G Proteins Direct Two Modes of Asymmetric Cell Division in the Drosophila Nervous System. *Cell*, *107*, 183–194.

Schenk, J., Wilsch-Brauninger, M., Calegari, F., & Huttner, W. B. (2009). Myosin II is required for interkinetic nuclear migration of neural progenitors. *PNAS*, *106*(38).

Schilling, B., Gafni, J., Torcassi, C., Cong, X., Row, R. H., Lafevre-bernt, M. A., Cusack, M. P., et al. (2006). Huntingtin Phosphorylation Sites Mapped by Mass Spectrometry. *The Journal of biological chemistry*, *281*(33), 23686–23697. doi:10.1074/jbc.M513507200

Schliwa, M., & Woehlke, G. (2003). Molecular motors. *Nature*, *422*(April), 759–765.

Schroer, T. a. (2004). Dynactin. *Annual review of cell and developmental biology*, *20*, 759–79. doi:10.1146/annurev.cellbio.20.012103.094623

Shah, J. V. (2010). Cells in tight spaces : the role of cell shape in cell function. *The Journal of cell biology*, *191*(2), 233–236. doi:10.1083/jcb.201004003

Shibata, M., Lu, T., Furuya, T., Degterev, A., Mizushima, N., Yoshimori, T., Macdonald, M., et al. (2006). Regulation of Intracellular Accumulation of Mutant Huntingtin by Beclin 1. *The Journal of biological chemistry*, *281*(20), 14474–14485. doi:10.1074/jbc.M600364200

Shimohata, M., Shimohata, T., Igarashi, S., Naruse, S., & Tsuji, S. (2005). Interference of CREB-dependent transcriptional activation by expanded polyglutamine stretches – augmentation of transcriptional activation as a potential therapeutic strategy for polyglutamine diseases. *Journal of neurochemistry*, 654–663. doi:10.1111/j.1471-4159.2005.03060.x

Shimohata, T., Nakajima, T., Yamada, M., Uchida, C., Onodera, O., Kimura, T., Koide, R., et al. (2000). Expanded polyglutamine stretches interact with TAF II 130 , interfering with CREB-dependent transcription. *nature genetics*, *26*(september), 29–36.

Shimojo, M. (2008). Huntingtin Regulates RE1-silencing Transcription Factor / Neuron-restrictive Silencer Factor (REST / NRSF) Nuclear Trafficking Indirectly through a Complex with REST / NRSF-interacting LIM Domain Protein (RILP) and Dynactin p150 Glued. *The Journal of biological chemistry*, *283*(50), 34880–34886. doi:10.1074/jbc.M804183200

Shitamukai, A., Konno, D., & Matsuzaki, F. (2011). Oblique radial glial divisions in the developing mouse neocortex induce self-renewing progenitors outside the germinal zone that resemble primate outer subventricular zone progenitors. *The Journal of neuroscience*, *31*(10), 3683–95. doi:10.1523/JNEUROSCI.4773-10.2011

Shitamukai, A., & Matsuzaki, F. (2012). Control of asymmetric cell division of mammalian neural progenitors. *Development, growth & differentiation*, *54*(3), 277–86. doi:10.1111/j.1440-169X.2012.01345.x

Siegrist, S. E., & Doe, C. Q. (2006). Extrinsic cues orient the cell division axis in Drosophila embryonic neuroblasts. *Development*, 529–536. doi:10.1242/dev.02211

Siller, K. H., Cabernard, C., & Doe, C. Q. (2006). The NuMA-related Mud protein binds Pins and regulates spindle orientation in Drosophila neuroblasts. *Nature cell biology*, *8*, 594–600.

Siller, K. H., & Doe, C. Q. (2008). Lis1/dynactin regulates metaphase spindle orientation in Drosophila neuroblasts. *Dev. Biol.*, *319*, 1–9.

Siller, K. H., & Doe, C. Q. (2009). Spindle orientation during asymmetric cell division. *Nature cell biology*, *11*(4), 365–374.

Simpson, J. M., Gil-Mohapel, J., Pouladi, M. a, Ghilan, M., Xie, Y., Hayden, M. R., & Christie, B. R. (2010). Altered adult hippocampal neurogenesis in the yac128 transgenic mouse model of huntington disease. *Neurobiology of disease*. doi:10.1016/j.nbd.2010.09.012

Sinadinos, C., Burbidge-king, T., Soh, D., Thompson, L. M., & Marsh, J. L. (2009). Live axonal transport disruption by mutant huntingtin fragments in Drosophila motor neuron axons. *Neurobiology of Disease*, *34*(2), 389–395. doi:10.1016/j.nbd.2009.02.012

Slep, K. C. (2009). The role of TOG domains in microtubule plus end dynamics. *Biochemical Society Transactions*, *37*, 1002–1006. doi:10.1042/BST0371002

Smith, R., Brundin, P., & Li, J. (2005). Synaptic dysfunction in Huntington ' s disease : a new perspective. *Cellular and Molecular Life Sciences*, *62*, 1901–1912. doi:10.1007/s00018-005-5084-5

Snell, R. G., Thompson, L. M., Tagle, D. A., Holloway, T. L., Barnes, G., Harley, H. G., Sandkuijl, L. A., et al. (1992). A recombination event that redefines the Huntington disease region. *American journal of human genetics*, *51*(2), 357–62. Retrieved from http://www.pubmedcentral.nih.gov/articlerender.fcgi?artid=1682687&tool=pmcentrez&rendertype=abstract

Son, J. H., Shim, J. H., & Kim, K. (2012). Neuronal autophagy and neurodegenerative diseases. *EXPERIMENTAL and MOLECULAR MEDICINE*, *44*(2), 89–98.

Sonbuchner, T. M., Rath, U., & Sharp, D. J. (2010). KL1 is a novel microtubule severing enzyme that regulates mitotic spindle architecture. *Cell Cycle*, 2403–2411.

Squitieri, F., Gellera, C., Cannella, M., Mariotti, C., Cislaghi, G., Rubinsztein, D. C., Almqvist, E. W., et al. (2003). Homozygosity for CAG mutation in Huntington disease is associated with a more severe clinical course. *Brain*, 946–955. doi:10.1093/brain/awg077

Steffan, J. S., Agrawal, N., Pallos, J., Rockabrand, E., Trotman, L. C., Slepko, N., Illes, K., et al. (2004). SUMO Modification of Huntingtin and Huntington ' s. *Science*, *304*(April), 100–104.

Steffan, J. S., Bodai, L., Pallos, J., Poelman, M., Mccampbell, A., Apostol, B. L., Kazantsev, A., et al. (2001). Histone deacetylase inhibitors arrest neurodegeneration in Drosophila. *Nature*, 739–743.

Steffan, J. S., Kazantsev, A., Spasic-boskovic, O., Greenwald, M., Zhu, Y., Gohler, H., Wanker, E. E., et al. (2000). The Huntington ' s disease protein interacts with p53 and CREB-binding protein and represses transcription. *PNAS*, (12).

Steinmetz, M. O., & Akhmanova, A. (2008). Capturing protein tails by CAP-Gly domains. *Trends in biochemical sciences*, *33*(October), 535–545. doi:10.1016/j.tibs.2008.08.006

Stepanova, T., Slemmer, J., Hoogenraad, C. C., Lansbergen, G., Dortland, B., De Zeeuw, C. I., Grosveld, F., et al. (2003). Visualization of microtubule growth in cultured neurons via the use of EB3-GFP (end-binding protein 3-green fluorescent protein). *The Journal of neuroscience : the official journal of the Society for Neuroscience*, *23*(7), 2655–64. Retrieved from http://www.ncbi.nlm.nih.gov/pubmed/12684451

Stewart, M. P., Helenius, J., Toyoda, Y., Ramanathan, S. P., Muller, D. J., & Hyman, A. a. (2011). Hydrostatic pressure and the actomyosin cortex drive mitotic cell rounding. *Nature*, *469*(7329), 226–230. doi:10.1038/nature09642

Stowers, R. S., & Isacoff, E. Y. (2007). Drosophila Huntingtin-Interacting Protein 14 Is a Presynaptic Protein Required for Photoreceptor Synaptic Transmission and Expression of the Palmitoylated Proteins Synaptosome- Associated Protein 25 and Cysteine String Protein. *The Journal of Neuroscience*, *27*(47), 12874–12883. doi:10.1523/JNEUROSCI.2464-07.2007

Strehlow, A. N. T., Li, J. Z., & Myers, R. M. (2007). Wild-type huntingtin participates in protein trafficking between the Golgi and the extracellular space. *Human molecular genetics*, *16*(4), 391–409. doi:10.1093/hmg/ddl467

Su, T. T., & O'Farrell, P. H. (1998). Size control : Cell proliferation does not equal growth. *Current biology*, 687–689.

Sugars, K. L., & Rubinsztein, D. C. (2003). Transcriptional abnormalities in Huntington disease. *Trends in genetics*, *19*(5), 233–238.

Sun, Y., Savanenin, A., Reddy, P. H., & Liu, Y. F. (2001). Polyglutamine-expanded Huntingtin Promotes Sensitization of N-Methyl- D -aspartate Receptors via Post-synaptic Density 95. *The Journal of biological chemistry*, *276*(27), 24713–24718. doi:10.1074/jbc.M103501200

Szebenyi, G., Morfini, G. A., Babcock, A., Gould, M., Selkoe, K., Stenoien, D. L., Young, M., et al. (2003). Neuropathogenic Forms of Huntingtin and Androgen Receptor Inhibit Fast Axonal Transport. *Neuron*, *40*, 41–52.

Tabrizi, S. J., Cleeter, M. W., Xuereb, J., Taanman, J. W., Cooper, J. M., & Schapira, A. H. (1999). Biochemical abnormalities and excitotoxicity in Huntington's disease brain. *Annals of neurology*, *45*(1), 25–32. Retrieved from http://www.ncbi.nlm.nih.gov/pubmed/9894873

Taddei, I., Deugnier, M.-A., Faraldo, M. M., Petit, V., Bouvard, D., Medina, D., Fässler, R., et al. (2008). Beta1 integrin deletion from the basal compartment of the mammary epithelium affects stem cells. *Nature cell biology*, *10*(6), 716–22. Retrieved from http://www.pubmedcentral.nih.gov/articlerender.fcgi?artid=2659707&tool=pmcentrez&rendertype=abstract

Tanenbaum, M. E., Galjart, N., van Vugt, M. a T. M., & Medema, R. H. (2006). CLIP-170 facilitates the formation of kinetochore-microtubule attachments. *The EMBO journal*, *25*(1), 45–57. doi:10.1038/sj.emboj.7600916

Tanenbaum, M. E., & Medema, R. H. (2010). Mechanisms of centrosome separation and bipolar spindle assembly. *Developmental cell*, *19*(6), 797–806. Retrieved from http://www.ncbi.nlm.nih.gov/pubmed/21145497

Tartari, M., Gissi, C., Sardo, V. L., Zuccato, C., Picardi, E., Pesole, G., & Cattaneo, E. (2008). Phylogenetic Comparison of Huntingtin Homologues Reveals the Appearance of a Primitive polyQ in Sea Urchin. *Mol Biol Evol*. doi:10.1093/molbev/msm258

Taverna, E., & Huttner, W. B. (2010). Neural progenitor nuclei IN motion. *Neuron*, *67*(6), 906–14. doi:10.1016/j.neuron.2010.08.027

Thakur, A. K., Jayaraman, M., Mishra, R., Thakur, M., Chellgren, V. M., Byeon, I. L., Anjum, D. H., et al. (2009). Polyglutamine disruption of the huntingtin exon 1 N terminus triggers a complex aggregation mechanism. *NATURE STRUCTURAL & MOLECULAR BIOLOGY*, *16*(4), 380–389. doi:10.1038/nsmb.1570

The Huntington's Disease Collaborative Research Group. (1993). A Novel Gene Containing a Trinucleotide That Is Expanded and Unstable on Huntington ' s Disease Chromosomes. *Cell*, *72*, 971–983.

Thomas, L. B., Gates, D. J., Richfield, eric K., O'brien, thomas F., Schweitzer, john B., & Steindler, D. A. (1995). DNA end labeling (TUNEL) in Huntington's disease and other neuropathological conditions. *Experimental neurology*.

Thompson, L. M., Aiken, C. T., Kaltenbach, L. S., Agrawal, N., Illes, K., Khoshnan, A., Martinez-vincente, M., et al. (2009). IKK phosphorylates Huntingtin and targets it for degradation by the proteasome and lysosome. *The Journal of cell biology*, *187*(7). doi:10.1083/jcb.200909067

Théry, M., & Bornens, M. (2006). Cell shape and cell division. *Current opinion in cell biology*, *18*(6), 648–57. doi:10.1016/j.ceb.2006.10.001

Théry, M., & Bornens, M. (2008). Get round and stiff for mitosis. *HFSP Journal*, 65–71. doi:10.2976/1.2895661

Théry, M., Jiménez-Dalmaroni, A., Racine, V., Bornens, M., & Jülicher, F. (2007). Experimental and theoretical study of mitotic spindle orientation. *Nature*, *447*(7143), 493–6. doi:10.1038/nature05786

Théry, M., Racine, V., Pépin, A., Piel, M., Chen, Y., Sibarita, J.-B., & Bornens, M. (2005). The extracellular matrix guides the orientation of the cell division axis. *Nature cell biology*, *7*(10), 947–53. doi:10.1038/ncb1307

Tian, L., Nelson, D. L., & Stewart, D. M. (2000). Cdc42-interacting protein 4 mediates binding of the Wiskott-Aldrich syndrome protein to microtubules. *The Journal of biological chemistry*, *275*(11), 7854–61. Retrieved from http://www.ncbi.nlm.nih.gov/pubmed/10713100

Tong, Y., Ha, T. J., Liu, L., Nishimoto, A., Reiner, A., & Goldowitz, D. (2011). Spatial and Temporal Requirements for huntingtin (Htt) in Neuronal Migration and Survival during Brain Development. *The Journal of neuroscience : the official journal of the Society for Neuroscience*, *31*(41), 14794–9. doi:10.1523/JNEUROSCI.2774-11.2011

Toyama, Y., Peralta, X. G., Wells, A. R., Kiehart, D. P., & Edwards, G. S. (2008). Apoptotic Force and Tissue Dynamics During Drosophila Embryogenesis. *Science*. doi:10.1126/science.1157052

Toyoshima, F., Matsumura, S., Morimoto, H., Mitsushima, M., & Nishida, E. (2007). PtdIns(3,4,5)P3 regulates spindle orientation in adherent cells. *Developmental cell*, *13*(6), 796–811. doi:10.1016/j.devcel.2007.10.014

Toyoshima, F., & Nishida, E. (2007a). Spindle Orientation in Animal Cell Mitosis : Roles of Integrin in the Control of Spindle Axis. *Journal of Cellular Physiology*, (June), 407–411. doi:10.1002/JCP

Toyoshima, F., & Nishida, E. (2007b). Integrin-mediated adhesion orients the spindle parallel to the substratum in an EB1- and myosin X-dependent manner. *The EMBO journal*, *26*(6), 1487–98. doi:10.1038/sj.emboj.7601599

Trettel, F., Rigamonti, D., Hilditch-maguire, P., Wheeler, V. C., Sharp, A. H., Persichetti, F., Cattaneo, E., et al. (2000). Dominant phenotypes produced by the HD mutation in STHdh(Q111) striatal cells. *Hum. Mol. Genet*, *9*, 2799–2809.

Trottier, Y., Lutz, Y., Stevanin, G., Imbert, G., Devys, D., Cancel, G., Saudou, F., et al. (1995). Polyglutamine expansion as a pathological epitope in Huntington's disease and four dominant cerebellar ataxias. *Nature*, *378*(6555), 403–6. Retrieved from http://www.ncbi.nlm.nih.gov/pubmed/7477379

Trushina, E., Dyer, R. B., Ii, J. D. B., Eide, L., Tran, D. D., Vrieze, B. T., Mcpherson, P. S., et al. (2004). Mutant Huntingtin Impairs Axonal Trafficking in Mammalian Neurons In Vivo and In Vitro Mutant Huntingtin Impairs Axonal Trafficking in Mammalian Neurons In Vivo and In Vitro. *Molecular and cellular biology*. doi:10.1128/MCB.24.18.8195

Tsai, J., Chen, Y., Kriegstein, A. R., & Vallee, R. B. (2005). LIS1 RNA interference blocks neural stem cell division, morphogenesis, and motility at multiple stages. *The Journal of cell biology*, 935–945. doi:10.1083/jcb.200505166

Tsai, J.-W., Bremner, K. H., & Vallee, R. B. (2007). Dual subcellular roles for LIS1 and dynein in radial neuronal migration in live brain tissue. *Nature neuroscience*, *10*(8), 970–9. doi:10.1038/nn1934

Tsai, L.-H., & Gleeson, J. G. (2005). Nucleokinesis in neuronal migration. *Neuron*, *46*(3), 383–8. doi:10.1016/j.neuron.2005.04.013

Tzingounis, A. V., & Wadiche, J. I. (2007). Glutamate transporters : confining runaway excitation by shaping synaptic transmission. *Nature Reviews Neuroscience*, *8*(DECEmBER). doi:10.1038/nrn2274

U, M., Miyashita, T., Ohtsuka, Y., Okamura-Oho, Y., Shikama, Y., & Yamada, M. (2001). Extended polyglutamine selectively interacts with caspase-8 and -10 in nuclear aggregates. *Cell Death and Differentiation*, 377–386.

Usdin, M. T., Shelbourne, P. F., Myers, R. M., & Madison, D. V. (1999). Impaired synaptic plasticity in mice carrying the Huntington ' s disease mutation. *Human molecular genetics*, *8*(5), 839–846.

Valenza, M., Rigamonti, D., Goffredo, D., Zuccato, C., Fenu, S., Jamot, L., Strand, A., et al. (2005). Dysfunction of the Cholesterol Biosynthetic Pathway in Huntington ' s Disease. *The Journal of Neuroscience*, *25*(43), 9932–9939. doi:10.1523/JNEUROSCI.3355-05.2005

Vallee, R. B., & Tsai, J.-W. (2006). The cellular roles of the lissencephaly gene LIS1 , and what they tell us about brain development. *Genes & Development*, 1384–1393. doi:10.1101/gad.1417206

Van Der Burg, J. M. M., Björkqvist, M., & Brundin, P. (2009). Beyond the brain : widespread pathology in Huntington ' s disease. *The Lancet Neurology*, *8*(8), 765–774. doi:10.1016/S1474-4422(09)70178-4

Velier, J., Kim, M., Schwarz, C., Kim, T. W., Sapp, E., Chase, K., Aronin, N., et al. (1998). Wild-Type and Mutant Huntingtins Function in Vesicle Trafficking in the Secretory and Endocytic Pathways. *Experimental neurology*, *40*(152), 34–40.

Vonsattel, J. P., & DiFiglia, M. (1998). Huntington disease. *Journal of neuropathology and experimental neurology*, *57*(5), 369–84. Retrieved from http://www.ncbi.nlm.nih.gov/pubmed/9596408

Vonsattel, J. P., Myers, R. H., Stevens, T. J., Ferrante, R. J., Bird, E. D., & Richardson, E. P. (1985). Neuropathological classification of Huntington's disease. *Journal of neuropathology and experimental neurology*, *44*(6), 559–77. Retrieved from http://www.ncbi.nlm.nih.gov/pubmed/2932539

Waelter, S., Scherzinger, E., Hasenbank, R., Nordhoff, E., Lurz, R., Goehler, H., Gauss, C., et al. (2001). The huntingtin interacting protein HIP1 is a clathrin and α -adaptin-binding protein involved in receptor-mediated endocytosis. *Human Molecular Genetics*, *10*(17), 1807–1817.

Walczak, C. E., Cai, S., & Khodjakov, A. (2010). Mechanisms of chromosome behaviour during mitosis. *Nature Reviews Molecular Cell Biology*, *11*(2), 91–102. doi:10.1038/nrm2832

Walczak, C. E., & Heald, R. (2008). Mechanisms of Mitotic Spindle Assembly and Function. *International review of cytology*, *265*(07). doi:10.1016/S0074-7696(07)65003-7

Wang, X., Lui, J. H., & Kriegstein, A. R. (2011). Orienting fate: spatial regulation of neurogenic divisions. *Neuron*, *72*(2), 191–3. doi:10.1016/j.neuron.2011.10.003

Wanker, E E, Rovira, C., Scherzinger, E., Hasenbank, R., Wälter, S., Tait, D., Colicelli, J., et al. (1997). HIP-I: a huntingtin interacting protein isolated by the yeast two-hybrid system. *Human molecular genetics*, *6*(3), 487–95. Retrieved from http://www.ncbi.nlm.nih.gov/pubmed/9147654

Wanker, Erich E. (2000). Protein aggregation in Huntington ' s and Parkinson ' s disease : implications for therapy. *MOLECULAR MEDICINE TODAY*, *6*(October), 387–391.

Warby, S. C., Chan, E. Y., Metzler, M., Gan, L., Singaraja, R. R., Crocker, S. F., Robertson, H. a, et al. (2005). Huntingtin phosphorylation on serine 421 is significantly reduced in the striatum and by polyglutamine expansion in vivo. *Human molecular genetics*, *14*(11), 1569–77. doi:10.1093/hmg/ddi165

Warby, S. C., Doty, C. N., Graham, R. K., Shively, J., Singaraja, R. R., & Hayden, M. R. (2009). Phosphorylation of huntingtin reduces the accumulation of its nuclear fragments. *Molecular and cellular neurosciences*, *40*(2), 121–7. doi:10.1016/j.mcn.2008.09.007

Watanabe, N., Madaule, P., Reid, T., Ishizaki, T., Watanabe, G., Kakizuka, A., Saito, Y., et al. (1997). p140mDia , a mammalian homolog of Drosophila diaphanous , is a target protein for Rho small GTPase and is a ligand for profilin. *The EMBO journal*, *16*(11), 3044–3056.

Watson, P., & Stephens, D. J. (2006). Microtubule plus-end loading of p150Glued is mediated by EB1 and CLIP-170 but is not required for intracellular membrane traffic in mammalian cells. *Journal of cell science*, *119*(Pt 13), 2758–67. doi:10.1242/jcs.02999

Weisbrich, A., Honnappa, S., Jaussi, R., Okhrimenko, O., Frey, D., Jelesarov, I., Akhmanova, A., et al. (2007). Structure-function relationship of CAP-Gly domains. *Nature structural & molecular biology*, *14*(10), 959–67. doi:10.1038/nsmb1291

Wellington, C. L., Ellerby, L. M., Gutekunst, C., Rogers, D., Warby, S., Graham, R. K., Loubser, O., et al. (2002). Caspase Cleavage of Mutant Huntingtin Precedes Neurodegeneration in Huntington ' s Disease. *The Journal of Neuroscience*, *22*(18), 7862–7872.

Wellington, C. L., Leavitt, B. R., & Hayden, M. R. (2000). Huntington disease: new insights on the role of huntingtin cleavage. *Journal of neural transmission. Supplementum*, (58), 1–17. Retrieved from http://www.ncbi.nlm.nih.gov/pubmed/11128600

Wexler, N. S. (2004). Venezuelan kindreds reveal that genetic and environmental factors modulate Huntington ' s. *PNAS*, *101*(10).

Wheeler, V. C., Auerbach, W., White, J. K., Srinidhi, J., Auerbach, A., Ryan, A., Duyao, M. P., et al. (1999). Length-dependent gametic CAG repeat instability in the Huntington's disease knock-in mouse. *Human molecular genetics*, *8*(1), 115–22. Retrieved from http://www.ncbi.nlm.nih.gov/pubmed/9887339

White, J. K., Auerbach, W., Duyao, M. P., Vonsattel, J. P., Gusella, J. F., Joyner, A. L., & MacDonald, M. E. (1997). Huntingtin is required for neurogenesis and is not impaired by the Huntington's disease CAG expansion. *Nature genetics*, *17*(4), 404–10. Retrieved from http://www.ncbi.nlm.nih.gov/pubmed/9398841

Williams, S. E., Beronja, S., Pasolli, H. A., & Fuchs, E. (2011). Asymmetric cell divisions promote Notch-dependent epidermal differentiation. *Nature*, *470*(7334), 353–358. doi:10.1038/nature09793

Wu, L. L., Fan, Y., Li, S., Li, X., & Zhou, X. (2010). Huntingtin-associated Protein-1 Interacts with Pro-brain-derived Neurotrophic Factor and Mediates Its Transport and Release * □. *The Journal of biological chemistry*, *285*(8), 5614–5623. doi:10.1074/jbc.M109.073197

Wynshaw-Boris, A. (2007). Lissencephaly and LIS1: insights into the molecular mechanisms of neuronal migration and development. *Clinical genetics*, *72*(4), 296–304. doi:10.1111/j.1399-0004.2007.00888.x

Xia, J., Lee, D. H., Taylor, J., Vandelft, M., & Truant, R. (2003). Huntingtin contains a highly conserved nuclear export signal. *Human molecular genetics*, *12*(12), 1393–1403. doi:10.1093/hmg/ddg156

Xie, Z., Moy, L. Y., Sanada, K., Zhou, Y., Buchman, J. J., & Tsai, L.-H. (2007). Cep120 and TACCs Control Interkinetic Nuclear Migration and the Neural Progenitor Pool. *Neuron*, 79–93. doi:10.1016/j.neuron.2007.08.026

Yamashita, Y. M., Jones, D. L., & Fuller, M. T. (2003). Orientation of Asymmetric Stem Cell Division by the APC Tumor Suppressor and Centrosome. *Science*, *1547*(2003). doi:10.1126/science.1087795

Yanai, A., Huang, K., Kang, R., Singaraja, R. R., Arstikaitis, P., Gan, L., Orban, P. C., et al. (2006). Palmitoylation of huntingtin by HIP14 is essential for its trafficking and function. *Nature neuroscience*, *9*(6), 824–831. doi:10.1038/nn1702

Yingling, J., Youn, Y. H., Darling, D., Toyo-Oka, K., Pramparo, T., Hirotsune, S., & Wynshaw-Boris, A. (2008a). Neuroepithelial stem cell proliferation requires LIS1 for precise spindle orientation and symmetric division. *Cell*, *132*(3), 474–86. doi:10.1016/j.cell.2008.01.026

Yingling, J., Youn, Y. H., Darling, D., Toyo-Oka, K., Pramparo, T., Hirotsune, S., & Wynshaw-Boris, A. (2008b). Supplemental Data Neuroepithelial stem cell proliferation requires LIS1 for precise spindle orientation and symmetric division. *Cell*, *132*(3), 474–86. doi:10.1016/j.cell.2008.01.026

Yoon, K., & Gaiano, N. (2005). Notch signaling in the mammalian central nervous system : insights from mouse mutants. *Nature neuroscience*, *8*(6), 709–715. doi:10.1038/nn1475

Yoon, K.-J., Koo, B.-K., Im, S.-K., Jeong, H.-W., Ghim, J., Kwon, M.-C., Moon, J.-S., et al. (2008). Article Mind Bomb 1-Expressing Intermediate Progenitors Generate Notch Signaling to Maintain Radial Glial Cells. *Neuron*, 519–531. doi:10.1016/j.neuron.2008.03.018

Young, A. B., Greenamyre, J. T., Hollingsworth, Z., Albin, R., Amato, C. D., Shoulson, I. R. A., & Penney, J. B. (1988). NMDA Receptor Losses in Putamen firom Patients with Huntington ' s Disease. *Science*, *5867*(1977), 1986–1988.

Yu, F., Kuo, C. T., & Jan, Y. N. (2006). Drosophila Neuroblast Asymmetric Cell Division : Recent Advances and Implications for Stem Cell Biology. *Neuron*, 13–20. doi:10.1016/j.neuron.2006.06.016

Zala, D., Colin, E., Rangone, H., Liot, G., Humbert, S., & Saudou, F. (2008). Phosphorylation of mutant huntingtin at S421 restores anterograde and retrograde transport in neurons. *Human molecular genetics*, *17*(24), 3837–46. doi:10.1093/hmg/ddn281

Zeitlin, S., Liu, J. P., Chapman, D. L., Papaioannou, V. E., & Efstratiadis, A. (1995). Increased apoptosis and early embryonic lethality in mice nullizygous for the Huntington's disease gene homologue. *Nature genetics*, *11*(2), 155–63. Retrieved from http://www.ncbi.nlm.nih.gov/pubmed/7550343

Zhadanov, A. B., Provance, D. W., Speer, C. A., Coffin, J. D., Goss, D., Blixt, J. A., Reichert, C. M., et al. (1999). Absence of the tight junctional protein AF-6 disrupts epithelial cell-cell junctions and cell polarity during mouse development. *Current biology*, *9*(16), 880–8. Retrieved from http://www.ncbi.nlm.nih.gov/pubmed/10469590

Zhai, Y., Kronebusch, P. J., & Borisy, G. G. (1995). Kinetochore Microtubule Dynamics and the Metaphase-Anaphase Transition. *The Journal of Cell Biology*, *131*(3), 721–734.

Zhang, R., Zhang, Z., Zhang, C., Zhang, L., Robin, A., Wang, Y., Lu, M., et al. (2004). Stroke transiently increases subventricular zone cell division from asymmetric to symmetric and increases neuronal differentiation in the adult rat. *The Journal of neuroscience : the official journal of the Society for Neuroscience*, *24*(25), 5810–5. doi:10.1523/JNEUROSCI.1109-04.2004

Zhang, S., Feany, M. B., Saraswati, S., Littleton, J. T., & Perrimon, N. (2009a). Inactivation of Drosophila Huntingtin affects long-term adult functioning and the pathogenesis of a Huntington's disease model. *Disease models & mechanisms*, *2*(5-6), 247–66. doi:10.1242/dmm.000653

Zhang, S., Feany, M. B., Saraswati, S., Littleton, J. T., & Perrimon, N. (2009b). Inactivation of Drosophila Huntingtin affects long-term adult functioning and the pathogenesis of a Huntington's disease model. *Disease models & mechanisms*, *2*(5-6), 247–66. doi:10.1242/dmm.000653

Zhang, X., Lei, K., Yuan, X., Wu, X., Zhuang, Y., Xu, T., Xu, R., et al. (2009). SUN1/2 and Syne/Nesprin-1/2 complexes connect centrosome to the nucleus during neurogenesis and neuronal migration in mice. *Neuron*, *64*(2), 173–87. doi:10.1016/j.neuron.2009.08.018

Zhang, Y., Leavitt, B. R., Jeremy, M., Raamsdonk, V., Dragatsis, I., Macdonald, M. E., Hayden, R., et al. (2006). Huntingtin inhibits caspase-3 activation. *The EMBO journal*, *25*(24), 5896–5906. doi:10.1038/sj.emboj.7601445

Zhao, Z.-S., Lim, J. P., Ng, Y.-W., Lim, L., & Manser, E. (2005). The GIT-associated kinase PAK targets to the centrosome and regulates Aurora-A. *Molecular cell*, *20*(2), 237–49. doi:10.1016/j.molcel.2005.08.035

Zheng, S., Clabough, E. B. D., Sarkar, S., Futter, M., Rubinsztein, D. C., & Scott, O. (2010). Deletion of the Huntingtin Polyglutamine Stretch Enhances Neuronal Autophagy and Longevity in Mice. *plos genetics*, *6*(2). doi:10.1371/journal.pgen.1000838

Zuccato, C., Belyaev, N., Conforti, P., Ooi, L., Tartari, M., Papadimou, E., Macdonald, M., et al. (2007). Widespread Disruption of Repressor Element-1 Silencing Transcription Factor / Neuron-Restrictive Silencer Factor Occupancy at Its Target Genes in Huntington ' s Disease, *27*(26), 6972–6983. doi:10.1523/JNEUROSCI.4278-06.2007

Zuccato, C., & Cattaneo, E. (2007). Role of brain-derived neurotrophic factor in Huntington ' s disease. *Progress in Neurobiology*, *81*, 294–330. doi:10.1016/j.pneurobio.2007.01.003

Zuccato, C., Ciamola, A., Rigamonti, D., Leavitt, B. R., Goffredo, D., Conti, L., Macdonald, M. E., et al. (2001). Loss of Huntingtin-Mediated BDNF Gene Transcription in Huntington's Disease, *493*(2001). doi:10.1126/science.1059581

Zuccato, C., Marullo, M., Conforti, P., Macdonald, M. E., Tartari, M., & Cattaneo, E. (2008). Systematic Assessment of BDNF and Its Receptor Levels in Human Cortices Affected by Huntington ' s Disease, *18*(57), 225–238. doi:10.1111/j.1750-3639.2007.00111.x

Zuccato, C., Tartari, M., Crotti, A., Goffredo, D., Valenza, M., Conti, L., Cataudella, T., et al. (2003). Huntingtin interacts with REST/NRSF to modulate the transcription of NRSE-controlled neuronal genes. *nature genetics*, *35*(1), 76–83. doi:10.1038/ng1219

Zuccato, C., Valenza, M., & Cattaneo, E. (2010). Molecular Mechanisms and Potential Therapeutical Targets in Huntington ' s Disease. *Physiological Reviews*, 905–981. doi:10.1152/physrev.00041.2009.

Zucker, B., Luthi-carter, R., Kama, J. A., Dunah, A. W., Stern, E. A., Fox, J. H., Standaert, D. G., et al. (2005). Transcriptional dysregulation in striatal projection- and interneurons in a mouse model of Huntington ' s disease : neuronal selectivity and potential neuroprotective role of HAP1. *Human molecular genetics*, *14*(2), 179–189. doi:10.1093/hmg/ddi014

des Portes, V., Pinard, J. M., Billuart, P., Vinet, M. C., Koulakoff, A., Carrié, A., Gelot, A., et al. (1998). A novel CNS gene required for neuronal migration and involved in X-linked subcortical laminar heterotopia and lissencephaly syndrome. *Cell*, *92*(1), 51–61. Retrieved from http://www.ncbi.nlm.nih.gov/pubmed/9489699

van der Burg, J. M. M., Bacos, K., Wood, N. I., Lindqvist, A., Wierup, N., Woodman, B., Wamsteeker, J. I., et al. (2008). Increased metabolism in the R6 / 2 mouse model of Huntington ' s disease. *Neurobiology of Disease*, *29*, 41–51. doi:10.1016/j.nbd.2007.07.029

HUNTINGTINE ET MITOSE

La maladie de Huntington (MH) est une maladie neurodégénérative héréditaire autosomique dominante. Elle résulte d'une expansion anormale de glutamines (polyQ) dans la partie N-terminale de la protéine huntingtine (HTT ; codé par *HTT*). La MH est caractérisée par la dysfonction et la mort de cellules neuronales dans le cerveau, entraînant l'apparition de symptômes cognitifs, psychiatriques et moteurs, dévastateurs chez les patients. De nombreuses études sur des modèles animaux et cellulaires montrent que l'expansion polyQ dans la protéine mutante conduit à un gain de nouvelles fonctions toxiques, ainsi qu'à la perte de fonctions neuroprotectives de la protéine sauvage.

Pendant ma thèse, je me suis intéressée à la description et à la validation fonctionnelle d'un nouvel outil pour étudier la HTT : pARIS-htt. pARIS-htt est un gène synthétique construit pour faciliter le clonage et le marquage de la protéine HTT totale. En utilisant différentes approches cellulaires, nous avons montré que pARIS-htt peut remplacer le rôle de la HTT endogène dans le transport de vésicules du Golgi ainsi que du brain derived neurotrophic factor (BDNF). La version mutante de pARIS-htt ne peut pas restaurer cette fonction. Parallèlement, nous avons généré deux variants de pARIS-htt avec soit une délétion dans la région d'interaction de la HTT avec la dynéine, moteur moléculaire se dirigeant vers l'extrémité négative des microtubules, soit avec la huntingtin associated protein 1 (HAP1), l'un de ses interacteurs. Dans les expériences de remplacement du gène, aucun des deux mutants n'a restauré le transport vésiculaire.

Un autre aspect de ma thèse a été d'étudier le rôle de la HTT au cours de la mitose. Nous avons mis en évidence l'importance de la HTT dans le contrôle de l'orientation du fuseau. Cette fonction est perdue lorque la HTT est mutée, mais restaurée lorsque celle-ci est phosphorylée par Akt à la sérine 421. Le contrôle de l'orientation du fuseau est particulièrement important durant la neurogénèse puisque cette orientation ainsi que le mode de division sont impliqués dans la détermination des devenirs cellulaires. Cette fonction de la HTT est conservée chez la *D. melanogaster.*

Cette étude a donc permis de mieux comprendre les fonctions de la HTT, et de proposer de nouvelles cibles thérapeutiques pour traiter la MH.

Mots clés : maladie de Huntington, huntingtine, polyglutamines, transport intracellulaire, mitose, neurogenèse, Akt, phosphorylation, moteurs moléculaires.

Laboratoire d'accueil

Institut Curie, Équipe Huntingtine, Neurogènese et Cancer

CNRS UMR 3306/INSERM U1005/Université Paris-Sud 11

Orsay, France